MICRO AND NANO ANALYSIS OF A NOVEL POLYMERIC BIORESORBABLE SCAFFOLD AND ITS DRUG RELEASE

Tamara Mahmood, BSc. (Hons)

School of Pharmacy

Thesis submitted to the University of Nottingham for the degree of Doctor of Philosophy

September 2017

DECLARATION

I hereby certify that this thesis represents my own work, that where the language of others is set forth, quotation marks so indicate, and that appropriate credit is given where I have used the language, ideas, expressions or writings of another. I declare that the thesis describes original work that has not previously been presented for the award of any other degree of any institution.

Tamara Mahmood

ABSTRACT

The composition of the top-most molecular layers of solid materials is of great importance in the understanding of many technologically important processes. This is especially so, for example for devices exposed to the *in vivo* environment of our bodies especially if long term functionality is required. Cardiovascular stents or scaffolds are a biomedical implant that must maintain structural and functional integrity for periods of months to achieve their therapeutic goal. In this work, the fully polymeric drug-eluting bioresorbable scaffold, ArterioSorb^{TM} is characterised, paying particular attention to surface and near surface properties.

The introduction of cardiovascular stents has considerably enhanced the potential of surgical intervention via angioplasty. Biomaterials used for implants may be metallic, ceramic, polymeric or composite. A new generation of drug eluting stent are now emerging, such as the Poly (L-lactide) (PLLA) based fully biodegradable stents studied here, that have the potential to increase the therapeutic potential of this approach even further. PLLA is a bioabsorbable semi-crystalline polymer that possesses a low elongation and high tensile strength, which makes it appropriate for this medical application. Using a spray-coating method a sirolimus/PDLLA layer was coated onto the surface of a bioresorbable PLLA scaffold by Arterius Ltd. The aim of this thesis is the study of the drug distribution and physiochemical properties of the biomedical device and to relate this information to likely drug release mechanisms under physiological conditions. Complementary surface and near-surface analysis techniques including scanning electron microscopy (SEM), atomic force microscopy (AFM), time-of-flight secondary ion mass spectrometry (ToF-SIMS), X-ray photoelectron spectroscopy (XPS) and confocal Raman imaging (CRM) have been used to assess structure, composition and their relation to drug release.

Primarily, this work was carried out on a series of extruded and orientated (die-drawn) PLLA tubing before considering the actual bioresorbable medical device (uncoated, coated expanded and crimped scaffolds). ToF-SIMS has been used to confirm the chemical homogeneity of the PLLA coating and provide evidence of some minor surface elemental contamination likely due to transfer of fluorine from packaging/sample

handling. The drug (sirolimus) was clearly observed and mapped at the microscale at the surface and in the bulk of the scaffold coating. In addition, the physical properties of these materials were investigated using nano and micro thermal analysis. The percentage of crystallinity of the PLLA materials was studied using Differential Scanning Calorimetry (DSC). Attenuated total reflection infrared (ATR-IR) helped in assessing the structure of PLLA. Factors including the manufacturing process used have been shown to have an effect on the materials. The degradation *in vitro* has been shown to be influenced by the molecular weight of the polymer and the concentration of the drug.

This thesis is organised into six chapters. Chapter 1 provides an introduction to the technical requirements needed for bioresorbable stent and outlines the literature review and research context for the development of the scaffold, including materials used for the manufacturing of the scaffold, spray coating method and laser cutting techniques. Chapter 2 describes the instrumentation and methodology used for characterising such medical device as well as a description of laser cutting used in manufacture. Chapter 3 presents a feasibility study on the extruded and oriented tubing. Chapter 4 describes the characterisation of the drug distribution in the drug/polymer matrix. Chapter 5 provides a detailed characterisation of the *in vitro* degradation of sirolimus/PDLLA coating layer revealing the release kinetics of the device. Finally, Chapter 6 gathers information learnt throughout this thesis and explored future directions to improve release and performance of such a device.

ACKNOWLEDGEMENTS

I wish to offer my sincerest gratitude to Professor Clive J Roberts and Morgan R Alexander from University of Nottingham, Dr Kadem Al-Lamee and Dr Nial Bullett from Arterius Ltd (Leeds) for their encouragement, and guidance throughout this research project. With their expertise and enthusiasm, I managed to overcome many challenges. I would also like to acknowledge Professor Xinyong Chen for his technical assistance with the AFM. I would like to thank Dr David J Scurr for his operational and assistance with ToF-SIMS and continual support over the last four years of my research. The Nanoscale and Microscale Research Centre (NMRC) are gratefully acknowledged for providing me access to the Raman Spectroscopy in particular Dr Andrew Davies (University of Nottingham) for his excellent contribution and advice on Raman imaging and experimental optimisation. I would like to acknowledge Nexus facility at Newcastle University for allowing me to use XPS and would like to thank particularly Dr Jose Portoles and Dr Naoko Sano for their invaluable help with XPS data acquiring and operation of the instrument. I also wish to acknowledge Kratos Analytical Ltd, especially Dr Jonathan Counsell for his advice on XPS peak-fitting. The BBSRC and Arterius Ltd kindly funded this study under the iCASE scheme. Scholarship Reference number: BB/K013300/1. Thank you to Kayla Friedman and Malcolm Morgan of the Centre for Sustainable Development, University of Cambridge, UK for producing the Microsoft Word thesis template used to produce this document.

To my colleagues and friends from the former LBSA and AMHT, I must thank them for being there when needed. Thanks to Dr Andreea Iuras, Dr Emanuela Cingolani, and Mr Jawaad Ismail, who helped me to keep things in perspective and supported me on several occasions. The friends I have made while at Nottingham have been absolutely amazing. Nottingham wouldn't have been the same without Emanuela, Victoria, Georgina, Rosa, Abdul and Sergey. You guys were some of the kindest, happiest and friendliest people I have met. Thank you for putting up with me. Finally, I owe all that I am and all I have accomplished to my loving parents and loved ones. Without their love, and motivation, I would have never achieved a fraction of what I am proud of today.

TABLE OF CONTENTS

Declaration ..... *ii*

Abstract ..... *iii*

Acknowledgements ..... *v*

Table of Contents ..... *vi*

Glossary ..... *x*

1 Introduction *12*

1.1 Biomedical Materials **12**

1.2 Coronary Artery Disease, Clinical Management and Stenting **18**

1.3 Generations of Coronary Stents **22**

1.3.1 Bare Metallic Stents 22

1.3.2 First and Second-Generation Drug Eluting Stents 24

1.3.3 Next Generation Stents: Fully Bioresorbable Scaffolds (BRSs) 26

1.4 Drugs used in Bioresorbable Stents **31**

1.4.1 Anti-proliferative Actives 31

1.5 Poly L Lactide (PLLA)/Poly D, L lactide (PDLLA) **35**

1.6 Surface Characterisation and Example of Surface Analytical Techniques used for Drug Delivery **38**

1.7 Example of Surface Characterisation in the Field of Drug Eluting Stents **40**

1.8 Controlled Drug Delivery for Biodegradable Drug Eluting Stents **44**

1.9 Aims of this Study **48**

2 Experimental Methods and Instrumentation *50*

2.1 Materials **50**

2.2 Stent Manufacturing and Geometry **53**

2.3 Bioresorbable Spray Coating Layer **62**

2.4 Sample Preparation **64**

2.4.1 Polymeric Tubing 64
2.4.2 Fully Bioresorbable Stents 65
2.5 Instrumentation 66
2.5.1 Scanning Electron Microscopy (SEM) 66
2.5.2 Atomic Force Microscopy (AFM) 67
2.5.3 Time-of-Flight Secondary Ion Mass Spectrometry Chemical Mapping (Tof-SIMS) 71
2.5.4 X-Ray Photoelectron Spectroscopy (XPS) 75
2.5.5 Confocal Raman Microscopy (CRM) 78
2.6 Other Complementary Characterisation Techniques 79
2.6.1 Scanning Thermal Microscopy (Nano Thermal Analysis) NTA 79
2.6.2 Bulk Analysis: Differential Scanning Calorimetry (DSC) 81
2.6.3 Attenuated Total Reflectance Infrared (ATR-IR) 82
2.6.4 Zeta Profilometry 82
2.6.5 Nano IR-AFM 83
3 Surface Characterisation of Bioresorbable Polymeric Tubing 84
3.1 Objective 86
3.2 Materials and Methods 87
3.3 Results and Discussion 87
3.3.1 Microstructural Characterisation of Polymeric Tubing 87
3.4 Physiochemical Characterisation of the Polymeric Tubing by AFM 92
3.4.1 Surface Imaging 92
3.4.2 Thermal Bulk Characterisation by DSC 96
3.5 Surface Thermal Characterisation 101
3.5.1 Nano Thermal Analysis by AFM 101
3.5.2 Micro Thermal Analysis (μ-TA) 103
3.6 Near Surface Chemistry by ATR-IR 105
3.7 Surface Chemistry by ToF-SIMS 109
3.7.1 Surface Analysis 109
3.7.2 ToF-SIMS Depth Profiling 113
3.8 Elemental Composition by XPS 115
3.9 Conclusions 121

4 Distribution of Sirolimus in PDLLA Coating Layer from the ArterioSorb™ Drug Eluting Stent Pre-Dissolution 122

4.1 Objective 124

4.2 Materials and Methods 124

4.2.1 Environmental Scanning Electron Microscopy (ESEM) 125

4.2.2 Atomic Force Microscopy (AFM) Analysis 125

4.2.3 ToF-SIMS Analysis 126

4.2.4 3D Profilometery 127

4.2.5 X-Ray Photoelectron Spectroscopy Analysis (XPS) 128

4.2.6 Confocal Raman Spectroscopy (CRM) 129

4.3 Results and Discussion 129

4.3.1 Surface Morphology 129

4.3.2 Thermal Analysis 145

4.3.3 Nano-IR Measurements 148

4.3.4 ATR-IR 150

4.4 Surface Chemical Analysis 152

4.4.1 ToF-SIMS Characterisation 152

4.4.2 ToF-SIMS Depth Profiling and Chemical Imaging 155

4.4.3 3D Image Reconstruction 162

4.4.4 Surface Composition of Sirolimus/PDLLA Coating in ArterioSorb™ Scaffold by XPS 166

4.4.5 XPS Depth Profiling 172

4.5 Compositional with Depth by Raman Spectroscopy 175

4.6 Conclusions 179

5 Understanding the Distribution of Sirolimus and Release from the PDLLA Coating Layer 181

5.1 Experimental Methods and Materials 183

5.1.1 In Vitro Drug Release Studies 184

5.2 Results and Discussion 184

5.2.1 Release Profile 184

5.2.2 Surface Morphology of Dissoluted Stents 189

5.2.3 Surface Chemical Chemistry by ToF-SIMS 201

5.2.4 Surface Chemical Composition by XPS 210

5.2.5 XPS Depth Profiling 215

5.2.6 Raman 219

5.3 Near Surface Chemistry by ATR-IR 221

5.4 Conclusions..... 223

6 General Conclusions and Future Directions..... 226

Appendix A: SEM 233

APPENDIX B: AFM 239

Appendix C: ToF-SIMS 241

Appendix D: XPS 253

Appendix E: Dissolution Testing 259

Appendix F: Crimping and expansion bench testing..... 263

Conferences and Awards..... 264

References..... 265

GLOSSARY

AFM	Atomic force microscopy
API	Active pharmaceutical ingredient
ATR-IR	Attenuated total reflection infrared
BRSs	Bioresorbable scaffolds
BVA	Bioabsorbable vascular scaffold
CABG	Coronary artery bypass grafting
CAD	Cardiovascular disease
CRM	Confocal Raman imaging
CT	Computed tomography
DAPT	Dual antiplatelet therapy
DES	Drug eluting stent
DSC	Differential scanning calorimetry
E	Young’s modulus
EDA/EDX	Energy dispersive X-ray analysis
ESCA	Electron spectroscopy for chemical analysis
ESEM	Environmental scanning electron microscopy
FDA	Food and drug administration
FTIR	Fourier transform infrared
FWHM	The full width at half maximum
HAZ	Heat affected zone
HPLC	High performance liquid chromatography
IR	Infrared
ISR	In-stent restenosis
LMIG	Liquid metal ion gun
LTA	Local thermal analysis
MI	Myocardial infraction
Mn	Number average molecular weight
MRI	Magnetic resonance imaging
mTOR	Mechanistic target of rapamycin
MTT	3-(4, 5-dimethylthiazolyl-2)-2, 5-diphenyltetrazolium bromide

Mw	Molecular weight
NTA	Nano thermal analysis
NMR	Nuclear magnetic resonance
PBS	Phosphate buffer solution
PCI	Percutaneous cardiovascular intervention
PCL	Poly caprolactone
PDLLA	Poly-D-L-lactide
PHB	Poly hydroxy butyrate
PLGA	Poly (lactic-co-glycolic acid)
PLA	Poly (lactic acid)
PLLA	Poly-L-lactide
PDMS	Polydimethylsiloxane
PTCA	Percutaneous transluminal coronary angioplasty
QNM	Quantitative nano mechanical
ROI	Region of interest
ROP	Ring opening polymerisation
RPM	Revolution per minute
RSF	Relative sensitivity factor
SEM	Scanning electron microscopy
SMCs	Smooth muscle cells
SThM	Scanning thermal Microscopy
Tc	Recrystallisation temperature
Tg	Glass transition
Tm	Melting point
ToF-SIMS	Time of flight-secondary ion mass spectroscopy
UHV	Ultra-high vacuum
XPS	X-ray photoelectron spectroscopy
ΔHc	Recrystallisation enthalpy
ΔHm	Melting enthalpy

1 INTRODUCTION

1.1 Biomedical Materials

Biomaterials, natural or synthetic are used to make structures or implants to replace damaged or diseased biological structures, or support the body to fully repair[1]. Such materials include synthetic polymers, inorganics, ceramics, metals and biopolymers, that are processed to be appropriate to be used in medical devices[2]. The field of biomaterials is of immense importance to mankind, since their existence has played a significant role in improving quality of life and life expectancy. Table 1.1 shows some of the different materials that are used in a broad range of biomedical application. The field of biomaterials is not new, the Romans and Egyptian have used gold and iron for dental application and wood for the replacement as well as linen for sutures. Some other materials have been introduced for biomedical applications after the Second World War, these include silicon, Teflon, stainless steel, nylon and titanium. With the availability of improved diagnostic tools and advancement in the knowledge of biomaterials, biomaterials have found great significant in dentistry, cardiovascular surgery, and orthopaedics. In use, these biomaterials come in to contact with proteins, cells, organs and tissues. Materials that degrade predictably and slowly in the human body are suitable in numerous medical applications, particularly those performing a temporary function such as sutures, controlled release drug delivery devices, bone fixation devices related

to reconstructive surgery, scaffolding for cells that reconstruct diseased organs. Materials designed for blood contacting devices require understanding the many competing reactions that happen when blood interacts with a foreign surface: activation of blood enzymes, protein adsorption activation of the inflammatory pathways, adhesion and aggregation of blood platelets, attraction of white cells and fibrin formation. Blood contacting devices must work in conjunction with a complex feedback system in which enzymes in the blood can improve or inhibit thrombosis formation, depending on which pathways predominate [2].

Any medical device implanted into the human body will start a host reaction, which can be related to a wound healing process that can have an impact on the function of the device. The outcome of this process depends on material properties such as crystallinity, surface chemistry, degradation products and wettability[2,3]. It is very important that a medical device is made from materials that initiate a minimal host response. Some applications require materials to contribute in the biological response[4].

The living body is an aggressive environment for almost all types of devices, foreign materials, artificial organs and prostheses. This environment can generate changes in the mechanical, physical, chemical, and structural properties of biomaterials, i.e., biodegradation[5]. In the very early practice of implantation, a biological response is predicted to take place, blood interactions happen with protein adsorption to the surface of biomaterial and development of a blood-based transient form temporary matrix on and around the biomaterial.

Many of the challenges in manufacturing new biocompatible materials and medical devices are focused on attenuating the host foreign body response, which captures the implant in a fibrotic membrane. Post implantation, a typical process of tissue inflammation becomes persistent, producing a distinct, collagenous sheath around the implant[6]. The fundamental outcome of this body's response is to separate and neutralise the embedded device with predictable chronic inflammation[7]. Moreover, the surface properties of biomaterials play a significant role in modifying the foreign body reaction in the first four

weeks after implantation of a medical device, although the foreign body reaction at the tissue interface is existing for the *in vivo* lifetime of the medical device[6].

Table 1.1 Materials used for biomedical applications. Table adapted from ref.[2].

Materials	Application
Nondegradable Synthetics— Commodity Polymers	
Polyamides	Sutures
Polycarbonates	Housing materials
Polyesters	Vascular grafts
Polyformaldehyde	Heart valve stents
Polyolefins	Sutures, mesh for hernia repair
Polyvinyl chloride	Tubing, blood bags
Nondegradable Synthetics— Value-Added Polymers	
Fluorocarbons	Vascular grafts
Hydrogels	Contact lenses, catheter coatings
Polyolefin elastomers	Tubing, artificial heart bladder
Polyurethanes	Catheters, artificial heart bladders
Silicones	Soft tissue reconstruction, tubing
Ultrahigh molecular weight polyethylene	Acetabular cup
Biodegradables	
Albumin, cross-linked	Vascular graft coatings, cell encapsulation
Collagen/gelatin, cross-linked	Soft tissue reconstruction, vascular graft coatings
Polyamino acids	Controlled release, cell adhesion peptides
Polyanhydrides	Controlled release
Polycaprolactones	Controlled release, bone plates
Polylactic/glycolic acid copolymers	Sutures, bone plates
Polyhydroxybutyrates	Controlled release, bone plates
Polyorthoesters	Controlled release, bone plates
Biologically Derived Materials	
Bovine carotid artery	Vascular grafts
Bovine ligaments	Ligaments
Bovine pericardium	Pericardial substitute, heart valves
Human umbilical vein	Vascular grafts
Porcine heart valve	Heart valves
Bioderived Macromolecules	
Chitosans	Experimental, wound dressing, controlled release
Collagen	Soft tissue injectables, coatings, wound dressing
Elastin	Experimental, coatings
Gelatin, cross-linked	Artificial heart bladder coating
Hyaluronic acid	Coatings, wound dressing, surgical non-adhesion

Continued

Table 1.1 Continued

Tissue Adhesives	
Cyanoacrylates	Wound closure, microsurgery
Fibrin glue	Vascular graft coating
Molluscan glue	Enhancement of cell adhesion
Metal and Metallic Alloys	
	Orthopedic and dental implants, vascular stents
Cobalt chrome molybdenum alloys	Heart valve stents
Nitinol alloys (shape memory alloys)	Orthopedic wire
Stainless steels	Orthopedic wire
Titanium and titanium alloys	Artificial heart housing, heart valve stents
Ceramics, Inorganics, and Glasses	
Aluminum, calcium, and phosphorous oxides	Degradable bone filler, enhanced bone growth
Bioglass®	Bioactive phosphorous calcium glass, orthopedic coating
Glass ceramics	Encapsulation of implantable medical electronics
High density alumina	Acetabular cup, ball of hip prosthesis
Hydroxyapatites	Bioactive ceramic, orthopedic coating, bone fillers
Carbons	
Glassy carbons	Fibers for orthopedic composites
Pyrolytic (low temperature isotropic) carbon	Heart valves, dental implants
Ultralow temperature isotropic carbon	Coatings on heat sensitive polymers
Passive Coatings	
Albumin	Thromboresistance
Alkyl chains	Adsorbs albumin for thromboresistance
Fluorocarbons	Reduced drag for catheters, thromboresistance
Hydrogels	Reduced drag for catheters, thromboresistance
Silica-free silicones	Thromboresistance, improved wound healing for soft tissue reconstruction
Bioactive Coatings	
Anticoagulants, e.g., heparin and hirudin	Thromboresistance
Antimicrobials	Infection resistance
Bioactive ceramics and glasses	Bone adhesion and formation; soft tissue adhesion
Cell adhesion peptides	Enhanced cell adhesion, epithelium, endothelium
Cell adhesion proteins	Enhanced cell adhesion, epithelium, endothelium
Negative Surface Charge	Thromboresistance
Thrombolytics	Thromboresistance

The vast majority of polymers used today as biomaterials or in devices, prostheses, or artificial organs are considered bio-stable and are designed to resist the impact of the *in vivo* environment for the lifetime of the device or patient, whilst maintaining the required properties that satisfy the anticipated functions. As an additional approach, bioresorbable or biodegradable polymers are intended to degrade during their operational lifetime and be eliminated from the body by normal metabolic and physiological processes without adversely affecting in the longer-term, tissues, body fluids and organs[5]. For biodegradable materials to be useful, they should have acceptable shelf life with the appropriate mechanical properties and the breakdown products must be nontoxic; additionally, the body must have a mechanism for removing the by-products. The term bio-stability relates to the relative stability in the physiological environment as a function of time. Changes in the properties of polymers as a function of time can be caused by chemical degradation, leading to loss of mass and mechanical properties[5]. Another factor that must be taken into account for materials to help advance the quality of life and endurance of people, is biocompatibility. Biocompatibility (safety) is the capability of a material to prompt a suitable host response, to allow the body to repair without any toxic changes to the material or body[8]. Chronic inflammations, scarring and lesions are some of the adverse reactions that may take place in the site if the implant is not biocompatible. The lifetime of a medical device should be considered before selecting materials for the making of the device.

Table 1.2 shows a list of polymer properties and characteristics fabrication methods and sterilisation techniques that are needed to be considered as they can potentially control the lifetime and the degree of physiological interaction and the function of a medical device.

Table 1.2 A list of variables that can affect polymer biodegradation and stability. Table adapted from[5].

Polymer Characteristics and Properties
Chemical structure and chain regularity
Molecular weight and molecular weight distribution
Cross-linking
Residual monomer and/or catalyst residue
Additives
Antioxidants
Diffusion and permeability properties
Morphology and molecular orientation
Crystallinity
Mechanical properties
Surface energetics and wettability
Processing or Fabrication Methods
Injection molding
Melt extrusion
Compression molding
Blow molding
Vacuum forming
Solvent casting and welding
RF welding
Cleaning and Sterilization Techniques
Liquids
Glow discharge
Steam sterilization
Dry heat sterilization
Ethylene oxide
Radiation: UV or ionizing

The ultimate requirement of a biomaterial is that the material and the neighbouring physiological environment should co-exist without having any unwanted effect on one another. Since the surface is the interface where the biomaterials meet and interact with the biological environment (soft tissues or blood), the surface properties are the main factors that eventually regulate the recognition or elimination of a biomaterial in the body[9]. The surface chemistry of biomaterials is significantly fundamental within biomedical science, where the interfacial chemical structure will have an impact on the host bio-interactions[7]. Thus, the interfacial bio-interactions determines whether a biomaterial device is biocompatible[10].

1.2 Coronary Artery Disease, Clinical Management and Stenting

Coronary artery disease (CAD), also known as ischemic heart disease, is the foremost cause of death in the in the UK and worldwide[11] and has had a tremendous health impact across the globe. Resulting in more than seven million deaths worldwide among individuals aged less than 75 years each year[12] CAD can result from atherosclerosis or a build-up of plaque in the blood vessels, which inhibits blood supply to the myocardium, leading to narrowing of the arteries as shown in Figure 1.1 resulting in stenosis[13]. CAD costs the UK health care system around £8.7 billion and the UK economy £19 billion a year in total, as of 2009[14]. Atherosclerosis is a slow progressive disease characterized by chronic inflammation in the artery walls[14]. It is important to understand the pathophysiology of atherosclerosis in order to improve treatment strategies.

Clinical management can be categorised into revascularisation and medical therapy. The latter encompasses cardio-protective and anti-angina agents, accomplishing prognostic benefits through reduction in cardiac work load and peripheral vasodilation[15,16]. Second line of treatment involves prevention with the use of antiplatelet agents to prevent future cardiovascular events. The aim of revascularisation is to restore enough blood supply to ischemic myocardium supplied by acutely or chronically narrowed coronary vessels. Coronary artery by-pass grafting (CABG) was used initially by using autologous conduits anastomosed to proximal and distal points across the diseased vessel[16,17]. Technologies such as percutaneous transluminal coronary angioplasty (PTCA) also known as balloon angioplasty, atherectomy and stents may play a substantial role in percutaneous coronary intervention (PCI)[18]. Figure 1.2 shows coronary angioplasty using expandable balloon.

PTCA was introduced in 1977 as a new approach for the treatment of CAD. PTCA is a non-surgical procedure that involves making an incision in the femoral artery with the use of a catheter with a balloon at the tip, which is inflated at high pressure inside the blocked artery[18]. During the first decade of the PTCA procedure the outcome improved greatly, although PTCA is a minimally invasive procedure, however elastic recoil of the arterial wall[19] remains an issue. Recoil triggers the channel to become smaller soon after being enlarged by balloon expansion[20]. High rates of restenosis of around 30% have been

reported following the treatment with coronary balloon angioplasty. This procedure showed loss of luminal diameter due to recoil of the vessel and negative remodelling[21].

During the second decade of development, improved procedures such as atherectomy and stents were introduced[18,22]. Atherectomy is a non-balloon coronary device that was approved by the Food and Drug Administration (FDA) in 1989. Atherectomy is the removal of the atherosclerotic plaque from target lesions. It was reported that atherectomy led to a higher rate of complications and increased cost compared to angioplasty[23].

Developing new cardiovascular stents to widen the blocked artery to restore normal blood flow, hence became an important therapeutic approach to overcome the limitation of PTCA. In order to reduce the incidence of restenosis PTCA is often combined with implantation of a coronary stent[24]. These metallic stents of the time were capable of optimising vessel patency following balloon expansion by eliminating the effect of vessel recoil[24]. The stent market has developed significantly since this time.

The ideal properties of stents should include:

- Flexibility to ease the implantation of stent into the artery.
- Ability to release and encapsulate drugs to stop the reoccurrence of blocked artery.
- Biodegradability is crucial to avoid prolonged presence within the body.
- High radial, ductility and tensile strength to stop stent recoiling after implantation.
- Low crossing profile.
- Radio-opacity.
- Low shortening upon expansion.

Figure 1.3 (a) shows stent deployment in a coronary vessel and a cross section of an artery showing both angioplasty and stenting procedure. Figure 1.3 (b) shows frayed appearance for angioplasty compared to opening resulted by stent where it showed smoother and bigger opening.

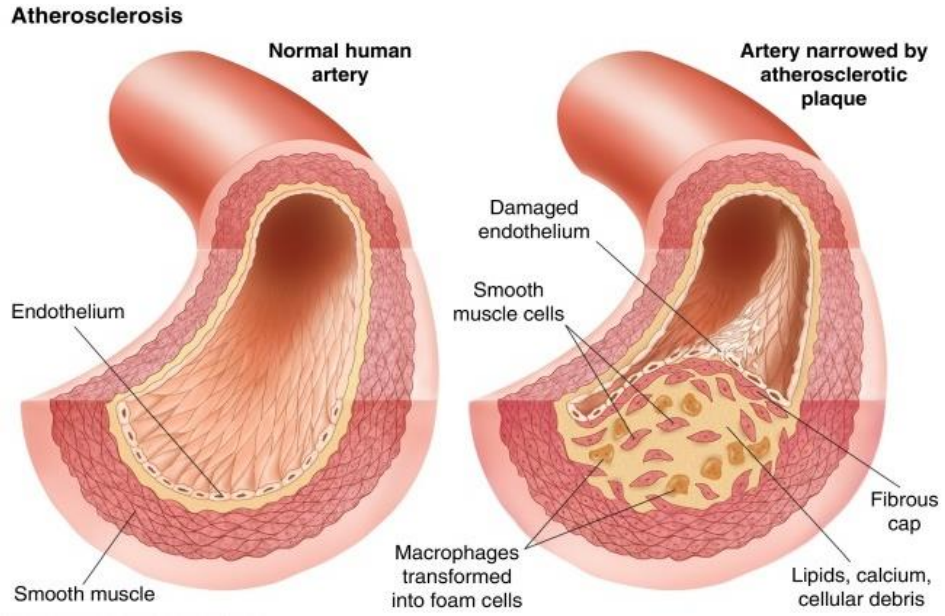


Figure 1.1 Schematic representation of atherosclerosis process showing re-blockage of a stented artery at the right and healthy artery comprising of intima, media and adventitia. Adapted from[25,26].

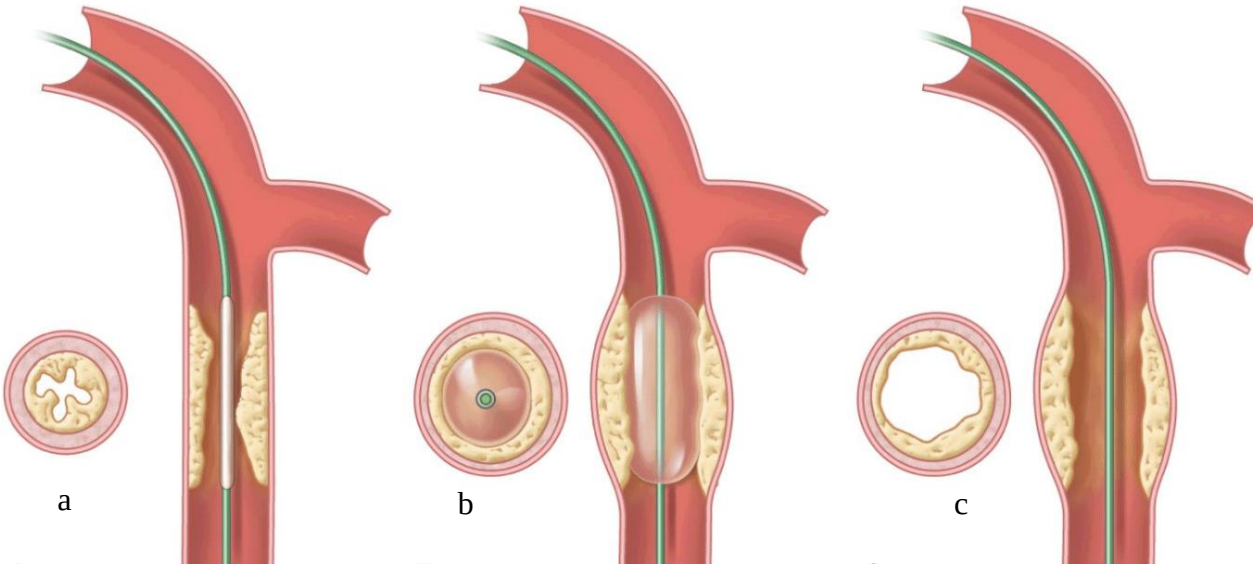


Figure 1.2 Schematic diagram showing the process of balloon angioplasty. A. represents deflated balloon positioned across stenosis, B. inflation of the balloon catheter within the stenosis section and C. follow balloon deflation. Figure adapted from[27].

a.

b.

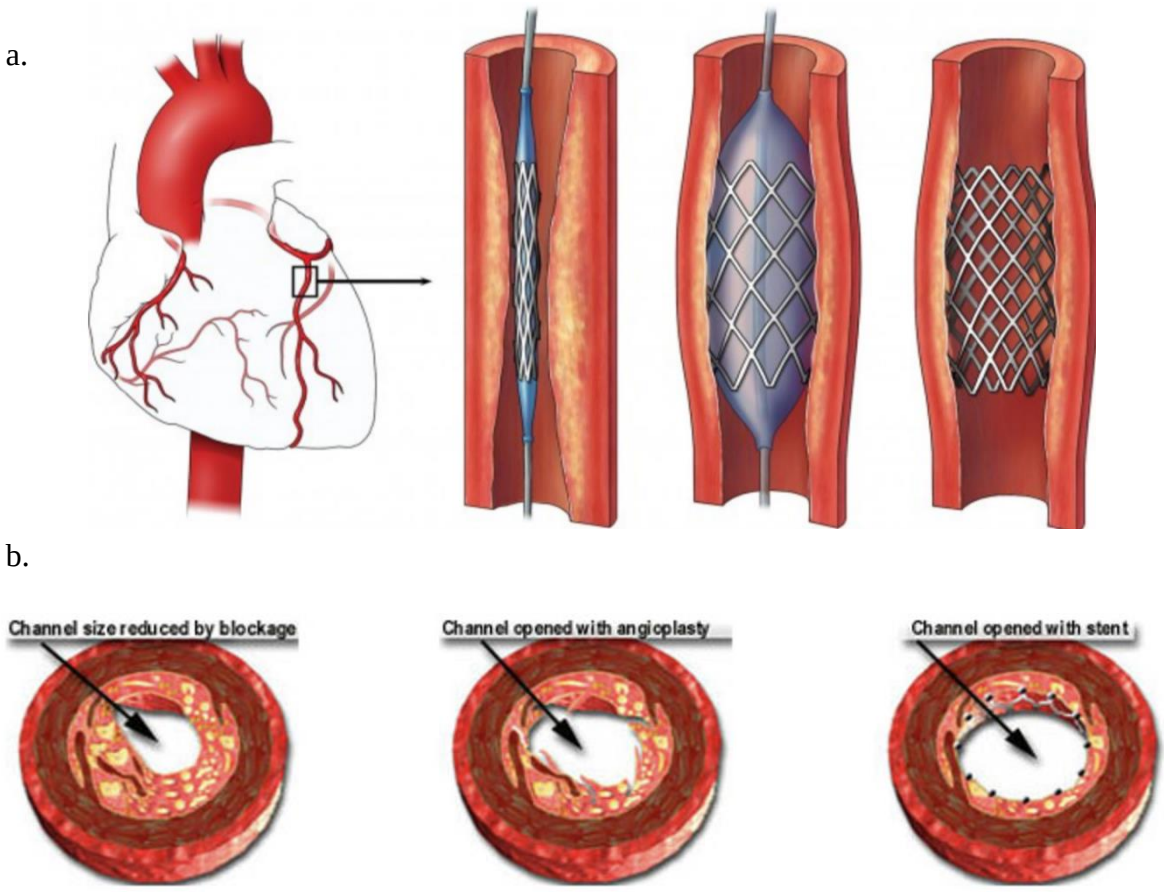


Figure 1.3 Schematic diagram of a. stent deployment, b. cross section of a coronary artery at the level of stenosis.

Coronary artery stents have progressed over the past three decades to become one of the most implanted prosthetic devices worldwide[28]. Stenting is a mechanical solution to a complex biomechanical matter. The choice of material for stents was initially mostly influenced by engineering concerns[29]. A scaffold (stent) needs to be deformable enabling it to be crimped on to a balloon and nevertheless maintain structural integrity upon expansion and deployment. Once a stent is implanted, adequate radial force is vital to counter act vessel recoil. Stent radio-opacity facilitates operator visualisation during stent deployment[30].

1.3 Generations of Coronary Stents

1.3.1 Bare Metallic Stents

Coronary artery stents are small mechanical devices in a cylindrical mesh tube-like scaffold that are implanted in arteries to hold open or expand a section of a blood vessel and restore physiologically healthy blood flow to the ischemic heart muscle[31]. Stenting involves the placement of a stent at the site of acute artery closure where stent is mounted on the balloon, expanded and positioned by inflating the folded angioplasty balloon. Once a stent is expanded to the required diameter, it is pushes against the artery wall and the stent remains in place once the balloon is deflated. After removal of the balloon, the stent tends to shrink in length and diameter[32]. This type of treatment has proved effective in decreasing myocardial ischemia and has become the most usual therapeutic intervention for coronary artery disease[33].

The introduction of metallic stents to flowing blood has showed the benefit in reduction of re-occlusion of the ischemia-related artery and lead to reduction in rates of restenosis as compared to angioplasty[34] due to mechanical scaffolding which can essentially reduce elastic recoil following implantation. However, there are issues associated with metal stents, one of these issues, the net electrical charge is a critical factor regulating the biological response once it comes in contact with blood. It is the adhesion of the platelet to surface that causes it to spread and activate that leads to thrombogenic reactions[35,36]. Figure 1.4 shows the progression of events once a metal stent is in contact with blood. Very rapidly after a metallic surface is exposed to circulating blood, a series of actions changes the surface in preparation for tissue establishment. At first, changes arise rapidly with a cascade of successively larger proteins adsorbing to the metal surface, within a few seconds. Later, the progression of events slows down as a biofilm (biofilm is usually used to refer to a film of bacterial (infection) in a mucoid matrix) forms and eventually tissue growth and engulfment of the stent occur. Implantation of metal stents has hence resulted in thrombus formation, acute thrombotic occultation of the stent and smooth muscle proliferation[33]. In addition as a result of the difference in mechanical behaviour

between the blood vessel and the metal stent, excessive intimal proliferation and thrombosis occur[37].

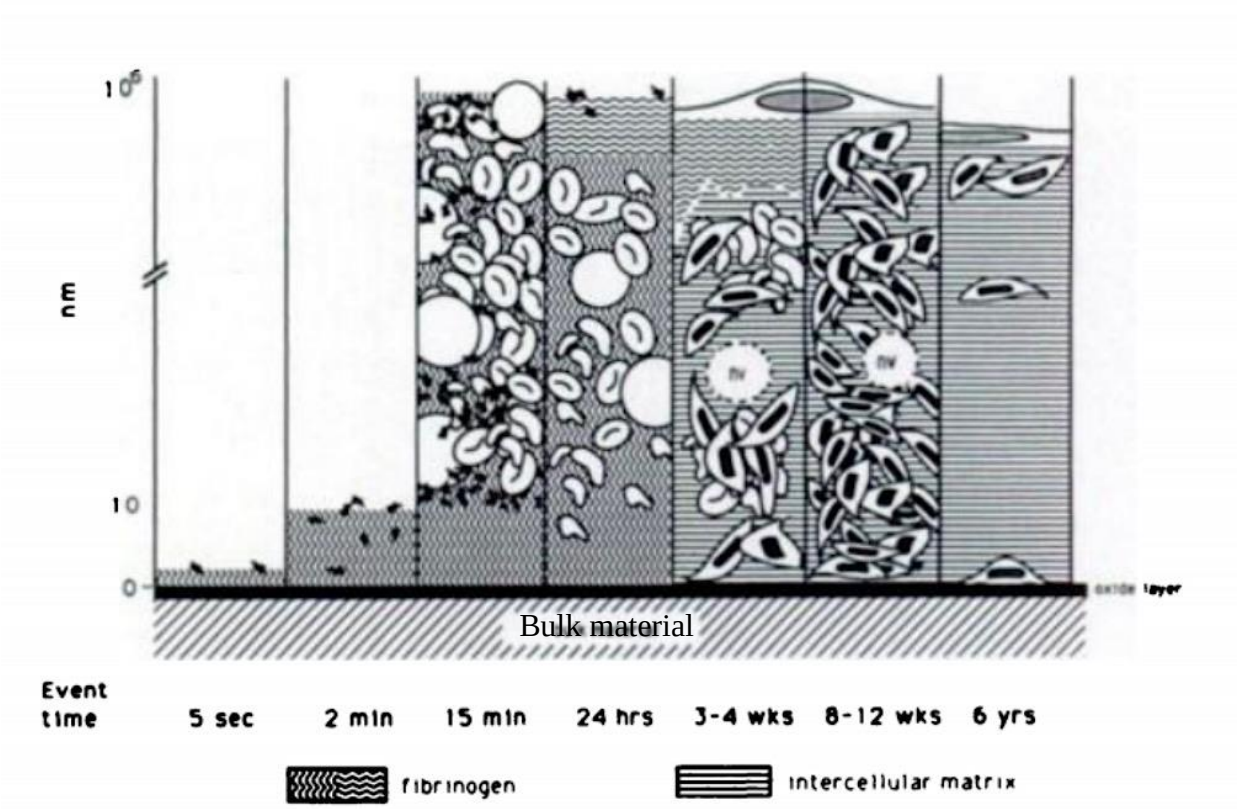


Figure 1.4 Schematic showing series of events post positioning of metal stent into a blood vessel. Thickness of tissue put on surface of prosthesis is not on a linear scale. nm = nanometers; nv = neo-vessel. Key point: collagen and ground substance (Parallel straight lines). Randomly oriented fibrinogen strands (Vertical lines). Fibrinogen strands oriented in the direction of flow (Horizontal lines). Figure adapted from[37].

Metal stents occasionally becomes re-narrowed causing restenosis, that is the reduction of the luminal size and is the most critical long-term limitation of stent implantation occurring in 15-60 % of patients[38]. Bare metal stents were presented with a high incidence of thrombotic formation in the early 1990 and long term endothelial dysfunction as well as mismatches in mechanical behaviour between non-stented and stented areas[39]. Bare metal stents require the need for long-term dual antiplatelet therapy and lifelong impact of a metal scaffold in the artery intrusive with adequate computed

tomography (CT) or magnetic resonance imaging (MRI), vascular remodelling, and coronary vasomotion. Moreover, extensive stenting makes future coronary artery bypass grafting (CABG) procedures difficult, if not impossible[40]. Bare metal stents made from stainless steel have thick struts which can cause poor flexibility and a high in-stent restenosis (ISR) rate, therefore stents with thinner struts were developed where the stainless steel was replaced by chromium and cobalt alloys to maintain the radio-opacity, strength and deliverability[34]. However, the problem associated with ISR is still quite high at around 15% after 6 months of follow-up[41,42]. Between May and September in 1999, a group studied PCI databases and concluded more than a third of patients presented with myocardial infraction (MI) and required hospitalisation[43]. Therefore, efforts have been made to advance stents with a biocompatible coating containing an anti-proliferation drug[44]. Most drug eluting stents consists of a metallic stent platform with a coating of an active pharmaceutical agent usually dispersed in a polymer that is intended to reduce intimal hyperplasia[45]. Such stents are commercially available, and some stents are still undergoing clinical trials. An example is the XIENCE stent, a stent made with a polyester coating that controls the release of the drug, and everolimus to prevent reclogging[33].

1.3.2 First and Second-Generation Drug Eluting Stents

The advent of drug eluting stents (DES) has reduced rates of stenosis. The first generation of drug eluting stents was based on stainless steel scaffold coated with a drug-eluting polymer layer. The most commonly used DES in 2003 were Taxus® Paclitaxel DES (Boston Scientific, Natick, MA, USA) and the Cypher® Sirolimus DES (Cordis Corporation, Miami Lakes, USA), (detailed description shown in Table 1.3 of other available stents). Both of these stents have a strut thickness of about 135 μm and a coating layer consisting of sirolimus or paclitaxel that can inhibit endothelial healing and smooth muscle migration. First generation DES have been reported to have a better efficacy with a lower rate of ISR than bare metal stents with a reduction of 60-70% of target vessel revascularisation being reported[46].

Table 1.3 Food and Drug Administration (FDA) approved commercial metallic and drug eluting stents and their manufactures.

Manufacturer	Trademarks	Stent					
		Bare metallic stents		Drug eluting stents			
		Device name	Platform	Device name	Platform	Drug	Coating
Abbott vascular	Vision, Xience VTM, Xience Prime™, Multilink Vison ST stents	MULTILINK 8LL Coronary stent system	MULTI LINK 3-3-3, nonlinear link stent design (L-605 cobalt chromium)	XIENCE Everolimus Eluting coronary stent system	Multi-link Vison® coronary stent	Eveolimus	PLGA (Biodegradable)
Cordis Corpoation/Johnson & Johnson	Cypher™, Cypher Select™ stents	Palmaz-Schatz stent	316L stainless steel	Cypher ® sirolimus eluting stent	Closed cell FLEXSEGMENTTM Technology	Sirolimus	P(EVA)-PBMA top coat
Boston Scientific	OMEGA, PROMUS, TAXUS,TAXUS Express and TAXUS Liberte stents	OMEGATM Platinum Chromium coronary stent system	Platinum chromium stent	PROMUSTM eveolimus eluting coronary stent system	Multi-Link Vision™ stent platform	Everolimus	Promus-PVDF-HFP TAXUS - SIBS
Medtronic Vascular	Endeavor™, Driver ™ stents	Diver bare metal stent	Cobalt alloy stent	Endeavor ® Drug eluting coronary stent	Cobalt alloy stent	Zotarolimus	PC polymer

Only XIENCE DES (Table 1.3) has a biodegradable coating, the rest are non-biodegradable. The polymer used in the coating of DES controls the release of the drug for approximately 30-60 days. The drug helps to suppress biological response to the affected area caused during stent implantation, thus reducing restenosis incidence. After 60 days of drug release, the rate of released drug reduces towards zero, due to complete elution of the drug in this case Cypher® stent or could be due to drug entrapment within the coating in this case Taxus®[47,48]. There are some concerns associated with first generation stents besides issues with biocompatibility. Defects and irregularities in the polymer coating after stent expansion have been reported in the Cypher SELECT (uneven polymer coating and round small defects), XIENCE V (rare polymer flaking), and TAXUS Liberte (bridging defects) stents implanted in healthy swine for seven days[49].

Such defect could be responsible for coronary micro-embolism, late inflammatory and thrombosis post stent placement[50].

1.3.3 Next Generation Stents: Fully Bioresorbable Scaffolds (BRSs)

In the light of the drawbacks associated with permanent metallic stents, the general consensus among medical practitioners over recent years has been the desire to move away from using permanent stents and towards using non-permanent biodegradable scaffolds[51]. Biodegradable (bioresorbable) biomedical materials are hence of high interest. Their capability to degrade progressively in the body makes them suitable for applications that do not involve surgical removal. For biodegradable products to be beneficial, the breakdown products must be harmless; also, the body must have a mechanism for removing the by-products[2]. Fully bioresorbable stents have the potential advantage of no longer being existent as a foreign material in arteries once they have scaffolded the vessel for an appropriate period of time[52] and follow a 'do and disappear' strategy. Table 1.4 and Figure 1.5 demonstrates various designs of fully bioresorbable scaffolds.

Bioresorbable scaffolds provide the advantage of not needing an anti-platelet therapy, as required for metallic stents. Di Mario *et al.,* have produced a bioresorbable stent based on magnesium alloy[53] and other versions based on iron and zinc , demonstrating that bioresorbable stents are not limited to polymeric materials. The stent developed by Di Mario's group is capable of providing anti-preoperative and anti-thrombotic properties with no side effects and provides considerable reduction in acute stent thrombosis[53]. In terms of polymer-based systems, poly L-lactide (PLLA) based stents are being investigated extensively as a drug delivery technology[54-57]. The drug used in such PLLA stent coatings must show anti-inflammation and anti-proliferation propertied[58].

Table 1.4 Summary of the structure and the design of various types of clinically tested BRS[59] stents .

Scaffold	Strut material	Coating material	Eluted drug	Strut thickness (μm)	Resorption (month)	Current status
Igaki-Tamai	PLLA	None	None	170	24–36	CE mark for peripheral use
AMS-1	Mg	None	None	165	<4	Discontinued
DREAMS-1	Mg	PLGA	Paclitaxel	125	9	Clinical trials
DREAMS-2	Mg	PLLA	Sirolimus	150	9	Clinical trials
Absorb BVS 1.0	PLLA	PDLLA	Everolimus	156	18–24	Discontinued
Absorb BVS 1.1	PLLA	PDLLA	Everolimus	156	24–48	CE mark
Absorb BVS-New generation	PLLA	PDLLA	Everolimus	<100	NA	NA
DeSolve	PLLA	None	Myolimus	150	12–24	CE mark
DeSolve 100	PLLA	PLLA	Novolimus	100	24	CE mark
IDEAL biostent	Polymer salicylate	Salicylate	Sirolimus	175	>12	Clinical trials
REVA	PTD-PC	None	None	200	24	Discontinued
ReZolve	PTD-PC	None	Sirolimus	115–230	4–6	Clinical trials
ReZolve2	PTD-PC	None	Sirolimus	100	48	Clinical trials
Fantom	PTD-PC	-	Sirolimus	125	36	Clinical trials
Fortitude	semicrystalline polylactide	-	None	150–200	3–6	Clinical trials
Mirage BRMS	PLLA	-	Sirolimus	125–150	14	Clinical trials
MeRes	PLLA	PDLLA	Sirolimus	100	24	Clinical trials
Xinsorb	PLLA	PDLLA	Sirolimus	160	24–36	Clinical trial
ART 18AZ	PDLLA	None	None	170	3–6	Clinical trials



Figure 1.5 Bioresorbable scaffolds with different design characteristics in clinical or preclinical use.

To date the most investigated BRS stent is the Abbot Vascular biodegradable stent[60]. Bioabsorbable vascular scaffold (BVS) ABSORB (Abbott Vascular) is a fully re-sorbable stent, consisting of a PLLA platform coated with PDLLA which helps control release of the drug, everolimus. This stent can be combined with anti-proliferative drug; thereby avoiding potential problems associated with metallic stents and long-term dual antiplatelet therapy (DAPT). The strut design and modification of polymer manufacturing process is an essential strategy, which resulted in a lower hydrolysis rate of the polymer to preserve its mechanical integrity for a longer period. Therefore, Arterius Ltd has come up with a novel design that utilise a thinner strut than one used by Abbott Vascular. Recent study was recently published in the European Heart Journal[61], where they provided *in vivo* comparison between endothelial shear stress computations for Absorb 3.0 x 18 mm (Abbott vascular , US) and ArterioSorb™ 3.0 x 14 mm (Arterius, UK). The data obtained had showed that thinner struts like the ones used for the manufacturing of

ArterioSorb™ has resulted in less disruption of the arterial blood flow and higher endothelial shear stress values were achieved with Absorb stent during coronary flow periods.

Two of the largest players in the stent developments, Abbott's bioresorbable and Boston scientific stents have abandoned their bioresorbable stents due to poor performance.in clinical studies where data showed due to fundamental issues with the design as the design of their stents.

Arterius Ltd initiated a preclinical study where the fully bioresorbable ArterioSorb™ scaffold was implanted into porcine model with encouraging results[61]. The study sought to evaluate the scaffold for acute performance. Figure 1.6 shows optical coherence tomography data showing good apposition of the struts to the vessel wall. The scaffold in Figure 1.6 was observed to be clearly visible by angiography due to the radiopaque markers. During the delivery of the device it was reported by an experienced cardiovascular preclinical specialist that the device was easy to position and to deploy and showed no irregularity following implantation, with comprehensive perfusion of the blood flow. Upon implantation, the ArterioSorb™ scaffold became fully encapsulated within the vessel wall and was fully bioresorbed within a 12 to 24-month time frame. Furthermore, this would lessen "stent jailing" where the stent obstructs an artery which branches off the main artery and could be predominantly useful in paediatric cases, where vessel growth dictates that metal stents must be surgically removed[61]. In silico and *in vitro* studies were carried out by the Patrick Serruys group, where they also compared ArterioSorb™ and Absorb BVS (Abbott Vascular, USA) upon implantation in pigs. 3D reconstruction of the right coronary of two healthy pigs post implantation was performed using optical tomography coherence, (Figure 1.6b).

a.

b.

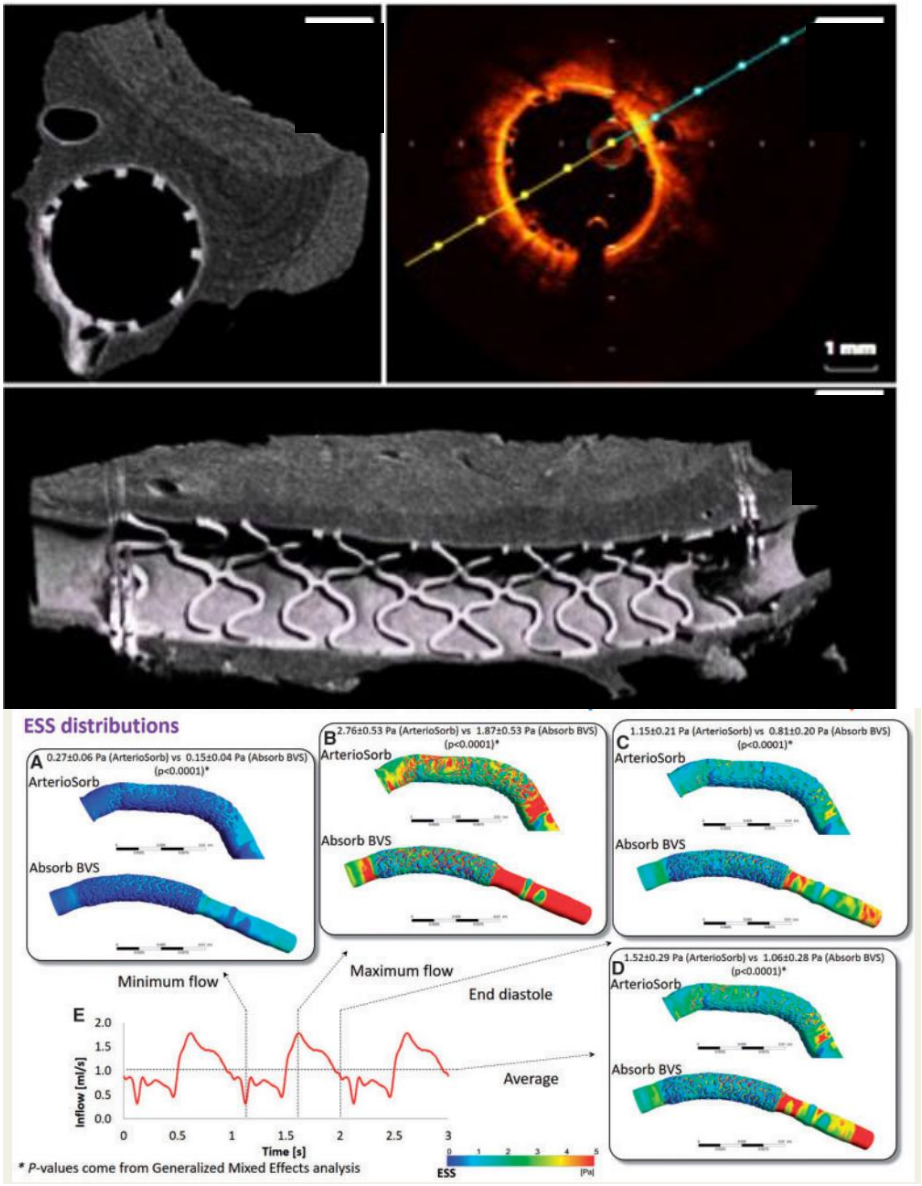


Figure 1.6 a. Optical coherence tomography of ArterioSorb™ scaffold, b Non-Newtonian pulsatile simulation of ArterioSorb™ (95 μm) and Absorb (157 μm) comparison of ArterioSorb 3.0x14 mm with strut thickness of 95 μm (Arterius, UK) and Absorb BVS 3.0 x18 mm with strut thickness of 157 μm (Abbott, USA) upon implantation in pigs. Figures adapted from[61].

A pulsatile non-Newtonian study shows endothelial shear stress is higher at the top of the strut (as indicated in red in Figure 1.6b) whereas the inner strut areas show lower endothelial shear stress values (dark blue). Pulsatile simulation shows low endothelial

shear stress areas at maximal flow which therefore could lead to thrombus and fibrin formation. Figure 1.6b shows 21.6% of luminal surface of ArterioSorb™ was exposed to low endothelial shear stress, while 47.2% of the Absorb luminal surface was subjected to low endothelial shear stress.

1.4 Drugs used in Bioresorbable Stents

1.4.1 Anti-proliferative Actives

The physicochemical properties of the chosen drug are fundamental in determining its release kinetics[10]. The drug used in such PLLA stent coatings must show anti-inflammation and anti-proliferation properties [58]. Table 1.5 shows the different drugs used for stent therapy[10]. The most common drugs eluted from drug eluting stents are paclitaxel and sirolimus. These arrest the proliferation of smooth muscle cells (SMCs) in the arterial wall and therefore inhibit vascular restenosis. In this study, we have used sirolimus. Sirolimus is a naturally occurring macrolide antibiotic derived from streptomyces hygroscopicus. Sirolimus is a highly hydrophobic drug, following delivery it diffuses slowly therefore a high dose is needed to be maintained in the blood vessel. Sirolimus mode of action is distinct from other immunosuppressive agents. It inhibits DNA synthesis as illustrated in Figure 1.7. Sirolimus binds to the FK binding protein-12 (FKBP-12), which regulates the action of the mechanistic target of rapamycin (mTOR). mTOR hinders interleukin-2-mediated signal transduction, causing the cell cycle to stop in G1-S phase and eventually prevents proliferation and blocks the response of B and T cell activation by cytokines[62]. Figure 1.8 shows the chemical structure and molecular weight of sirolimus.

Ring cleavage is a classic reaction that sirolimus follows under a range of experimental conditions. Seco-Rapamycin (sodium salt) is a nonenzyme-dependent degradation product of rapamycin, developing from ester hydration (C25 ester bond had been hydrolysed) followed by dehydration[63]. Degradation products of sirolimus like the ester hydrolysis and the ring-opened rapamycin isomer are described in Figure 1.9[64], including seco rapamycin, in the cytoplasm or in homogenates of Caco-2 cells. Seco rapamycin is

secreted from cells by P-glycoprotein and metabolized to a common dihydro species[65]. Seco-rapamycin poorly activates mTOR, it mimics rapamycin in its ability to inhibit the proteasome[66].

Table 1.5 Candidate drugs used in DES.

Anti-restenotic drug	Mode of action	Binding target	Final outcome
Curcumin	Intercalates between RNA and DNA prohibiting replication	Microtubules	Inhibits platelet aggregation Smooth muscle cell replication arrested in G0-G1 phase
Pimecrolimus		Macrophilin-12	Binds to macrophilin-12 Prevents inhibition of calcineurin
Dexamethasone	Prevention of IL-1 and IL-2 transcription Binds with cytoplasmic receptor to form steroid-receptor complex Complex associates with DNA and directs production of apoptotic proteins	Specific steroid-binding protein receptor	Reduction in inflammatory response
Sirolimus	Prevents activation of mechanistic target of rapamycin (MToR) Binds to cytosolic FKBP-12	FK-5-6 binding protein 12	SMOOTH MUSCLE CELL CYCLE ARREST IN g1-s PHASE
BIOLIMUS a9 ZOTAROLIMUS Everolimus Novolimus			Smooth muscle cell and T-lymphocyte cell cycle arrest in G1-S phase
Tacrolimus	Prevents activation of calcineurin Inhibition of IL2 transcription Prevents activation of calcineurin Binds to cytosolic FKBP12 Inhibition of T-lymphocyte signal transduction		T-lymphocytes cell cycle arrest in G1-S phase

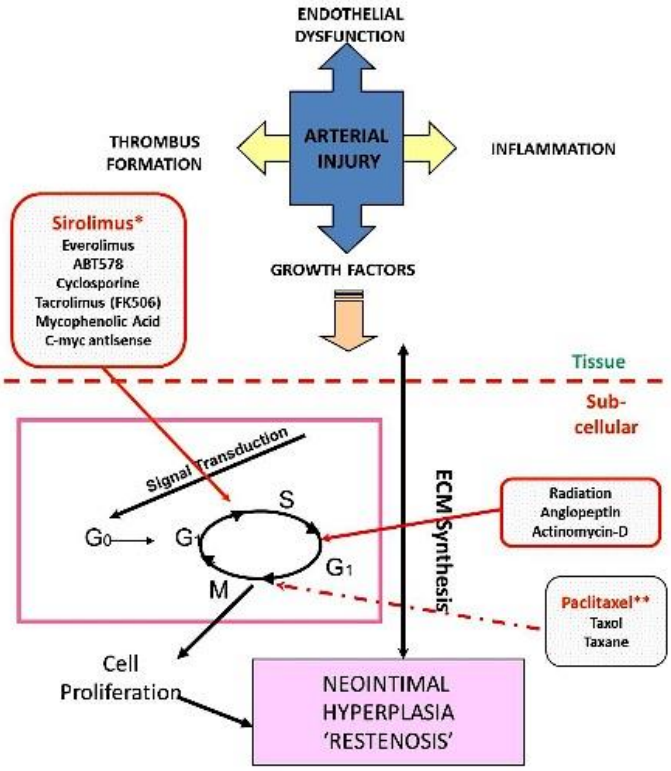


Figure 1.7 Active pharmaceutical drugs at subcellular level. Showing sirolimus and other immunosuppressive drugs targeting the G1/s phase of the cycle[19].

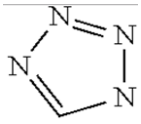
The degradation of sirolimus and its ring-opened isomers under basic conditions was studied previously by Yuri *et al*[67]. Sirolimus degradation under highly basic conditions, is via fragmentation and water addition reactions. After less than one hour of degradation sirolimus was reported to be completely decomposed in 3 mM NaOH (pH 12.2).

$C_{51}H_{79}NO_{13}$ MW= 914.17g/mol

Some analogues modified here:

Everolimus R = O-CH_2-CH_2-OH

Biolimus R= O-CH_2-CH_2-OR

Zotarolimus R= 

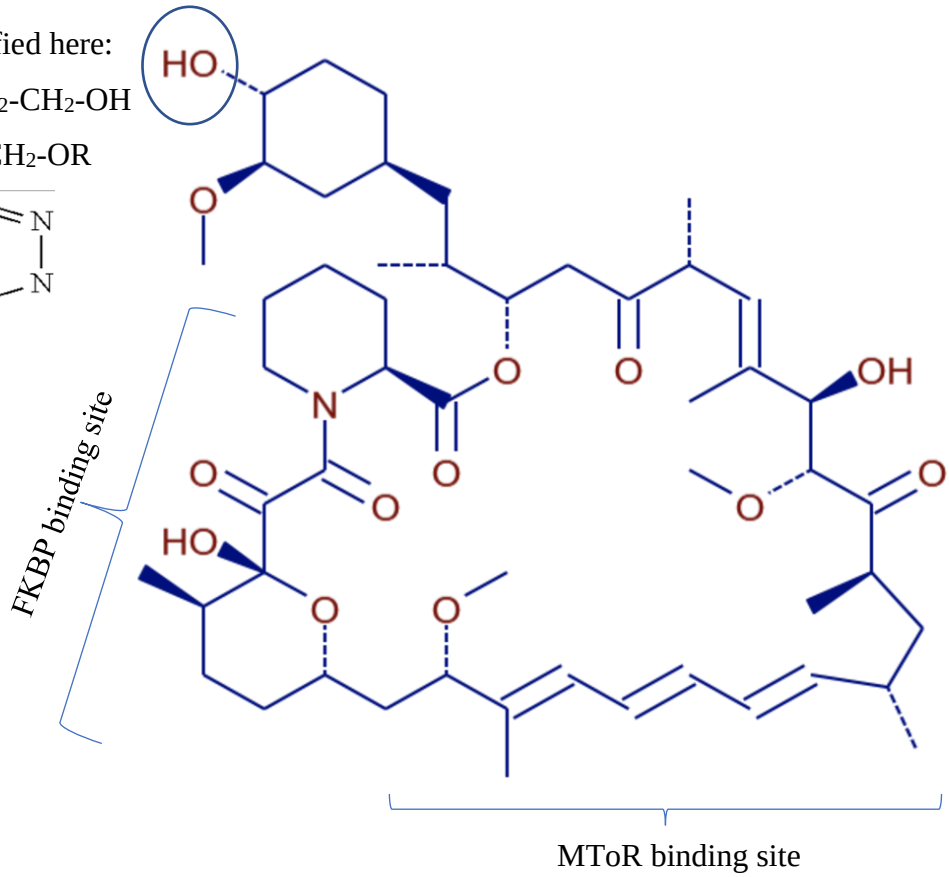


Figure 1.8 Molecular chemical structure of Sirolimus, chemical formula and molecular weight.

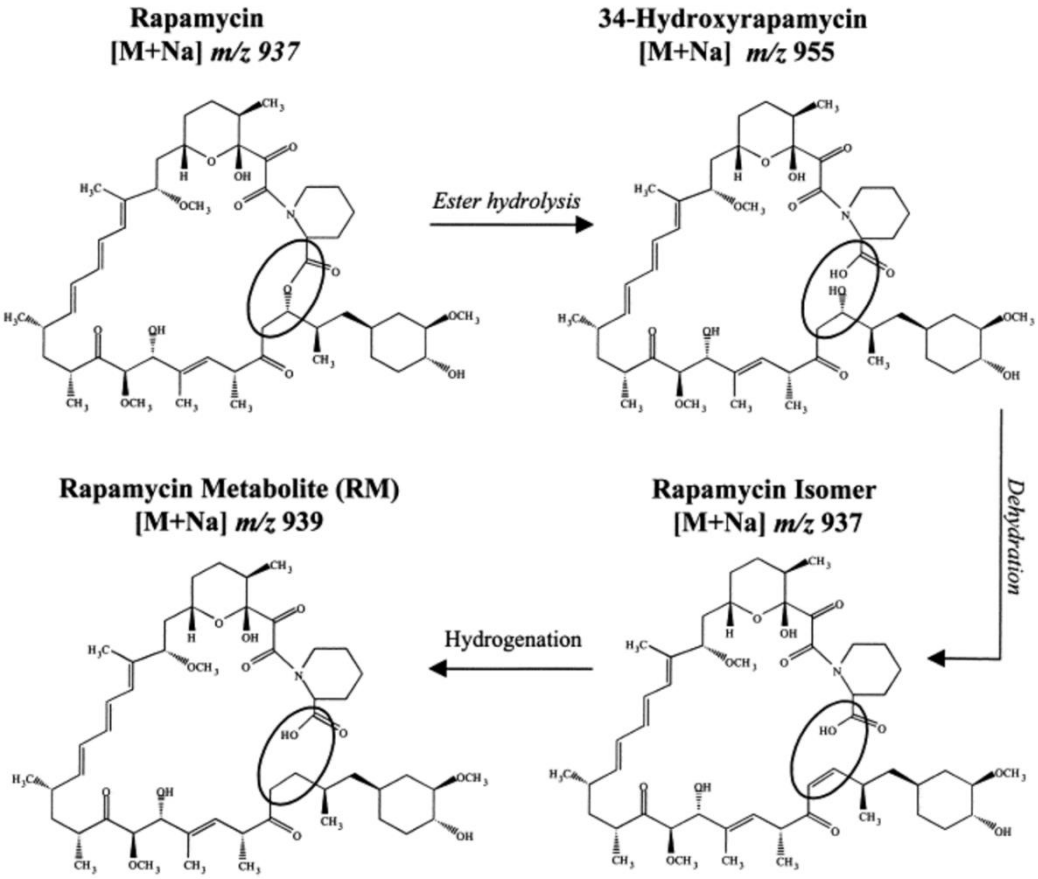


Figure 1.9 The degradation product of sirolimus[68] .

1.5 Poly L Lactide (PLLA)/Poly D, L lactide (PDLLA)

Polymers, which are capable of degrading, releasing drugs, or mimicking biological functionalities, are of great interest for the development of vascular implants[69].The drug delivery system presented in this thesis utilises poly-l-lactic acid (PLLA) and poly-*D*,*L*-lactide (PDLLA), which are gradually eroded by cleavage of ester bonds and eventually will degrade into lactic acid[70]. PLA is a biodegradable polyester polymer most commonly used in medical devices due to its ability to be resorbed *in vivo* in a timeframe that can vary from months to a few years. Its applications include tissue engineering scaffolds, sutures, implants and drug delivery devices. PLA is an aliphatic polymer obtained either by direction condensation polymerisation of lactic acid monomers or by ring opening

polymerisation (ROP) through lactide (Figure 1.10). PLA derived from 2-hydroxypropionic acid and has chiral molecules, polylactides come in four forms: poly (L-lactic acid) (PLLA), poly (D-lactic acid) (PDLA), poly (D, L-lactic acid) (PDLLA) a racemic mixture of PLLA and PDLA, and meso-poly (lactic acid). As far as use in biomedical research, only PLLA and PDLLA have been extensively studied, in particular PLLA of high molar mass as it has sufficient strength[71,72]. PLLA has been widely tested as a temporary stent material in cardiology due to its long track record of *in vivo* biocompatibility[73,74]. The mechanical property of PLLA are shown in Table 1.6. When a stronger mechanical property is required, semi-crystalline poly lactic acid is desirable. It was reported semi-crystalline polymers have a tensile strength of 50-70 MPa and tensile modulus of 3 GPa[75].The degree of crystallinity of the polymer has a significant impact on the mechanical properties. Although PLLA has been used in medical application extensively, the crystalline domains tend to degrade slowly. The crystallinity could be induced by PDLLA, leading to amorphous polymer with faster degradation profile.

The degradation of the polymer happens via random hydrolysis process. The hydrolysis of the polymer begins with water uptake phase followed by hydrolytic splitting of the ester bonds in a random manner. Thus, the degradation begins with the amorphous region, in which molecular fragments are hydrolysed. As a result, great mobility is achieved, leading to reorganisation of the polymer chains[76,77] The hydrophobicity of PLLA limits the water uptake of thin films to about 2%, thus reducing the rate backbone hydrolysis compared to other polymers such as lactic-co-glycolic acid (PLGA)[78].

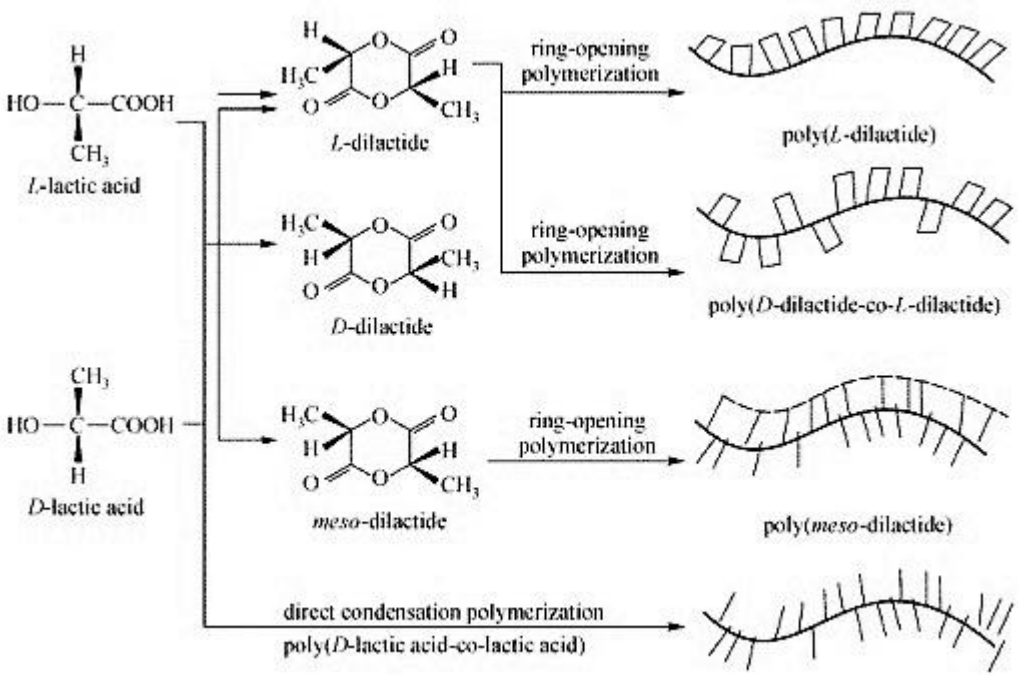


Figure 1.10 L-Lactic acid and D-lactic acid polymerisation scheme[79].

The general physical properties of PLLA depends on its crystallinity, spherulite size, morphology, degree of orientation and molecular characteristics[80]. The crystallinity of PLLA can be reduced on laser irradiation as used to machine the stent architecture. The melting temperature of PLLA varies from 130 to 203 °C[71,80,81]. Addition of PDLLA to matrix can make the spherulite structure of PLLA more disordered. It was also reported that the melting temperature of PLLA was depressed due to the presence of PDLLA[82,83]. Molecular orientation of PLLA can also have an impact on the mechanical strength of PLLA. For instance, if the molecular orientation is done at low temperature by extrusion or drawing under hydraulic pressure, the resulting polymer will have an improved strength without any substantial increase in crystallinity[83,84].

Table 1.6 Physical properties of PLLA and PDLLA[80].

Properties	PLLA	PDLLA
Melting temperature (°C)	170-190	-
Equilibrium melting temperature (°C)	200 - 215	-
Tg (°C)	50 - 60	50 - 60
ΔHm (xc = 100%)/(J/g)	93	
Density (g/cm^3)	1.25 - 1.29	1.27
Solubility parameter(25°C)/ (J/cm^3)$^{0.5}$	22.7	21.1
Tensile strength (kg/mm^2)	12-230 of oriented film	4 - 5 non-oriented film
Young's modulus (kg/mm^2)	700 - 1000 of oriented film	150-190 of non-oriented film

1.6 Surface Characterisation and Example of Surface Analytical Techniques used for Drug Delivery

When a biological system encounters an implant, interactions are induced at the implant-tissue interface[85]. The surface chemistry of biomaterials is of considerable importance within biomedical science, where the interfacial chemical structure will have a major effect on the host bio-interactions[86,87]. To more completely understand the relationship between surface properties and biological performance, it is fundamental to characterise the biomaterial surface in detail. The potential difference between the surface and bulk properties mean that surface analysis is required in complement to traditional bulk analysis approaches[88,89]. Polymers as intricate macromolecules can present quite complex surface behaviours and also reorientation with time and/or environment[90]. An investigation of a surface phenomenon requires complementary techniques to be used as usually no single approach provides satisfactory information to comprehend the surface chemical structure of a material[89,91]. Here AFM, ToF-SIMS, XPS and confocal Raman microscopy are the main complementary techniques used for the chemical characterisation of the ArterioSorb^{TM} scaffolds. These techniques will be briefly described in Chapter 2 in terms of the theory of operation and the experimental protocols used throughout the thesis. Table 1.7 below illustrates a summary of the most commonly used surface analytical techniques. AFM is capable of nanometre spatial resolution with some

degree of sensitivity to material properties but is generally unable to provide spectroscopic chemically specific analysis. In contrast ToF-SIMS and XPS can provide chemical and elemental composition.

Table 1.7 Comparison of different surface analytical techniques used in vascular application[92].

Technique	Principal	Depth	Spatial resolution	Measured Parameter	Sensitivity	Limitation	Advantages
AFM	Atomic contact using cantilevers	Surface	Molecular level	Topography	Highly sensitive	Visualisation only	High spatial resolution
SEM	Secondary electron emission following electron	5 Å	1 Å	Topography	High (not quantifiable)	Damages sample, artefacts	Capable of analysing wide variety of applications
ToF-SIMS	Secondary ion emission following ionic bombardment	0.01 – 1μm	500 Å	Secondary ion count	Very high	Damages sample	Semi-quantitative technique with high spatial resolution
XPS	Secondary Auger electron emission following electron bombardment	10 -250 Å	10 – 150 μm	Composition	0.1 % at.	Damages sample, complex interpretation	Quantitative technique
Raman	Vibrational spectroscopy	>1μm	1 μm	Chemical composition	High	Limited for depth, 1 μm	Wide variety of application
ATR-IR	IR causing molecular vibrations	1-5μm	Good in the order of μ	Chemical composition	1 mol %	Water subtraction	Wide variety of application

1.7 Example of Surface Characterisation in the Field of Drug Eluting Stents

The Taxus™ DES (Boston Scientific Inc) has been studied extensively. This metal stent has a polymer-based drug delivery coating containing poly styrene-b-isobutylene-b-styrene (SIBS). The Taxus stent is the first commercial application of this polymer in a drug delivery platform. *In vitro* release study of this DES were conducted in PBS at physiological condition[93]. The surfactant Tween 20 was used to prevent drug loss through passive adsorption. Physiochemical characterisation of the paclitaxel/SIBS coating matrix was analysed using many analytical techniques, including SEM and AFM. The stent was examined by SEM pre-and post-expansion showed smooth conformal coating that lack of cracking and flaking, indicating the ability of the coating to withstand the rigours of sterilisation, expansion and handling. Figure 1.11 shows the surface morphology of the Taxus™ stent comprising of 8.8% paclitaxel (Figure 1.11b) showing that the drug exists as discrete particles. SIBS in Figure 1.11b phase separated and this shows two phases with the drug sitting in one of phases.

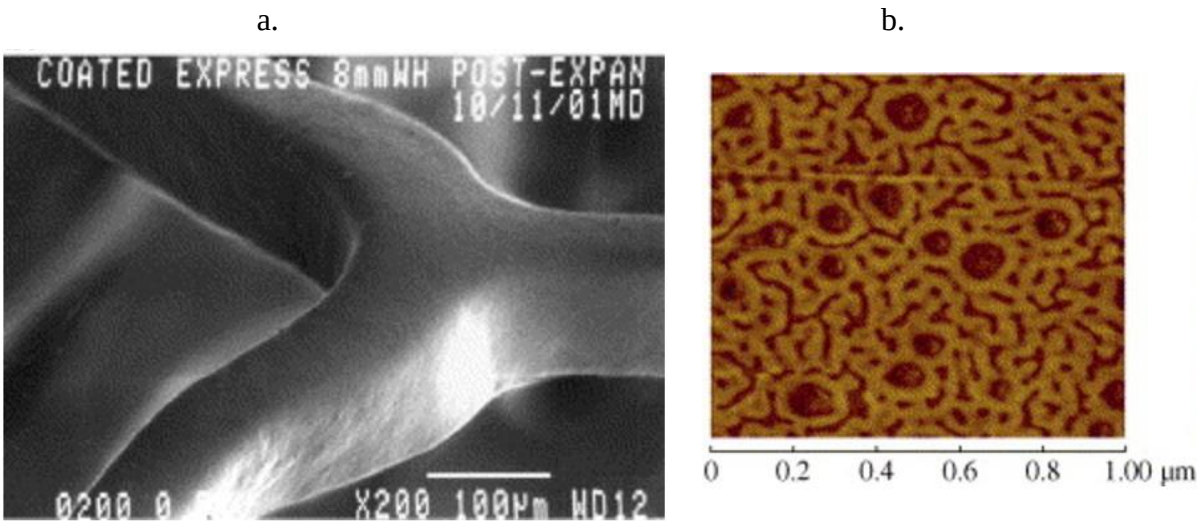
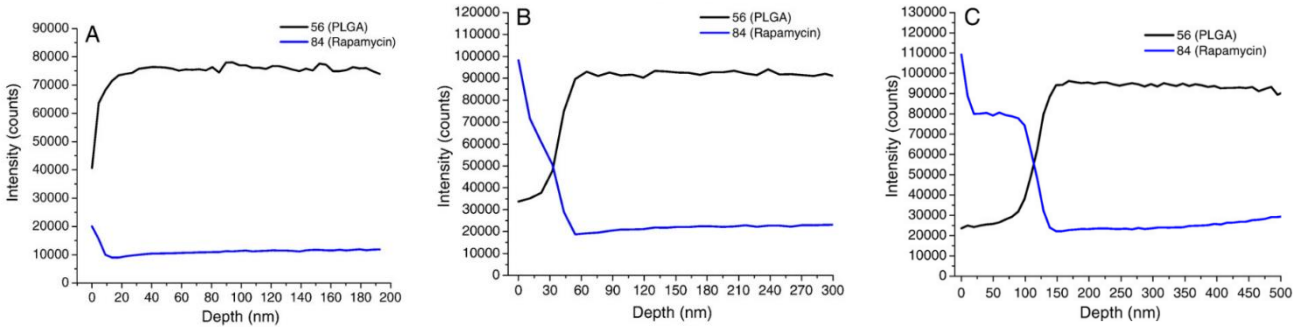


Figure 1.11 Images of Taxus™ stent a. post sterilisation and expansion[94], b. AFM surface imaging of paclitaxel-SIBS matrix 8.8% w/w.[93].

Another example where chemical images of the surfaces and the bulk of the coatings of rapamycin in poly (lactic-co-glycolic acid) (PLGA) was produced by Wormuth *et al*., where they investigated different coating formulations ranged from 5 to 50 wt % rapamycin in PLGA with and without a top layer of PLGA on coupons and stents (made of MP35N alloy)[95,96]. The work presented combined different analytical techniques including ToF-SIMS and Raman to give a clear understanding of rapamycin distribution in the coating film. Upon sputtering with ToF-SIMS the coating layers with 50% drug concentration were damaged, However Raman was able to image the chemical distribution of such thick coatings. As the rapamycin concentration increased from 5 wt.% to 50 wt.%, an increased segregation of rapamycin within the bulk of the coating was apparent[97] as seen in Figure 1.12.

1.



2.

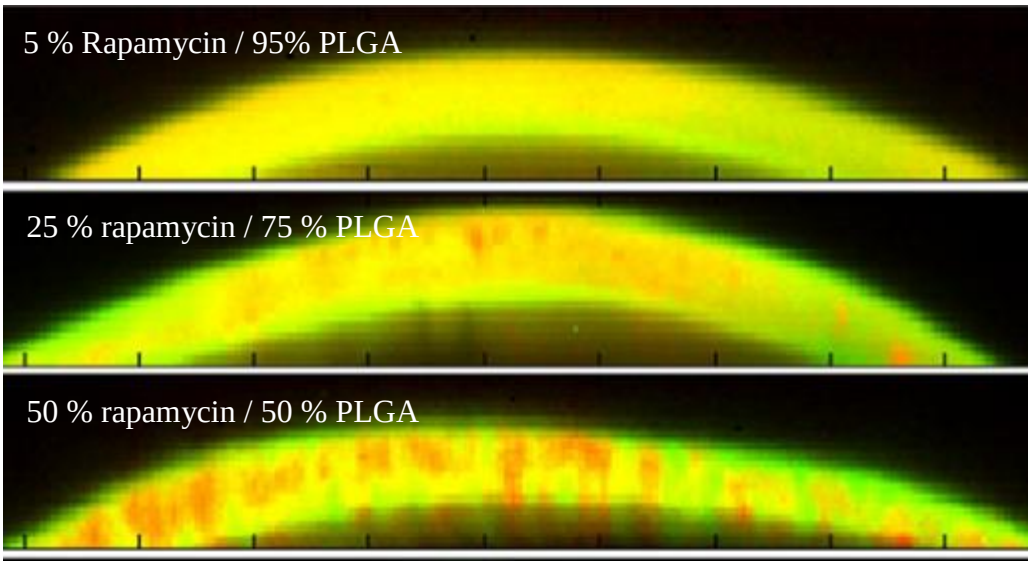


Figure 1.12 Acquired data from coatings of rapamycin in PLGA. 1. ToF-SIMS depth profiles of coating layer of 5% Rapamycin /95% PLGA coating. B) Profile of 25% Rapamycin /75% PLGA coating. C) Profile of 50% Rapamycin/50% PLGA coating.

Data acquired on polymer film on metal coupon. 2. Raman images of stent coating from as a function of increasing concentration, rapamycin is in red and PLGA is in green. Data from[97].

Another example of surface characterisation analysis of DES , where Grabow *et al*., have developed a slotted tube biodegradable stent based on PLA and poly (4-hydroxybutyrate) (P4HB) as shown in Figure 1.13[98]. The key finding from their investigation was that the PLA/P4HB blend delivers superior load-bearing capacity and rapid expansion in contrast to a bare polymeric stent[98]. Nevertheless, degradation properties and *in vivo* performance of these stents still need to be assessed.

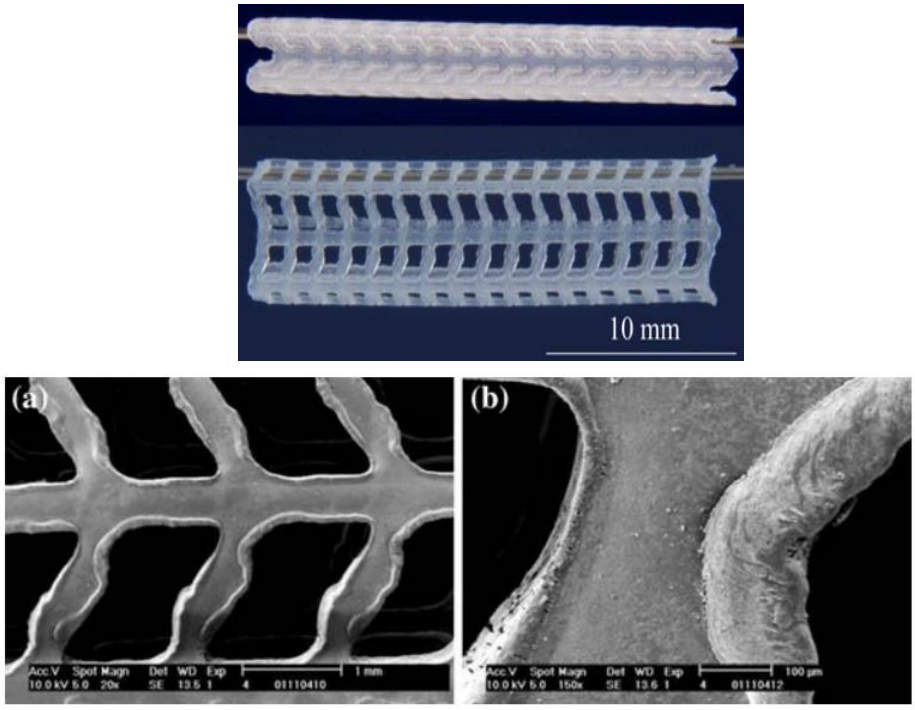


Figure 1.13 Slotted tube PLLA/P4HB stent, the top image shows the stent prior and post expansion and bottom images show SEM of a. the expanded stent and b. the melted edges caused by laser cutting (CO_2) and the deformation zones post expansion.

Many other surface coatings of drug eluting stents have been investigated including, characterisation of a curcumin-loaded PLLA film[99] The inflammatory and anti-proliferative properties were tested and found that the curcumin reduced phagocyte accumulation and

significantly reduced their proliferation, however the adhesion of human coronary artery smooth muscle cell was not reduced [100].

Yamawaki *et al*. inspected the likelihood of delivering specific tyrosine kinase inhibitors from PLA based stents. Tyrosine kinases control various extracellular signals inducing proliferation and differentiation[101]. The device loaded with ST638 helped to reduce geometric remodelling. Neointimal formation is still in the need of further investigation in terms of biocompatibility.

Lewis *et al*.[102] have investigated the suitability of a phosphorylcholine (PC) coated stent as a drug delivery vehicle. Phosphorylcholine based polymer reported to be a non-thrombogenic and stable *in vivo* for over six months [103]. Two types of phosphorylcholine coronary stents have been reported in terms of *in vitro* and *in vivo* protein adsorption. The study showed that the catatonically charged monomer choline methacrylate coating was able to absorb various drugs with a range of molecular weights in a controlled manner[104].

Vog *et al*.[105] have developed a novel biodegradable double-helical stent. They tested 12 paclitaxel loaded poly lactide stents. This novel device showed satisfactory mechanic stability, and by addition of paclitaxel, a substantial potential to diminish restenosis development after vascular intervention was seen.

Another example of surface characterisation, Wu *et al*.,[54] characterised two different types of stents, poly (ethylene vinyl alcohol) copolymer (EVAL)/everolimus and PLA/everolimus using many analytical techniques. These stents provided different surface morphologies, with homogenous drug distribution for the EVAL coated stent and phase separation of the drug at the surface for the PLA coated stent. In addition, they conducted release studies revealing a loss of drug on both surfaces. The EVAL coated stent showed an intact surface after 28 days in contact with aqueous solution, whilst the PLA surface presented matrix erosion.

1.8 Controlled Drug Delivery for Biodegradable Drug Eluting Stents

Drug delivery technology is an evolving field, with many new technologies emerging in both delivery of biological materials such as gene based, protein and peptides and pharmaceuticals [106]. Combination products have become vital in device-based technology[107] , in this case DES with fully bioresorbable coating. Drug release can result from the migration of the solvated drug from the bulk of the polymeric system to the polymer's outer surface and to the release medium[108].

Drug transport through the vessel wall occurs *via* various forces and partitions to both specific and non-specific binding sites[109]. The transport of drug described in Figure 1.14, shows radial and planar transport, respectively. The pharmacokinetics of an active agent within the arterial wall delivered *via* drug eluting stent are dependent on transport forces (Figure 1.14) such as convection (directed always from inside out) and diffusion (drug moves away from the release device), as well as physiochemical properties of the drug[109]. Furthermore, the geometry of the stent and placement of the device influence the local drug deposition and the distribution of the drug from the stent. In summary, the release of the drug can be affected by many factors such as, the physiochemical properties of the solute, release environment and the characteristic structure of material systems; Table 1.8 shows a summary of these influencing factors.

In vitro drug release profile models are an essential part of drug eluting stents development process. These models are important for establishing the reproducibility of the drug release as well as the coating procedure. *In vitro* release should be scrutinised at 37℃, under sink conditions, and with small agitation to inhibit boundary layer effects until completion of release or no major change in release is further anticipated[110]. Dissolution testing is usually used as part as part of product characterisation. There are different types of dissolution apparatus used specifically for DES, noncompendial and compendial apparatus. Apparatus 2 (paddle) require large volumes of media and therefore not appropriate for DES application. Flow-through (USP 4) and reciprocating (USP 7) apparatus offer the advantage of using low volume of medium which is ideal for

DES application due to low drug level of formulation. In this thesis, USP 4 was considered, into however, obstacles were encountered (Appendix E).Therefore stents used in this thesis were incubated in release medium and samples were then transferred to fresh medium at predetermined time points. Suitable selection of the release medium is recommended as this may affect the rate of drug release. The release media used can change the release profile, as the drug and polymer used can be sensitive to alterations in media composition, with such effects being a common feature of accelerated drug release tests. For example, addition of solvents such as acetonitrile can increase the solubility of the drug[111].

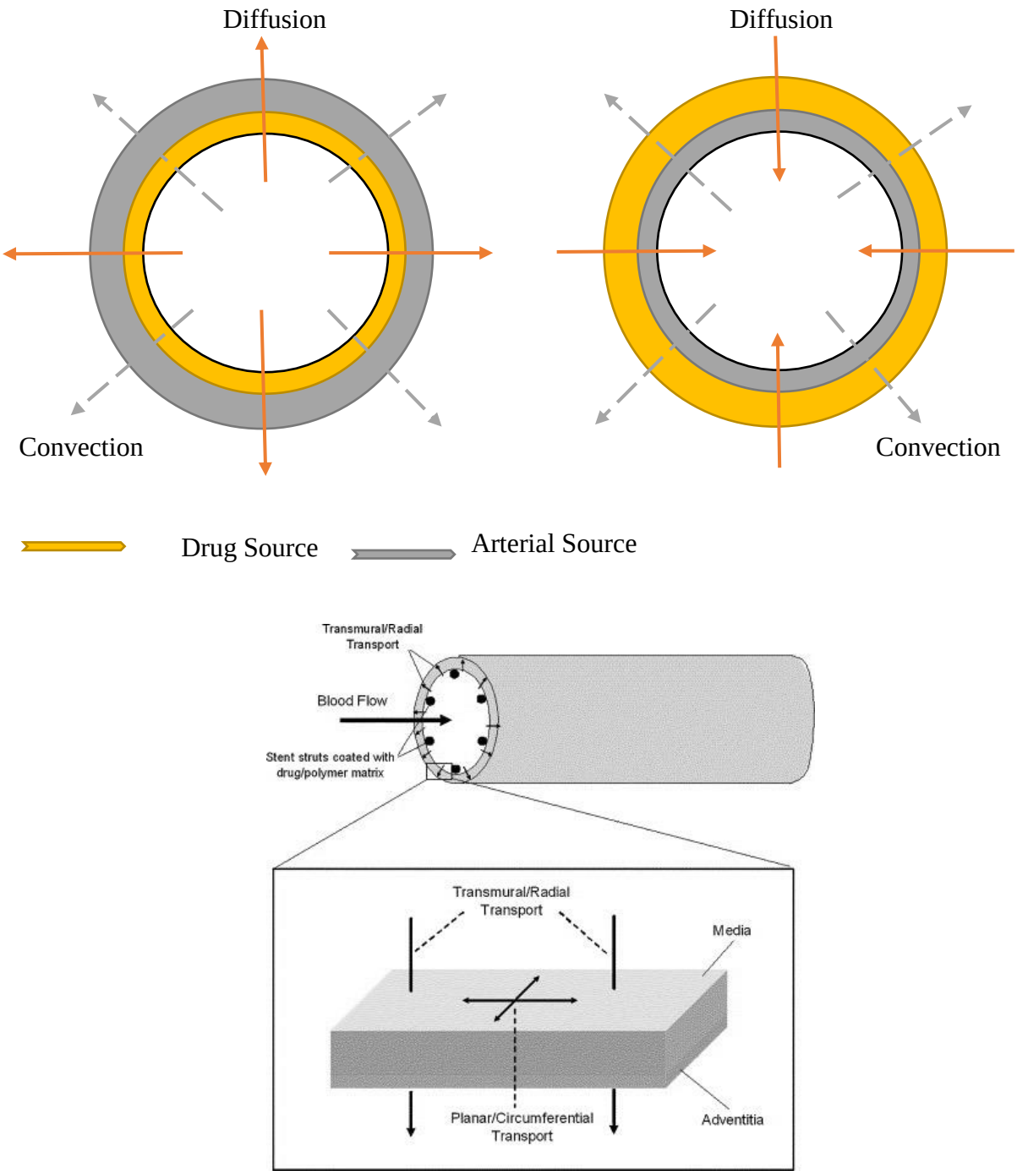
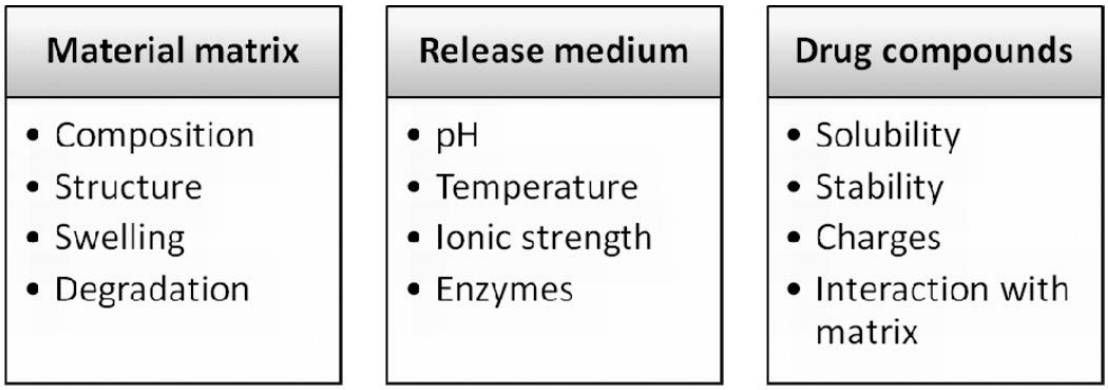


Figure 1.14 Schematic showing the directional transport of drugs across and within the vessel walls. Circumferential transport is within the arterial tissue layer and radial transport the arterial is across the arterial vessel wall. Schematic adapted from[109,111].

Table 1.8 Factors affecting drug release kinetics, Figure adapted from [112].



Sirolimus has been broadly used in drug coating formulations in large clinical trials and showed high efficacy[113] as it carries both anti-proliferative and anti-inflammatory properties and possess immuno-regulatory function. The use of sirolimus in biodegradable polymer coated stent inhibits smooth muscle cell proliferation without affecting the healing process. Stent coatings and polymers have a significant role in management of drug release to the vessel wall[113]. In order to establish a controlled drug delivery from polymeric systems such as the one used in the making of the ArterioSorb™ device, parameters affecting polymer degradation should be considered.

Drug release profile of sirolimus depends on drug solubility and stability in the release medium [111]. It was reported in the literature[114], cumulative release of sirolimus is utmost in saline isopropyl alcohol mix, as compared to phosphate buffered saline (PBS) with pH 7.4 at 37 ºC. The reason for this is due to hydrolysis of sirolimus to form new products with an open lactam ring at alkaline pH[114]. An investigation was carried out by Mikkonen et al[115] examining the drug eluting properties of a novel drug-eluting biodegradable stents *in vitro* with four different drugs; simvastatin, indomethacin, dexamethasone and ciprofloxin. The relative hydrophilicity and the concentration of the drug has a good influence on the drug elution profile with different rates of elution for each drug[115]. Paclitaxel and sirolimus are hydrophobic agents. In other word, hydrophobic agents have superior distribution rate and are more homogeneous into the vessel arterial wall compared to hydrophilic drugs[116].

Different kind of drug-eluting biodegradable polymer coatings made up on stainless steel stents, studied by Pan *et al*[117], reported that depending on the drug category, different DES shown different drug release profile. Polymeric implants usually have either a bi or tri-phasic drug release profile as a result of heterogeneous polymer degradation and drug diffusion of bioresorbable polymer. Drug release from the polymer coating can occur via multiple or single mechanisms, including degradation of the polymer, dissolution and diffusion[54,108].

The polymer in the coating serves as a carrier for drug elution and helps controlling diffusion by self-erosion with the drug. The polymer should deliver the drug in a manner that assures it has reached the desired target at the physiologically appropriate time. There are three phases of the initial drug release in terms of permeability. The first phase of high permeability corresponds to very high initial release rate due to drug coming out from the surface or due to the rupture of polymer surface structure triggered by osmotic pressure. A pore density at the surface increases and shape of pores becomes round. The phase of high permeability is followed by the phase of medium and low permeability, which relates to an increase of swelling and a decrease in the release rate. Decrease in permeability results from polymer chain reorganisation and surface pores closure. During this period a diffusion barrier develops with a porous core and less porous surface. Additionally, amorphous PDLLAs undergo degradation in aqueous medium, which occurs heterogeneously[118]. After the initial burst release, phase II follows. This phase is a lag phase. The phase II is characterised by a slow drug release through relatively dense polymer. Formation of pore closing, and polymer-drug interaction or drug-drug interaction can be a reason for the lag phase. In the typical tri-phasic profile, the phase III is a period of faster release due to rapid polymer erosion and thus faster drug diffusion[119].

1.9 Aims of this Study

The primary aim of this work is to establish and develop an understanding of the methods and instruments used for the characterisation of bioresorbable ArterioSorb™ scaffold. PLLA tubes were used as models to mimic key aspects of the scaffold. Understanding the chemical composition and surface characteristic of these materials will make it feasible to understand and learn about the interface interactions between the

physiological environment and the surface. Practicability and limitations of the surface analysis techniques were established using these PLLA tubes models. The PLLA tubes extruded and die drawn acted as reference samples.

This study is aimed at characterising the surface properties of PLLA used in biodegradable scaffolds with micro and nano resolution by techniques includes AFM, SEM, ToF-SIMS, XPS, Raman spectroscopy, DSC, and IR-ATR. Using the above techniques helps in choosing the optimal experimental procedures and operating parameter. The purpose of surface characterisation is identifying any contaminants and defects in PLLA tubes and to monitor the consistency of coating processes in the final product. Complementary surface techniques have proven successful in characterising drug eluting stent device. The surface coating morphology, location distribution, drug for and *in vitro* drug release profiles are examples of properties, which can provide valuable insight into the final product performance such as efficacy, *in vivo* drug release and safety.

2 EXPERIMENTAL METHODS AND INSTRUMENTATION

2.1 Materials

All starting materials and chemicals were used as received. Phosphate buffered saline (PBS) tablets were obtained from Sigma-Aldrich (Dorset, UK). The scaffold material used for the stent/scaffold is poly-L-Lactide (PLLA) and for the coating sirolimus and poly-D-L-lactide (PDLLA). Bioresorbable polymeric tubes were supplied in a sealed moisture proof container by Arterius Ltd (Mayesbrook House, Leeds, UK) processed via extrusion and orientation (die-drawing) into tubes 2.5 - 3.5 mm outer diameter and a wall thickness of 0.095 - 0.120 mm approximately. The weight average molecular weight (Mw) before processing was 425,000 g/mol and the number average molecular weight (Mn) is 283,333 g/mol with a polydispersity of 1.5. The ratio Mw to Mn is known as the polydispersity index, which is a measure of the breadth of the molecular weight distribution.

First generation ArterioSorb™ [1]scaffolds provided by Arteries Ltd (Leeds) were ~3.5 mm 0.17–0.19 mm wall thickness (WT) (the six-crown design). However, second generation scaffolds, were 0.095 or 0.120 mm approximately 3.0 mm diameter, with 8-crown design, (design of 6 and 8 crown will be described in Appendix). This is because Arterius Ltd changed the design, but the drug coating did not change apart from the total content. The larger 6-crown scaffolds, were 3.2 mm OD, 170 μm WT, and the recent design 8 crown scaffolds were 2.54 mm and 95 um/120 um WT. The tubes had an outer diameter of 2.4

ArterioSorb™ is an innovative medical implant product currently being developed by UK medical device SME, Arterius Ltd, to assist in the treatment of coronary artery disease which affected 110 million people and resulted in 8.9 million deaths in 2015

and 3.4 mm and wall thickness of 120 and 95 µm. Post tube manufacturing, the polymeric tubing was cut into small segments using a sharp sterilised scalpel and a steel pin (pin gauge) of similar internal diameter fits inside the tube to support it during cutting, as illustrated in Figure 2.1 for surface analysis.

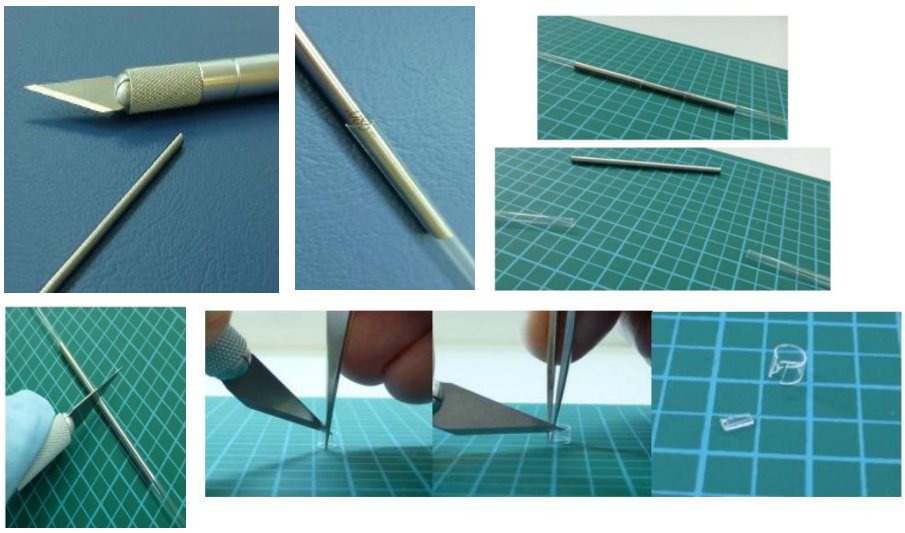


Figure 2.1 Photographs of the tube cutting procedure using a steel pin gauge.

A Series of bioresorbable coronary scaffolds (ArterioSorb^{TM}) (coated, uncoated, crimped, and expanded) were provided by Arterius Ltd. The device was produced in different sizes 3.5 x 14 mm and 2.5x14 mm. The stent under investigation had a coating thickness of the abluminal[2] coating of 15 µm and around 2 µm on the luminal[3] surface and the strut thickness was150 µm in profile.

Powdered PLLA (Purasorb PL38) and PDLLA (Purasorb PDL 02) were supplied by Corbion Purac Biomaterials (Gorinchem, Netherlands) and are used as reference materials throughout the thesis. Sirolimus powder purchased from Sequoia Research Products Ltd (Pangbourne, UK) was used for construction of calibration curve for the *in vitro* degradation study. Solutions for calibration curves were made in methanol

[2] Abluminal: The outer surface of the stent

[3] Luminal: The inner surface of the stent

(analytical grade). Deionised water of 18.2 MΩ was used for making up solutions. In addition, was used in extracting ToF-SIMS, XPS and IR spectra.

Several stents were eluted/dissoluted for various time intervals using 3 mL of PBS solution (pH 7.4) that has been reconstituted from PBS tablets obtained from Sigma Aldrich. The samples were suspended in PBS at 37 °C with gentle agitation 180 revolution per minute (RPM). The entire volume was sampled and replenished with fresh PBS at each time point. The elution curve was generated by measuring the amount of drug each stent released into buffer by TECAN Spark 10M Multimode Microplate Reader at 278 nm after 1, 5, 7, 9, 12, 15, 18, 20, 22, 26, 31, 32, 34, 37, 41, 45, 48, 50, 53, 56, 60, 63, 67, 70, 76, 83, and 91 days. Surface characterisation of samples post dissolution testing was carried out on 0, 1 day, 2 weeks, 1 month, 2 months and 3 months. The calibration curve was constructed by dissolving sirolimus in methanol of known concentrations, (calibration curve described in Appendix E).

The techniques used in this thesis are extremely sensitive to contamination, therefore when preparing samples for analysis it is essential to make sure all glassware, and stages are thoroughly cleaned. Surface morphology of the tubes and the bioresorbable stents (coated and uncoated) was observed using a FastScan AFM (BrukerNano, Coventry, UK) with PeakForce QNM (quantitative nano mechanical) operation mode. Tap150A part: MPP-12120-10 and RTESPA-150 AFM cantilevers with an average spring constant of 5 and 6 N/m respectively were purchased from Budget sensor (Sofia, Bulgaria). The spring constant of the cantilever was determined experimentally using thermal tuning method. The spring constant was observed to be in the range of 5 – 6 N/m. In the force measurement, the sensitivity measurements were performed on a piece of silicon wafer, to ensure no indentation taking place during force measurement experiment. QNM peak force mode uses special algorithm and feedback system, which can monitor image quality and adjust the set point automatically. In this thesis, the system was set to automatic mode, however the gain was adjusted physically as required. Thermal analysis cantilevers 1610-00, part: 1610-00, temperature coefficient: 0.00165/K; VITA-MM-NANOTA-200 with spring constant of 0.5-3.0 N/m were used. AFM data were evaluated using Gwyddion software (version, 2.36). Materials used for microthermal calibration

were polycaprolactone (PCL), polyethylene (PE) and polyethylene terephthalate (PET) films with a melting point of 55 °C, 116 °C, and 235 °C respectively were supplied by Anasys Instruments (Norwich, UK).

The crystallinity of the starting materials as well as scaffolds was investigated using a Perkin-Elmer DSC instrument equipped with an aluminium pan (Tzero pans). Crystallinity of the scaffold was not presented in this thesis. However, crystallinity was reported by Arterius to be around 35-40 %. ToF-SIMS depth profiling studies were performed on ION-TOF instrument (Muenster, Germany). ToF-SIMS spectra and secondary ion images were obtained using Ionspec and Ion-image version 4.1 and surface Lab 6 (IONTOF Gmbh, Munster, Germany). The composition and chemical state information of coating-layer surfaces were studied using a XPS ThetaProbe MKII / K-Alpha instruments at Nexus, University of Newcastle and Kratos Axis ULTRA (kratos Analytical, Manchester). Confocal Raman microscope (Horiba LabRAM HR) using a laser at 523.02 nm was applied in the Raman mapping mode to monitor composition as function of depth.

The supplied bioresorbable stents and polymeric tubing were handled with tweezers, polyethylene gloves and stored in a freezer until analysis. Polyethylene gloves were used in order to avoid contaminating residues from commonly used free nitrile glove. Silicon wafers purchased from Rockwood (Ridings, UK), were used for mounting samples on using double-sided tape.

2.2 Stent Manufacturing and Geometry

To date, little has been reported on the mechanical aspect and the design of fully bioresorbable stents. The stringent design criteria of bioresorbable arterial stents require high precision technologies to perform fabrication of mesh-like tubular scaffold. The first laser cut stent called Palmaz-schatz stent was approved by FDA for clinical practice in the USA in 1994[48]. The general fabrication process of arterial stent is illustrated in Figure 2.3.

The design of the stent was reported to a have a significant effect on stent delivery performance. The candidate material for such medical device should have specific

mechanical properties ideally close to those 316L stainless steel, or more ideally Cobalt-chromium, which allows thinner struts, in reality, the properties of magnesium-alloy also used in BRS are achievable, in order to provide mechanical support to diseased vessel. Such properties include high Young's modulus, high fracture toughness to allow crimping of the stent and high radial strength. Mg alloy stents has low elastic recoil[51], with minimum shortening after inflation. Despite having these properties Mg alloy stents experienced limited success due to rapid rate of degradation of 60 to 90 days[51]. Given these issues, PLLA scaffolds made from extruded and oriented tubing are currently used in the clinic. Stent requirements are illustrated in Table 2.1. PLLA has a Tg higher than the normal body temperature, which makes the polymer maintaining its rigid property and resistant to short creep deformation after stent implantation. Bioresorbable polymers such as poly lactide have been extensively studied to optimise their biocompatibility and properties.

Table 2.1 Polymeric scaffold material requirement.

General properties	Mechanical properties	Surface properties
• **Small outer diameter.** • **Low elastic recoil after expansion.** • **Thin struts.** • **High flexibility.** • **Sufficient x-ray visibility.** • **Sufficient radial stability.** • **High expandability.** • **Low longitudinal contraction after expansion (foreshortening)**	• High modulus of elasticity (Young's modulus) to minimize the recoil. • High plastic formability for a large expansion.	• Support the Growth of endothelial cells. • High biocompatibility. • Non-corroding. • Low thrombogenicity.

Laser cutting is one of the key fabrication technologies applied to coronary stent manufacture. Scaffolds can be manufactured from raw material shape such as wire, ribbon, sheet or tubing. Tubing and wire are widely used profiles in making self-expanding and expandable stents. Some conventional stent fabrication methods include etching, welding, braiding and knitting. These types of stents are outlined in Figure 2.2. However, this thesis focuses only on laser cutting stents from polymeric tubing. This method is the most effective method in stent manufacturing as compared to other conventional methods that take considerable processing times. In order to generate different pattern and design of the scaffold, laser cutting was used. Laser machining of stents from thin walled tubing is the most common form of stent fabrication for metal and polymer based systems[120,121]. Laser cutting is very sensitive to fluctuations in the quality and quantity of material being machined. When cutting away the wall of the polymer tubing to make the required mesh-like scaffolding, the tube must have a consistent wall thickness along its length and be of a uniform shape in order for laser cutting process to proceed[122]. Laser cutting is reliable in cutting large production volumes therefore, making it the most preferable method in stent manufacturing. Some of the advantages laser cutting provides fast and low cost high precision. All metallic stents are finished by surface modifications because laser-cutting process leaves sharp edges and burrs. Therefore, various surface modification or finishing steps to remove these features, as they would potentially cause injury to the vessel, disrupting blood flow which causes thrombosis. Whereas polymeric stents do not have these sharp edges but there has been reported some issues with melting which occurs during laser cutting (will be described in Chapter 3 and 4 and SEM images of such areas will be described in Appendix A). Certainly, heat affects the polymer and there is a laser cut “heat affected zone”, which the laser cutter attempts to minimise by modifying the parameters. Moreover, metallic stents experience some issues with adhesion of the polymer (drug loaded) coating to the metal, therefore surface modification helps to improve the adhesion and reduce flaking and cracking. For polymer stents, the substrate (scaffold) is the polymer and the coating is a bioresorbable polymer, therefore no problem associated with adhesion.

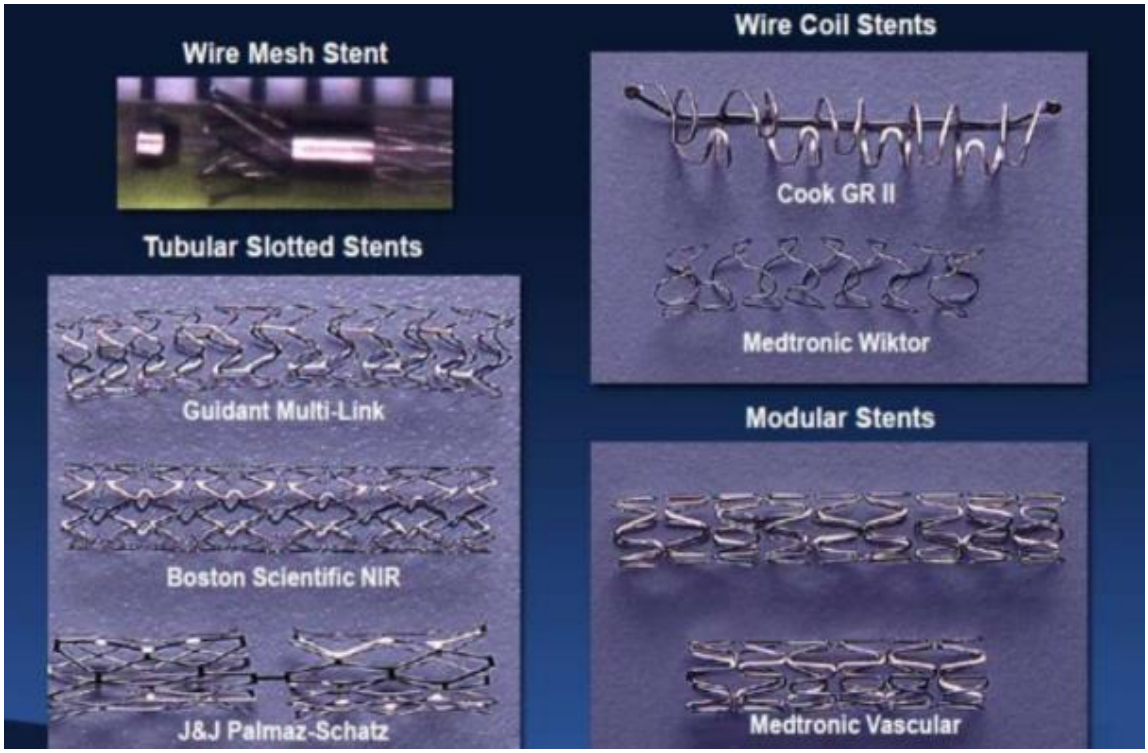


Figure 2.2 Different stent types.

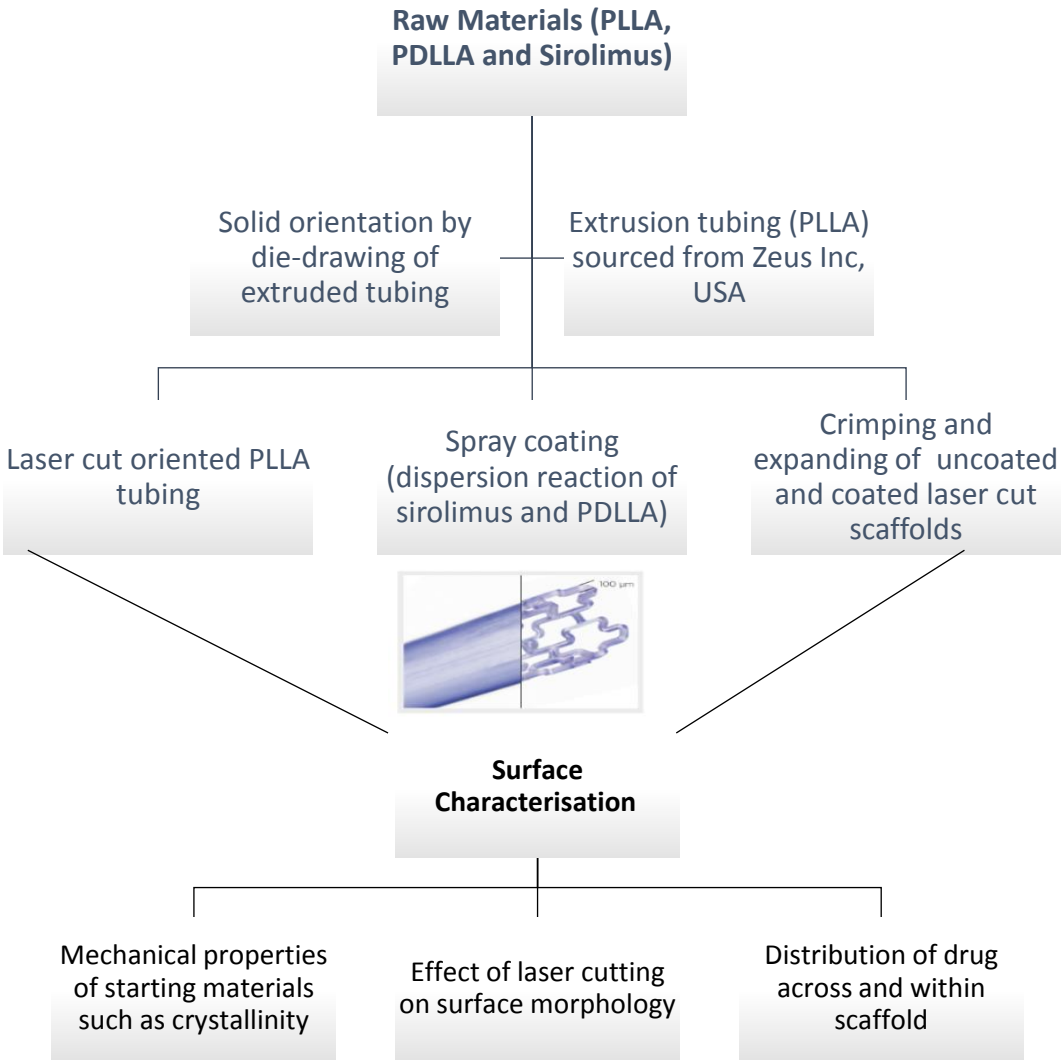


Figure 2.3 Schematic illustrating the multistep process of stent manufacturing.

Manufacture of scaffold is a complex process with many parameters that contribute to how well this device (ArterioSorb^{TM}) will work in releasing the anti-restenosis (vessel narrowing) drug. This thesis was focused on characterisation aspect of the device. Most of the commercial coronary stents are manufactured by laser cutting of tubular materials [123] (in this case die-drawn PLLA tubing). The polymer is extruded (Figure 2.4) into tight tolerance tubing then expanded radially and axially, and laser machined into a scaffold pattern. Other processes accompany the extrusion process of making bioresorbable scaffold include surface coating the scaffold with a bioresorbable polymer that carries a drug (sirolimus in this case) and radio-opaque marker bands were added on each end of

the scaffold, to aid for follow up procedures and help identify the stent during positing in the artery. During the production of the polymeric tubing, the molten PLLA was cooled down triggering an increase in the degree of crystallinity. The fraction of amorphous material is mostly at the top surface of the tube, this surface tends to cool down quicker than the bulk material.

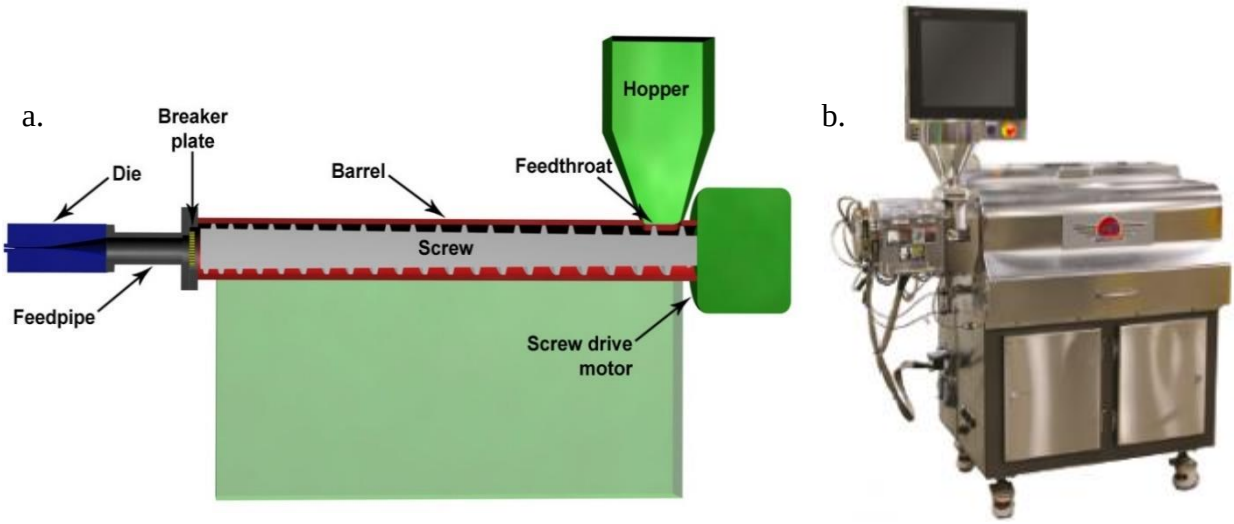


Figure 2.4 a. Plastic extruder cut showing its components, and b. micro extruder machine.

The device was first manufactured through an extrusion process, where polymer resins are melted into shape of tubular geometry[51]. A processing condition such as die drawing[51] was selected to achieve predictable and acceptable decrease in polymer molecular weight and tight dimensional control. A die-drawing process was used by Arterius Ltd in the making of the device studied here, ArterioSorb™. Molecular orientation can greatly improve the mechanical and physical properties of PLLA. Whereby a polymeric material is heated to a temperature between its glass transition and melting temperature and pulled through a die to change its cross-sectional area. Orientation of the polymer chains as shown in Figure 2.5 is caused by this cross-sectional event leading to an improvement of the scaffold with regard to its stiffness and strength[51].

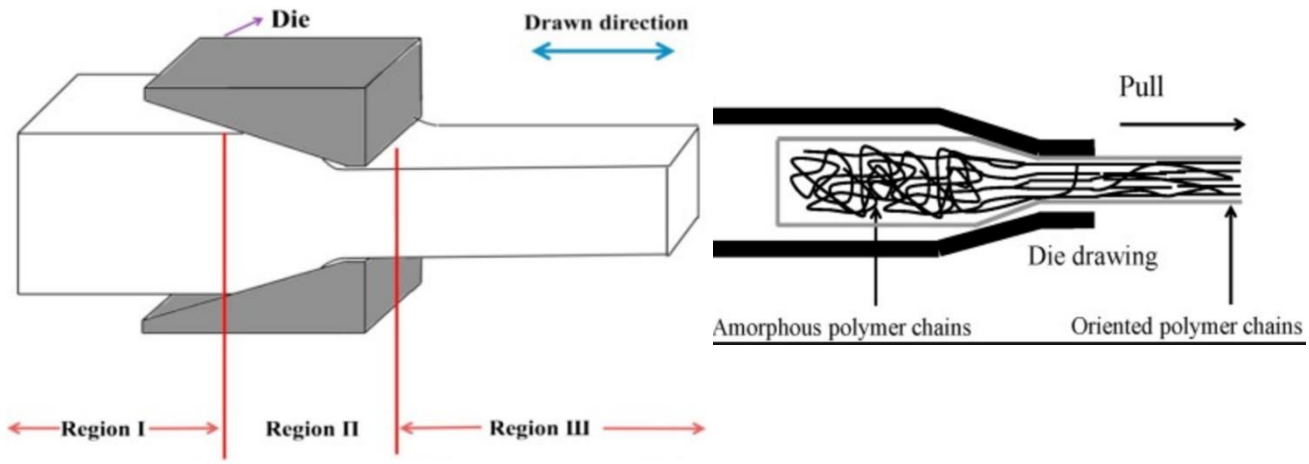


Figure 2.5 Schematic of PLLA die-drawing through a die, illustrating length of the tube, internal diameter and thickness. Region I: the sample moves towards the die entrance, deformation has begun in this region, at region II, the sample gets drawn out of the exist of the die and undergoes die drawing. Region II the sample gets cooled at distance of 100 mm from the exist of the die. Figure adapted from[122].

In summary, bioresorbable scaffolds were manufactured from PLLA that was extruded into tubing that is secondarily radially and axially expanded, then laser machined into a scaffold pattern. The alignment of these molecules in axial and radial directions improves the overall properties of the tubing. Die-drawing technique enables to deform polymeric tubing in the light of inducing molecular orientation of the polymer molecules, in bi- or uniaxial fashion, hence strengthening the polymeric tubing

Laser processing can be classified into two groups:

1. Conventional laser processing (non-chemical).
2. Laser chemical processing (chemical).

Conventional laser processing is done in an inert atmosphere and can take place without any changes in the overall chemical composition of the processed materials. Whilst, chemical laser processing is characterised by an overall change in the chemical composition of the material processed[124].

There are different types of laser which are used in material processing, these include:

- Neodymium-doped yttrium aluminium garnet (Nd: YAG) lasers.
- Ultra-short pulse lasers (Ti: Sapphire).
- Carbon dioxide (CO_2) lasers.
- Ytterbium-doped fibre lasers.

The stent geometry was first modelled in a computer-aided design (CAD) software package (This work was done at the university of Southampton), due to confidentiality of this project, details cannot be disclosed. However, CAD data were used to generate a computer numerical control (CNC) programme that essentially help define cutting path necessary to design the stent by pulsed fibre laser machine. The tube specimen was loaded into the workstation horizontally and guided by a brushing mechanism as illustrated in Figure 2.6.

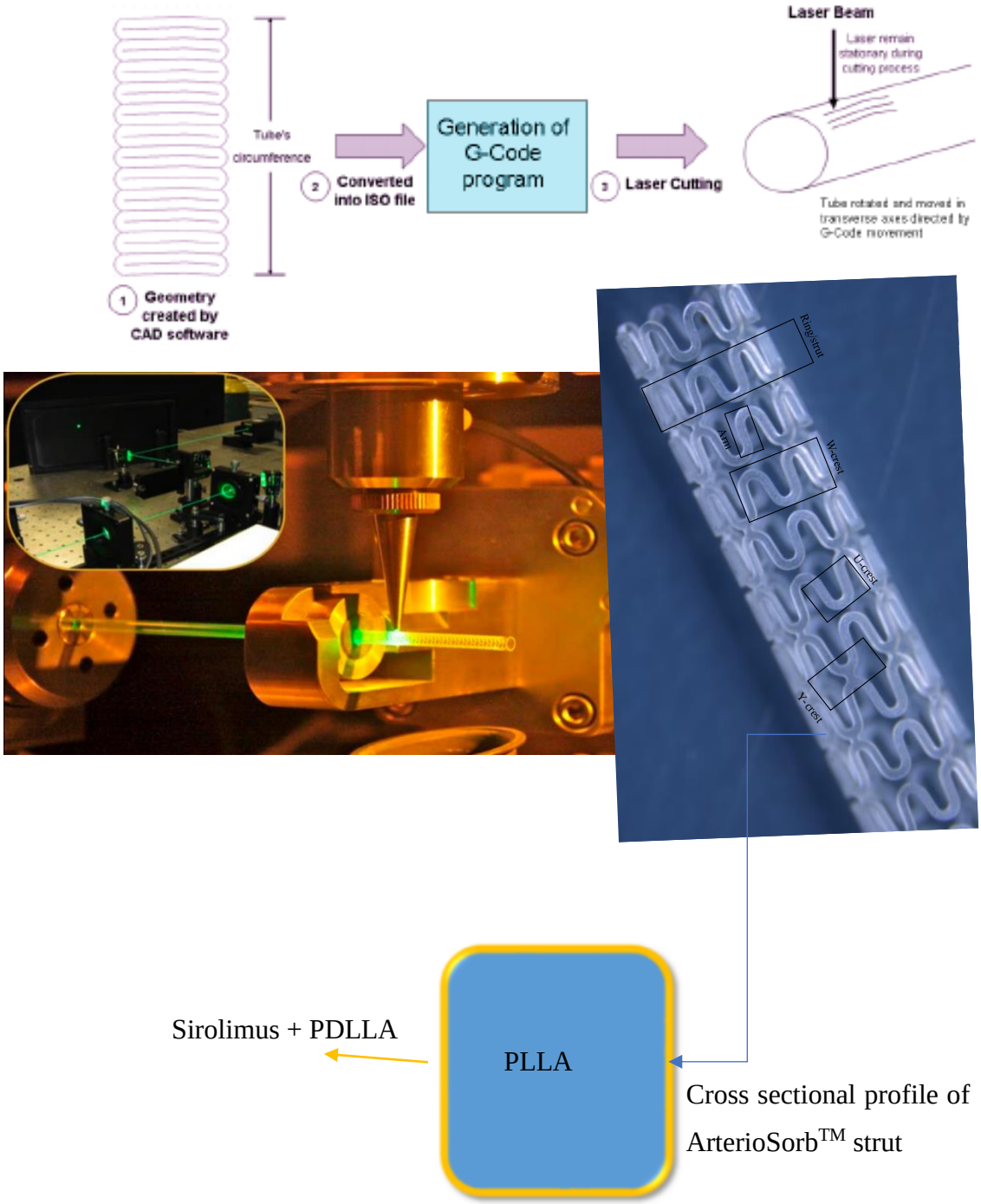


Figure 2.6 Representation diagram of laser tube cutting process. The final laser cut scaffold pattern shows number of interconnecting members include U, W, Y, arm and ring.

After laser cutting additional processes include surface coating the scaffold with a bioresorbable polymer that carries a drug, and radio-opaque markers added on each end of scaffold[125]. Visualisation of the device by ultrasonic imaging is achieved by using a radiopaque marker. Radiopaque materials are used for imaging by X-ray (fluoroscopy) as this is used during stent implantation.

2.3 Bioresorbable Spray Coating Layer

The coating layer could be liable for adverse effects such as stent-thrombosis, in-stent restenosis and hypersensitivity reactions. Therefore, biocompatible materials promote the re-endothelialisation of the polymeric surface and possess anti-inflammatory effect. The coating acts as a carrier to deliver the drug to the artery tissue to the lumen, therefore a carrier is needed in metallic bio stable polymer but in BRS, biodegradable polymer is needed, and this controls the release profile as well as time of degradation. Since 1980s, coatings were usually applied ultrasonically to medical devices and to stents in 2001[126]. Ultrasonic spray nozzles are advantages in probing complex stent geometries, ensuring full coverage of all strut surfaces without webbing. Moreover, stents coatings sprayed using ultrasonic are much thinner than with dip coating. Dip-coating can result in the bridging between struts, particular where they join each other and could lead to breaking off of the bridged coating and entering the blood stream[127]. To avoid coating bridges between struts, ArterioSorb™ was spray coated.

High drug concentration in coating process can result in lower drug release resulting in higher coating evaporation and therefore reducing the time for the drug phase to separate from the polymer matrix[126].

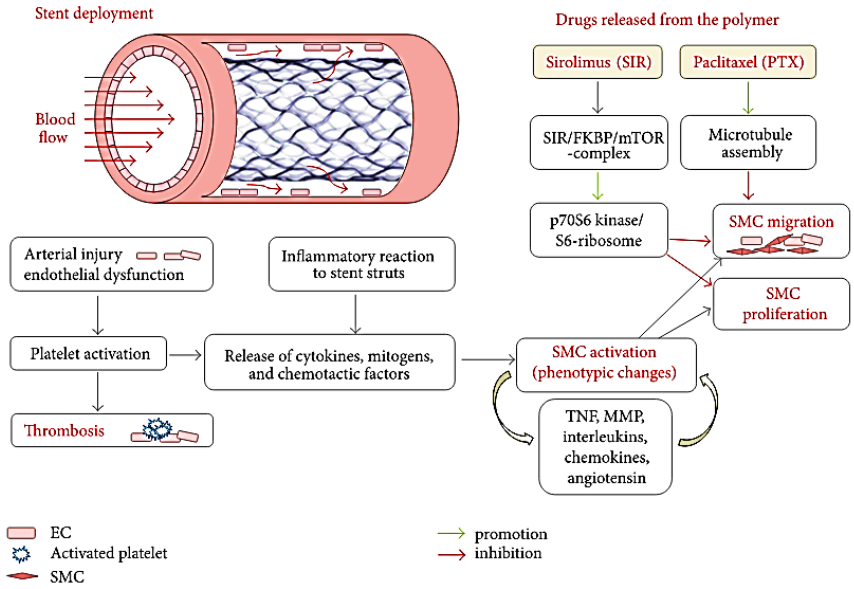


Figure 2.7 Schematic showing the impact of stent deployment and anti-proliferative API[69].

Spray coating techniques (Figure 2.8) are one of the common manufacturing methods used for stent coating. This technique ensures perfect coatings on a variety of surfaces with different morphologies. Spray coating offers the possibility of coating arbitrary shaped and textured substrate that would not easily be coated by spin coating. Spin coating is considered the most reproducible and consistent deposition technique; however, it is not scalable to roll-to-roll production. Therefore, spray coating methods have demonstrated large area coverage[128]. Some parameters need to be taken into account to achieve a smooth and defect free spray coating layer, these include, spray distance, environment, flow rate, and spray solvent. The research carried out by Girotto *et al.*[128] developed two methods to deposit materials by spray coating. These methods obtained by spraying SiO_2 substrate with a single cycle at high solution flow rate and a multiple pass technique, where the active layer was a build-up of superposition of several ultra-thin sub layers produced with a minimum solution flow rate.

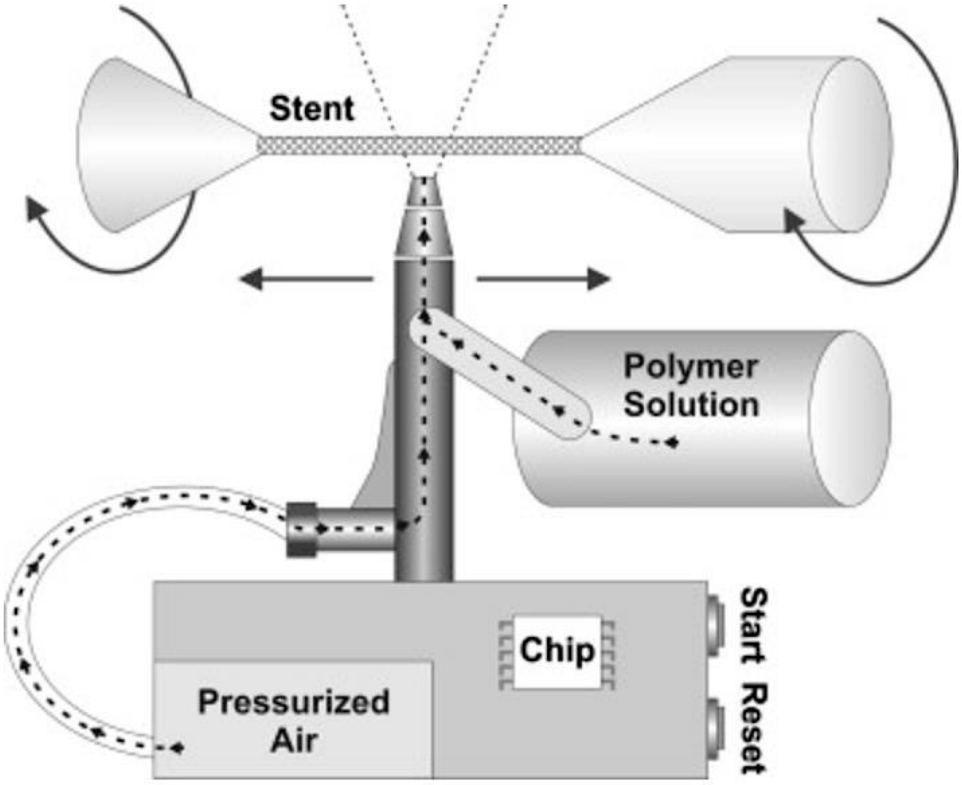


Figure 2.8 A diagram explaining the process of spray coating sirolimus/PDLLA solution with an ultrasonic atomising spray.

2.4 Sample Preparation

2.4.1 Polymeric Tubing

Series of PLLA tubes were provided by Arterius Ltd (Leeds) extruded and oriented polymeric tubing. Some of the oriented PLLA tubing was spray coated with a PDLLA/drug coating by Arterius Ltd. The polymeric tubing are manufactured by using extrusion and orientation of PLLA (sourced from Zeus Inc. (USA), where molecular orientation of the polymer was achieved using, die drawing to deform the polymeric tubing to induce orientation of the polymer molecules in both the radial and axial directions[51]. The tube thickness was calculated at the time of production using a pin gauge and micrometre, to

be between 0.17-0.19 mm[51]. The results of the outer diameter and wall thickness of the tubing are illustrated in Table 2.2.

Table 2.2 Approximate values for tubing of absorbable materials processed by Zeus Inc.

Capabilities				
Product ID	**Outer diameter (OD) range**		**Wall thickness range**	
	inch	Mm	inch	inch
Tubing prior orientation	0.012-0.0250	0.305 – 6.350	0.001-0.079	0.025-2.01
Oriented (die-drawn) tubing	0.059-0.138	1.499-3.505	0.004-0.008	0.102-0.203

With die-drawing tubing consistent dimensions can be achieved because the tube was drawn over a mandrel and through a die. The drawing process of the tube enhances tube cosmetics by creating a bright finish with no weld lines. The draw process improves the surface of the tube by removing extrusion die lines and other surface irregularities. In terms of bending of the die-drawing tubing, better dimensions and temper characteristics greatly enhance tube-bending operations. Even dimensions and temper reduce bender setup time and need less machine tunings. Tube spring back is enhanced therefore, obtaining precise bends. The drawn tube superior strength and hardness characteristics improve tube machinability; this assures a better-machined surface with less gumming. Die-drawing involves cold-work and this increases tube strength and is stronger than extruded tubing[129].

2.4.2 Fully Bioresorbable Stents

The stents were manufactured from polymeric tubes by laser cutting away the wall of the tube to produce the mesh-like scaffolding structure that provides a platform for the drug coating and the required mechanical properties of a stent. Arterius Ltd supplied series of stents with different dimensions and shapes for surface characterisation and drug release

studies. Some of these stents were supplied crimped and expanded and some un-crimped (Figure 2.9). Stent drug-polymer coating solution was prepared by dissolving the PLLA in chloroform with a desired amount of sirolimus. The coated stent's scaffold thickness was reported by Arterius Ltd to be 0.14 mm. For analysis, the tubes/stents were cut open and flattened out using gentle pressure onto acetone and chloroform cleaned glass slides and mounted onto a metal sample disk with double sided tape. Three different areas were analysed on the abluminal and luminal sides of all samples.

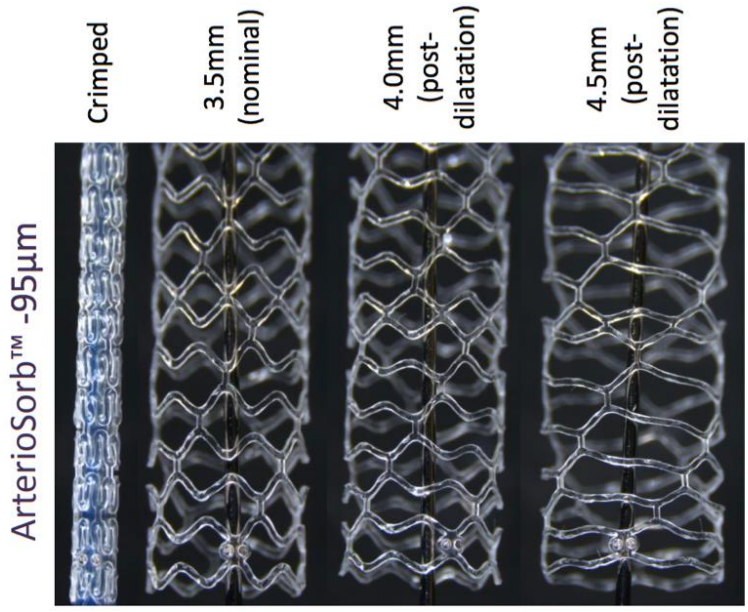


Figure 2.9 Schematic of un-crimped and crimped ArterioSorb™ scaffolds.

2.5 Instrumentation

2.5.1 Scanning Electron Microscopy (SEM)

SEM can reveal surface features at nm lateral resolution. SEM is hence preferred over optical microscopy when an increased depth of field at low resolution or high resolution is required, although SEM is limited by its depth of field <<1 µm at high magnification[130]. SEM utilises a beam of electrons that interact with the sample (typically) in a vacuum environment to form an image (Figure 2.10). The electron beam follows a vertical path through lenses and electromagnetic field, which enables focusing of the beam on the surface of the sample. The primary beam is rastered over the surface (typically coated in a conducting layer to avoid surface charging), emitted secondary electrons and x-rays

are collected from the sample to produce an electron micrograph (as shown in Figure 2.10).

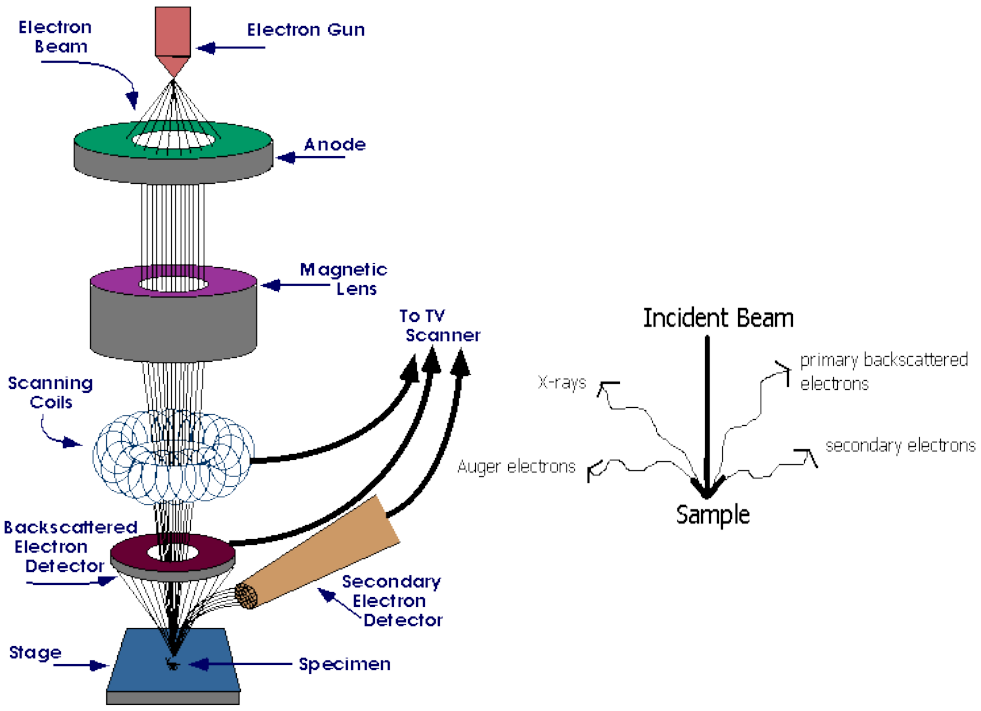


Figure 2.10 Schematic diagram of a scanning electron microscope (reproduced from *https://www.purdue.edu/ehps/rem/rs/sem.htm*).

The SEM images in this thesis were taken using A Philips XL30 SEM as well as FEI 650 Quanta ESEM with Dispersive X-ray Analysis (EDX/EDA) in high vacuum mode. Some samples were gold coated and other majority were imaged using low vacuum SEM. Samples that have been gold coated are described in Appendix A.

2.5.2 Atomic Force Microscopy (AFM)

2.5.2.1 Imaging Mode

The invention of scanning tunnelling microscope (STM), the original members of what was to a new class of microscopy in 1982 opened up a new capability of visualising and manipulating individual atoms on conducting semi-conductors and metallic surfaces. A few years later, the AFM was invented by Binnig *et al.*, in 1986[131] able to image and analyse insulating samples[131]. AFM has become a common tool in nano-mechanical characterisation and topography imaging in a range of disciplines, include

pharmaceutical and biomedical research. AFM is capable of imaging individual molecules and atoms on a solid surface and can probe information related to electrical, mechanical, magnetic and chemical properties at the nano scale[132]. AFM imaging operates on the principal of mechanical rather than electronic or optical interaction between the sample surface and the probe. The probe tip is mounted on a flexible micro-cantilever. As the probe tip approaches and contacts a sample the resultant interaction forces between the tip and the sample surface bend the cantilever (as shown in Figure 2.11). This bend can be measured, typically using an optical level set-up and hence using Hooks law and knowing the spring constant of the cantilever the force can be determined. The interaction between sample and the tip as the tip approaches and leaves a surface can be described by a force distance (see Figure 2.12)[133]. The force-distance curve in Figure 2.12 shows, how the force changes when the sample surface approaches the cantilever tip.

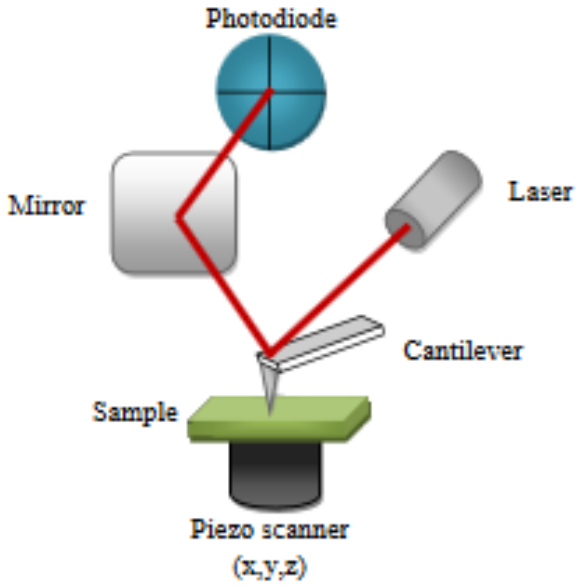


Figure 2.11 Schematic figure of the essential components of an atomic force microscopy[134].

When the tip approaches a (clean, uncharged and in vacuum) surface from a long distance, it typically senses an attractive force due to van der Waal's forces; this is counteracted and eventually exceeded by a repulsive force due to Pauli repulsion. There are three basic AFM imaging modes, termed contact, non-contact and tapping modes. In this thesis we will be focusing on tapping mode as provides the imaging resolution

required without inducing excessive damage to a sample surface as can occur in contact mode[135]. In tapping mode, the cantilever is oscillated near or at its resonance frequency (typically via acoustic excitation) and the AFM feedback control system is used to monitor the amplitude, frequency or phase change of the oscillation cantilever. In this mode, the tip passes the attractive repulsive force dominant regions as it is oscillated, and lateral friction is reduced dramatically in this mode due to the intermittent tip-sample contact as the bottom of each oscillation cycle compared to that induced by the continuous contact between the sample and tip as on contact mode (Figure 2.12). Tapping mode experiments here were carried out in air under ambient conditions.

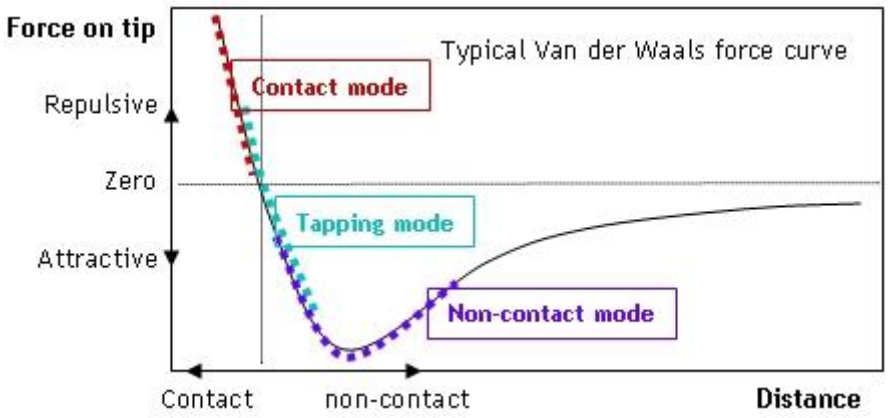


Figure 2.12 Schematic of sample-tip interaction force as a function of distance and different imaging modes of an AFM. Adapted from Ref.[136].

2.5.2.2 AFM-QNM Force Mode

PeakForce QNM is a relatively new AFM mode developed by Bruker, this technique involves use of standard probes, and however, the correct choice of cantilever is vital for best performance (Table 2.3). This technique uses peak force tapping technology[137]. Peak force tapping is suited for biological and delicate live cells imaging as it provides a lower average force of contact than standard (acoustic) tapping mode. Also offers simultaneous quantitative information on tip-sample adhesion, sample deformation and modulus. In this QNM mode the tip is actively oscillated at a low frequency (well below resonance) between 1-2 kHz. On each oscillation, a force curve recorded (as shown in Figure 2.13). The peak (or maximum) recorded force is then used as the trigger point. This allows the user to minimise the maximum force of the tip on the sample and as a

force curve is produced an on-the fly quantitative nano mechanical mapping. Peak force tapping hence helps to protect the sample and the probe from damage at the same time allows the probe-sample contact area to be minimised. Figure 2.13 (a) demonstrates what happens when the probe comes in contact with the sample. Point A on Figure 2.13 (a) shows little or no force on the probe, as the tip is far away from the surface. The cantilever is pulled down as the tip approaches the surface by capillary forces (if in air), electrostatics or van der Waal's forces.

Table 2.3 General AFM cantilever properties for different imaging modes.

Use for	K (N/m)	F (KHz)
Non-contact	10-100	100-300
Contact	0.1-1	1-50
Intermittent contact	1-10	20-100

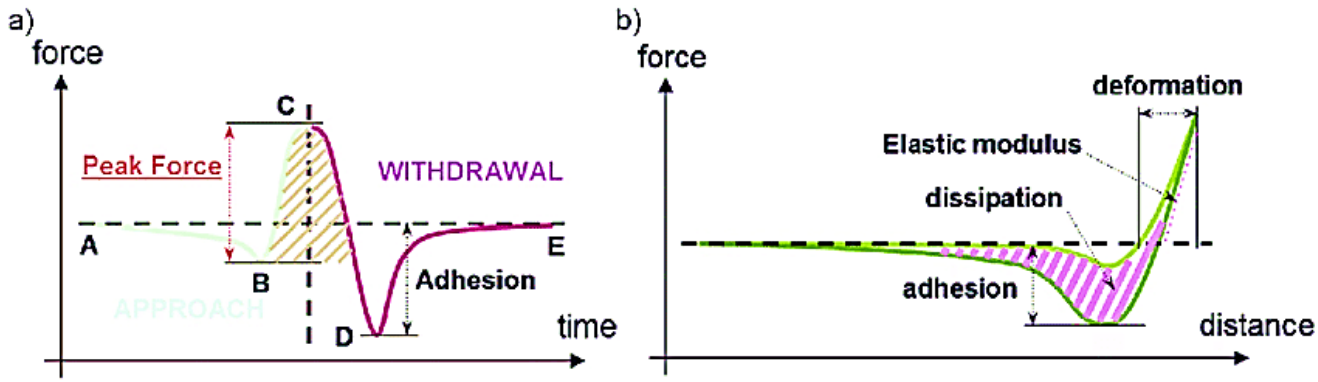


Figure 2.13 Schematic plot showing the principal of PeakForce QNM operation system. (a) One cycle of the peak force curve and (b) resulting different peak force channels that can be obtained from force curve. Figure adapted from ref.[138].

The tip is pulled to the surface at point B by attractive forces overcoming the cantilever stiffness. While the tip is on the surface at this point, the force increases until the z position of the modulation reaches position C (where the tip reaches its maximum force, as set by the user). The force at this point (C) stays constant due the feedback system. As the

probe starts to withdraw the force reduces until it reaches its minimum at point D[137]. This cycle repeats on each oscillation.

In this work AFM was used in both tapping and contact mode, however the main work of this thesis was focused on tapping mode. Although AFM has a surface specificity, but it also presents several limitations such as requiring a flat surface and significant number of replicates needed for numerical calculations, in addition, it can only be employed to a small area (at most 100 μm x 100 μm) and it is very time consuming.

2.5.3 Time-of-Flight Secondary Ion Mass Spectrometry Chemical Mapping (Tof-SIMS)

ToF-SIMS is an ultrahigh vacuum (UHV) surface sensitive technique that provides mass spectra from the top 1-2 nm of a surface following layer by layer etching by a charged ion beam[139]. The first SIMS instrument was developed in the early 1950s by Herzog followed by the development of static SIMS instrument by Benninghoven in 1970s. Ion bombardment in ToF-SIMS generates extensive molecular fragmentation leading to a mass spectrum made up of hundreds of peaks. This pattern of peaks contains information about surface chemistry and is also influenced by surface morphology. To understand this information, it is essential to investigate and comprehend not only the specific peaks but also their many combinations, ratios, and interrelationships[140]. SIMS instruments comprise of an air lock, primary ion gun, main analysis chamber, ion optical system and a mass spectrometer. A Schematic of ToF-SIMS is shown in Figure 2.14.

In the so-called static SIMS condition, the primary ion dose is set to a very low dose of usually 1 x 10^{12} ions/cm^2. During analysis, using static condition only 1 % of the top layer is sputtered, consequently, the majority of the surface remains undamaged and the obtained spectra are only containing atomic and molecular ions that are characteristic of the unchanged surface. The static SIMS process is illustrated in Figure 2.15[139,141], where the sample is bombarded by a primary ion beam, and the kinetic energy of which is transferred to the sample via a collision cascade process. Secondary particles are emitted from the surface once the transferred recoil energy exceeds the surface binding energy. Around 1 % of the ejected secondary particles are ionised, either negatively or

positively. A negative and/or positive mass spectrum is collected via mass spectrometer and this reflects the surface chemistry of the sample analysed[141]. The most common primary ion source used includes ions of bismuth, gallium and caesium.

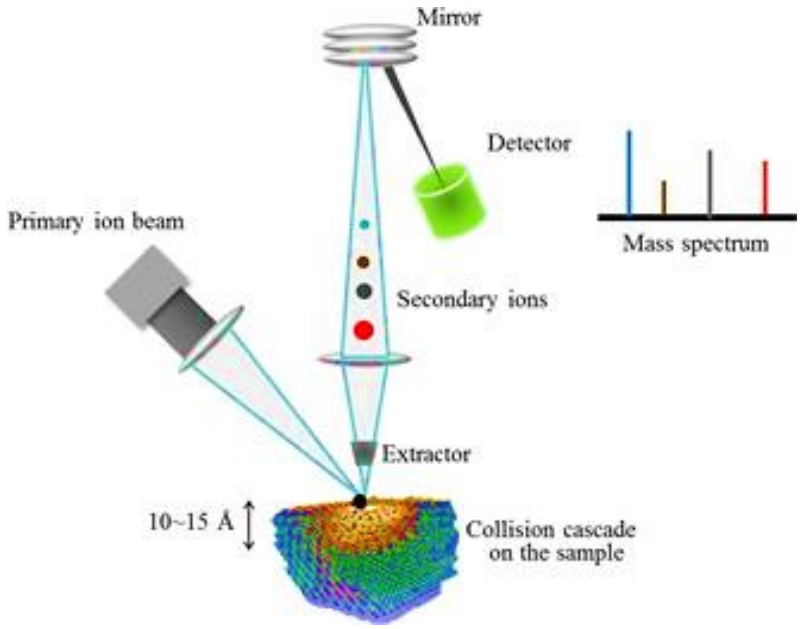


Figure 2.14 Schematic diagram showing ToF-SIMS operation.

SIMS instruments are typically equipped with a time-of-flight analyser due to their high transmission and parallel detection[142]. ToF-SIMS provides high mass resolution of about 10,000 at a mass of 29 amu for polymeric materials, enabling the identification of isobaric peaks.

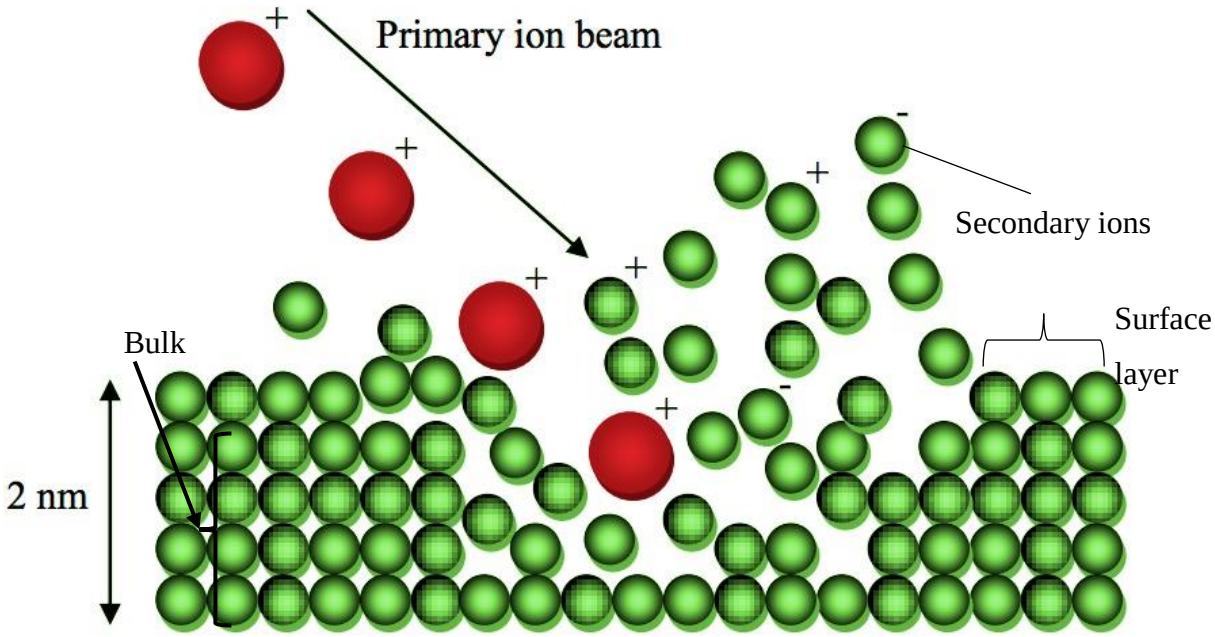


Figure 2.15 Schematic diagram of collision cascade in the sample that can occur during SIMS analysis[143].

Polymers are insulating materials and when dosing with positive primary ions and emission of secondary electrons they gain a net of positive charge. Therefore, when using ToF-SIMS to analyse such materials, it is essential to employ a charge compensation[144]. This charge compensation is in the form of an electron gun and helps to stabilise the surface potential. Molecular depth profiling allows polymeric materials to be analysed along the depths as well as at the surface. SIMS depth profiling is a surface analytical technique capable of determining the elemental concentrations of atoms within a material as a function of depth. SIMS depth profiles are generated from a mono-energetic beam of mass filtered ions, as the primary ion beam is scanned over the sample surface. Short lived collision cascades are generated when each primary ion penetrates into the surface, causing the breaking of bonds[145]. SIMS depth profile craters are usually between 10 nm and a few micrometres deep. The depth is measured by either measurement of the crater after analysis or by recognisable feature at a known depth[146]. ToF SIMS data of the luminal and abluminal surfaces of PLLA tubes were acquired by using a ToF-SIMS IV

time-of-flight secondary ion mass spectrometer (IONTOF Gmbh, Munster, Germany) equipped with a Bi_3 cluster ion source operating at 25 keV liquid metal ion gun (LMIG) and 10 KeV $C60^{++}$ /Ar_{1446} cluster.· The LMIG was operated in pulsed mode to deliver discrete packages of primary ions. The primary ions impact the surface of the analysed area and produce secondary ions through a collision cascade (as shown in Figure 2.15). Several repeats per sample were undertaken for each negative and positive polarity. The LMIG was used to perform the analysis, whereas the $C60^{++}$ and Ar cluster sources were used for etching the sample during depth profiling.

The analysis was carried out on abluminal surfaces of two samples of each of the extruded and die-drawn PLLA and was quite difficult to get into the inside of the tube due to the curvature thus bad topography. The analysis beam was rastered over a (300 x 300) and (400 x 400) μm area for the surface analysis work. In order to compare relative compositions between samples, a peak list for positive and negative was generated from each analysis. The positive and negative ion spectra mass was calibrated by using surface-lab6 (ION TOF GmbH). Correct intensities for the selected peak areas were measured and tabulated. The corrected positive and negative peak intensities for each mass in the peak list were normalised to the total ion count for that measurement, and peak intensities were then exported into Excel for further analysis. ToF-SIMS images were taken at two different locations of the samples.

Different mounting methods were carried out in order to check which one has the less contamination. Drug loaded stents were mounted on metal stubs using glue and adhesive double-sided tape, it was proved in this investigation level of contamination was less in tape method although we know this method could have some silicon in. Depth profiling is used for the determination of material composition with depth[147]. Depth profiling was performed at room temperature for all samples using a Eurothermal unit (IONTOF). A Faraday cup was used to measure the ion beam currents at approximately 200 and 0.1 pA for the $C60^{++}$ / Ar and Bi_3^+ ion beam sources. Only positive ion data were extracted from the sample into a reflection type time of flight mass spectrometer. A microchannel plate detector with post acceleration energy of 10 kV was used to detect the secondary ions. In the analysis mode, a low energy flood gun used for charge compensation. It was

expected that any damage to the surface from the electron beam is minimal in contrast to primary ion beam damage[148,149].

To summarise, SIMS is a powerful method for surface characterisation due to its lateral spatial resolution, surface specificity and mass resolution. The most common limitation of SIMS is the nature of samples and data analysis. For non-conductive samples with complex geometry such as scaffolds, charge compensation by flood gun is not a straightforward process. Data analysis of the spectra is another challenge to this technique due to its non-quantitative traits.

2.5.4 X-Ray Photoelectron Spectroscopy (XPS)

The surface chemistry of the samples was examined using XPS. XPS also known as electron spectroscopy for chemical analysis (ESCA), is one of the most widely used technique to monitor the surface chemistry of solid materials[150]. XPS surface analysis provides qualitative and quantitative information on all elements apart from helium and hydrogen. Table 2.4 illustrates the main features of XPS surface analytical technique. The main XPS features are an ultra-high vacuum (UHV) system, electron-energy analyser, x-ray gun and data acquisition system, as illustrated in Figure 2.16. XPS technique is capable of generating quantitative information from its analysis depth of 5-10 nm[151]. Kai Siegbahn invented XPS in the 1960s, where a beta-ray spectrometer was built by him to test the spectrometer. The generated photoelectrons emitted and their kinetic energy is measured. The kinetic energy (Ek) is determined by the difference of the photon energy of the incident X-ray radiation (hv), the binding energy (Eb) of the electron for solid and the sum of the work function of the sold (Φ). The signal comes from the outermost 5-10 nm of material.

The binding energies of the electrons represent the strength of interactions between the nucleus and the electron. The concentration of each element within the XPS sampled region is represented by the intensity of the peak and the shape of peaks at particular binding energies indicate the presence of a specific element in the sample[152].

Table 2.4 Main features of XPS surface analytical technique.

Feature	XPS
Main information	Elemental composition and type of chemical bonds of surface atoms
Surface sensitivity	From 3–6 nm for polymers
Sensitivity for elements	All, except H and He
Need for ultra-high vacuum ambient	Yes
Spatial resolution	1–100 μm
In-depth information for thin films	Yes
faautoImaging	Limited
3D analysis	No
Quantification	Yes
Typical acquisition time for high resolution spectrum	1–3 min
Required expertise for data interpretation	High

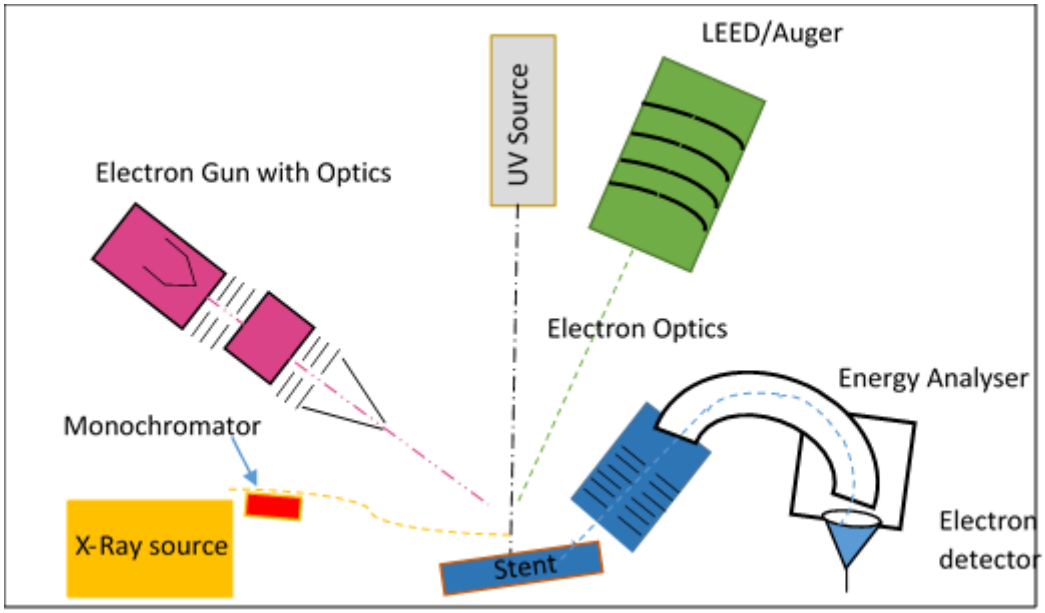


Figure 2.16 Schematic diagram of XPS set up.

The surface to be analysed was initially put into the XPS vacuum chamber and irradiated with photons, where the photon source was in the x-ray energy range. After direct transfer of energy from the photons to the core level electron, atoms emit photoelectrons of energy as define by Equation 1. The intensity (number) of emitted electrons and their energies are determined. Figure 2.17 illustrates the steps of XPS work.

Equation 1 $E_k = h\nu - E_b - \Phi$

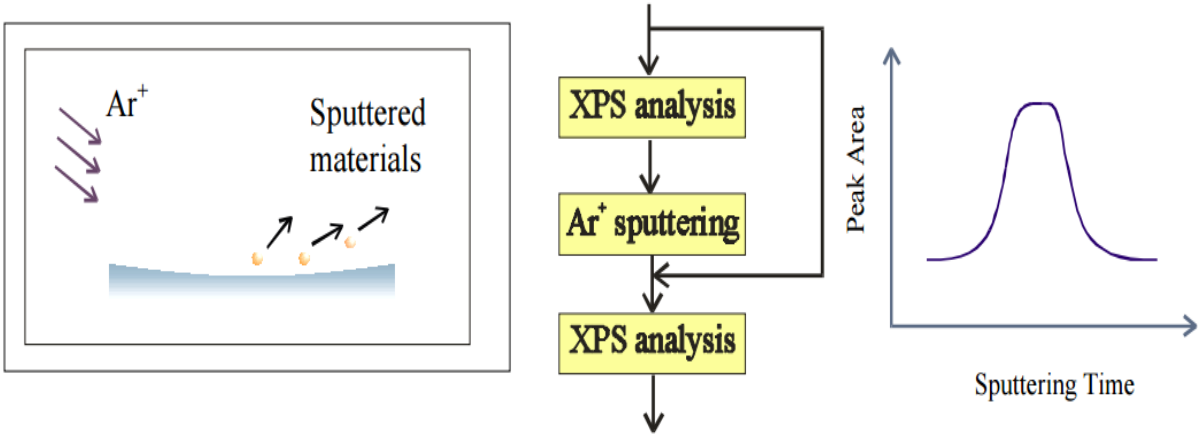


Figure 2.17 Schematic of XPS depth profiling.

Whilst XPS has the ability to distinguish elements and their bonding environments (and hence the 'chemistry') it is not possible to differentiate between aliphatic and aromatic carbons in XPS[153]. Nevertheless, XPS can provide a quantitative understanding of the distribution of the drug within the samples as there is a distinctive element or bonding environment related to that drug[154]. Two types of spectra are usually recorded during XPS analysis, a wide energy scan spectra and high energy resolution spectra of characteristic peaks of the elements. Energy concentration is calculated by dividing the peak intensities with the relative sensitivity factors provided by XPS software[155].

In this thesis, the spectra collected were taken from a wide/survey scan spectra and high resolution C 1s, N 1s, O 1s, Si 2p and Na 1s. Survey scans were performed from 0 to 1400 eV. A set of surface measurements in the form of scanned spectra acquired on three different positions on each sample with a non-overlapping analysis areas. In this research, more than one XPS instruments were used to evaluate if there a difference in measurement. The samples were scanned with x-ray source of 1486.6 eV (TheatProbe, Nexus). The atomic percentages were quantified using empirically derived relative sensitivity factors provided by the Scofield library [156] for the ThetaProbe XPS/ (Nexus, Newcastle) and Kratos library for the Kratos AXIS ULTRA, Manchester. Aluminium Kα monochromated radiation was used by sputtering the samples using argon ion gun. The pressure in the analysis chamber was maintained below 2 x 10^{-8} mbar for data acquisition and the area of analysis was fixed at 1 x 2 mm. The obtained XPS data were converted

to VAMAS format and processed using the CasaXPS software package, version 2.3.18PR1.0. Peak areas and positions were tabulated, and O 1s, C 1s, Na 1s, Si 2p and N 1s ratios were calculated.

2.5.5 Confocal Raman Microscopy (CRM)

Raman spectroscopy has been widely used in the investigation of biodegradable polymers to assist determining the degradation level and changes in the molecular weight of the PLLA material[157]. The samples were analysed using a Raman Spectrometer HORIBA equipped with a 532 nm near-infrared (NIR) diode laser used as the excitation source for the Raman spectra. Extruded and die-drawn PLLA samples were cut into small segments and mounted on aluminium foil. Scans were recorded from 400 - 3300 cm^{-1} using a x100 visible objective, the instrument was wavelength calibrated using a Si wafer.

Raman microscopy offers a powerful non-contact and non-destructive method of spatially resolved sample analysis[158]. Raman spectroscopy is highly specific and does not require significant sample preparation; work can be carried out in solid or solution and is easily automated[159]. One of the features of confocal Raman microscope is that it enables a very small sample volume or area to be analysed down to the micron scale and hence chemical mapping is possible. However, there are some limitations to Raman imaging such as spectral interferences, which comes from materials with similar chemistries and a depth resolution only on the order of 250 nm (compare ToF-SIMS of ca 1 nm).

Raman offers the opportunity to image and map samples. Images are recorded line-by-line and point-by-point while scanning the sample through the excitation focus. Raman mapping gives the opportunity in this work to investigate the drug distribution of sirolimus in eluting stent. Confocal Raman sectioning arises from the illuminated focal volume within the sample. Therefore, the size of the pinhole should be chosen according to the size of the illumination spot to compensate for magnification from final focusing lens and the microscope objective (2.18). In this thesis, confocal Raman microscope (HORIBA) (Kyoto, Japan) was utilised with the WITec Project v1.92 software. A schematic of the machine is outlined in Figure 2.18.

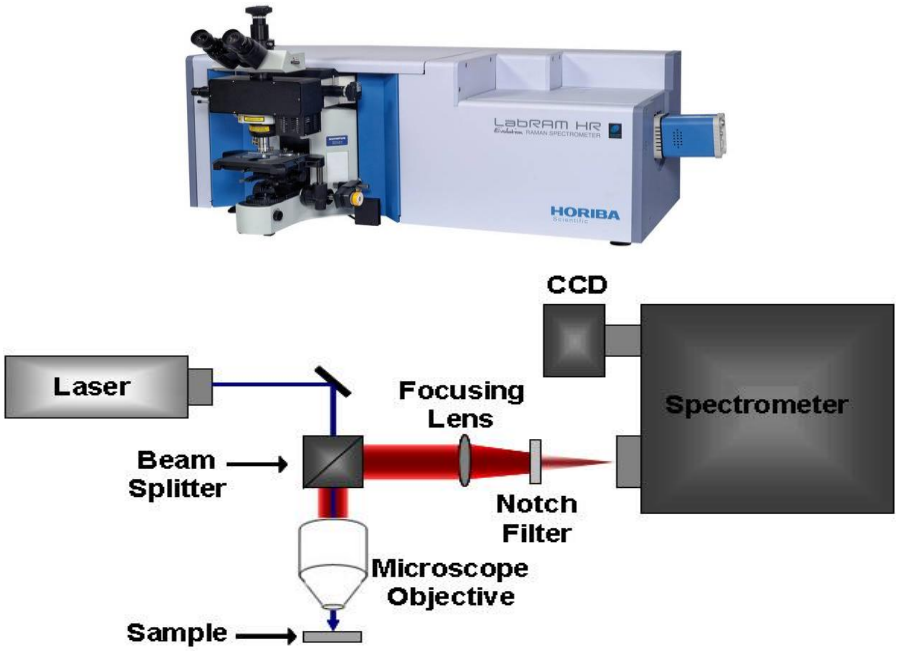


Figure 2.18 Schematic showing the LabRAM HR confocal Raman microscopy

Raman imaging is not a surface specific method, the depth of information in the order of micrometre. The acquisition time for depth analysis was considerably long (~15 hours) depending on the sample acquisition and topography of analysed sample.

2.6 Other Complementary Characterisation Techniques

2.6.1 Scanning Thermal Microscopy (Nano Thermal Analysis) NTA

In NTA the AFM conventional tip is substituted by a miniature heater which facilitates a surface to be imaged according to its response to the input of heat[160]. Nano thermal analysis can be considered as localised (surface) thermal analysis (LTA) and hence has spatial resolution unlike the more common bulk technique of DSC. There are two different probe-microscopy based methods of LTA; scanning thermal microscopy (SThM) and nanothermal analysis (NTA) having a spatial resolution of 500 nm and 100 nm respectively (Figure 2.19), related to the size of probe used[161]. NTA has been used to

characterise non dispersed pharmaceutical forms to determine their heterogeneity[162], while SThM has been utilised for example to distinguish different components in a pharmaceutical formulation[163]. The topography and conductivity of the samples were investigated before and after using SThM. In this mode, the probe was rastered over the PLLA outer surfaces at a constant temperature. As this mode works in contact mode the heat flow between the sample surface and the probe varies with contact area making it difficult to model on rough surface[164]. Extruded and die-drawn PLLA samples were investigated using a Multimode Nanoscope equipped with nanoTA2 module (Ansays Instruments, Ca) that is an accessory enables the Multimode AFM to undergo LTA. The topography of the samples was imaged using a thermal probe (AN2-200, Anasys instruments) moved to contact at a particular position. When the desired sampling region was identified, the scan size was reduced to 0 and the operative mode was switched to contact mode. With increasing the voltage, the temperature rises, and the deflection of the cantilever was recorded. The NTA was operated between room temperature and 200 °C at a temperature ramp of 1-2 °C/s in ambient conditions.

Temperature calibration of the probe was carried out against the known melting point of three polymers polycaprolactone, polyethylene and polyethylene terephalate have melting points of 55, 116 and 238 °C respectively. Once the material under the probe was molten, the probe penetrated into the sample surface, and the deflection of the cantilever was recorded as a function of temperature. Images were recorded in tapping and contact mode. LTA was performed by first bringing the probe into contact with the sample surface. The probe was heated at a controlled rate of 2 $°Cs^{-1}$. Thermal events such as a glass transition and melting produce a characteristic deflection of the cantilever. Nano-TA2 has the ability to produce high thermal scan rate up to 10000 °C/s and high temperature resolution of 0.1 °C[165] .The tip radii used in the Nano-TA2 system is about 30 nm which helps in giving a high topography close to a normal AFM tip[166].

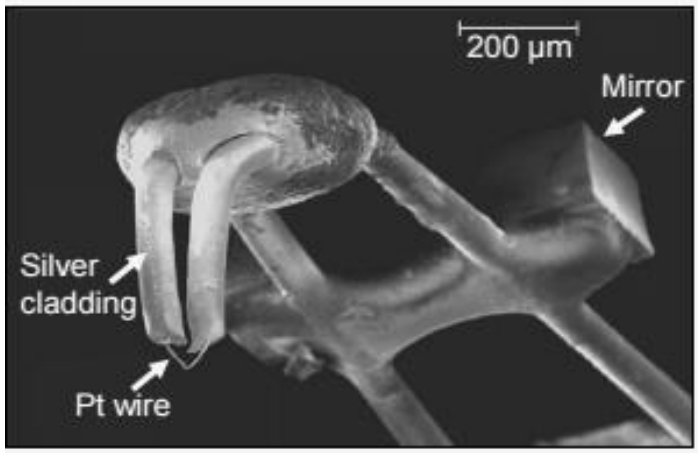


Figure 2.19 SEM image of Wollaston wire probe as used in SThM[167].

2.6.2 Bulk Analysis: Differential Scanning Calorimetry (DSC)

DSC is a widely used techniques in pharmaceutical industry to investigate physical and energetic characteristic of a sample, such as melting, transition and crystallisation. There are several operational modes including modulated DSC, thermal cycle (heat-cool-heat). In this thesis heat-cool-heat method was used. A Q2000 differential scanning calorimeter (TA instruments, USA) was used to obtain DSC scans of the starting materials and degraded samples. Thermal properties of both extruded and die-drawn PLLA tubes were analysed. The DSC was calibrated using an indium standard. An empty aluminium pan (Tzero pans) was used as a reference while another empty pan served as the sampling pan in which samples weighing between 3 - 10 mg were placed and heated at 10 °C/min from 18 - 250°C, cooled to -40 at 10 °C/min and reheated back to 250 °C at 10 °C/min so the melting point could be studied. The heat of melting and the melting temperature were collected during the first cycle to determine the percentage of crystallinity. Measurements were repeated three times. The information from the DSC was used to determine the glass transition temperature (Tg), recrystallisation temperature (Tc), melting point (Tm) and enthalpy of fusion needed to melt the samples, which is then used to calculate the % crystallinity. The enthalpy of fusion of a 100 % crystalline PLLA was reported to be 93 J/g[168]. Heat of fusion is directly proportional to crystallinity and calculated by

Equation 2 : $$X\ \% = \Delta H_f / \Delta H_0 \times 100$$

Where ΔHf is the fusion enthalpy of the sample and ΔH0 is the theoretical heat of fusion for crystalline PLLA.

2.6.3 Attenuated Total Reflectance Infrared (ATR-IR)

In the ATR, the IR beam passes through an optical dense crystal and reflects at the surface of the crystal to which the sample is in contact multiple times. The Agilent Cary 630 FTIR (Agilent Technologies, Inc, USA), is a small, mid-infrared spectrometer designed to deliver the capabilities of much larger traditional FTIR, but without the cost or complexity. The Cary 630 FTIR is computer-controlled using Agilent MicroLab PC software. FTIR uses an infrared light that passes through the sample and onto a detector; the amount of light absorbed by the sample was measured. This particular instrument equipped with a crystal. The crystal was cleaned using Azo wipes and the samples was placed on the window making sure it is in optical contact with the crystal and the dial path was turned to required path length. FT-IR was applied to identify the chemical information of the near surface region to approximately 1µm in depth. Characterisation of the sample was initially implemented on the PLLA tubing and the drug powder in order to obtain the reference IR spectra before analysing a series of bioresorbable stents. Each spectrum consisted of 64 co-added scans scanned in the range from 600 cm^{-1} to 4000 cm^{-1} at a resolution of 4 cm^{-1}.

2.6.4 Zeta Profilometry

Optical Profilometry was used to obtain topographical data from a surface. The benefits of profilometry is that it can rapidly attain surface morphologies, step heights and surface roughness. These tasks can be achieved by using a physical probe (stylus) or by using light. Nanoscience Instruments offers two distinctive profilometers which use the light-based approach: a structured grid confocal microscope and a white light interferometer. The Zeta profiler from Zeta Instruments is a true colour, 3D, non-contact surface profiler with multimode optics technology[169].

2.6.5 Nano IR-AFM

IR can be used to excite molecules in sample and in a nano IR-AFM cause rapid local expansion of sample sensed by cantilever to isolate[170]. The AFM probe can be used to collect an AFM image and then the probe placed at a location in the image. After this the multichip QCL can be tuned over a broad range of the mid-IR (1200–1900 cm^{-1}) to gather a spectrum at a single point.

3 SURFACE CHARACTERISATION OF BIORESORBABLE POLYMERIC TUBING

Surface characterisation is a powerful approach to facilitate optimising and validating the characteristic features of drug delivery devices. The outermost molecular surface of biomaterials constitutes the important interface between the external biological environment and the biomaterial, and hence plays an essential role in the biological and chemical interactions. Surface features of coatings play a great role in determining not only the initial biological response but also long-term device performance. Therefore, achieving adequate surface quality and biomechanical behaviour of medical devices has attracted considerable attention when treating cardiovascular disease[171]. It is proposed that materials should be employed to mimic the mechanical behaviour of arteries and veins, such features include a high elastic modulus material to withstand high stress solicitation and a viscoelastic material to dominate the low pressure mechanical response[172]. The use of cardiovascular biomaterials is subject to blood compatibility and integration with the surrounding environment where it is implanted. Whenever a cardiovascular biomaterial is used, two main factors should be considered, first physical and mechanical properties such as deformation, wear resistance, friction, creep, fatigue and strength, and second biocompatibility. The application of medical devices based on fully bioresorbable polymers is of value as it has the potential to reduce long-term issues

that maybe associated with persistent materials such as metallic stents. The bioresorbable scaffold must also be flexible enough to be delivered distally into the artery via balloon expansion without fracturing the struts of the scaffold. Therefore, the design of the scaffold is a crucial process and must be studied and tested thoroughly to avoid strut breakage post dilation as this may lead to adverse clinical events. The tube material used for making the scaffold must be suitable for formation by extrusion, subsequent laser-cutting of the complex stent geometry and also satisfy a number of mechanical requirement such as being capable of withstanding the structural load and radial compressive forces imposed on the stent once it supports the wall of a vessel, thus a stent must pose rigidity and radial strength. As cut, the stent must be crimped (compressed) onto a balloon catheter and is expanded during implantation (ideal characteristic of a stent material discussed in Chapters 1 and 2).

Polymers can either be semi crystalline or amorphous. They can never be fully crystalline due to the lattice defects that form amorphous regions. Polymers with small side groups and chain regularity tend to crystallise more than polymers with disordered regions. The presence of crystallites in the polymer helps to enhance mechanical properties and thermal behaviour. PLLA is a semi-crystalline biocompatible aliphatic homopolymer with processing it has high mechanical strength ideal for extruded bioresorbable coronary stent scaffolds[173]. The uniformity of the extruded tubing wall thickness along the length of the stent is a critical design parameter. The mechanical properties of the PLLA scaffold can be significantly reduced by thermal degradation of the polymer and consequent weight loss, caused from extreme thermal history such as the temperature exposure and time during the extrusion process. Moisture content prior to extrusion and secondary exposure to gamma radiation sterilisation or e-beam also has an influence on molecular weight loss. The molecular weight (Mn) of polymers is a significant factor in determining mechanical properties. The Mn can be reduced during a manufacturing process by more than 70 %, depending on the moisture content prior to extrusion, the thermal history during extrusion, and the radiation dose applied after extrusion[174]. It is hence very important to minimise process. The chemical and physical properties of the PLLA samples were assessed using SEM, AFM, nano and micro thermal analysis, ToF-SIMS with depth profiling and XPS. The percentage of crystallinity of two different manufactured

PLLA materials was assessed by DSC. ATR-IR helped in assessing the structure of PLLA. Confocal Raman spectroscopy was also used to determine surface property of the samples prior spray coating.

The main aspect of this chapter is to focus on the characterisation of the PLLA tubes, chemically, physically and mechanically and be able to use this material in the future as a biodegradable stent. Due to the geometric constraints of the stent and the roughness of the surface previous work has also attempted to characterise similar drug delivery systems[54,175], where a set of model films had been spray coated on a cleaned silicon wafers with various ratios of PDLLA and the drug everolimus and used to facilitate an understanding of such complex medical device. In this thesis, instead of using spin coated model films, the polymeric tubing used in the actual manufacturing process were investigated. Two types of polymeric tubing were used, extruded and oriented (die-drawing) tubing. The polymeric tubing were used, termed ‘extruded’ and ‘orientated’ (die drawn) tubing.

3.1 Objective

The introduction of cardiovascular stents has considerably enhanced the potential of angioplasty and improved clinical outcomes for patients[176]. Further, the addition of an anti-proliferation drug release coating to bare metallic stents has further improved this treatment[177]. Next generation stents now look to make the whole system bioresorbable to avoid potential long-term complications. PLLA is a bioabsorbable semi-crystalline polymer that possesses a low elongation and tensile strength of ~ 60- 70 MPa, which makes it suitable for medical applications such as a biodegradable cardiovascular drug eluting stent. The work in this chapter was carried out on a series of plain extruded and die-drawn PLLA tubes before conducting any further work on drug loaded stents (crimped and expanded). This chapter develops and establishes methods for characterisation that were used later on fully bioresorbable drug eluting stent using the polymeric tubing as model to determine the feasibility and limitations of the surface analysis techniques used.

3.2 Materials and Methods

In this chapter, series of polymeric tubing extruded and oriented (die-drawing) were supplied by Arterius Ltd (Leeds). Extruded tubing has less tensile strength in contrast to orientated tubing. These were R&D material, not the final product or production intermediates, used as model samples. Supplied materials were used without further treatment. The outer diameter of extruded PLLA tubing was 3.2 mm with a 1.7 mm inner diameter. For the die-drawn PLLA tubing, range of tube diameters were supplied, 3.4 mm with a 3.07 mm inner diameter and 2.5 - 2.7 mm diameter for second generation scaffold. Some tubes were drug coated in house (Arterius Ltd). The coating layer on the tube was made by spray coating sirolimus/PDLLA formulation (1% w/w in methanol) onto die-drawn PLLA tubing and allowing the coating to dry in air. The tubes were 10 cm in length. The drug loading was given as between 1 and 2 μg/mm^2. These tubes were used later to investigate the chemical distribution of the drug at the surface and through the coating-layer (will be described in Chapter 4). Test samples (tubing) were cut longitudinally and opened up by tweezers. A detailed description of the instrumentation, preparation and materials used can be found in Chapter 2.

3.3 Results and Discussion

3.3.1 Microstructural Characterisation of Polymeric Tubing

3.3.1.1 SEM

The polymer tube (oriented) used in the fabrication of making an implantable device (ArterioSorb^{TM}). Processes involved in fabricating a bioresorbable stent include: forming a polymeric tube by extrusion then radially and axially deform the tube (as described in Chapter 2). A stent is formed by cutting a stent pattern in the deformed tube (laser cutting). Finally, coating the stent with an active agent such as sirolimus and crimping it onto a balloon catheter. The physiochemical characterisation of the polymeric tubes was investigated by SEM (XL30 Philips, Eindhoven, Netherlands). SEM was utilised to investigate surface properties of the sample, which could help in identifying micro-crack formation and any foreign particle quantification [54]. The surfaces for both extruded and die-drawn polymeric (PLLA) tubing are shown in Figure 3.1-3.4. These appear to be

relatively homogenous and there are no significant differences between the two surfaces, although some dark patches up to the 100-micron scale or so can be observed on the extruded surfaces (Figure 3.1).

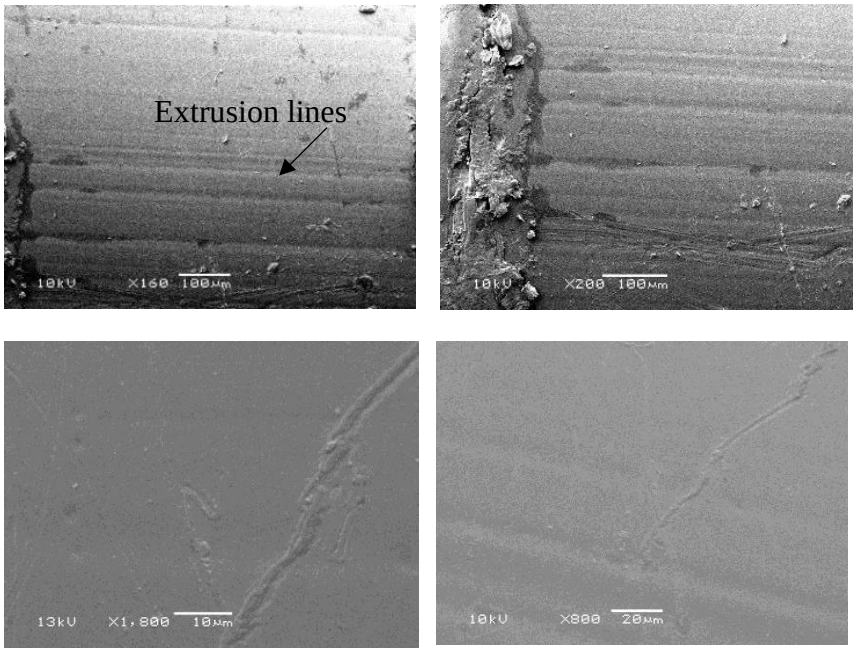


Figure 3.1 SEM images showing the abluminal areas of extruded polymeric tubing at various magnifications. The surface was gold sputtered.

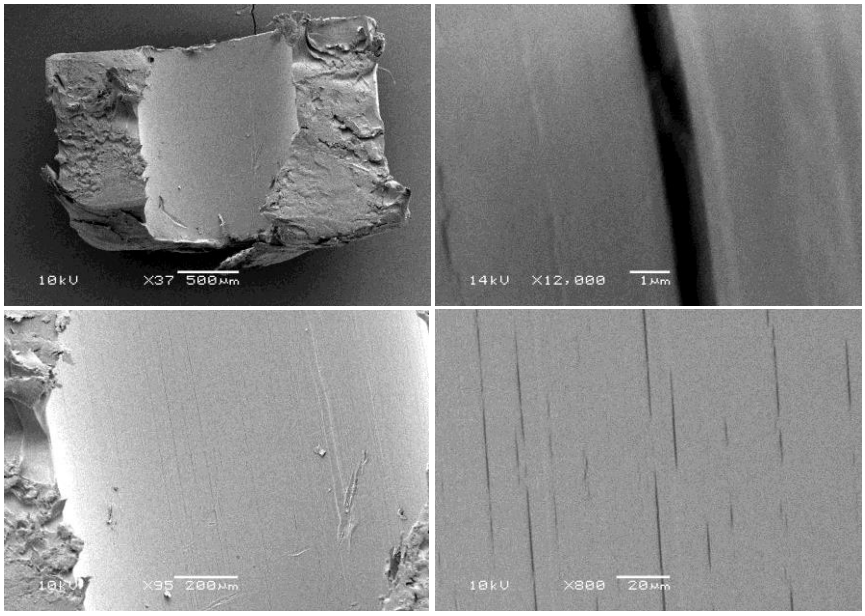


Figure 3.2 SEM images showing the luminal surface of PLLA extruded tubing at various magnifications. The surface was gold sputtered.

Extruding lines could be seen on the surface of extruded tubes some particles are present on the surface of the extruded tube and these particles could be due incomplete melting polymer particles caused by non-uniform melt-mixing during extrusion process. Some fibril lines could be seen in SEM for die-drawn PLLA tubes.

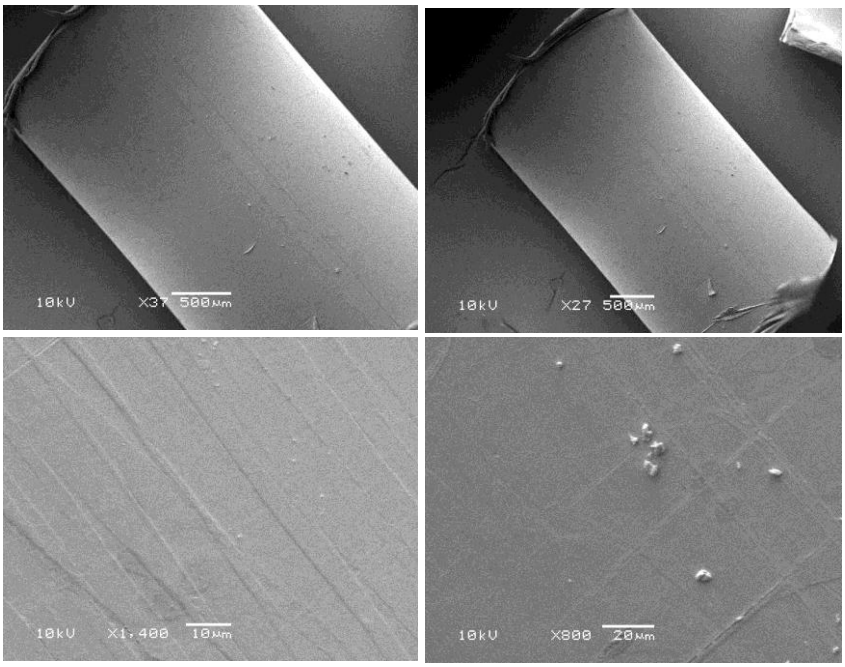


Figure 3.3 SEM images showing the abluminal surface of the die-drawn polymeric tubing at various magnifications. The surface was gold sputtered.

No drug loaded into these samples.

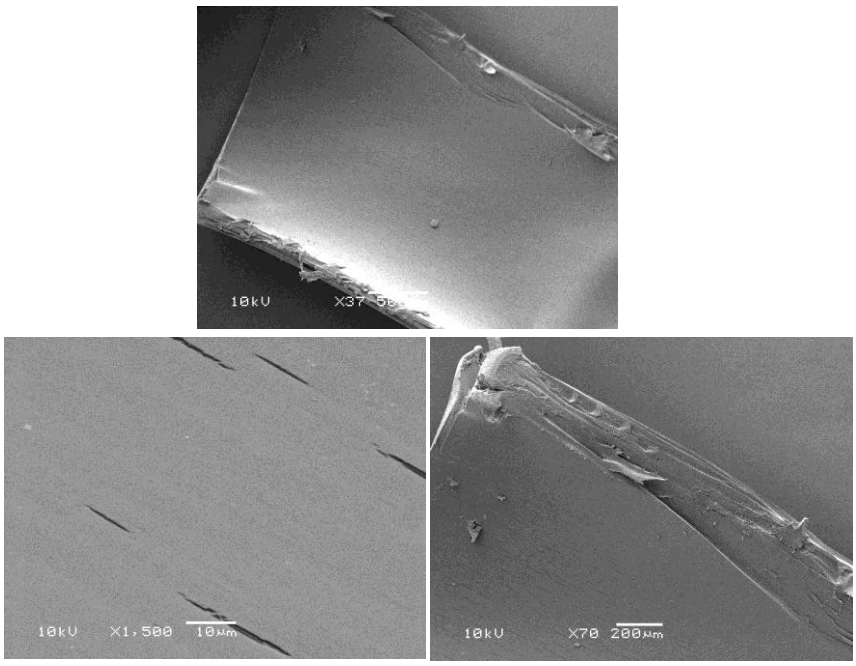


Figure 3.4 SEM images showing the luminal surface of the die-drawn polymeric tubing at various magnifications.

The topside of the polymeric tubing (extrusion or oriented) in the figures above show stress fractures and extrusion lines in both images due to the manufacturing processes of the tubes. Stress fracture is a known defect that often develops during manufacturing processing[178]. The stress fracture lines in the die-drawn PLLA tubing are larger than in the extruded tubing presumable due to the additional manufacturing step of the die-drawn tubing and could have been formed during sample preparation (cutting open the stent and opening it flat).

A scaffold pattern was formed in the deformed (oriented tubing) by laser cutting. The surface morphology of the laser cut scaffold was investigated using low vacuum SEM, as shown in Figure 3.5.

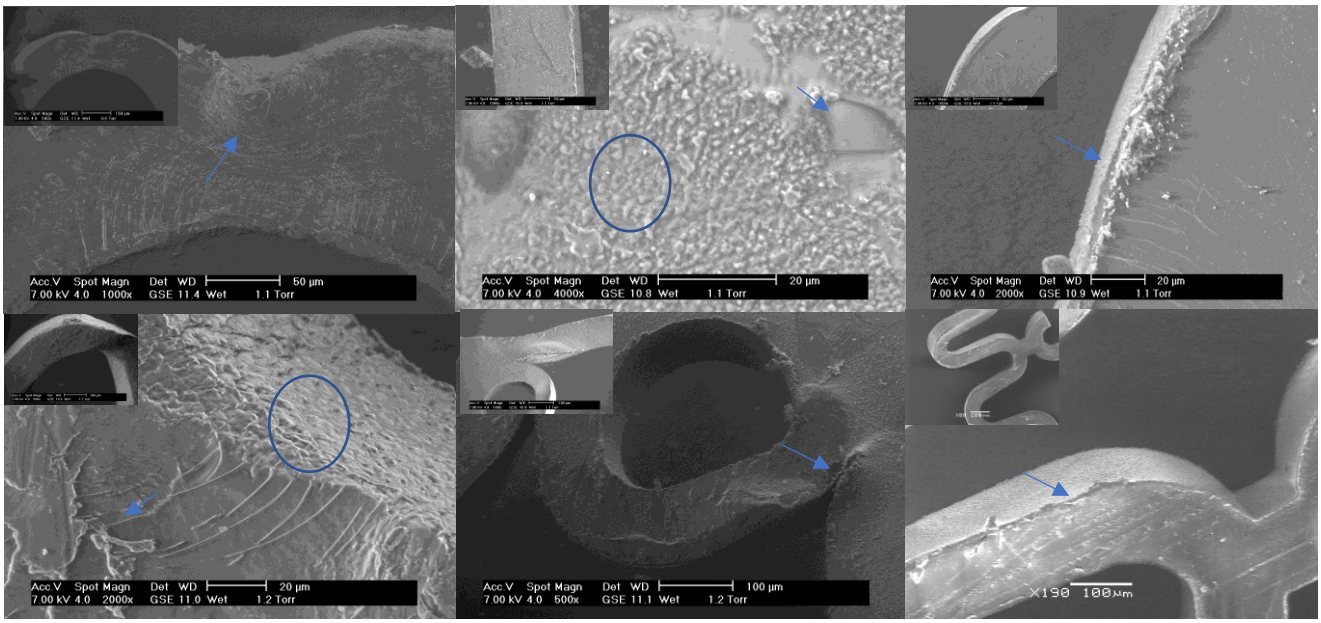


Figure 3.5 SEM images of the abluminal surface for uncoated laser cut polymeric stents (8 crowns design), using different laser cut parameters. Blue circles highlighting Diamond-shaped voids and blue arrows refer to heat affected zones. Blue arrows refer to melted areas and blue circles small voids.

The images in Figure 3.5 show formation of melted areas on the side walls of the scaffold, as highlighted by the blue arrows. These melted areas are presumably heat affected zones. A heat affected zone in a target substrate is unfavourable for a number of reasons[179]. This heat can produce thermal distortion and roughness at the machined surface (roughness of the coating surface will be discussed in AFM section). The heat can also change properties of a polymer such as degradation rate and mechanical properties, also causing chemical degradation which could have an influence on the degradation rate[179]. Change in the mechanical properties may lead to non-uniform distribution[124]. Upon crimping, diamond-shaped voids form in the scaffold. There is still considerable ambiguity with regard to these features[180]. These features are highlighted in Figure 3.5 (blue circle). The diamond shaped voids are believed to be present in a deployed U crest of laser cut scaffold. Once a stent is deployed the inner bend is placed under tension. This event does not cause the stent to fracture, despite the brittle property of PLLA, instead a diamond shaped features form in the scaffold , these features are not observed in metal scaffolds[181]. Reports in the literature indicate that the deformation of

diamond shaped voids along the PLLA scaffold is associated with the semi-crystalline morphology and orientation of chains in the polymer[19,182]. It can be seen that the cutting process is connected to melt shearing and vaprisation[181]. Consequently, it leads to the formation of a heat-affected zone and the re-solidification of molten material on cut edges.

Luminal surface morphology of laser cut scaffold will be described in Appendix A.

3.4 Physiochemical Characterisation of the Polymeric Tubing by AFM

3.4.1 Surface Imaging

Surface topography analysis was carried out using AFM, which can, for example be used to investigate drug distribution within a coating layer and any degree of separation of block copolymers such as PDLLA[183].

Primarily, AFM was used to characterise the surface of bare PLLA tubing (extruded and orientated) before investigating the final medical device (ArterioSorb™). PLLA can be crystallised by slow cooling from melt, annealing at various temperatures above glass transition. PLLA are known to crystallise by chain folding, making lamellae perpendicular to the chain axis and thickness of the order of 10–30 nm[184]. Studies carried out by Vasanthakumari *et al*., on crystallinity of PLLA have shown that the kinetics of melt crystallisation of polymer are moderately slow as compared with other semi-crystalline polymers therefore, the potential to impact its crystallinity using laser processing[185]. In this study, we focused on the AFM height and phase images, where AFM imaging revealed that the PLLA presents a relatively homogenous (in terms of properties) surface on the tubing. The stripped lines observed in Figure 3.6 were caused by a high set point voltage, therefore resulted in surface damage produced by AFM probe. In such AFM phase images bright and dark areas were observed and these areas relate to regions of different tip-sample interactions[186], in this case the observed contrast is believed to primarily related to topographic effects causing changes in tip-sample contact area. Tapping mode phase images hence indicate a homogenous surface in terms of surface

composition. The difference in roughness (Figure 3.6) due to the release of residual stresses imposed by the manufacturing processing during the final stage of the solvent evaporation [187].

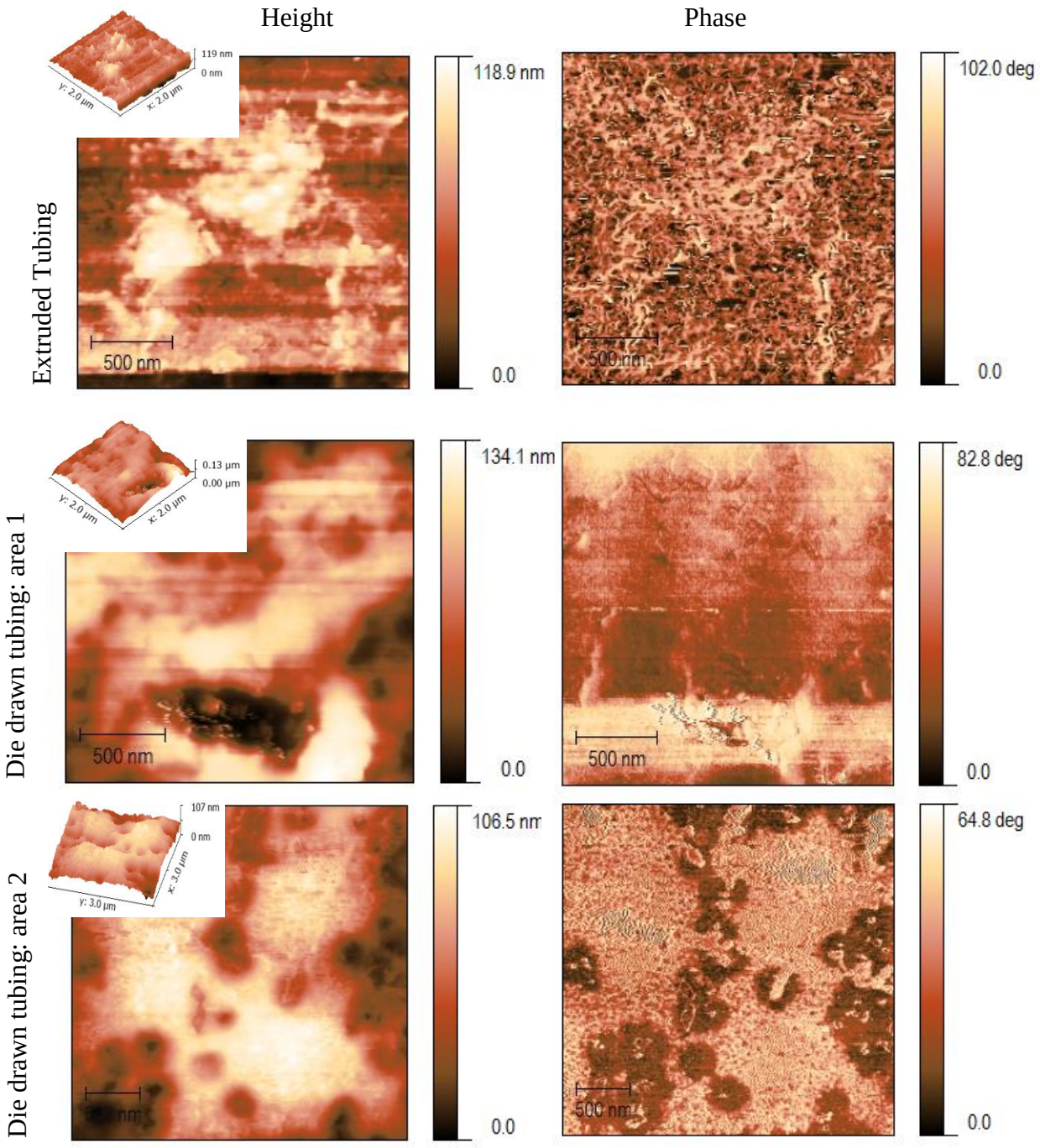


Figure 3.6 AFM Topography and phase images in tapping mode (in air) of the abluminal extruded and die-drawn PLLA tubing. Extruded tube shows roughness

of 13 nm, whilst die-drawn shows roughness of 17 nm and 15 nm. Blue arrows indicate extrusion lines.

Analysis of the laser cut scaffolds were obtained on several areas using tapping mode. The nature and mechanical properties of features observed in Figure 3.7 will be investigated later in Chapter 4. The laser cut surface shows to be dominated by fibres and spherulite features. Another characteristic of the laser cut samples is the presence of pits on the PLLA scaffold surface (Figure 3.7, area 3). The shape of these pits varies from round to elongate. These features may have originated from either the condensation of material from the laser induced plume or heat associated during the laser cutting process, where the laser melts materials to form pit like features. Previous studies established the significance of using multiple pulses in designing pattern in a polymeric material with femtosecond lasers. Surfaces patterned with multiple pulses proved clean cutting with little or no melting[188].

AFM phase images are related to tip interaction and can be modelled as the amount of energy the tip loses to the surface. The loss in energy could be due to adhesion to on the surface, therefore the tip of the cantilever gets trapped and loses energy. Another reasons could be due to sample being soft which thus indents further, leading to an increased surface area of contact. Changes in tip-sample interaction could be due to topography contact area change.

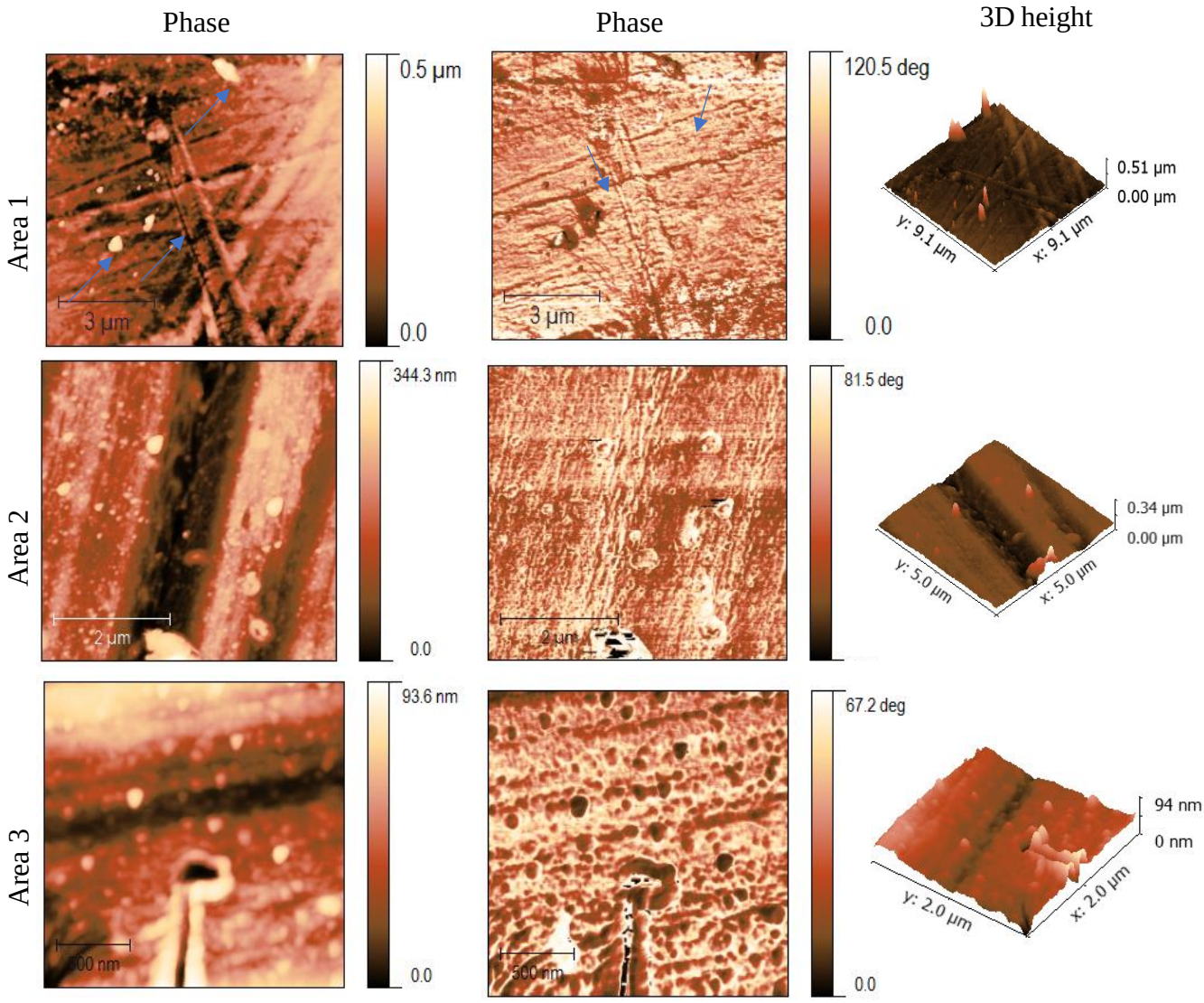


Figure 3.7 AFM topography and phase image in tapping mode (in air) of the abluminal surface of uncoated laser cut scaffold. Left: height image, middle: phase image. Right: 3D height image. Area 1 shows roughness of (27.5 nm), area 2 (23 nm) and area 3 (10 nm). Blue arrows indicate extrusion lines.

The lines on the uncoated tube might be related to the extrusion process. Hence this related to structural heterogeneity on these samples and not mechanically homogenous. Laser cut processing promotes formation of amorphous materials leading to the formation of pits and fibres on the surface of the coating.

3.4.2 Thermal Bulk Characterisation by DSC

DSC was performed to examine the level of crystallinity after the extrusion and orientation processes. DSC was helpful in determining the melting temperature (Tm) and glass transition temperature (Tg)[189,190] .The degree of crystallinity can be influenced by many factors such as cooling rate, additives, and polymer type. Cooling the polymer more quickly could form fewer crystals. Additives could either increase the degree of crystallinity or disrupt the formation of the crystals leading to a low degree of crystallinity[191].

Figures 3.8, 3.9, 3.11 show the DSC traces for pure extruded PLLA and die-drawn. Extruded polymer tubes made of semicrystalline polymer and may have variable crystallinity. The degree of crystallinity effects the thermal and mechanical properties of PLLA materials. The crystallization of a molten polymer is proposed to occur by growth and nucleation processes. Upon cooling through the melting temperature nuclei form in which small regions of tangled and random molecules become ordered in a more regular manner[192]. Gada *et al*., reported extruded tubes resulted in a crystallinity of 17-24 %.

Extruded tubing shows crystallisation peak at around 100 °C, whilst this peak is not present post orientation. The thermal phase transitions could be affected by the sample size. The extruded tube was thicker and easier to handle than oriented PLLA tubing. The size of oriented PLLA tubing was different to those measured for extruded tubing. This difference in sample size might lead to the different ranges of the Tg and crystallinity. During the measurement process, extruded materials recrystallise as they are heated up, this might be due to low crystallinity. The process of PLLA orientation could enhance the molecular orientation along the drawing direction, therefore the crystallinity of PLLA could be improved via orientation process[193].

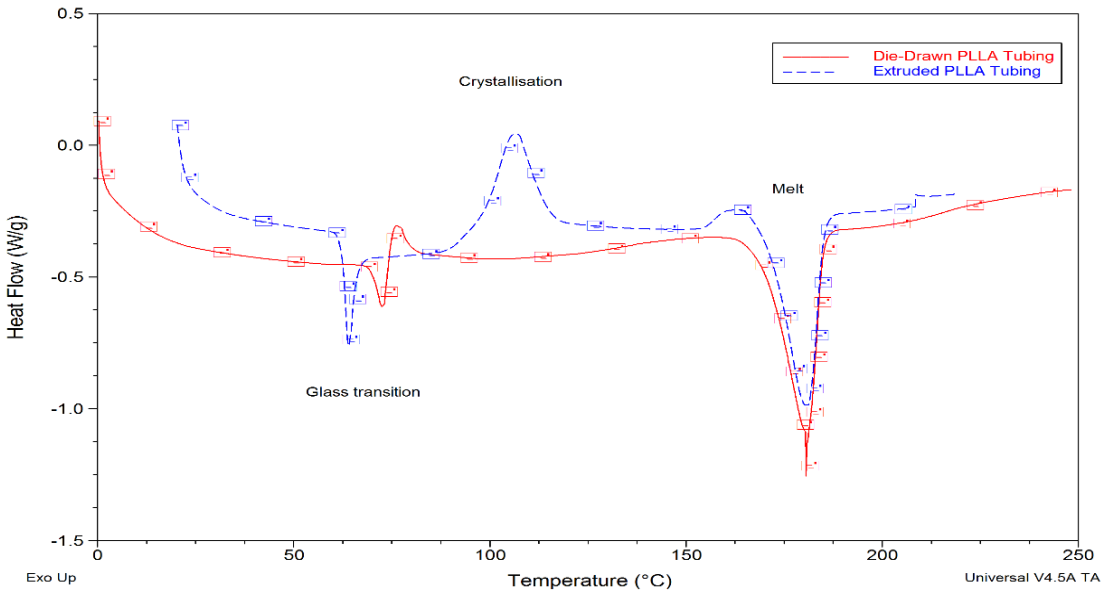


Figure 3.8 DSC thermograph of extruded (blue) and die-Drawn (red) PLLA tubing. The first peak is the Tg and second peak (extruded tubing) is the crystal dehydration temperature and melting temperature for both polymeric tubing is at 170 °C.

It should be noted that an overshoot in the DSC trace was initiated by enthalpy relaxation, this occurrence is dependent upon the thermal history of a polymer. The higher Tg for the die-drawing tube suggests modification has been made which may be due to the raised temperature at which the tube was exposed to during assessment and from strain induced crystallisation during the die drawing method[51]. The exothermic peak decreased with increasing crystallinity, thus no exothermic peak could be observed for the fully annealed specimens (specimens with around 40% crystalline content). The degree of crystallinity affects the water uptake and the degradation kinetics, as a consequence having an amorphous region on the stent coating (PDLLA) offers a good mobility and accessibility to water molecules, thus degradation occurs at higher rate. PDLLA was used for better drug delivery application[194].

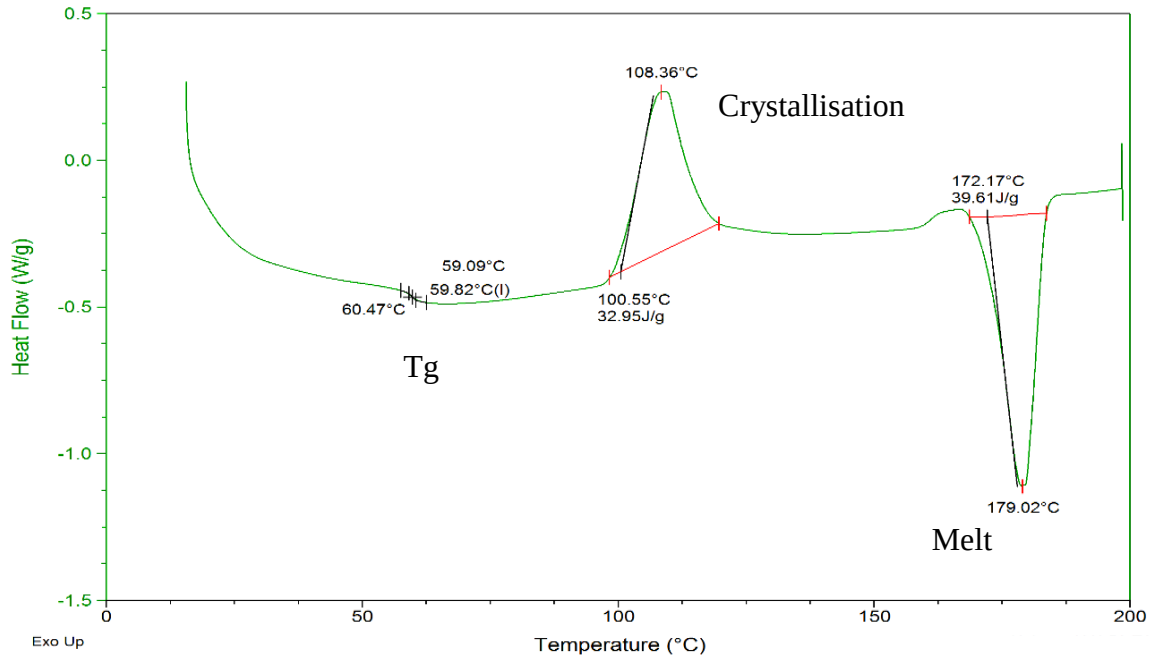


Figure 3.9 DSC thermograph for extruded PLLA tubing (heating rate 10 °C/min).

The step change that occurs at 55-60 °C relates to the glass transition temperature (Tg) of the polymer. The temperature at which the polymer experiences transition change from rubbery into rigid form is known as Tg[195]. The DSC traces above confirm that the samples are not amorphous as there is cold crystallisation temperature (Tc), i.e., crystallisation on heating above the Tg and melting point (Tm), thus confirming the crystallinity nature of the polymer. Amorphous materials do not have a melting point, but they continue to soften more until they behave more like a liquid. Crystalline structure forms when molecules have enough kinetic energy to form crystal growth[196]. Crystallinity content (X) has been evaluated according to the following equation:

Equation 3: $X\ \% = 100\ (\Delta Hm - \Delta Hc) / \Delta H0m$

Where ΔHm and ΔHc are the melting and crystallisation enthalpies and ΔH0m is the reference ΔHm (93.6 J/g) for PLLA. X% = 100 (39.61-32.95)/ 93.6 = 7.12 %.

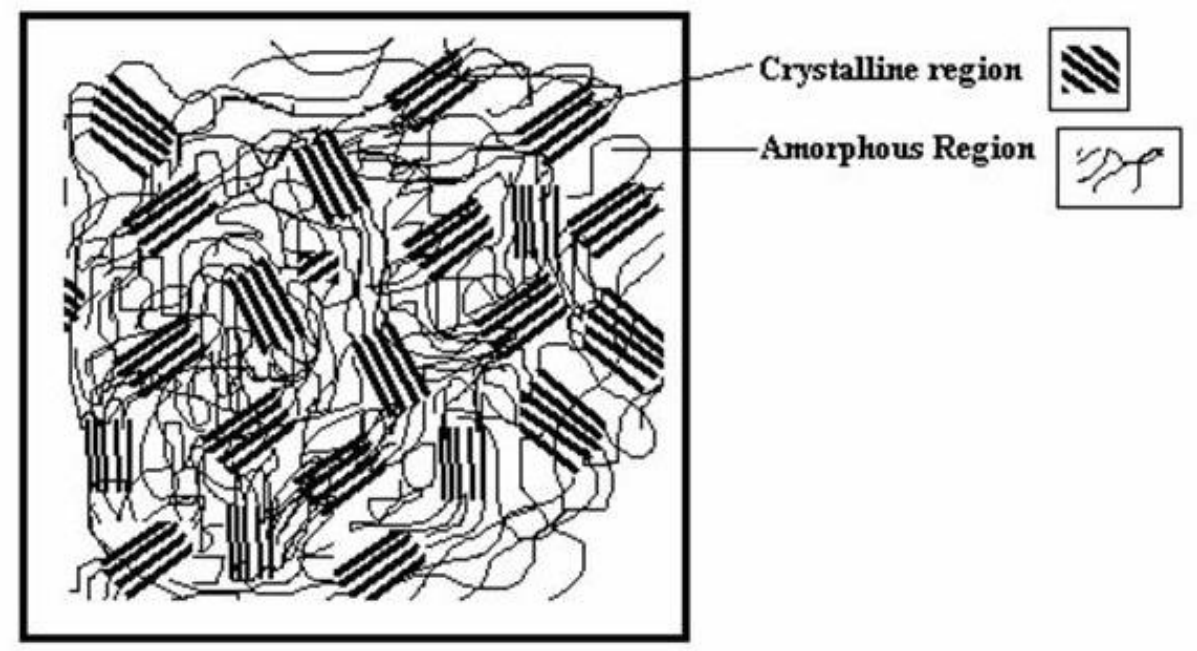


Figure 3.10 Schematic of amorphous versus Crystallinity.

The DSC thermograph for both extruded and die-drawn PLLA tubing show two distinctive thermal transitions. First, the glass transition with an onset temperature of 56 ˚C and the second transition is crystallisation upon cooling from the polymer melt[197]. The glass transition occurs in amorphous and semi-crystalline polymers and happens due to a reduction in motion of large segments of molecular chains.

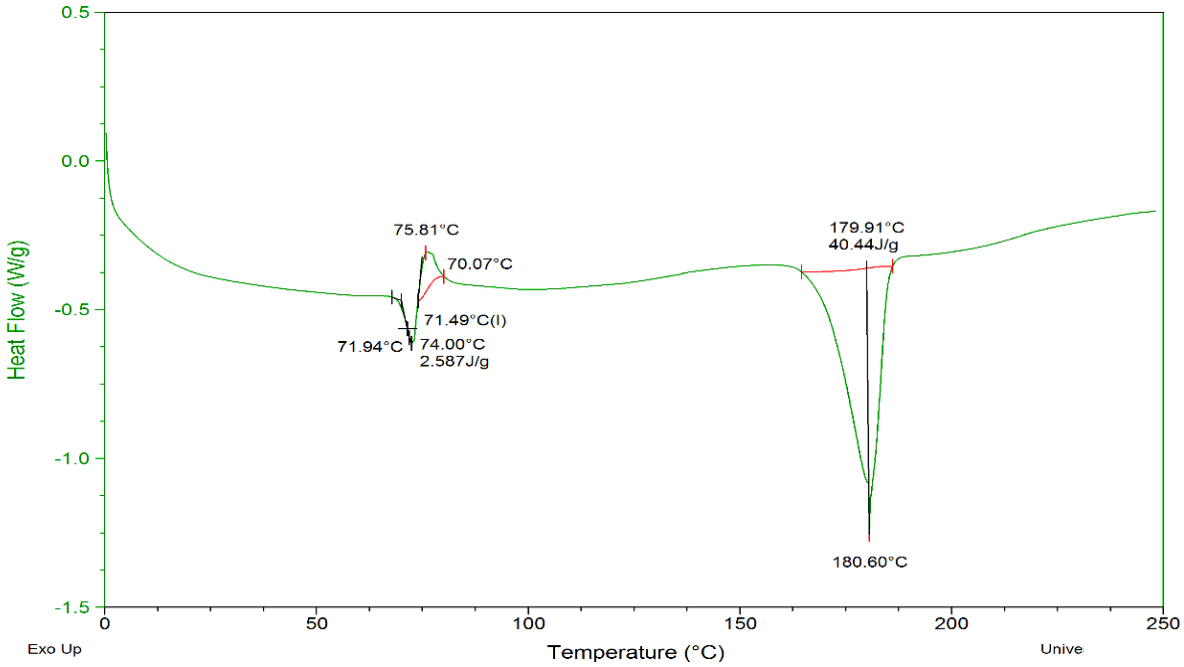


Figure 3.11 DSC thermograph for supplied orientated PLLA tubing (die-drawn). Measurements were registered at (heating rate of 10 °C/min) in nitrogen atmosphere. The first peak is the Tg and the second peak represent the melting point at 179.91 °C. PLLA crystallised at 108 °C, which is attributed to cold crystallisation. X% = 100 (40.44-2.587) / 93.6 = 40.44 %.

Both DSC curves for the homopolymer PLLA indicate a single endothermic peak at about 170 °C, which is in a good agreement with previous studies[198,199]. The crystallisation behaviour was monitored during the cooling process. With a melting point of at 179 °C, the melt crystallisation temperature (Tc) appeared at 75 °C. Overall that die-drawn PLLA sample displays a higher percentage of crystallinity than the extruded PLLA[191]. The control over crystallinity in these materials is very essential as it allows for constant modification for drug release profiles[200]. It was reported by Arterius Ltd the crystallinity and Mw of laser cut samples stayed similar (data not shown)

3.5 Surface Thermal Characterisation

3.5.1 Nano Thermal Analysis by AFM

Thermal properties of the PLLA samples have been studied using nano-TA technology. whereby a standard AFM probe is replaced with a micro fabricated-probe heater[201]. This method was used to reveal spatial distribution of components based upon their local thermomechanical properties[202]. Nano-TA used to map the thermal properties of PLLA and to carry out localised thermal analysis on particular points of the surface. This technique combines the high resolution imaging potentials of AFM with the capacity to characterise the thermal properties of PLLA samples[163].

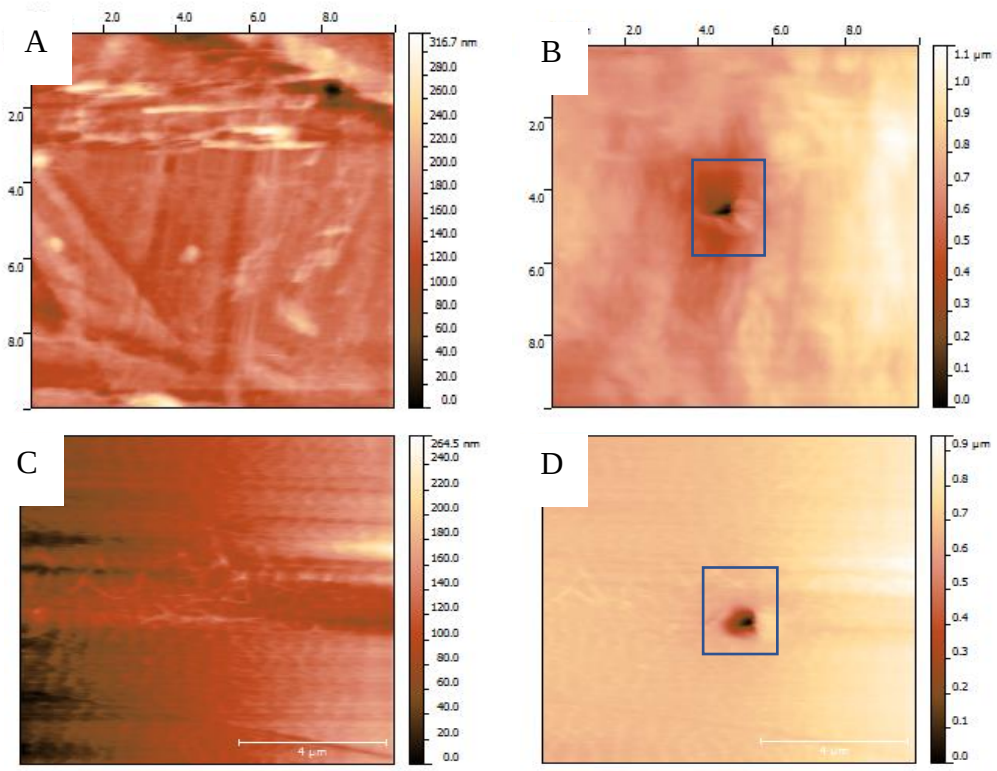


Figure 3.12 AFM images in contact mode of extruded and die drawn PLLA tubing before and after NTA measurement. A.: height image of extruded PLLA before thermal analysis. B. height image of extruded PLLA after NTA. C.: height image of die-drawn PLLA before thermal analysis. D. Height image of die-drawn PLLA after NTA.

Figure 3.12 shows that the surface of the extruded PLLA is homogenous. However, after the nano-TA tip was heated to 250 °C an area of localised damage can be seen (hole) highlighted in Blue Square (Figure 3.12). The processes that occurred during this measurement were monitored using the cantilever deflection[203] allowing the local surface melting (or softening) point of the PLLA samples to be obtained.

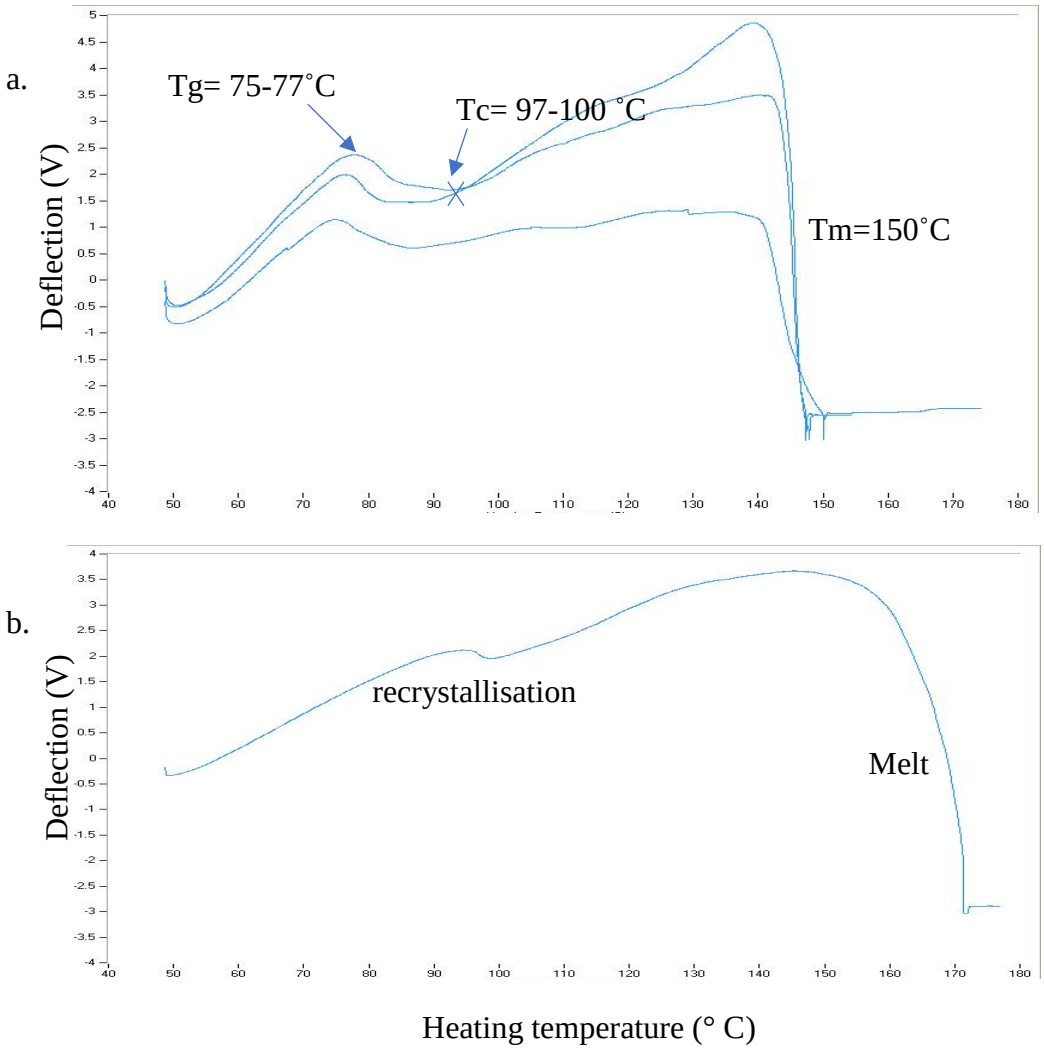


Figure 3.13 Nano-TA AFM curve of a. Three local analysis plots of the abluminal extruded PLLA using nano-TA AFM. The measurement was done on same sample however, three different locations about 100 nm apart, and b. die-drawn PLLA showing its transition phase, where sample melted at 170 °C and a hydration process occurred at around 95 °C.

The data in Figure 3.13 have confirmed that the extruded PLLA has a melting point of approximately 150 °C. The first peak is related to the glass transition at a temperature of 75 °C, crystallisation temperature at approximately 97-100 °C, and the final peak is the melting point of the sample at 150 °C. Different transitions observed for PLLA tubing suggesting changes in the thermal properties of samples post extrusion. Melting temperature of PLLA decreases with the presence of PDLLA[204,205].

PLLA has a bulk Tg varying from 50 to 80 °C[206].The exact melting point of the polymer depends on the processing conditions, the stereochemistry of the polymer, the molecular weight of the polymer has an impact on the Tg. The three main transitions observed in Figure 3.13 confirms presence of fibre features that were observed in the AFM, these features are generated from molten PLLA which solidified into crystalline and amorphous state. Supposedly the sample was presented with a single transition, then it would imply the presence of crystallinity and low level of amorphous which is not high enough to be detected by nano-TA. i.e. laser cutting increases the amount of amorphous material (data of laser cut scaffold will be discussed in Chapter 4).

3.5.2 Micro Thermal Analysis (µ-TA)

Micro-thermal analysis by scanning thermal microscopy is being used progressively for the analysis of pharmaceutical dosage forms. Nevertheless, there is not a great evidence to show that µTA data can compare directly with established approach of DSC[207]. The SThM thermal probe was used to transfer heat into the surface of the PLLA; upon heating the surface starts to expand causing an upward deflection of the probe then once melted the deflection signal drops downward.

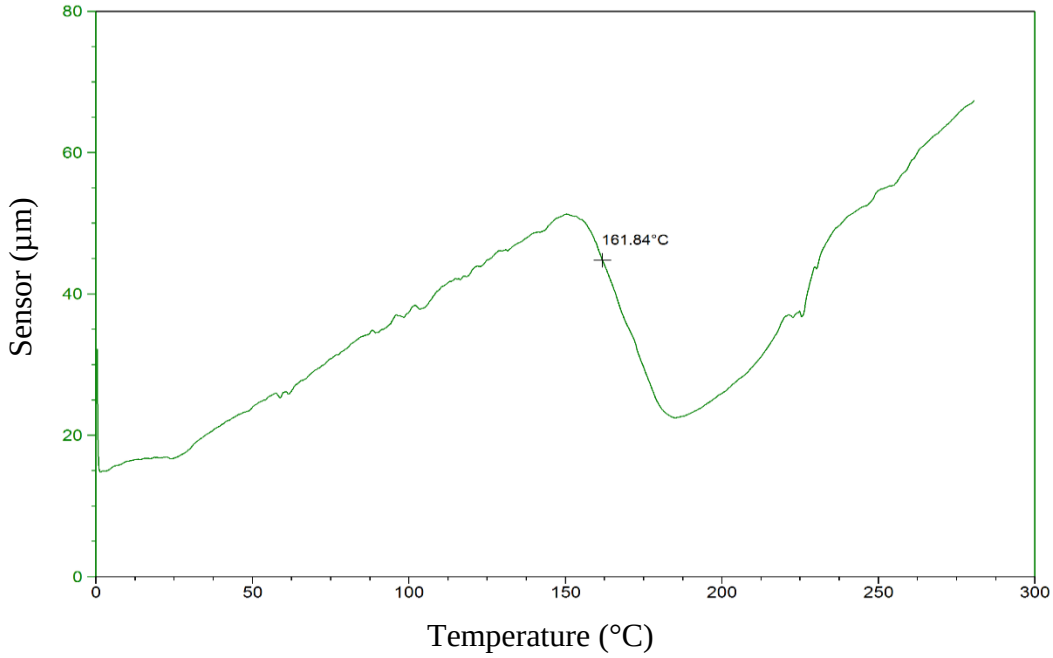


Figure 3.14 SThM local thermal analysis plot of extruded PLLA tubing. Heated from 0 to 280 °C; at 2 °C/s upward and 25 °C/s downward.

Both PLLA tubes yielded a melting temperature fairly close to each other, for the extruded tube it was at around 166 °C and for the die-drawn PLLA 162 °C. The transitions observed in the nano-TA system are not the same as the ones produced in the SThM. This is proposed to be due to differences in the heating rates of the techniques. Since the heating rate used in the nano-TA is below 10 °C/s, and for SThM 10 °C/min [207].

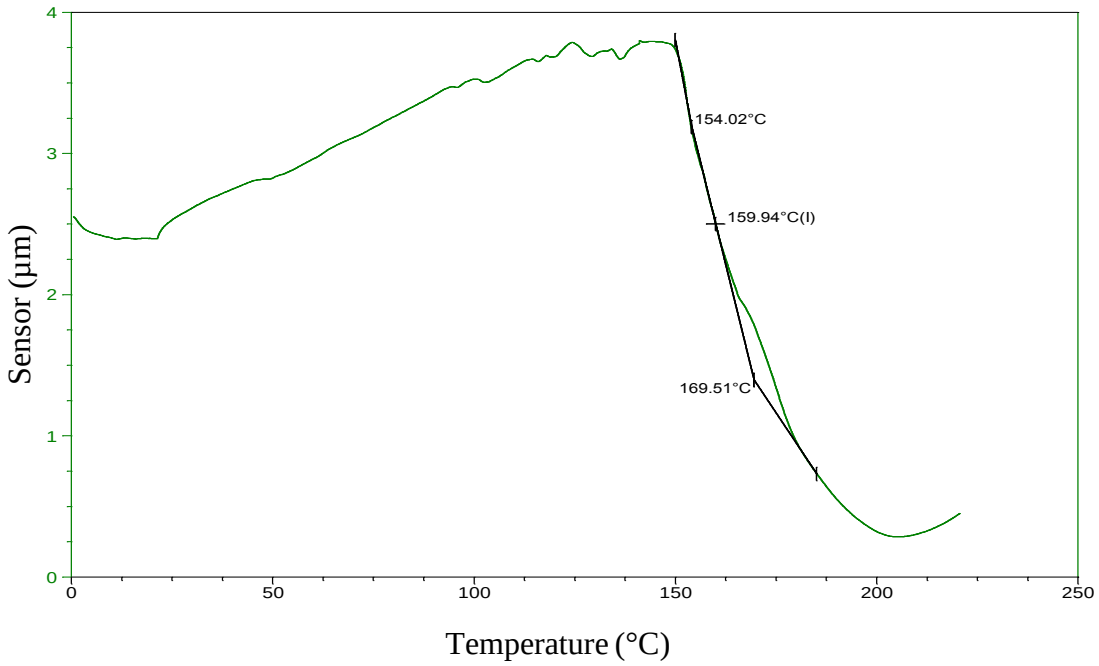


Figure 3.15 Localised thermal analysis (micro-TA) of the abluminal surface for the die-drawn PLLA tubing.

The tube was heated from 0-220 ˚C at 5.00 °C/s. There is a single transition observed which occurs at 169-170 °C (melting point), this implies that there are no granules, which can be induced by laser cutting, therefore the sample is semi-crystalline. The amount of amorphous fraction is not high enough to be detected by the microthermal cantilever. Only a single transition was observed in this sample (Figure 3.15). This observation suggest PLLA material is in the semi-crystalline state and the amount of amorphous fraction is not high enough to be detected by the cantilever.

3.6 Near Surface Chemistry by ATR-IR

IR spectroscopy can be used to verify the chemical characteristics of a polymer and the drug used in the preparation of the stent. IR has been used widely for the detection of crystal structure and conformational changes of the molecular chain[208]. Characterisation was first performed on the pure sirolimus and PDLLA as well as PLLA only and polymeric

tubing to obtain reference information before the latter analysis of the drug coated stent (ArterioSorb^{TM}).

PDLLA and PLLA are aliphatic polyesters with similar structures. The IR spectrum of the pure polymer is shown in Figure 3.16. The main IR peaks of the PLLA and PDLLA are ester bond stretching vibrations is situated at 1254 cm^{-1}, absorption at 1647, 1074, 963 and 709 are assigned to the aromatic bonds [209]. Absorption bands 2997-2965 (CH_2-CH_3), 1360-1450 (CH_3), 750 (CH), and 1759 (C=O) cm^{-1}.

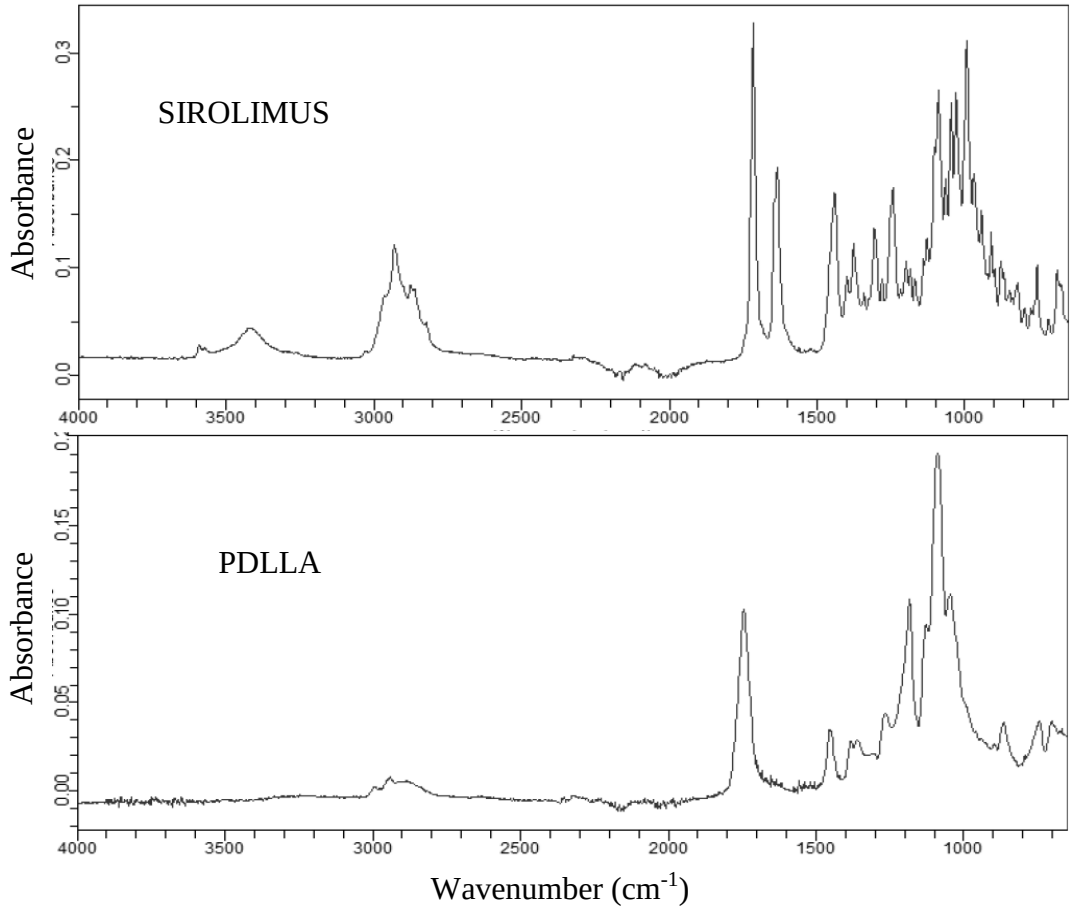


Figure 3.16 ATR spectra of powdered sirolimus and PDLLA respectively, these spectra used as referenced samples.

The ATR-IR spectrum of sirolimus (Figure 3.16) shows peaks at 3400, 2930, 1718 and 1634cm^1, which can be assigned to the stretching vibrations of O-H, C-H, C=O and C=O respectively. The peaks at 1443 and 1376 cm^{-1} are the asymmetric and symmetric C-H

bending vibration peaks, the peak at 1091 cm^{-1} is characteristic of C-N, and the peaks at 995 and 756 cm^{-1} are the out of lane vibration peaks of C=C and C-H, respectively.

Table 3.1 Band assignments of PLLA tubing in the range of 800 to 1500 cm^{-1}.[208]

Wavenumber cm^{-1}	**Assignments**	**Description**
1454	δ(CH3)	Conformation-sensitive
1209-1186	Uas(COC) + γas(CH3)	Inter-chain interaction
1267	Uas(COC) + δ (CH)	Conformation sensitive
956	Υ(CH3) + U (CC)	Amorphous specific
865	U (C-COO)	Crystalline specific

Strong absorption exists at 1750 cm^{-1} due to the existence of the abundant carbonyl groups in the bulk PLLA. The ATR-IR of non-laser cut tubing versus laser cut in Figure 3.17 shows no differences between laser machined substrate and the controls (extruded and oriented PLLA tubing). All spectra show the characteristic peaks of the polymer.

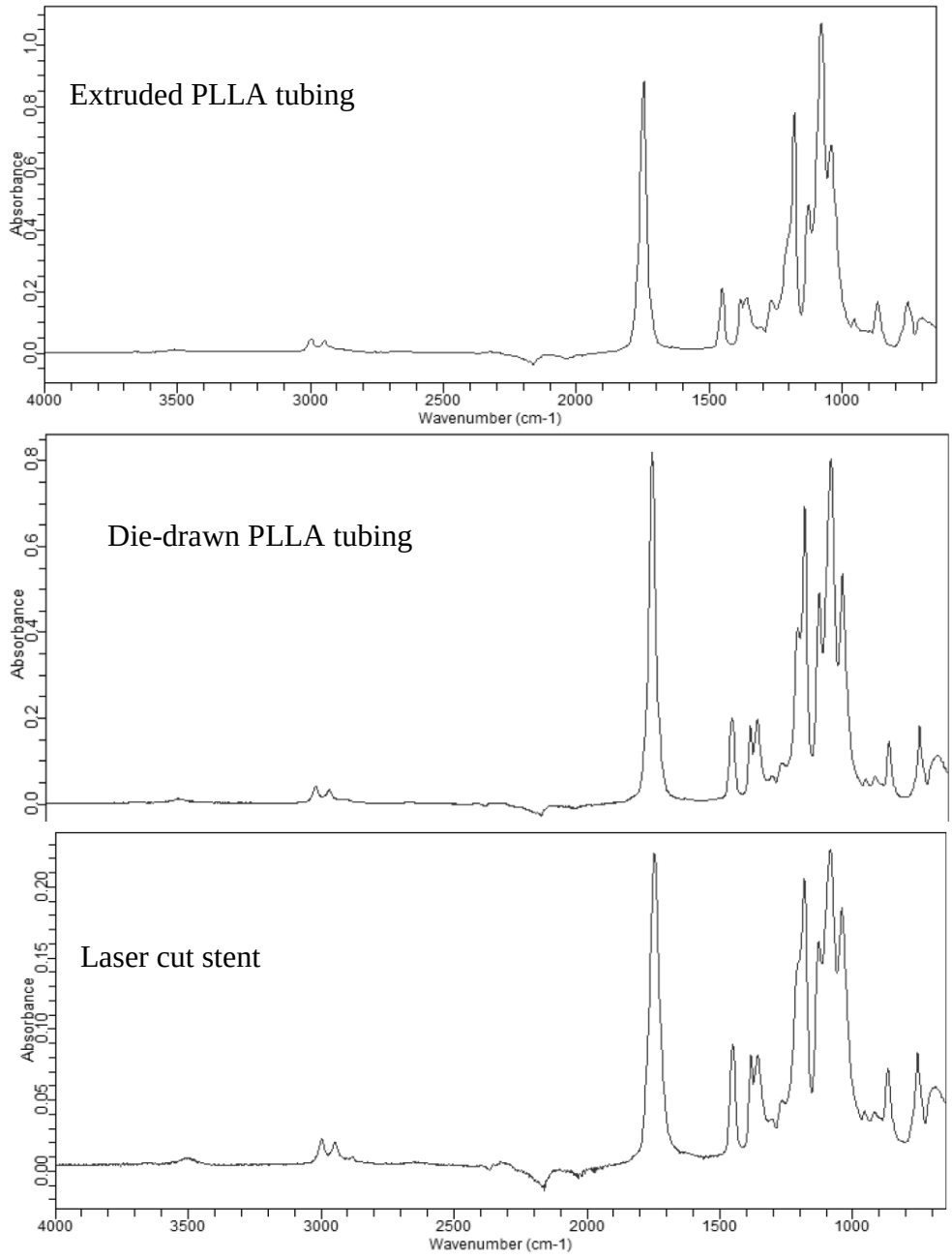


Figure 3.17 ATR-IR spectra for extruded, die-drawn PLLA tubing and laser cut uncoated polymeric stent from the region of 500 to 4000 cm^{-1}. The characteristic bands of the PLLA in the range of 1500-830 cm^{-1} and these bands are based on literature, Table 3.1 [208].

3.7 Surface Chemistry by ToF-SIMS

3.7.1 Surface Analysis

ToF-SIMS provides highly surface sensitive mass spectra to a depth of 1 to 2 nm, providing qualitative chemical information[210]. Both positive and negative polarities were collected and analysed, however positive secondary ions were established to be most useful for surface characterisation of polymeric tubing, due to having the best signal-to background which to achieve high contrast imaging[211]. Negative data are provided in Appendix C.

Table 3.2 illustrates the peaks established as most representative for the drug and the polymer. These characteristic ions were in agreement to those reported in the literature[211,212]. Secondary ion peaks for these diagnostic fragments are shown in Figure 3.18. These fragments are used for the characterisation of the stent during ToF-SIMS depth profiling.

Table 3.2 Positive secondary ions characteristics of the Drug and polymer materials.

Materials ID	Secondary ion	Mass (m/z)
Sirolimus	$C_5H_{10}N^+$	84.07
PLLA	$C_3H_4O^+$	56.03

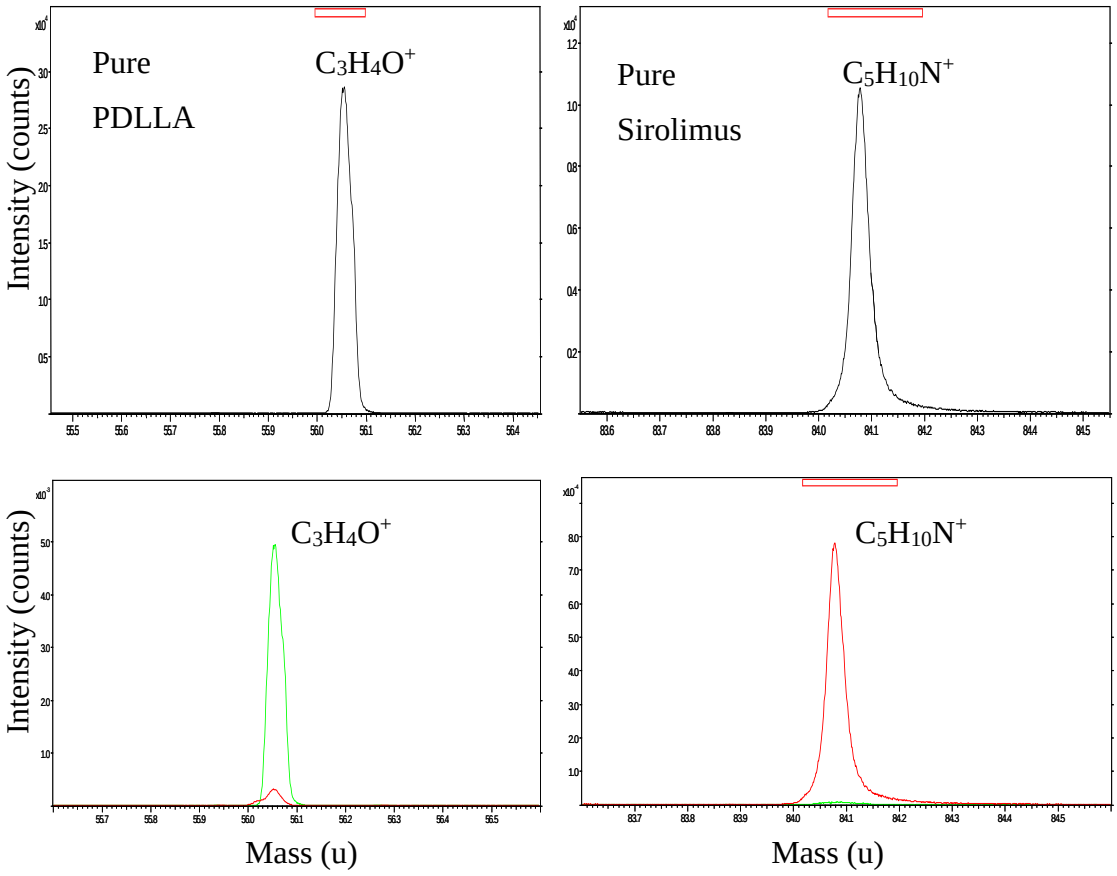


Figure 3.18 Positive secondary ion mass spectra of the diagnostic markers for powdered polymer and powdered sirolimus. PDLLA (green) at 56 m/z and sirolimus (red) at 84 m/z. The key m/z regions for the polymer (PDLLA) and sirolimus, $C_3H_4O^+$ and $C_5H_{10}N^+$ respectively.

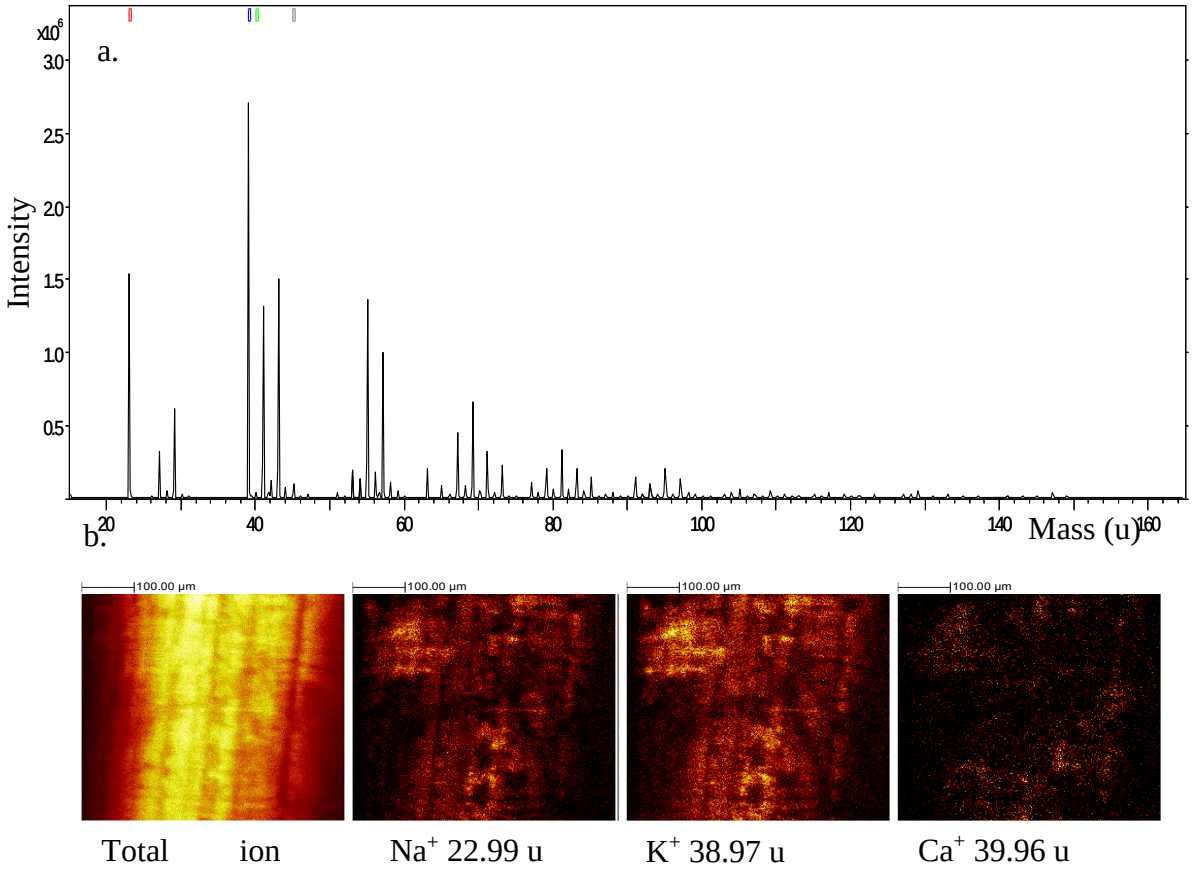


Figure 3.19 Positive ion intensity ToF-SIMS spectrum of the surface of a) positive extruded PLLA tubing and b) ToF-SIMS imaging of particular peaks identified in positive spectrum of extruded PLLA tubing from a mass range of 10 to 160. Calibration errors were kept below (10ppm).

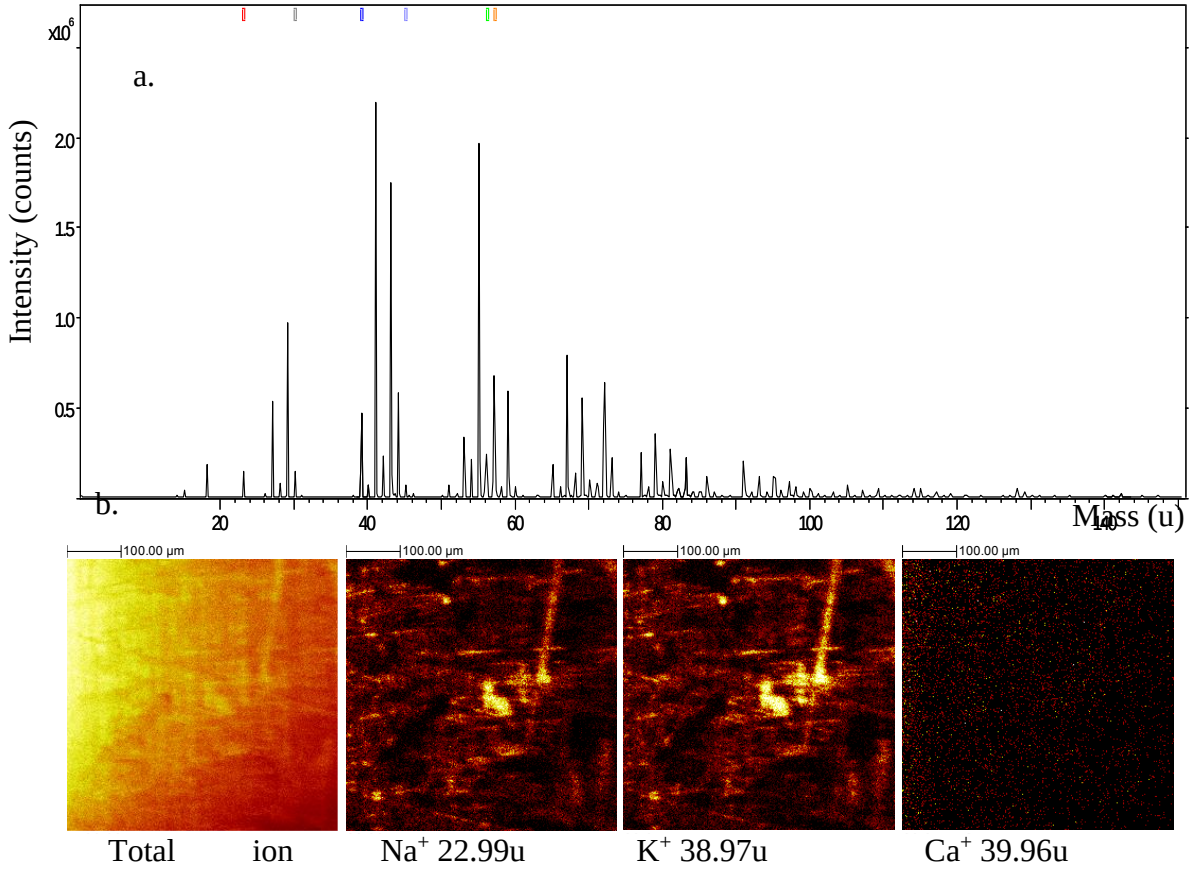


Figure 3.20 ToF-SIMS of a) positive secondary ions die-drawn PLLA tubing (b) ToF-SIMS imaging of particular ions identified in PLLA tubing. Calibration errors were kept below (10ppm).

Na, Ca and K were monitored as common surface contaminants. Spectra were calibrated using ions described in Table 3.3. The identity of the secondary ions assigned based on the lowest standard deviation, as compared by SurfaceLab 6.4 software. Some initial spectra of the starting materials are described in Appendix C.

T**able 3.3 Positive and negative ions used to calibrate ToF-SIMS spectra**.

Positive	Negative
H, C, CH, CH_2, C_2H_5, C_3H_7	O, OH, CN

3.7.2 ToF-SIMS Depth Profiling

Recent applications involving ToF-SIMS analysis of biomaterials have shown that much valuable chemical information below the surface can be probed by depth-profiling. In order to predict the depth distribution of diagnostic marks for the drug and polymer system, the sputter rate of the $C60^{++}$ source was calibrated using PDLLA/sirolimus spray coated polymeric tubing as well as actual stents. The rate was determined using ION ToF-SIMS software. The rate obtained from polymeric tubing was also compared with other studies, where the authors had used a spun cast film and sputter rate was established by dividing film thickness by the time required to reach 50 % of the silicon ions maximum intensity[213]. The depth profile was done on several samples to provide an accurate estimation of depth. Established sputter rate was used to determine the depth position of the drug and the polymer on the stent.

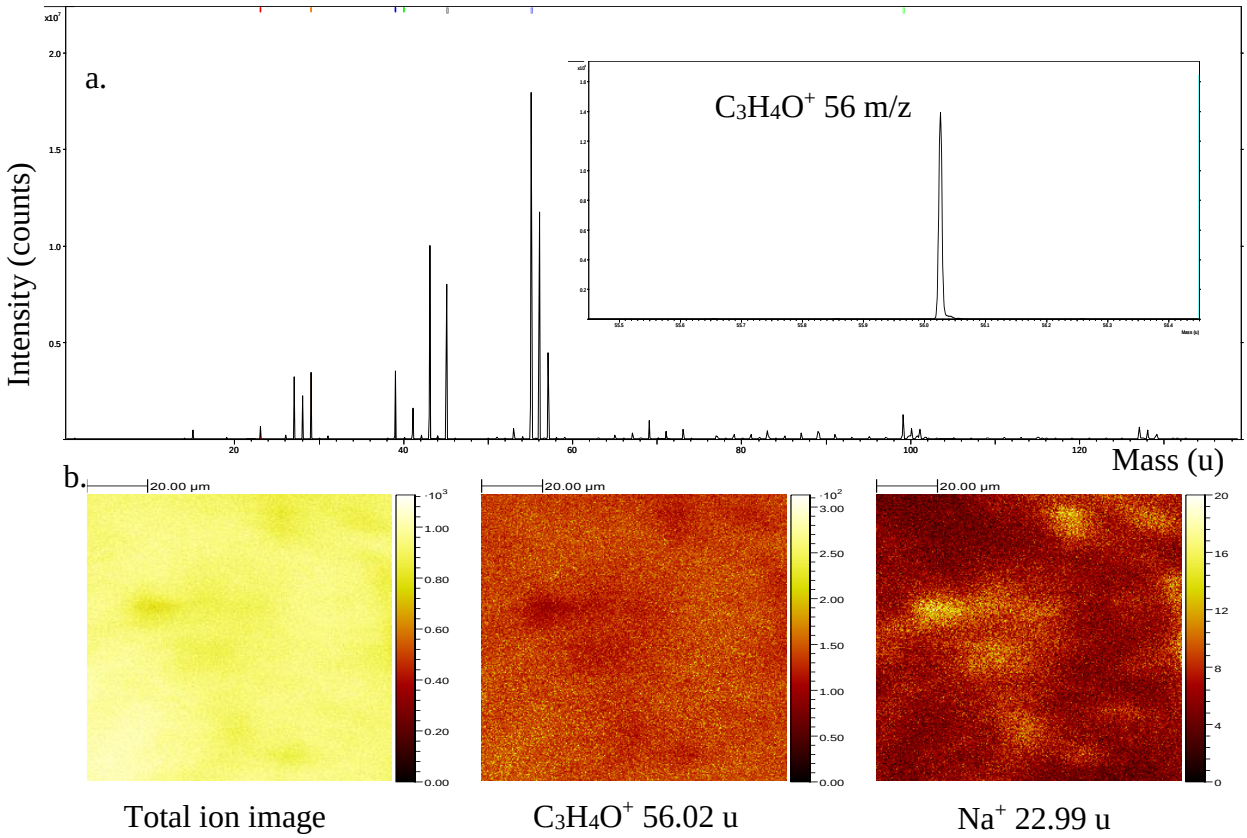


Figure 3.21 ToF-SIMS spectrum of a. Extruded tubing showing ions of significance for die-drawn PLLA tubing, in static mode, b. positive secondary ion distribution of the polymer as well as some common contaminant (Na^+). Poisson correction was applied on the polymer fragment due to saturation issue.

Using the characteristic ions highlighted above, the spectrum was reconstructed as images in order to understand the distribution of the PLLA. The highlighted peaks above were selected based on their relative intensities as well as the separation from other peaks.

For the depth profile work, only positive polarity was collected. Depth craters obtained from tubing were used to work out sputter rate in order to plot depth profile as a function of depth instead of time. This work will be further explored in Chapter 4.

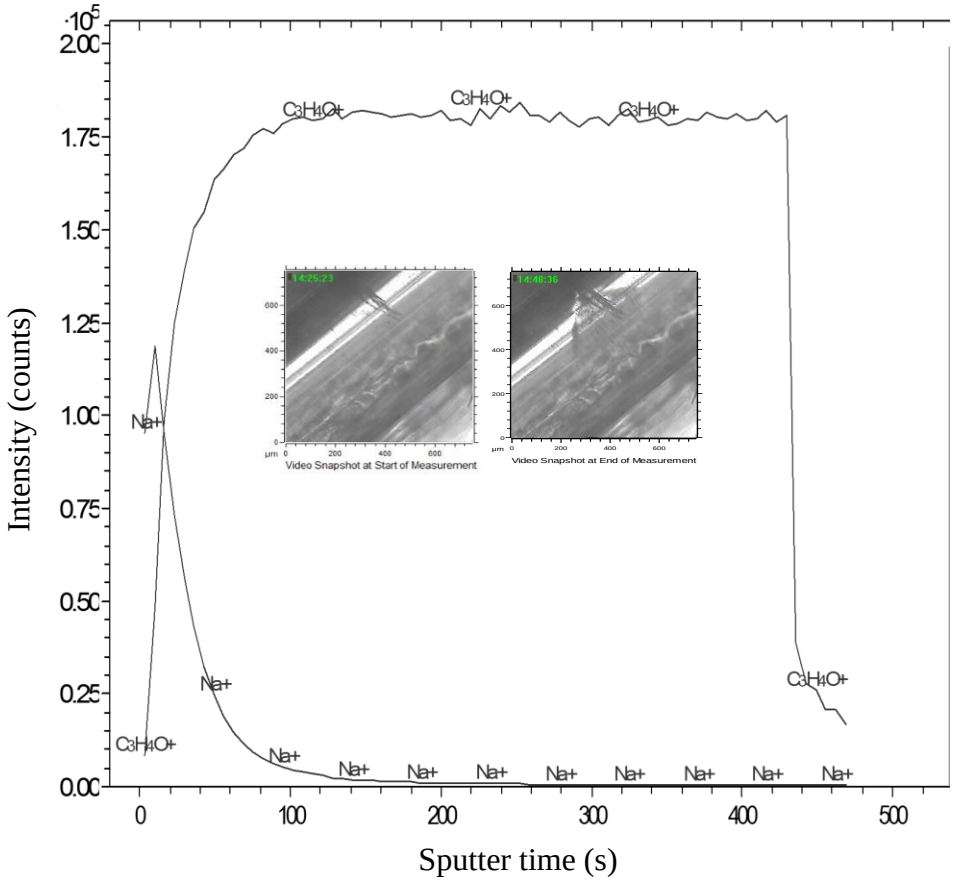


Figure 3.22 ToF-SIMS depth profile of abluminal surface of extruded polymeric tubing prior coating using Bi_3^+ ion beam analysis in conjunction with a $C60^{++}$ ion beam for sputter depth profiling. The experiment was performed under ambient conditions.

3.8 Elemental Composition by XPS

The surface composition of the tubing was determined by XPS. The detected elements that are present in the polymeric tubing by XPS are carbon and oxygen although other elements have been found at low levels such as silicon and nitrogen. Polymeric tubing prior to spray coating present three types of carbon bonding environment: C-O, C-C/(C-H) and O=C-O that correspond to their theoretical composition[214]. Table 3.4 illustrates the theoretical compositions of the materials and Figure 3.23 shows typical wide scan XPS spectra as well as high resolution spectra of the reference samples, powdered polymer (PDLLA) and drug (sirolimus).

Table 3.4 Theoretical composition for pure sirolimus and PDLLA. Sirolimus $C_{51}H_{79}O_{13}N$ - 1M Sirolimus=914.17 PDLLA $C_3H_4O_2$ - 1M PDLLA monomer unit= 72.

Description	at. % C	at. % O	at. % N
Sirolimus	78.5	20	1.5
Elemental Ratio	51	13	1
PDLLA	60	40	None
Elemental Ratio	3	2	

The spectra in Figure 3.23 shows peak intensities for C 1s, O 1s, and also highlights trace of nitrogen although it is difficult to see within the wide scan. The build-up samples were also analysed using high resolution scans of the important peaks, i.e. C, O, and N. The spectra show high presence of C 1s and O 1s in PDLLA and high presence of N in sirolimus.

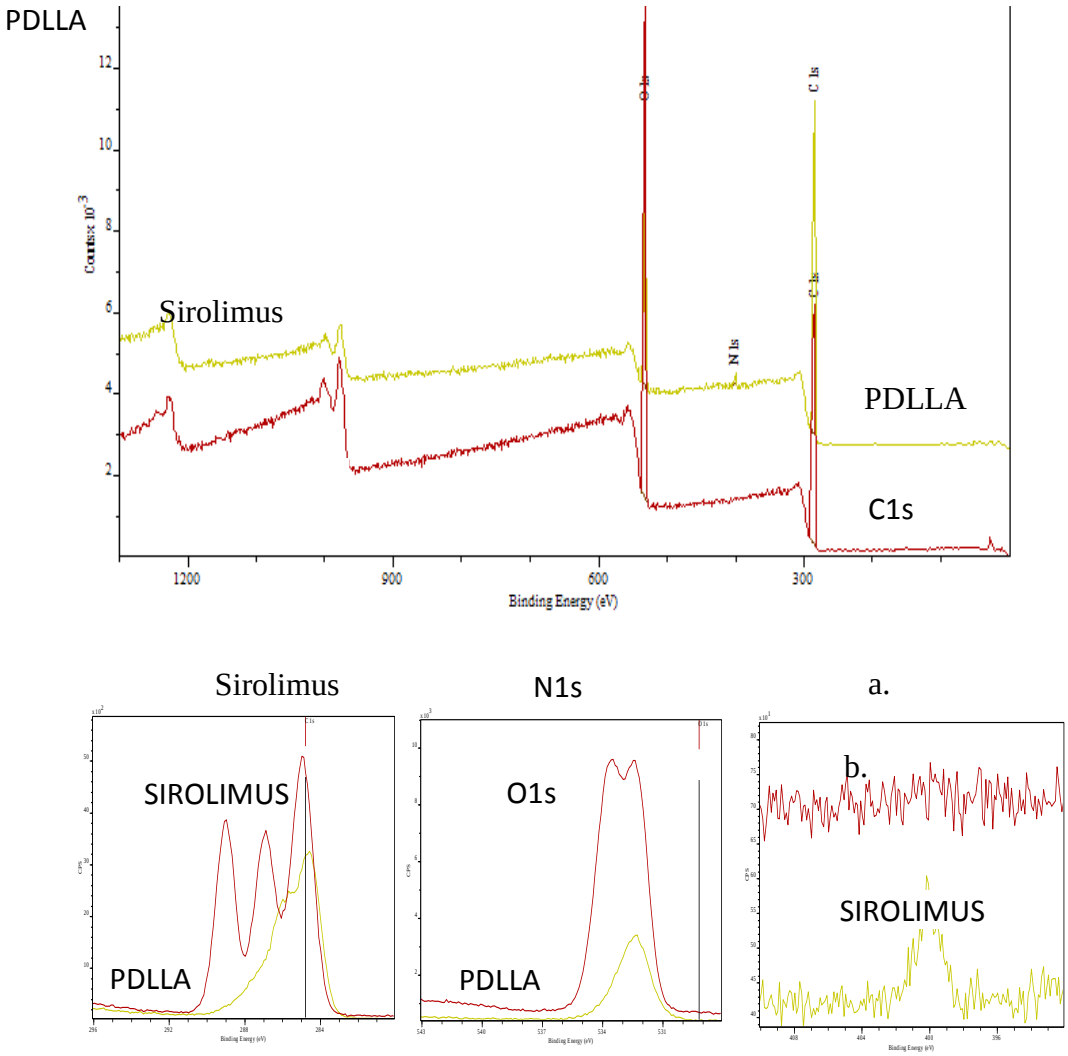


Figure 3.23 Overlaid XPS spectra of PDLLA and sirolimus, respectively, a. chemical composition spectra, and b. high resolution XPS component spectra showing the carbon, oxygen and nitrogen.

Figure 3.24 highlights the components within the C 1s envelope, which have been curve fitted using the Gaussian Lorentzian sum function[215], with chemical shifts relative to C-C, C-O and O-C=O for polymer and C=O for drug. All data sets were charge corrected to the C 1s peak at 284.98 eV. This was used as an internal standard for all spectra, to correct the binding energy shift due to charging. This correction was done for all elements

following a background subtraction or peak deconvolution to produce true binding energy values.

a. b.

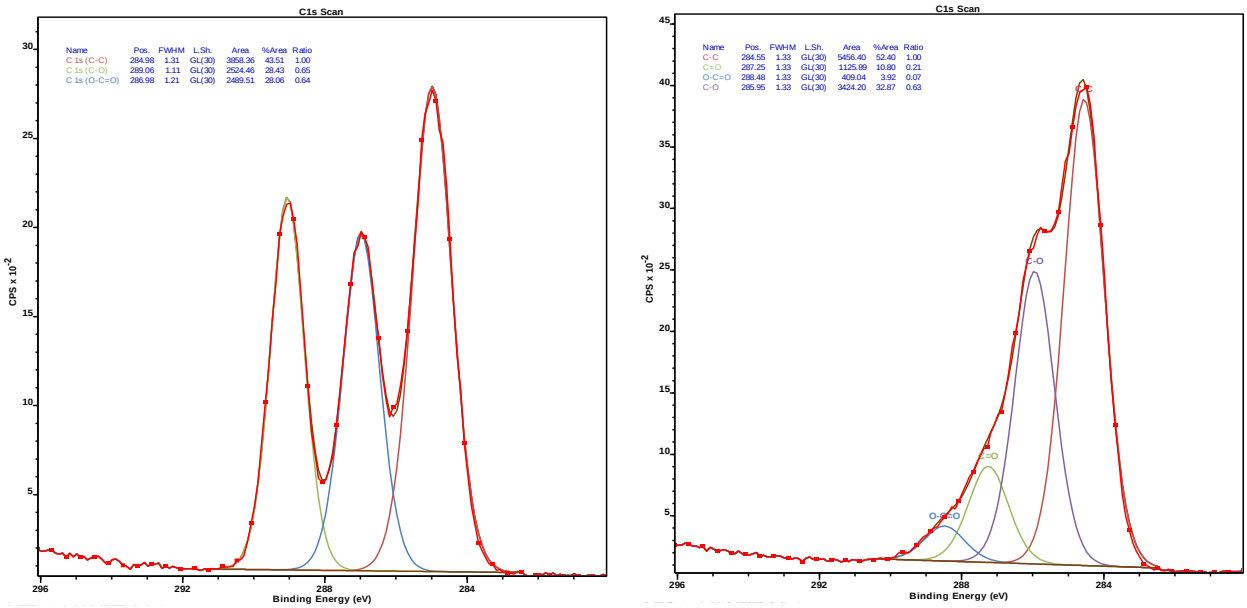


Figure 3.24 High resolution XPS spectra of a. powdered PDLLA and b. sirolimus showing the carbon region.

Carbon components for the polymer were found at 285, 287 and 289 eV and several carbon components peaks observed from sirolimus structure, where CN overlaps with C=O and CHO/R peaks, thus providing peak shape above.

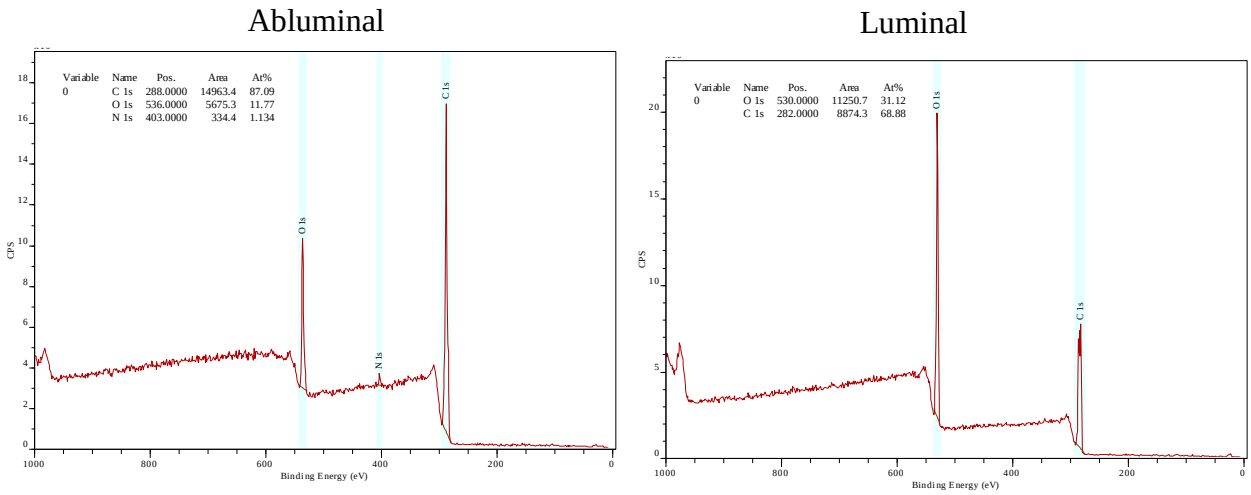


Figure 3.25 XPS spectra of abluminal and luminal surfaces of extruded PLLA tubing prior laser cutting.

Table 3.5 Atomic elemental % on the surface of extruded polymeric tubing prior laser cutting and drug spray coating. Atomic concentration is computed from the raw peak area divided by the relative sensitivity factor (RSF) parameter

Element	Extruded PLLA tubing: Abluminal (%)	Extruded PLLA tubing: luminal (%)
C 1s	87.09	68.88
O 1s	11.77	31.12
N 1s	1.134	0

The atomic composition of C1s on the abluminal and luminal side of the tube is slightly high, this value is considerably higher than the theoretical one (60 %), this can be due to deposition of adventitious hydrocarbons. The presence of N on the abluminal surface of the extruded tubing is presumably due to contamination.

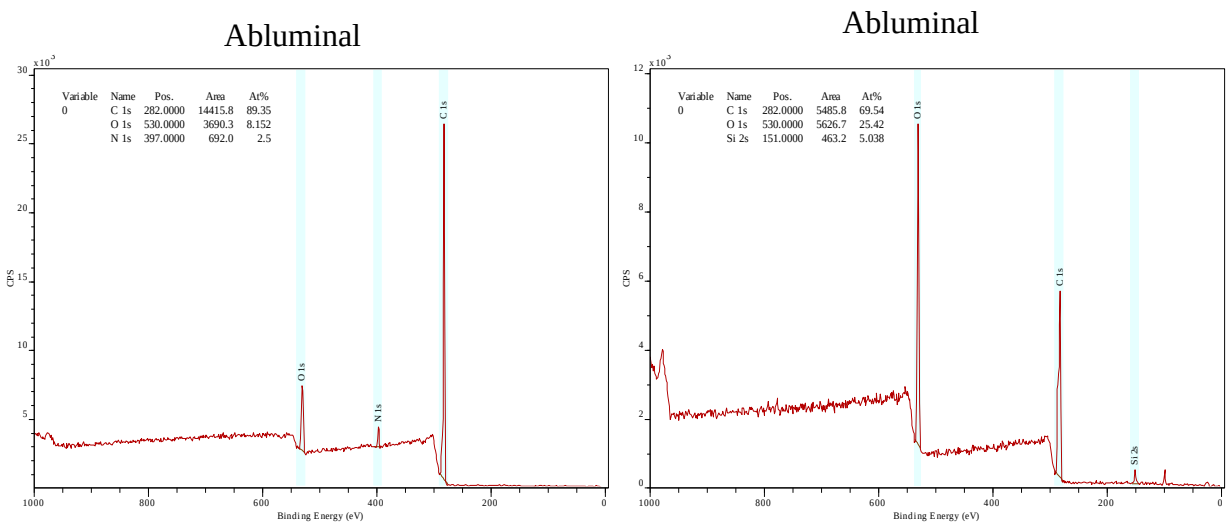


Figure 3.26 XPS spectra of abluminal and luminal surfaces of die-drawn PLLA tubing prior laser cutting.

Table 3.6 Atomic elemental % on the surface of die-drawn polymeric tubing prior laser cutting and drug spray coating. Atomic concentration is computed from the raw peak area divided by the RSF parameter.

Element	Die Drawn PLLA tubing: Abluminal	Die Drawn PLLA tubing : Luminal
C 1s	89.34	69.54
O 1s	8.15	25.42
N 1s	2.49	0
Si 2s	0	5.036

The C content for the die drawn tubing is even higher than the one in extruded tubing, this could be explained by the orientation process during the making of the tube. Nitrogen was observed on the abluminal surface of the tubing to be a common contaminant, as well as Si. Silicon might be another elucidation to the increase content of carbon at 285 eV. Polydimethylsiloxane (PDMS) molecules have two carbon atoms and one oxygen atom per silicon atom. We could recalculate the elemental composition of the tubing by subtracting the PDMS content to the carbon and oxygen, even by doing so the elemental composition of the carbon is considerably high suggesting deposition of adventitious hydrocarbons. Also, differences between theoretical and experimental atomic concentration could be due to polymer oxidation/ degradation or contamination during

experimental processing. The level of nitrogen increases post die drawing process. Traces of nitrogen level could be attributed to the handling of the samples, besides nitrogen is present in the atmosphere. Introduction of N trace might have happened during the deformation of the thermoplastic polymer tubing in the solid phase over a mandrel and through a die.

3.9 Conclusions

A series of extruded and die-drawn PLLA tubing were characterised before conducting further work on drug-loaded stents (crimped and expanded). SEM and AFM imaging revealed that the PLLA presents a homogenous surface. SIMS confirmed the general chemical homogeneity of the PLLA with evidence of some minor surface elemental contamination due to transfer of fluorine from packaging. The percentage of crystallinity of the PLLA tubing studied by DSC, in addition, the physical properties of these materials investigated using nano and micro thermal analysis. Data obtained though DSC and nano-TA are different, this difference is due to significant difference in heating rate. Attenuated total reflection infrared (ATR-IR) enabled us to assess the structure of PLLA, confirming the C=O, C-O-C and C-C peaks were visible at 1754, 1175 and 1200 cm^{-1}, respectively. ToF-SIMS employing $C60^{++}$ utilised to obtain in depth information from the PLLA tubing where sodium and nitrogen were found to be on the surface in small amounts.

The heat affected measurements taken from the laser cut scaffolds using SEM suggest that large areas of the scaffold struts are affected by heat propagation in laser cutting. Consequently, we believe that such scaffold have altered their mechanical properties in terms of the entire structure and hence the hydrolytic degradation process may vary from that of an untreated sample. Thus further research on biocompatibility and hydrolysis of laser-cut scaffolds should be taken into consideration. Taken together analysis conducted in this chapter, data showed that the manufacturing process such as extrusion and orientation, has shown an influence of surface morphology. Overall, the outcome of this study is a preliminary work to establish an understanding and knowledge on how these surface analysis techniques work.

4 DISTRIBUTION OF SIROLIMUS IN PDLLA COATING LAYER FROM THE ARTERIOSORB™ DRUG ELUTING STENT PRE-DISSOLUTION

Implantable medical devices are increasingly important in the practice of modern medicine. However, all medical devices to an extent provoke adverse reactions such as inflammation, fibrosis and thrombosis. Thus, to improve the function and the safety of medical implants, there is a need for a major development of materials that induce a desired tissue response without adverse reactions. In order for the use of bioresorbable stents in a clinical setting, they should possess the right mechanical strength, being able to endure the radial pressure applied upon the expanded stent when in the arterial lumen. Biocompatibility is another very important aspect of bioresorbable stents, as the degradation products are also capable of causing inflammatory immune responses [10,51]. For many biomaterials, especially controlled drug delivery system, their functionality is determined by the behaviour of the surface. For instance, if we consider a biodegradable polymer device whose function is to slowly release drug within the body as a result of hydrolytic surface erosion of the polymer, this function will be accomplished by the hydrolysis of polymer molecules at the polymer-aqueous interface. This hydrolytic action

will be determined by surface properties like hydrophobicity, which controls water permeation, and presence of chemical groups which are subjected to hydrolytic attack [216,217].

Polymers have found widespread applications in cardiology [218], in particular in coronary vascular intervention as stent platforms (scaffolds) and coating matrices for drug-eluting stents. Since some degrade once their function is fulfilled, their use might contribute to the reduction of adverse events like in-stent restenosis (ISR), late stent-thrombosis, and hypersensitivity reactions [69]. Bioresorbable stents have received significant attention over the past decade with and without drug eluting coatings. The coating here is made from the polymer PDLLA and the drug, sirolimus. Where the drug is dispersed within a thin polymeric film on the polymer scaffold, this helps in facilitating the drug release directly to the potential restenosis site. The purpose of the drug is to reduce the risk of restenosis after deployment of the stent. As the polymer degrades, the drug is locally released to the surrounding tissues in a controlled manner.

The characterisation of biomaterial surfaces over the last 20 years has led to many important improvements in the understanding of interfacial phenomena such as biocompatibility in such materials [219,220]. Laser stent manufacturing started more than twenties years ago and has become the primary choice of stent fabrication to achieve the complex architectures required.

Laser cutting techniques provide high precision, but a slight extent of melting can be observed in drawn film [221] , and hence there is the potential to alter polymer properties. In this work, stents were laser cut using ultra-short femtosecond or picosecond pulses. This method has been reported to minimise and eliminate the heat-affected zone [222]. Picosecond pulses are short enough to avoid thermal diffusion of energy and reach the required peak power densities necessary for high precision machining process [123,223]. Previous studies showed precision and fine structure laser cut patterns in a biocompatible polymer blend, such as poly-(hydroxybutyrate) (PHB) and PLLA using the femto-second laser machining process with negligible thermal damage and without the formation of melting at the cutting edge [224].

In general, the surface properties of material are different from the bulk properties, due to exposure of different species at the surface[225,226]. The interface considerably changes molecular behaviour, thus can create molecular orientation and properties, which can be dissimilar to the bulk. Thus, an understanding of the surface can offer insight into the nature of possible biological reaction. For drug-eluting stents, surface topography is considered to have an essential effect on stent performance[227,228], as mentioned in Chapter 1. If the stent has bridges and webbings between struts, the coating may break off from the stent when the stent is dilated [99]. The outer surface chemistry at the bio-interface, the interface between the human tissue and device, is of interest as it affects biocompatibility. Moreover, the chemical and physical state and degree of mixing the drug within the polymer are essential attributes which affect the release of the drug [97].

4.1 Objective

It is the aim of this chapter to analyse the surface chemistry of the novel scaffold device and study surface related phenomena. These drug eluting stents are designed to release sirolimus over approximately three months. The distribution of sirolimus in the matrix can influence the release behaviour, where possible surface drug enrichment at the surface of the scaffold may promote burst release effects. Different series of drug eluting stents have been investigated using complementary surface analysis techniques. The expertise gained from the analysis of the polymeric tubing (described in Chapter 3) has been applied to the study of laser cut scaffolds. This chapter focuses on investigating the physiochemical characterisation of series of ArterioSorb^{TM} medical devices, in particular the structure and composition of the drug-polymer coating layer. The coating of this device was studied to investigate its effect on the manufacturing process of this device. Such studies can support the regulatory approval of new medical devices.

4.2 Materials and Methods

A series of bioresorbable stents in the form of crimped and expanded and drug coated polymeric tubing were spray coated and supplied by Arterius Ltd (Leeds). All samples were analysed as received, apart from being cut to reduce sample size. The device was

produced in two sizes, 3.5 x 14 mm and 2.5 x 14 mm. The drug/polymer system under investigation has a coating thickness of the abluminal coating of 15 µm and around 2 µm on the luminal surface and a strut thickness of 150 µm in profile. All analysed scaffolds were crimped and expanded on to a balloon catheter. Such process may lead to the formation of features on the coating layer. The design of the uncoated stents is 8 crowns per ring (or peaks) with 2.40/2.64 mm ID/OD with a wall thickness of 120 µm. The dimensions for the first generation of coated stents were 3.06/3.38 mm ID/OD (the size of the tube from which the stent was cut, although this has now been crimped and expanded) with a wall thickness of 150 µm. The first generation of ArterioSorb^{TM} stents is a design, which has 6 crowns per ring. The second generation of ArterioSorb^{TM} scaffold with strut thickness of 95 µm and 120 µm will be described in Chapter 5 as a function of *in vitro* elution time as shown in Chapter 2 Figure 2.9.

4.2.1 Environmental Scanning Electron Microscopy (ESEM)

Drug/polymer spray coated orientated tubing and coated scaffolds were imaged using FEI 650 Quanta ESEM with Energy-Dispersive X-ray Spectroscopy (EDS) for elemental mapping in order to image the surface morphology of drug coated polymeric tubing. The samples were mounted onto standard SEM stubs with double-sided carbon tape (Agar Scientific Ltd, Essex, UK).

4.2.2 Atomic Force Microscopy (AFM) Analysis

Scaffold morphology was observed in the studies described in this thesis using two methods, FastScan AFM (BrukerNano, Coventry, UK) and AFM with PeakForce QNM (quantitative nano mechanical) and tapping operation modes. In addition, an AFM (Anasys Instruments) equipped with nano-IR has been used in collaboration with the University of Manchester, where the AFM images have been performed in contact mode. The scaffolds were cut open and flattened out using gentle pressure from an acetone and chloroform cleaned glass slide and mounted onto a metal disk with a double-sided tape (Figure 4.1). Three different areas were analysed, on the abluminal (top) and luminal (inner) surfaces of each drug-coated stent where topography, adhesion and deformation

images (QNM mode) were recorded simultaneously. Tapping mode in air was used for topography and phase images. The scan rate was adjusted in the range 1.0 – 1.7 Hz depending on the image quality. Each scan line contained 256 pixels, and a whole image was composed of 256 scan lines. All AFM topographical analysis was performed on Gwyddion, version 2.36.

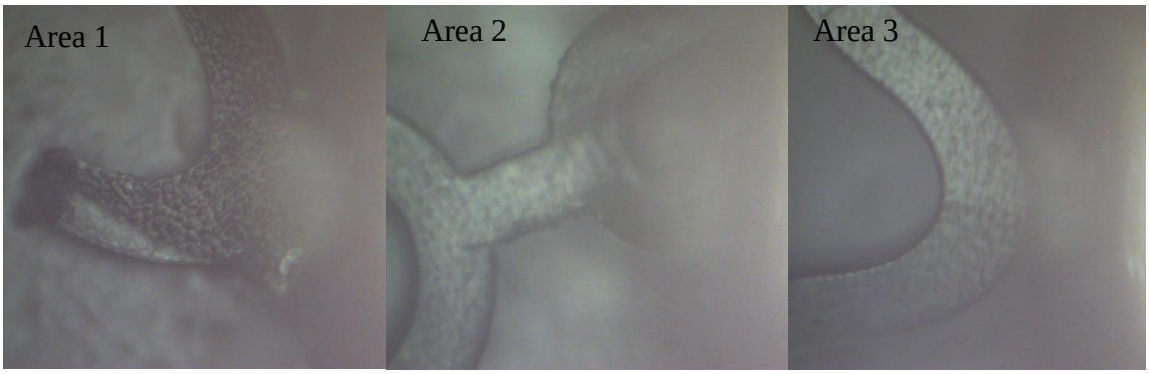


Figure 4.1 Optical images of abluminal area of ArterioSorb™ scaffolds used for AFM analysis.

For materials and methods of thermal analysis refer to Chapter 2.

4.2.3 ToF-SIMS Analysis

Scaffolds were prepared for SIMS analysis by cutting them longitudinally and opening them up with tweezers. The scaffolds were mounted onto a silicon free double-sided tape then placed into the analysis chamber at room temperature. ToF-SIMS experiments were performed using a ToF–SIMS IV instrument (ION-ToF GmbH, Munster, Germany) to acquire depth-profile data from the bioresorbable PLLA drug/polymer coated scaffolds. The instrument was equipped with a Bi liquid metal ion gun (LMIG) and an argon gas cluster ion gun (GCIB). Depth profiling was performed using a 25 keV pulsed Bi_3^+ analysis source and a 10 keV Ar_{1446}^+ sputtering. The Ar_{1446}^+ sputtering beam (target current of 10 nA) was rastered over the sample with a spot size of approximately 25 µm.

The Bi_3^+ analysis beam was used to analyse the central area between sputtering pulses. Both luminal and abluminal surfaces of scaffolds were measured with the $Ar_{1446/2500}^+$ beam sputtering a 400 x 400 µm area and the Bi_3^+ analysing the central 100 x 100 µm

region for stents as received. The target current was maintained at 10 nA throughout the depth profiling experiment and was tested using a Faraday cup prior and post profiling. Positive secondary ions were extracted from the samples into a reflectron-type time-of-flight mass spectrometer and reconstructed into 3D data. A low energy electron flood gun (<20 eV) was utilised for charge neutralization in the analysis mode. Data acquisition was performed using SurfaceLab 6 (ION-TOF).

4.2.4 3D Profilometery

Optical interferometry was performed on coated stents as well as drug/polymer coated tubing using a ZetaDots 3D profiler employing a x20 objective (Figure 4.2). Data was obtained over an area of 1169 x 876 µm, and the average thickness was calculated over this area. The measurements were taken at 8 evenly spaced locations along the length. Z ranges 224 µm and step size of 0.305 µm.



Figure 4.2 Optical interferometer image of ArterioSorb™ stent prior ToF-SIMS analysis. Oval shapes in red highlight some of the areas were analysed at using ToF-SIMS. Scale of the image = 149 µm, FOV= 3479 µm x 2609 µm.

4.2.5 X-Ray Photoelectron Spectroscopy Analysis (XPS)

The composition and chemical state information of coating-layer surfaces were accomplished using a ThetaProbe MKII instrument (Nexus, University of Newcastle). The X-ray probe used for this type of analysis was composed of micro-focused monochromated Al Kα X-ray source. The pressure in the test chamber was maintained at 1.5×10^{-9} Torr during the acquisition process. The setting parameters used were 8 kV Ar_{300}^{+}, with a total acquisition time of around 3 hours for full profile. A total etching time of 5000 seconds was used to collect the depth profile data. Each survey took 20 minutes. Survey spectra were obtained for powdered sirolimus and PDLLA, as well as uncoated polymeric scaffold. Narrow (high energy resolution) snapshot spectroscopy mode was used during the depth profile analysis of C 1s, N 1s, Na 1s, O 1s, and Si 2p regions for virgin stents. Data analysis and processing were performed with CasaXPS (Casa Software Ltd).

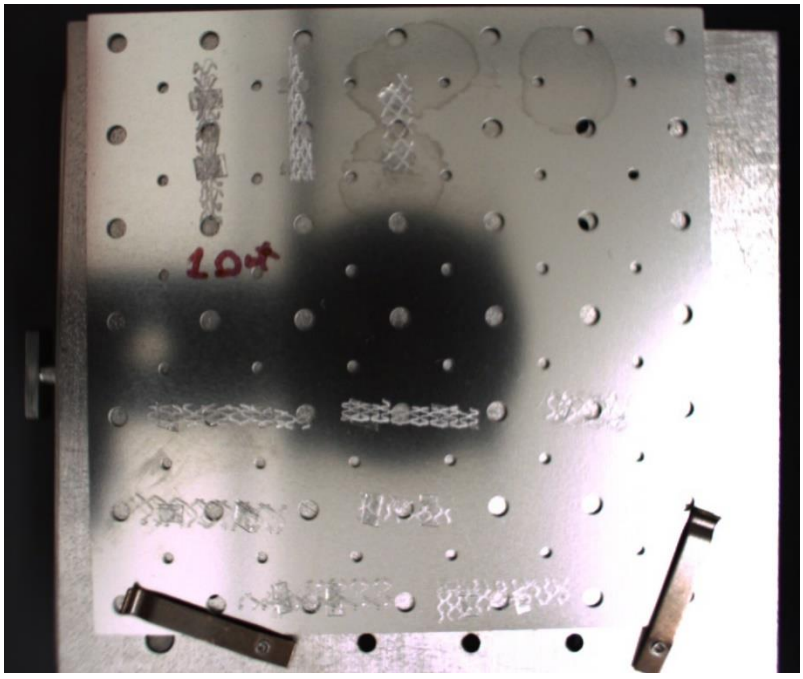


Figure 4.3 A picture of samples mounted on XPS stage.

4.2.6 Confocal Raman Spectroscopy (CRM)

Confocal Raman Spectroscopy (Horiba LabRAM HR Evolution) equipped with a Nd:YAG laser at 532 nm and a piezoelectric stage, was applied in the Raman imaging mode. The stent sample was placed upon a piezo-electrically driven table and the laser light was focused onto the samples using a x100 dry objective (50 µm pinhole) and finely focused laser spot scanned into the coating-layer. Raman spectra were collected over the spectral region of 50 - 4000 cm^{-1} with an integration time of 25 seconds per spectrum. Imaging of the coating-layer was taken over a region of 44 µm wide by 20 µm deep for scaffolds as received. Three areas (Figure 4.4) were analysed by Raman to confirm the trends described in the result section were reproducible.

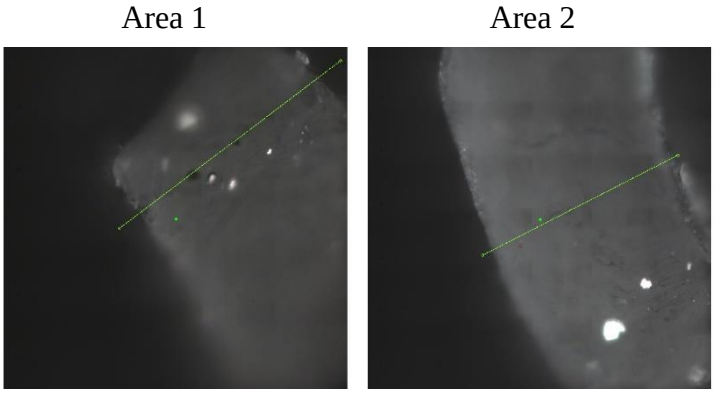


Figure 4.4 Optical images of abluminal; surface of ArterioSorb™ stents. Green line across the sample is where the measurement was taken place.

4.3 Results and Discussion

4.3.1 Surface Morphology

The influence of surface morphology is recognised by the presence of microscopy studies in many published papers on biomaterials. The surface morphology and composition of the drug/polymer coating-layer plays an important role in the clinical application of a drug-eluting coronary stent [117]. For example, the surface of the coating can promote thrombus formation, as defects and irregularities on the coating surface can increase the roughness of the scaffold surface [52]. Normally scaffolds require a uniform and smooth surface

without any ‘peeling-off’ [229], webbing between stent struts or cracking of the coating-layer. Scaffolds with a smooth surface cause less thrombus formation after deployment as compared with a rough surface [230].

In this thesis, the work focused on polymer stents, where the substrate polymer and the coating polymer are essentially the same. In order to assess the mechanical properties of coating layer used in ArterioSorb™ scaffold, the stent itself was subjected to a sequence of crimping and expansion onto a balloon. SEM and AFM were employed on drug coated tubing as well as drug coated stents with different drug loading to gain an understanding of the surface topography of the sirolimus/PDLLA coating-layer. In order to see the coating in its native state, all samples remained untreated (i.e. gold sputtering was not applied), although some samples were gold coated and EDS measurements was taken on some areas of the stent (Appendix A). Oriented polymeric tubing was drug/polymer (1%) spray coated and was used as a model for studying the final device, although the work in this thesis was mostly focused on laser cut scaffold rather than drug coated tubing.

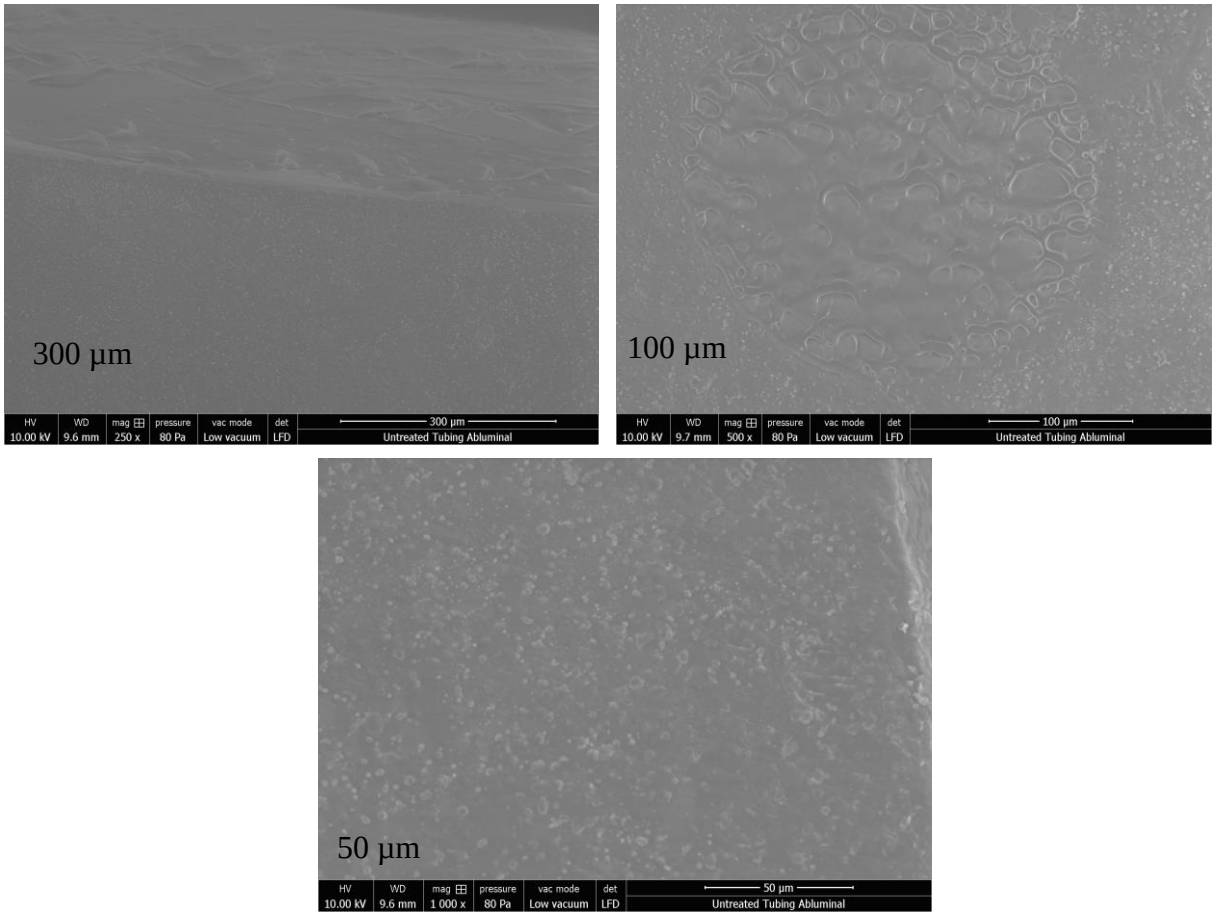
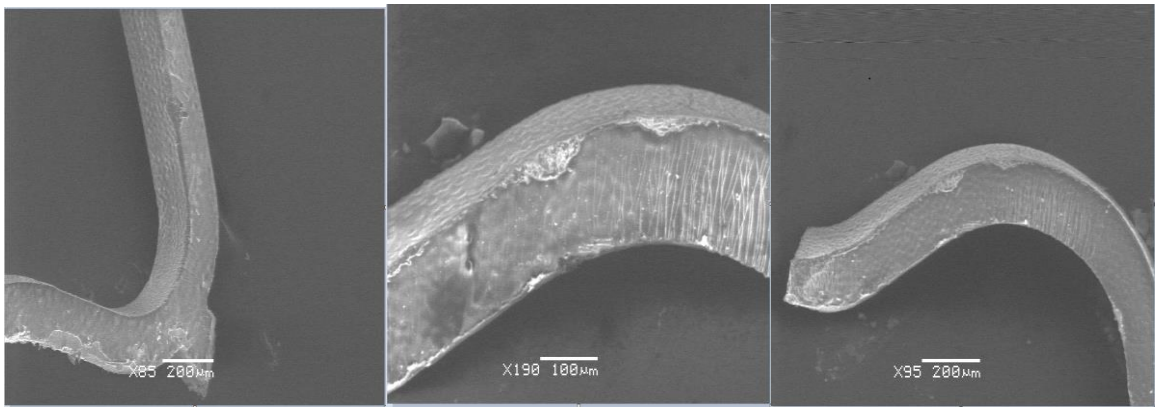


Figure 4.5 SEM images of the surface morphologies of the top surface of drug/polymer coated PLLA tubing taken from different regions at different magnifications (250x, 500x and 1000x), respectively). The SEM images demonstrate in general a relatively smooth surface.

The ESEM characterisation in Figure 4.5 shows images of sirolimus in PDLLA coating-layer coated on the oriented polymer tubing (die-drawn). It is important that the integrity of the coating is retained during crimping process and implantation, because peeling or cracking of the coating layer could cause severe inflammatory events and abrupt vessel closure [231-233]. Images of the coating layer displayed no cracking or peeling of the coating-layer, demonstrating that the sirolimus/PDLLA coating has strong adhesion to the stent surface; similar features are shown for the coated scaffolds in Figure 4.6. The roughness of samples is important, images obtained by SEM show relatively smooth areas.

Roughness of these samples was measured by AFM. For DES the roughness is important as the implant in direct contact with blood, the surface roughness affects the blood biocompatibility and increase roughness increase the likelihood of blood clotting. Whilst smooth surfaces have small surface area, thus providing better blood compatibility [233].

a. Abluminal



b. Luminal

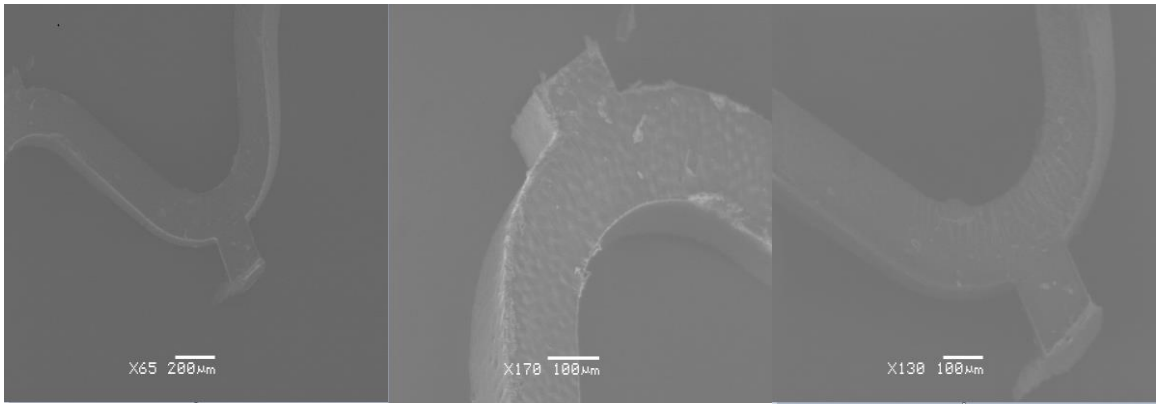


Figure 4.6 Representative SEM micrographs of the surface morphologies of a. top and b. inner surfaces of drug/polymer coated stents. The SEM images demonstrate a relatively smooth surface (abluminal and luminal). Some stress fractures are apparent in some areas on the stents; this could be due to manufacturing process or sample preparation.

None of the coating layers in the abluminal and luminal side of the stent exhibited significant damage from the crimping and expansion process. Data was confirmed by

Arterius Ltd, where bench testing of crimping and expansion was carried out on the whole scaffold and results obtained were compared to other bioresorbable scaffolds in the market. Data shown in Appendix F (Figure F.1) illustrates crimping test and Figure 2.9 demonstrates sent expansion of ArterioSob™ .

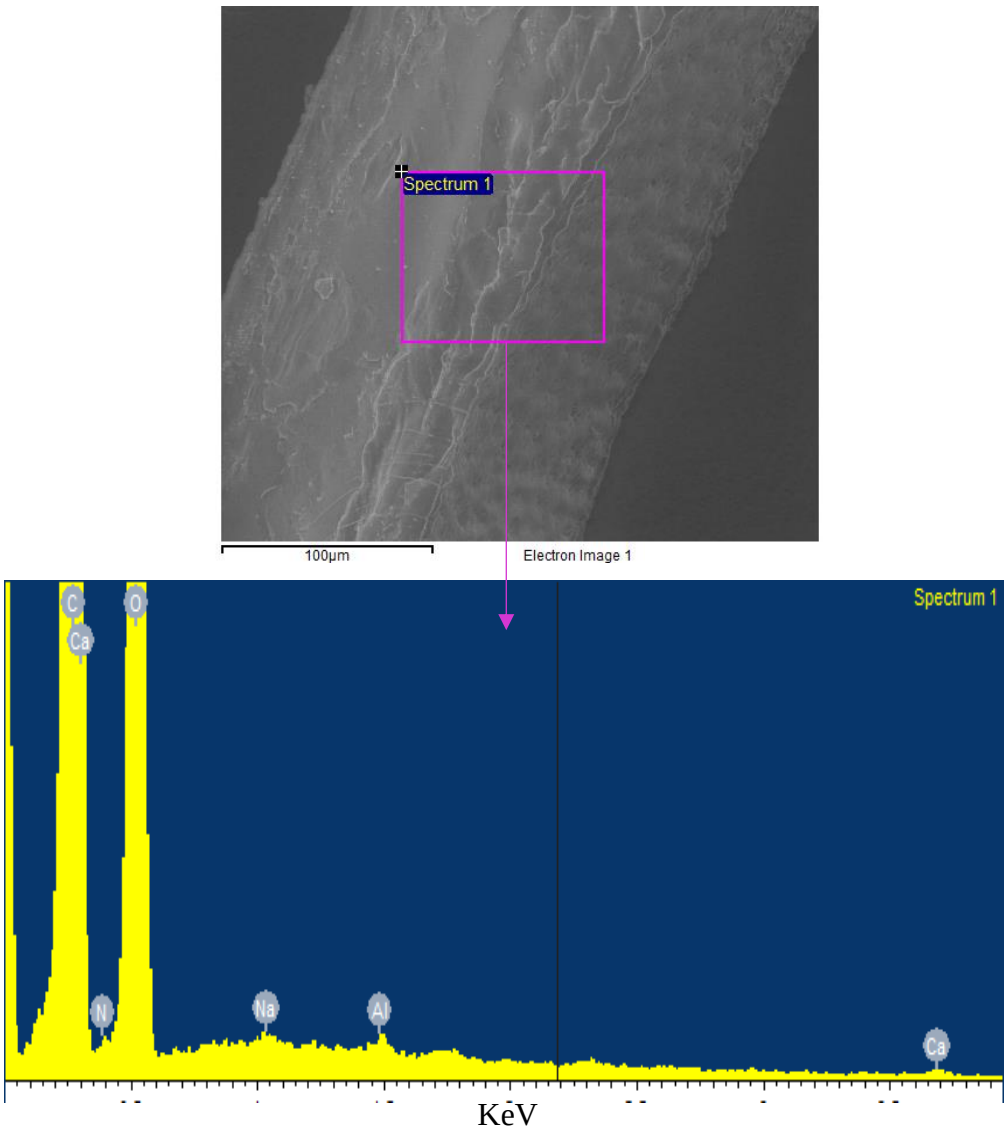


Figure 4.7 EDX spectrum of abluminal area of drug/polymer coated scaffold.

The smooth film coatings show evidence of 'islands' proposed to be related to the sirolimus on the surface of coated stents, as shown in the SEM image highlighted in pink (Figure 4.7). The EDX data shows presence of surface contaminants such as Na, Ca, Al as well as the C, O and N which are ion markers the device.

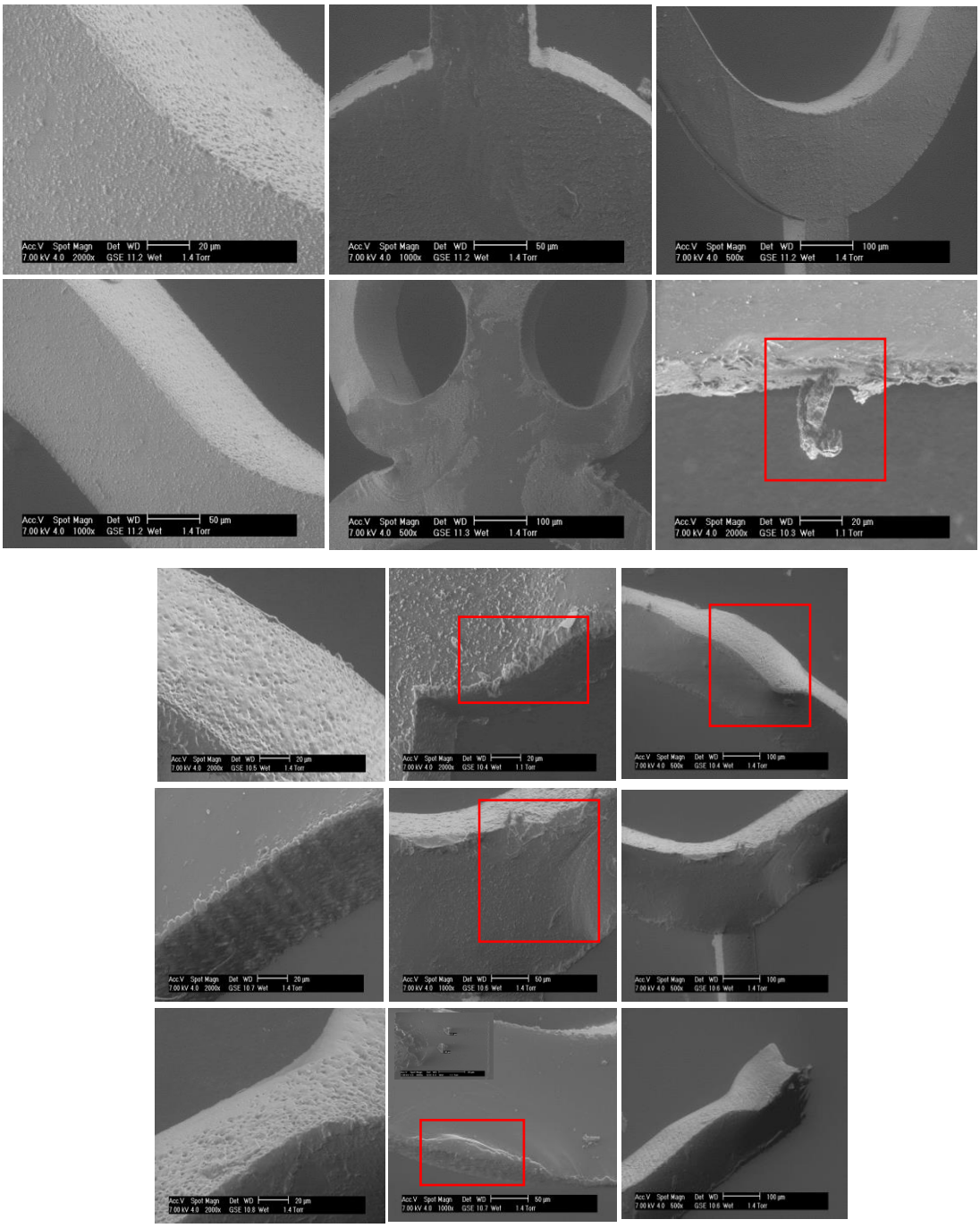


Figure 4.8 Representative SEM images of the top surface heat affected zone (HAZ) of uncoated laser cut bioresorbable stent. The stents were laser cut by femtosecond and picosecond laser. Red squares indicate molten areas on sidewalls of the stent.

The heat affected zone are characteristics highlighted in red in Figure 4.8 and have been investigated by means of microscopic examinations. The SEM images in Figure 4.8 present the SEM images of some areas possibly affected by heating during the laser cutting process. The topography and the roughness of the surfaces were measured using AFM tapping mode at room temperature (Figure 4.9). As previously observed from images in Figure 3.7 obtained by AFM, heterogeneity is apparent with fibre-like features and these features were also seen in Figure 4.7.

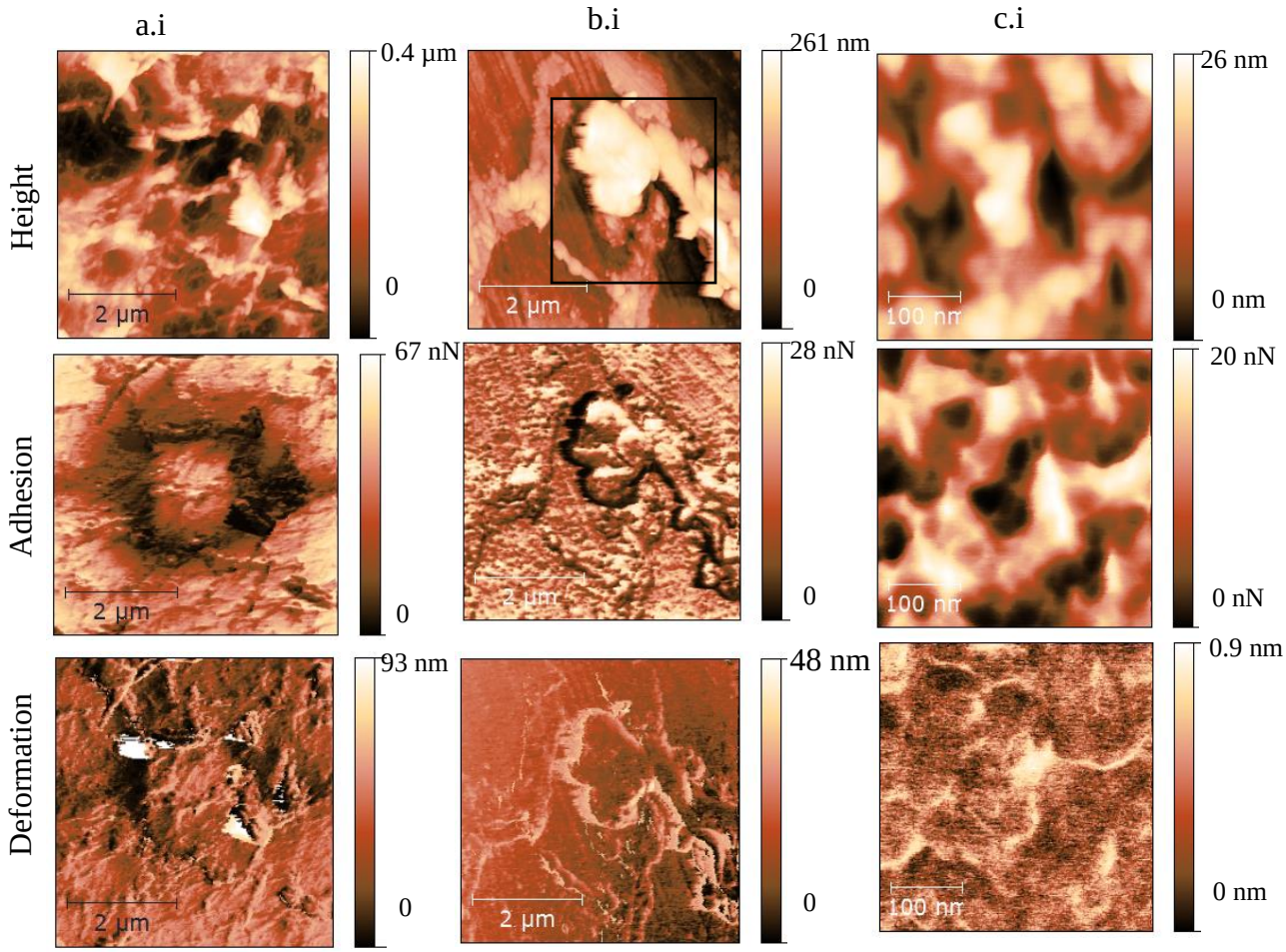


Figure 4.9 AFM images in QNM mode of heat affected zones of uncoated stents taken from two areas of stent that have been laser cut using different laser cutting methods (a.i scan size 5 x 5 µm with roughness RMS (sq) = 50 nm, b.i scan size 5 x 5 µm and roughness RMS (sq)= 48 nm, c.i is a magnified feature of the black square in b.i with a scan size of 0.37x 0.37 µm, RMS (sq) = 4 nm.

Laser cut samples seemed to be dominated by the appearance of fibrous and globular features and the presence of pits. The shape of these pits varies from rounded to elongated contour, as shown in Figure 4.9. Modifying the surface crystallinity by laser cutting has drawn much attention, as it is also an attractive method due to its ease of use, flexibility and spatial controllability [200]. Laser cut images in Figure 4.9 shows heterogeneity in topography with the presence of features like fibres. The mechanical property of these features was investigated via QNM AFM analysis. As seen in the adhesion images these fibres looking like features exhibit a clear contrast to the AFM probe with respect to the background indicating a mechanical heterogeneity, suggesting these features to be slightly different to the surrounding areas.

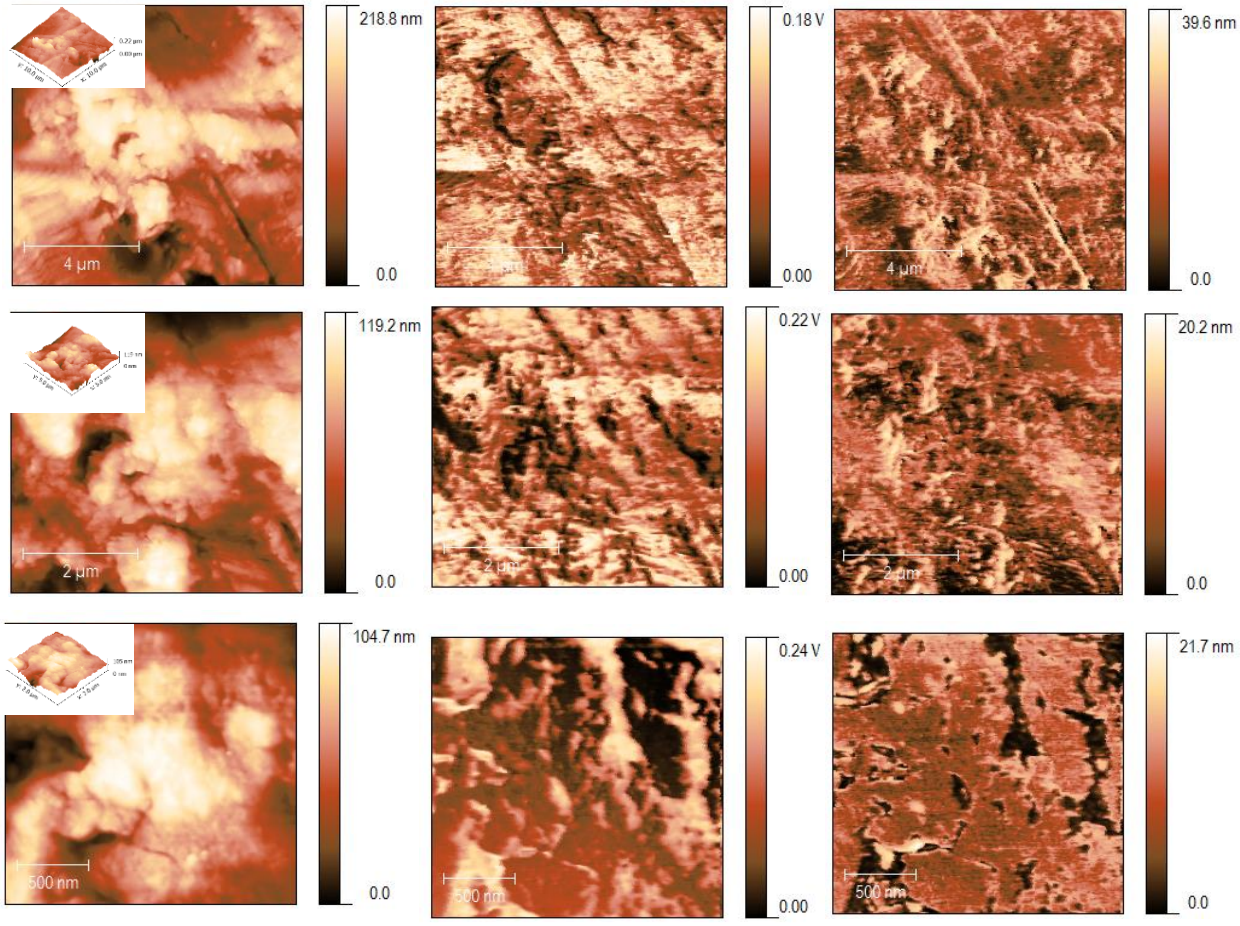


Figure 4.10 AFM images in QNM mode of abluminal surface of die-drawn tubing. a. scan size 10 x 10 µm, then zoomed into certain features 5 x 5 µm and 2 x 2 µm.

The surface of laser cut PLLA scaffold was compared to the surface of non-laser cut oriented PLLA tubing. The observed features in Figure 4.8 and Figure 4.9 were not present on the surface of oriented die-drawing tube in Figure 4.10. Laser cutting can induce rapid cooling rate, the recrystallisation process of the polymer may not be completely finished and leading to formation of semi-crystalline and amorphous features on the surface, such phenomena explains the mechanical heterogeneity in such samples.

The sirolimus/PDLLA coating in the ArterioSorb™ scaffold clearly shows globular features, these complex features are due to the variation in material properties, which are detected through variation in the degree and nature of the AFM probe interactions over these regions. These globular features on the coating layer were also observed in the ESEM images. The surface morphology observed in the AFM images, are similar to features seen previously on polymeric tubing in Chapter 3. Hence it is proposed that these features are due to the nature of PLLA material. The surface morphology of samples containing PLLA only without the drug was found to be relatively smooth and lacking in the spherlites structures. The surface topography of PLLA laser cut tubing is shown in Figure 4.10, showing a smooth structure disputed only by occasional aggregates. Polymeric samples only (uncoated) were observed to consist of a granular morphology (Figure 3.7 in Chapter 3 and Figure 4.8).

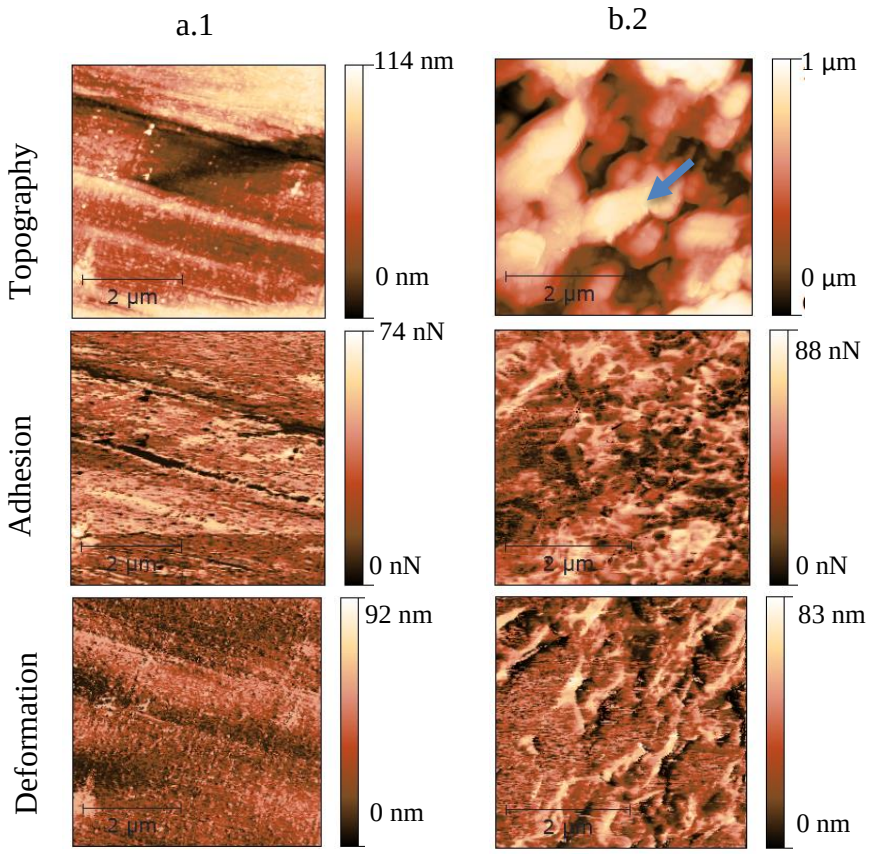


Figure 4.11 AFM images of abluminal surface of tubing prior laser cutting (a.1) and post laser cutting (b.2), showing, topography, adhesion and deformation. Scan size images, a.1 plain oriented tubing 5 x 5 µm, b.2 plain laser cut stent 4 x 4 µm.

Features observed in laser cut samples are in a different physical state from the background material. Such features could have initiated from melted areas developed during heating of the laser cutting process, these melted features are in the form of pits observed in Figure 4.11(b.2). Features observed in laser cut samples could be due to the condensation of materials from the laser cut induced plume. The heat associated with laser cutting could induce melting of the crystalline polymer. These crystalline features are held together by hydrogen bonds and van der Waals forces. During the ablation and melting involved in laser cutting these bonds are broken down, leading to disordered structure promoting the formation of amorphous material [71,234].

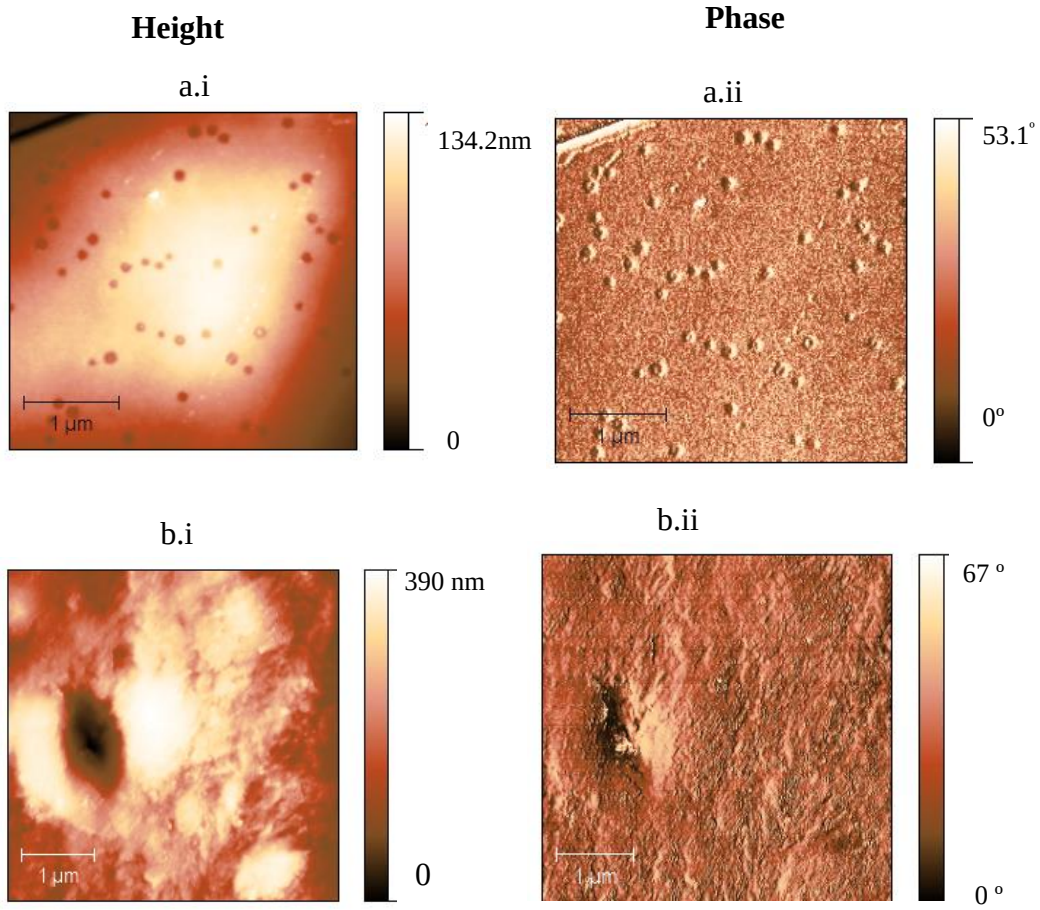


Figure 4.12 AFM images showing topography and phase images of sirolimus/PDLLA-coated stent of two areas of the abluminal (a.i, a.ii, b.i, and b.ii) surfaces of a laser cut bioresorbable-coated stents. Top surface (abluminal) area one is of scan size =3.6 x 3.6 µm, RMS (sq) = 14.1 nm and area two of scan size = 4.4 x 4.4 µm, RMS (sq) = 34 nm.

The correspondence phase images in Figure 4.12 show surface structures that maybe related to phase separation in the coating. Surface heterogeneity in the roughness and topography seems to be apparent on this coating layer. Increase of drug load in the coating layer produces globular/circular features that might be related to the drug and are drug-enriched regions. Laser cutting was investigated as it was apparent such features might occur due to laser cutting process. Laser cut stents have undergone through a heating process, this process could be the reason for the formation of such features that

are not observed in plain polymeric tubing. Figure 4.12 shows the surface topological features of ArterioSorb™ after spray coating and before being in contact with an aqueous environment. The phase images in Figure 4.12 indicate heterogeneity, this structural heterogeneity was responsible for the micro-domain separated morphologies observed. The mechanical property of the scaffold surface before spray coating and post spray coating was further investigated using AFM-QNM. Figure 4.13 illustrate the data recorded, topography, adhesion and deformation.

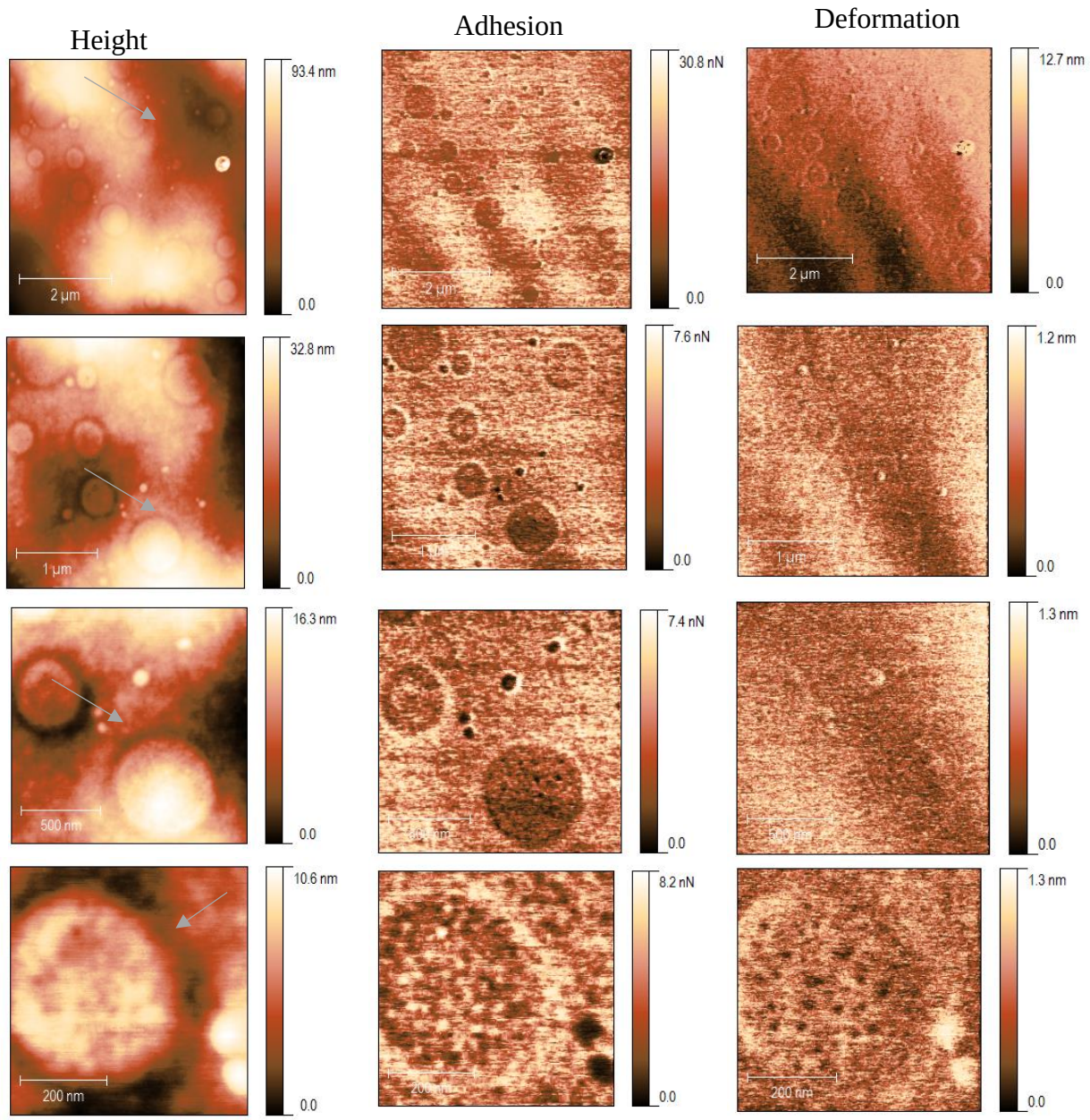


Figure 4.13 AFM images of abluminal surface of ArterioSorb™ Scaffold at different scales size. The blue arrows indicate circular features surrounded by a continuous

matrix, these domains could be related to drug-rich regions.

The results obtained in the AFM examination suggest that the spray-coated sirolimus/PDLLA was tightly adhered to the surface of the crimped and expanded ArterioSorb^{TM} scaffold. Additionally, the coating-layer was previously demonstrated by the SEM to be sufficiently flexible to allow balloon expansion of the scaffold without cracking or peeling.

The images in Figure 4.13 show the presence of circular features highlighted by blue arrows, which might be related to drug-rich regions or alternatively other features associated with forming the surface such as droplet drying marks. A heterogeneous surface at the nanoscale on the as-formed surface is clear from the AFM data. The spray-coated stents have showed a two-phase separated surface structure. This observation is due to the difference of materials used in the preparation methods. Little patches appeared on the surface these dark patches where more energy have been lost due to surface been sticky or softer than surrounding. Hence crystalisation takes places at these areas.

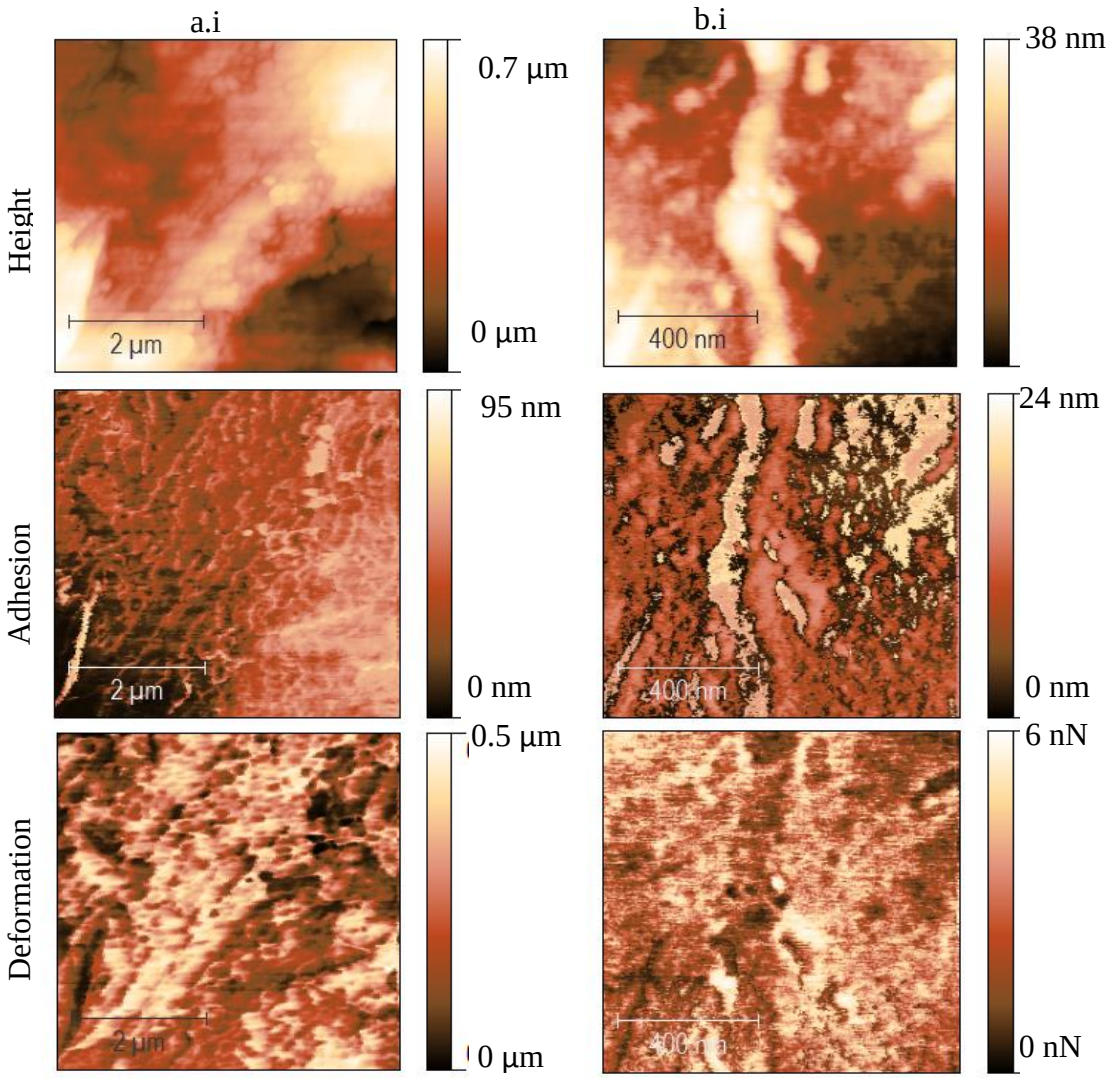


Figure 4.14 AFM images of abluminal surface of drug/polymer coated stent, showing topography, adhesion and deformation of a. 5 x 5 µm, b. 1.0 x 1.0 µm with roughness of RMS (sq) = 110.10 nm and RMS (sq) 6.12 nm, respectively.

Post spray coating the laser cut samples, showed a continuous film with shallow pits in the surface, as shown in Figure 4.12, Figure 4.13 and Figure 4.14. The diameter of the globular structure varies from one area to another. The deformation and adhesion force measurements established that the low valleys and high surface regions had dissimilar mechanical characteristics.

AFM height and phase images provided an insight into the phase separated regions and underlying morphologies. It is worth mentioning that the bright regions in the AFM images can be explained by the strong interaction forces between the surface and the AFM tip when the tip enters any pores that might be present on the coating surface. The presence of pore formation might be common on such coating and is usually observed in solvent casting polymer layers or stent coatings in general. This is formed due to solvent evaporation[235,236]. The formation of pore size will be discussed in more detail in Chapter 5.

Table 4.1 The root mean square (RMS) roughness of the surface measured using AFM under a tapping mode at ambient condition. The RMS roughness values were calculated as the average of three or more distinct spots (5 μm×5μm) on each sample.

Sample ID	Average roughness in root mean square (RMS) (nm)
Die-drawing PLLA tubing	13
Laser cut uncoated scaffold	50
Drug coated stent: Abluminal	110
Drug coated stent: Luminal	25

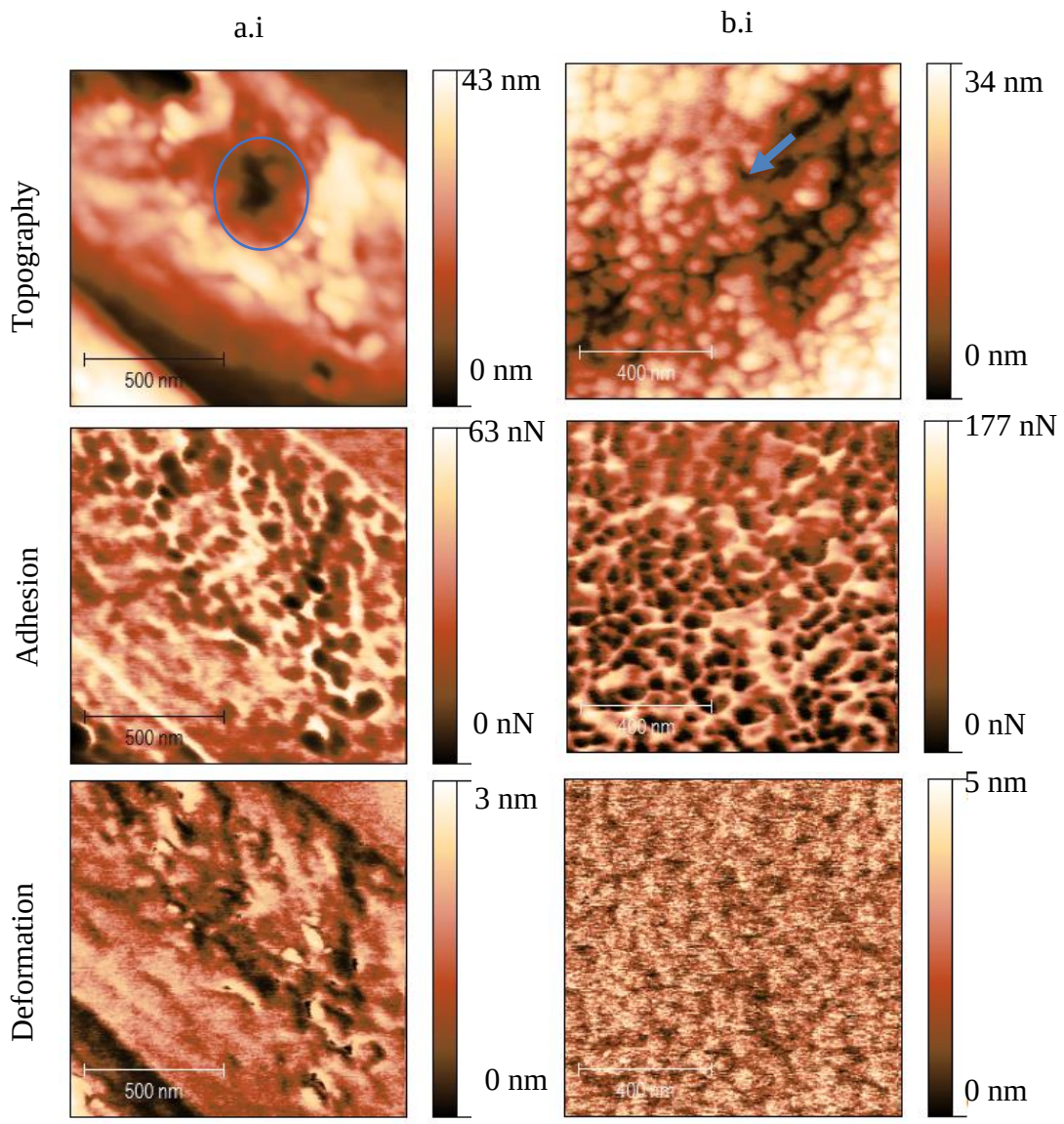


Figure 4.15 AFM images of luminal surface of drug/polymer coated stent taken from two areas (a.i and b.i) showing, topography, adhesion and deformation. The images show the presence of circular features highlighted by blue circle. Blue arrow refers to small spheres that might be related to drug or polymer.

Features in the sample above are representative of laser cut areas, where the presence of pits becomes quite pronounced. Mechanical heterogeneity was observed in this series of samples. This might arise from difference in solubility of the polymer and the drug in the solvent used during spray coating [237]. The coating appears to demonstrate region-to-region differences in the dimensions of the chemical morphologies. The surface

morphology can be influenced by many factors such as deposition method, drug loading as well as coating preparation solvent. Another reason as to why the drug distribution of samples present phase separation maybe due to use of high molecular weight of polymer or high solubility of the polymer in solvent. These factors are likely to generate phase separation in large scale of hundreds of microns. The morphology evolution is very much depended on the film thickness and the polymer blend ratio, for instance, if the polymer content of one of the blend is higher than the other one, then small holes are very likely to be observed on the surface of the coating and when the fraction decreases, the size of observed pits decreases and start to merge. The distribution of such pits is likely a key factor for determining the kinetics of release of the drug (this will be discussed in Chapter 5). Optimisation of spray coating parameters might affect the surface morphology. Previous studies have indicated that the rate of crystallization, crystal orientation, and rate of nucleation of thin films are quite different from the bulk PLLA [238]. Therefore, thermal analysis was conducted.

4.3.2 Thermal Analysis

In nano-TA, the Localized Thermal Analysis (LTA) is conducted by examining the cantilever deflection while scanning the heating power applied to the probe. The glass transition temperature (interpreted as a change in mechanical properties during heating) of sirolimus/PDLLA-coated stents was determined through LTA. The surface morphology and phase changes at elevated temperature were studied previously on oriented polymeric tubing (Chapter 3) by using AFM imaging. It was observed PLLA tubing presented a homogenous surface before the Nano-TA, however after the Nano-TA tip is heated a hole or indent occurred. A low gain-feedback was kept during LTA measurement was used to keep the defection signal constant during the temperature scan (Figure 4.16).

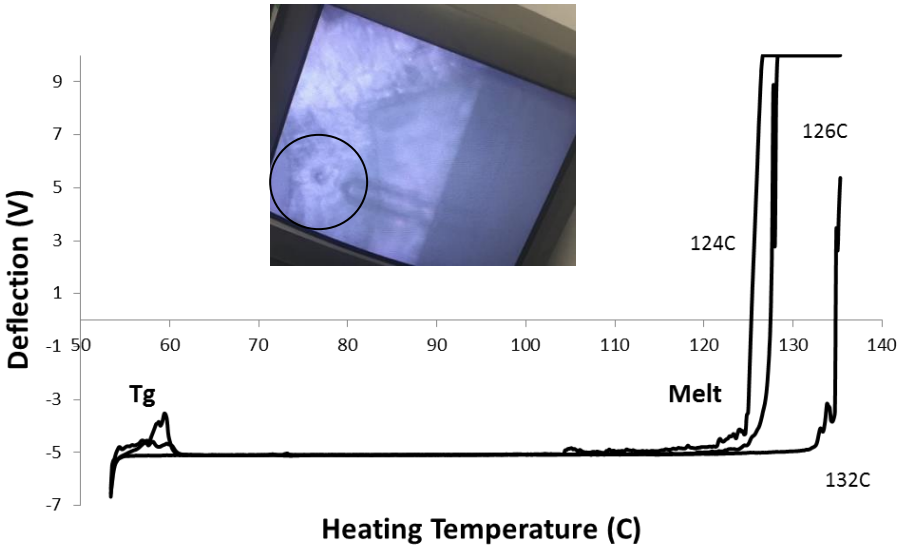


Figure 4.16 Microthermal measurements of sirolimus/ PDLLA coated bioresorbable stent showing the top surface. Circle highlights the hole that has been created post measurement.

The melting points of coated stents extracted from Nano-TA local thermal analysis are presented in Table 4.2.

Table 4.2 Melting points of sirolimus/PDLLA coated stents derived from Nano-TA analysis.

Sample ID.	Melting point ºC
Area 1	124
Area 2	126
Area 3	132

Nano-TA results show possible melting transitions starting in the range of 125-135˚C for as-fabricated stents. There is some variability in the data; this could be due to sample roughness. Since SThM is a relative new technique, appropriate interpretation of the data obtained from this technique still needs to be considered and confirmed with other techniques, therefore DSC was used for this purpose (data was previously considered in Chapter 3).

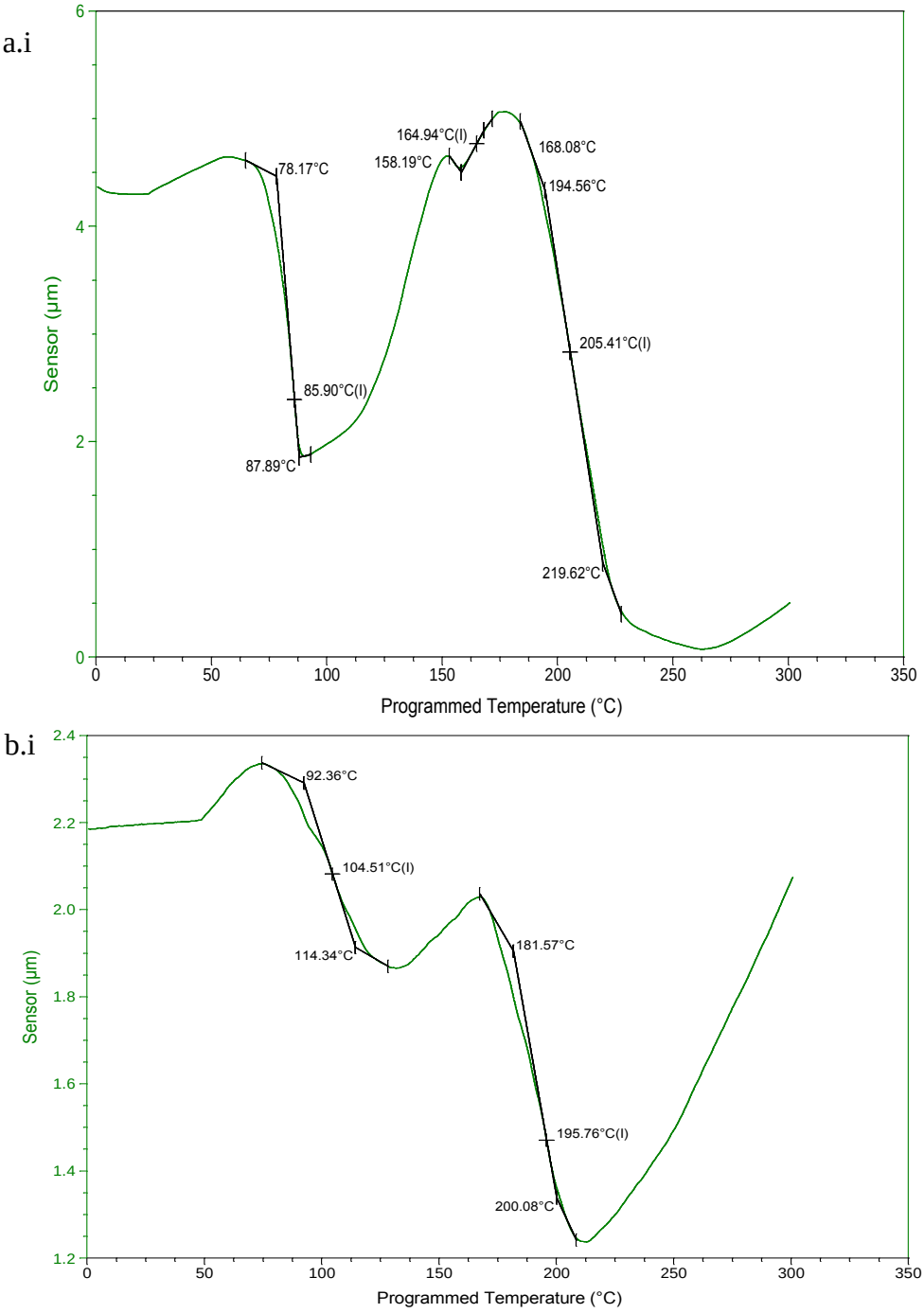


Figure 4.17 SThM micro thermal analysis of the a.i abluminal and b.i luminal area of sirolimus/PDLLA coated stent.

The melting points are not the same as the ones obtained previously using the lower resolution microthermal analysis. Micro-thermal analysis (SThM) was carried out using a micro-scale Platimum-Rhodium resistor tip using a much slower heating rate. The

variability in measurement indicate that laser cut samples may contain a fraction of amorphous material, as laser cutting process induces the formation of amorphous state, this fraction of amorphous domain is large enough to be detected by Nano-TA than those of non-laser cut samples. Representative sensor signals obtained are presented in Figure 4.17, demonstrating semi crystalline state. The presence of PDLLA can affect the melting temperature of the sample, also the processing conditions of the polymeric tubing during extrusion and orientation such as annealing time and temperature, may have played part in the fluctuating phase transitions. Moreover, the spring constant of the cantilever as well as room humidity and temperature may have had a part in fluctuating the measurement. The differences of measurements in the nano-TA and micro thermal analysis (SThM) is due to the surface sensitivity. Nano-TA can detect volume in the order of 100 nm, whilst SThM in the order of 1 μm.

4.3.3 Nano-IR Measurements

The AFM-IR was used to acquire IR absorption spectra and absorption images with spatial resolution on the 50 to 100 nm scale. All samples were measured using a nano-IR2 system in contact mode with the OPO IR source; this source is capable of covering a range of 900 – 3600 cm^{-1}. This technique was used to map the IR absorption properties of ArterioSorb™ coating layer.

Table 4.3 Absorption peaks of the drug and polymer.

Material	Structure	IR-Absorption CM^{-1}
$P_{DL}LA$	OH hydroxyl	3500
	CH_3	2945
	C=O	1756
	C-O	1300-1050
Sirolimus	C-H	2950
	C=N	1645-1717
	C-N	1636

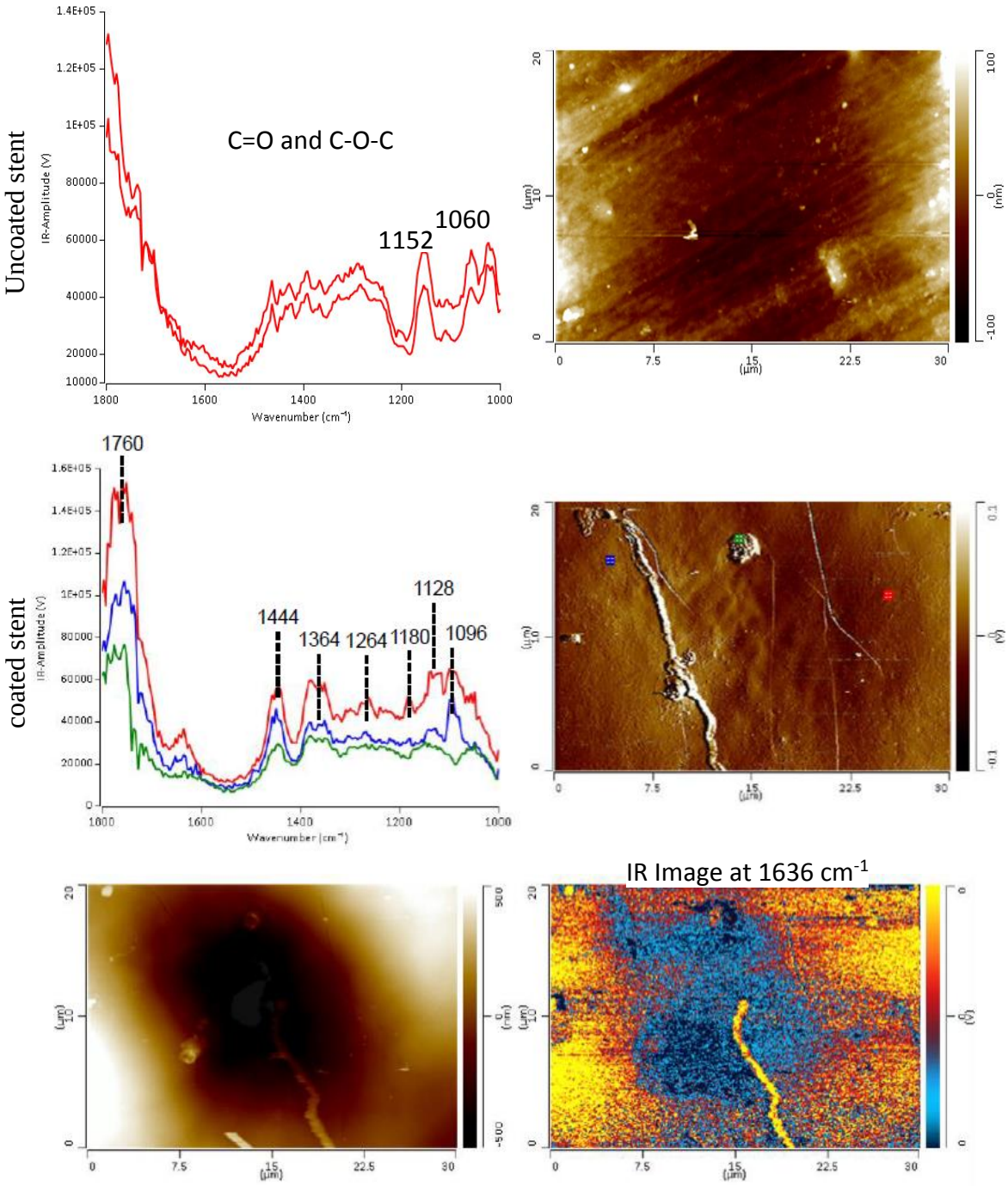


Figure 4.18 Nano-IR measurements of a. uncoated stent, b coated stent, AFM images 20 x 30 µm.

The observed bands at 1755, 1184 and 1088 cm^{-1} in the PLLA are caused by stretching vibration of the C=O group and the asymmetric and symmetric stretching vibration of the

C-O-C group. Sirolimus absorption peaks at 2950 (C-H), 1636 (C-N) were evident for the coated stent (Table 4.3).

4.3.4 ATR-IR

The ATR spectroscopies have the benefit of avoiding sample exposure to ultrahigh vacuum conditions, yet their application in biomaterials analysis is restricted by their high penetration depth which samples chemical data from a region of 1 to 5 μm below the boundary of the sample [239]. ATR-IR was applied to identify the chemical information of the near surface region. Characterisation of standard samples was previously performed on powdered drug and polymer and uncoated stents (described in Chapter 3) before the analysis of the drug/polymer coated stent.

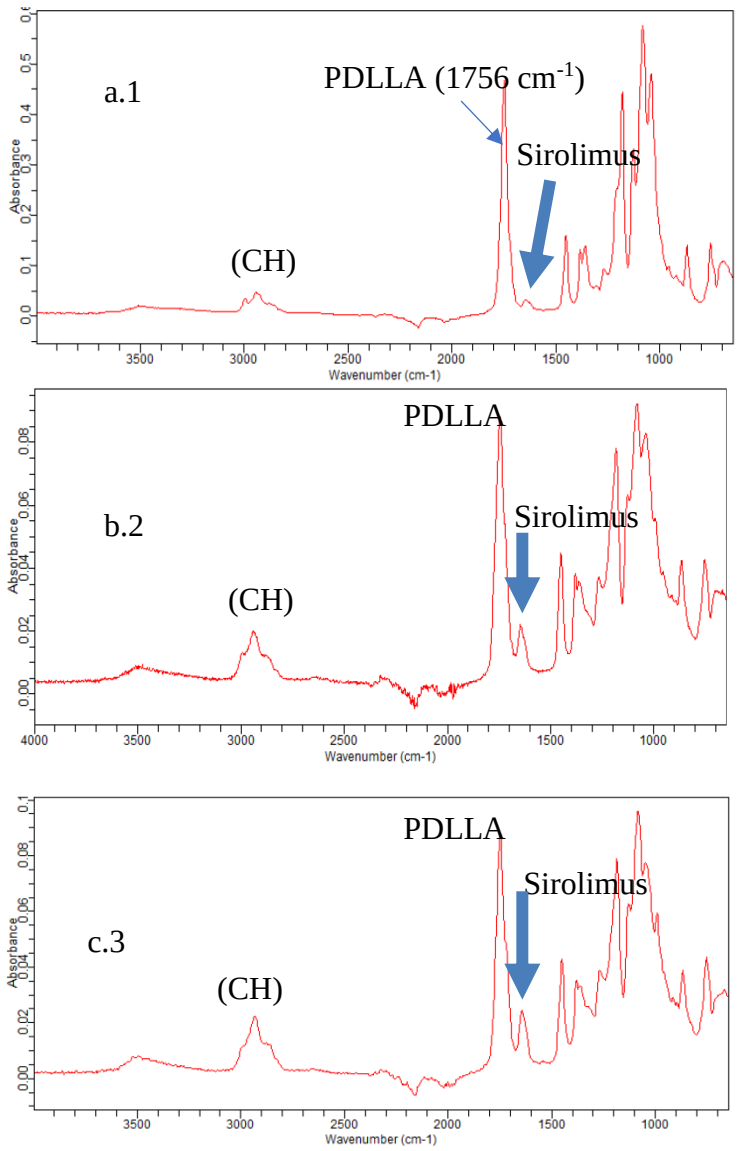


Figure 4.19 ATR-IR spectra of a.1 drug/polymer coated tubing, b.2 abluminal side of ArterioSorb™, c.3 luminal side of ArterioSorb™ scaffold. The peak at 1645 cm^{-1} was contributed from sirolimus only.

The IR spectrum in Figure 4.19 shows the characteristic peaks for the PLLA at 1756 cm^{-1} (C=O) and for the drug is at 1645 and 990 cm^{-1}. The ester group was detected in PDLLA was shown previously in Chapter 3, Figure 3.17. The ATR-IR spectra of the coating layer containing sirolimus showed similar peaks as PDLLA in addition to sirolimus characteristic peaks, in particular peaks observed at 3400, 2930, 1641, 1722 and 1750 cm^{-1}, were assigned to the stretching vibrations of sirolimus O-H, C-H, C=O. Figure 4.19(b) and (c) show incorporation of sirolimus in the blend.

4.4 Surface Chemical Analysis

4.4.1 ToF-SIMS Characterisation

ToF-SIMS depth profiling has been applied to obtain molecular ions information while sputtering and characterise the molecular chemistry of materials with efficient lateral and depth resolution 1-10 nm [97]. From Chapter 3, it has been established that it is feasible to monitor the distribution of the characteristic secondary ions PDLLA, ($C_3H_4O^+$) and sirolimus ($C_5H_{10}N^+$) as a function of depth profiling, this has led to the data reported in this chapter. Sputter depth profiling is one of the most versatile techniques to achieve in-depth chemical information about inorganic substrates with high surface sensitivity [240]. Depth profiling mass spectrometry was used to measure the distribution of the drug moieties in the coating, with depth, which is highly important in ensuring the potential efficacy of the slow release mechanism (drug release mechanism will be discussed in Chapter 5).

In this work, results are reported from molecular compositional profiling of a series of sirolimus/PDLLA coated stents and drug coated polymeric tubing using Ar ion sputter beam instead of the $C60^{++}$, as in Chapter 3. $C60^{++}$ has proven difficult to depth profile polymer films because the sample was thought to cross-link during sputtering process, leading to reduce sputter yield and result in making the sample immeasurable[241-243]. In fact, the change in ion guns makes it a valid study to compare the efficiency of the two different ion beams. The experimental set up remained the same despite of using a different ion gun. Initial experiments were performed on sirolimus/PDLLA coated oriented tubing, for this analysis positive polarity was established to be the most used polarity for the characterisation of these materials. This work was done in order to test feasibility of in-depth characterisation of bioresorbable materials using this approach, determine ideal operating conditions, obtain reference spectra, and determine sputter rates, as shown previously in Chapter 3. The ToF-SIMS spectrum consists of great number of peaks at different masses. The peaks assignment is quite complicated comparing to XPS method. Nevertheless, known groups of peaks at characteristic masses for the drug and the polymer of ArterioSorb™ were established in agreement with the literature.

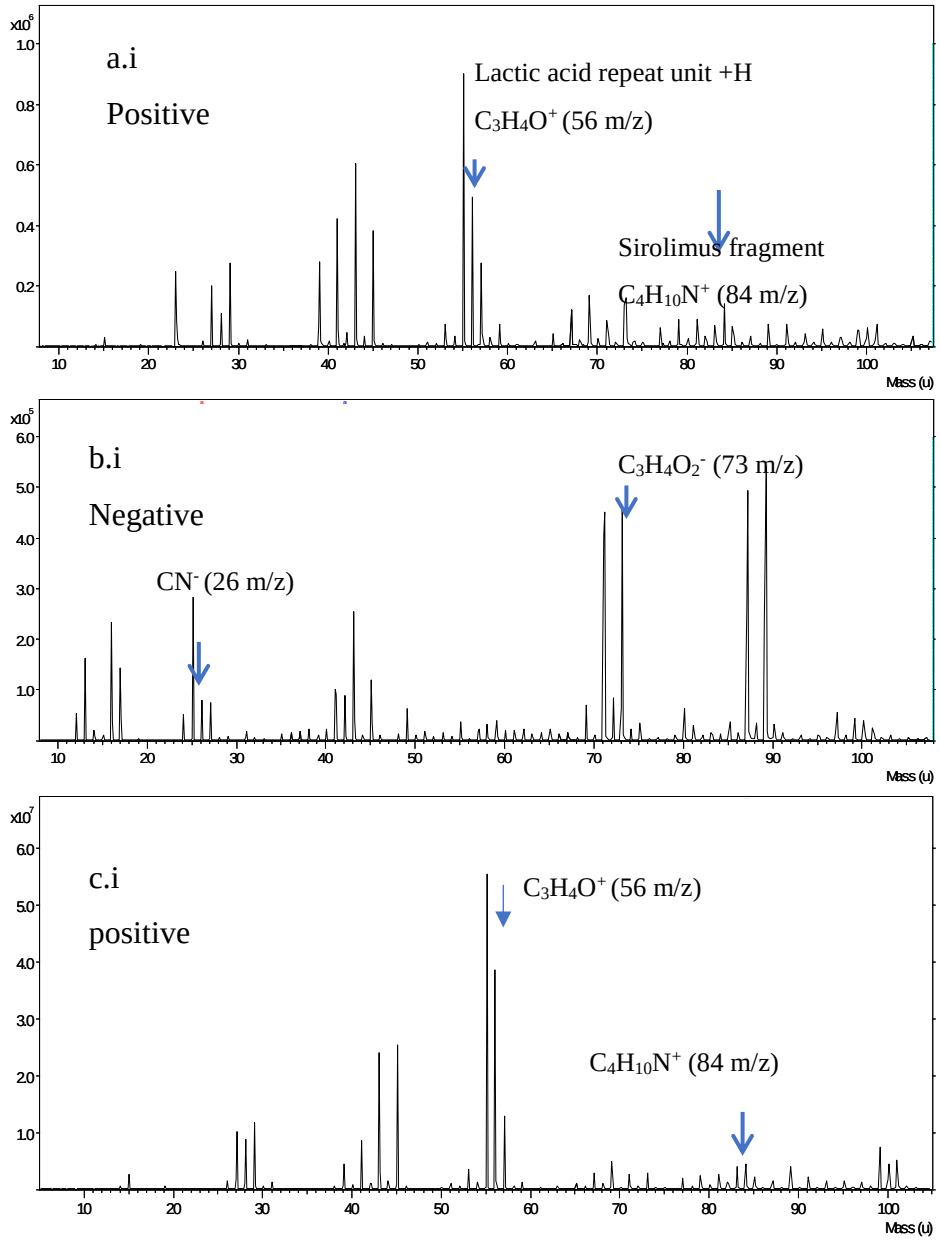


Figure 4.20 Positive and negative ion ToF-SIMS spectra of the top surface of sirolimus/PDLLA coated polymeric tubing, a.i (positive), b.i (negative) and c.i spectrum of drug/polymer-coated stent as received from a mass of 0 to 100. The masses chosen to represent the components include CN^- (sirolimus), $C_3H_4O_2^-$ (polymer), and $C_4H_{10}N^+$ (sirolimus) and $C_3H_4O^+$ (polymer).

The SIMS spectra show the main peaks at masses 84 m/z and 56 m/z. The diagnostic secondary ions for polymer and drug were determined in previous chapter; this has led to the optimisation of the depth profiling conditions that are reported in this chapter. The

reference spectra for the pure sirolimus, PDLLA and laser cut stents are shown in Figure 3.18 along with the corresponding chemical structures. The spectra of drug coated polymeric tubing and drug coated stents are shown in Figure 4.20. The degree coverage of drug on coated tubing as received was investigated with ToF-SIMS, data shown in Figure 4.20. Table 3.2 in Chapter 3 lists the positive secondary ions characteristic peaks of the drug and polymer and the spectra for the standard drug and the polymer materials, highlighting these diagnostic peaks are shown in Figure 3.18. These diagnostic markers are the most intense peaks in the spectra and most importantly they do not overlap with other ions. Depth profile of the extruded tubing showing characteristic secondary ion of PLLA is found in Chapter 3, Figure 3.22, although the ion intensity was reported as a function of $C60^{++}$. Depth profile of polymeric tubing using different ion beam (Ar cluster source) is shown in the appendix.

There is clear evidence of ions specific to the drug molecule within these spectra. Using the diagnostic ions highlighted above and in Chapter 3, ToF-SIMS spectra were reconstructed as images to understand the distribution of the sirolimus and PDLLA in the bioresorbable stent. Further analysis was carried out in the form of a search for common contaminants observed in the ToF-SIMS data, such as sodium and PDMS. However, these contaminants were not observed in significant quantities (data described in Appendix C). At each analytical cycle of the depth profile the lateral distribution of each chemical component is imaged, and these 2D images-at-depth may be extracted from the data file at any specified depth interval. Figure 4.21 shows ToF-SIMS images of the surface of the abluminal drug coated tubing and abluminal and luminal surface of drug coated stents.

a.i Abluminal tubing a.ii Abluminal stent a.iii Luminal stent

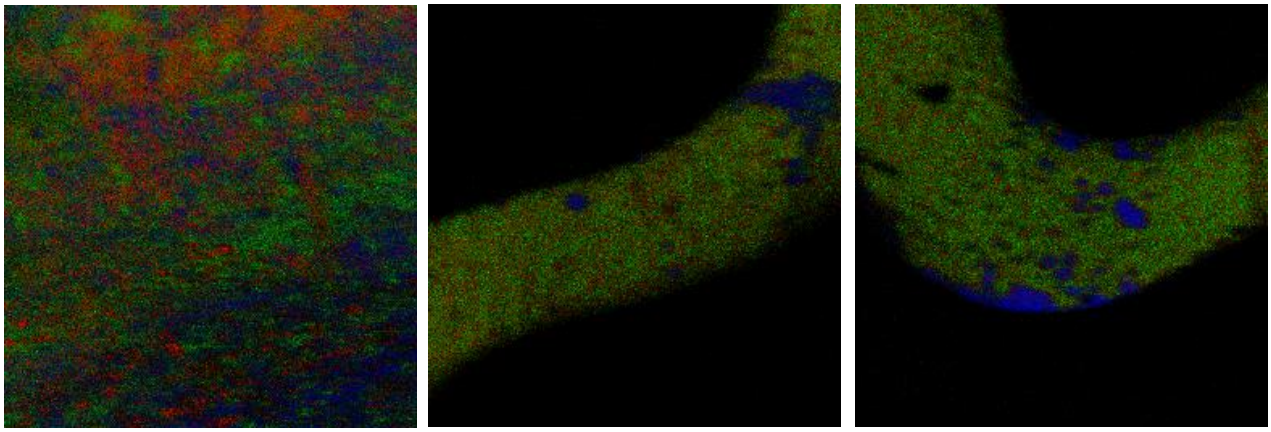


Figure 4.21 ToF-SIMS 2D chemical images taken in positive polarity of the characteristic peaks associated with the drug and the polymer. a.i abluminal drug coated tubing, a.ii abluminal and a.iii luminal surfaces of ArterioSorb™ scaffold prior depth profiling. Sirolimus is highlighted in red, polymer in green, sodium in blue and the overlay of the drug and polymer gives a yellow/orange shade.

The dark areas in images above, corresponds to the loss of signal due to accumulation of electrons at certain areas of the stent. Due to the curvature of the stent it is recommended to cut the stent into small segments although this method is not very practical as it makes sample handling quite fiddly and tricky. Another way to avoid edge effects and loss of signal where electron accumulation is the most intense is to analyse regions of interest, data shown in Appendix C.

4.4.2 ToF-SIMS Depth Profiling and Chemical Imaging

The high sensitivity of SIMS to chemical groups enables in the detection of elements with a concentration down to subsurface per million (ppm) levels , this makes the detection of elements with low concentration achievable [244]. The introduction of argon ion beam for ToF-SIMS imaging and sputtering depth profiling of polymeric materials by SIMS has provided a powerful capability and insight into the 3D imaging and chemical composition of medical devices [245]. 2D images of sirolimus and PDLLA are shown in Figure 4.22.

These images show that the drug (sirolimus) is enriched within the first 0.5μm of the surface. Eventually revealing enrichment of the polymer as shown in the figure presented in green.

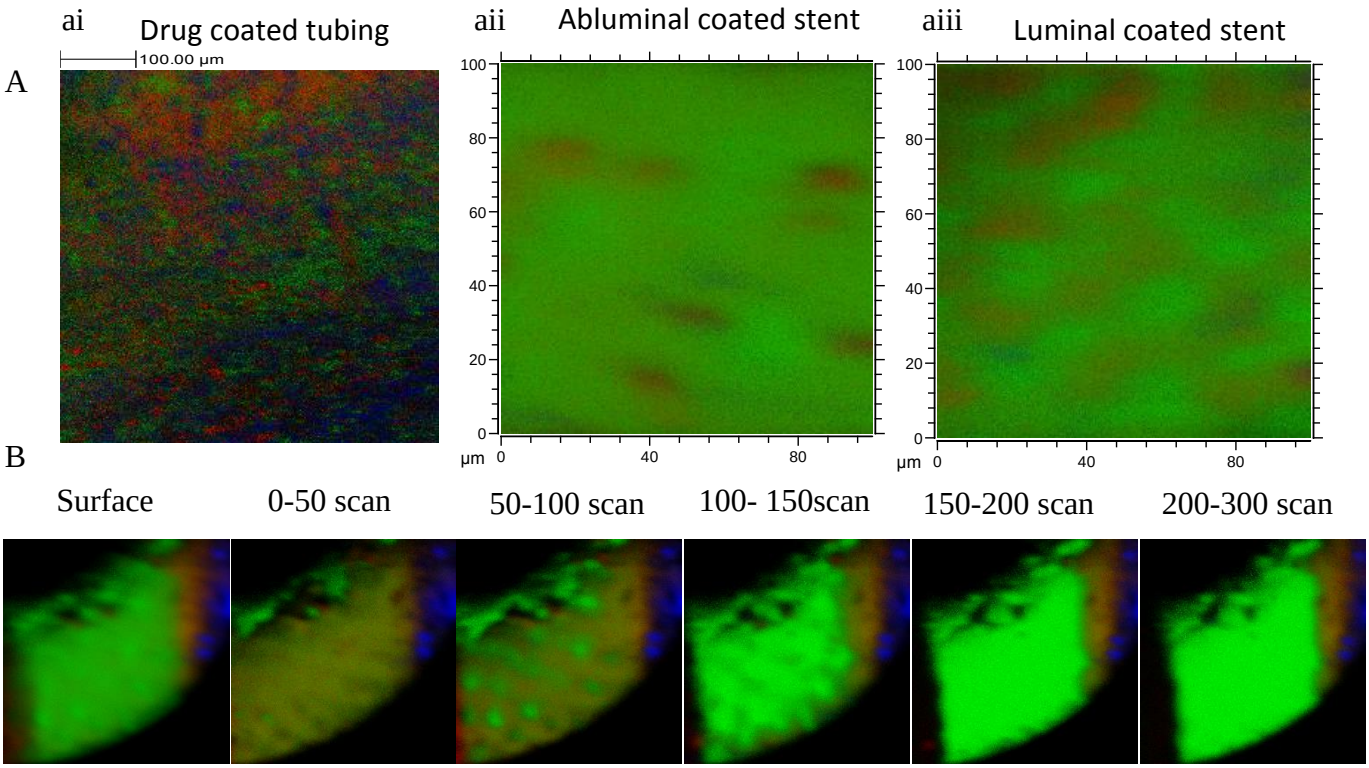


Figure 4.22 2D SIMS overlay chemical images of the characteristic peaks associated with the drug and the polymer. A- a. i abluminal surface of tubing a.i abluminal surface of ArerioSorb™ laser cut stent, a.ii luminal surface of ArterioSorb™ stent. B- ToF-SIMS 2D images at depth intervals of 300 seconds of sputter time over 200 x 200 μm of the abluminal surface of ArterioSorb™ (first generation).

The images at depth in Figure 4.22 reveal that the lateral distribution of PDLLA and sirolimus and how the percentage of each component changes as a function of depth from the surface of the coating.

The starting surface topography can have an important influence on depth resolution, since the surface of the stent is not flat to start with; it was not possible to etch a well-defined crater, Figure 4.23. Sputter rate was established to determine the depth position of the drug/polymer ions for the tubing and the stents. Erosion rate was established for

uncoated polymeric tubing, coated tubing as well as drug/polymer coated stent. Sputtering these materials did not have variability in samples containing drug only or polymer suggesting constant sputter rate.

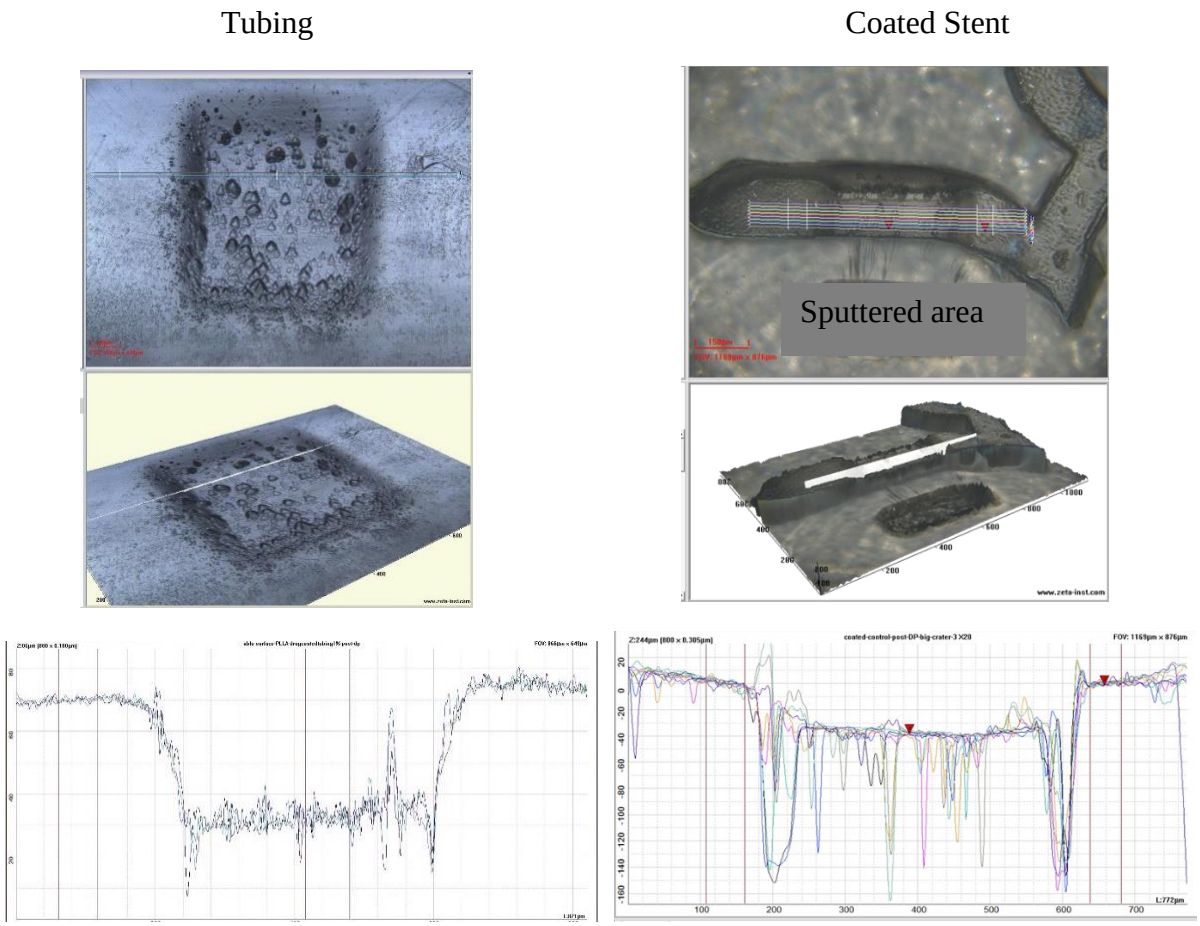


Figure 4.23 3D profiler of drug coated PLLA tubing and drug coated stent post depth profiling ToF-SIMS. Depth craters obtained from a.i tubing, b.i coated stents.

Ideally in depth-profiling, only the secondary ions emitted from the bottom crater are collected, but secondary ions are collected from the wall of the crater and these ions may contribute to the secondary ions in the analysis, however these ions do not represent the concentration of these elements. The only way to avoid this problem is to have an analysis area smaller than the crater size, hence the profile would not be affected by the crater wall, as shown in Figure 4.24. From Figure 4.25 it is clearly apparent that the drug is preferentially localised at the surface and followed by a decrease in the ion intensity

throughout the bulk until it reached a plateau. The drug (red) follows an opposing trend to the PDLLA. As mentioned in Chapter 3 the observed characteristic secondary ion for the PLLA scaffold and those for the PDLLA coating layer are the same as expected.

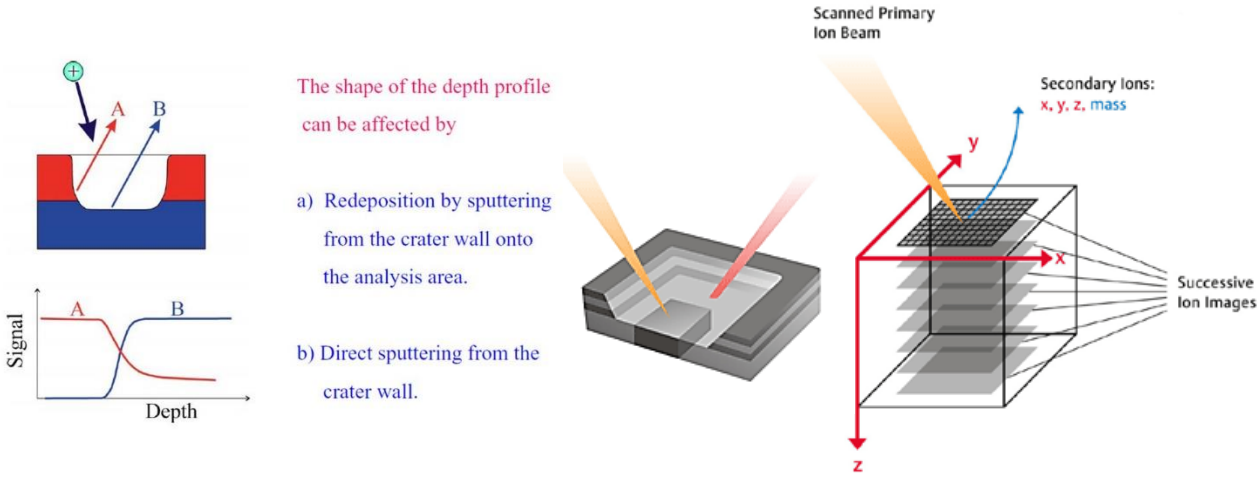


Figure 4.24 Schematic illustrating analysis area and crater bottom.

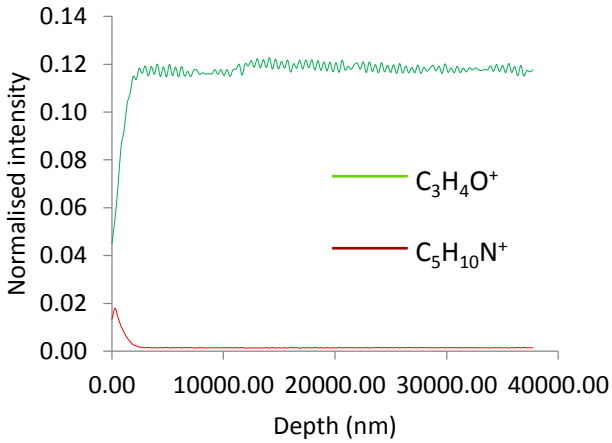


Figure 4.25 ToF-SIMS positive polarity depth profile of the abluminal side of coated tubing using Ar cluster source for depth profiling, in conjunction with Bi_3^+ for analysis. The colour in the green is the polymer (PDLLA) and the red is the drug (sirolimus).

The resulting depth profile in Figure 4.25 of sirolimus in PDLLA shows increase in PDLLA as the subsurface of sirolimus lessen as a function of depth. ToF-SIMS sputtering and profilometry analysis were applied to the surface of the scaffold as well as the tubing. The argon cluster ions were able to sputter through sirolimus/PDLLA spray coated tubing demonstrating that this tubing has potential applications as a ToF-SIMS calibration sample. The intensity profile from drug/polymer coated tubing shows high intensity of the polymer in the near-surface region as compared with sirolimus, both reach a relatively uniform intensity, i.e. steady state.

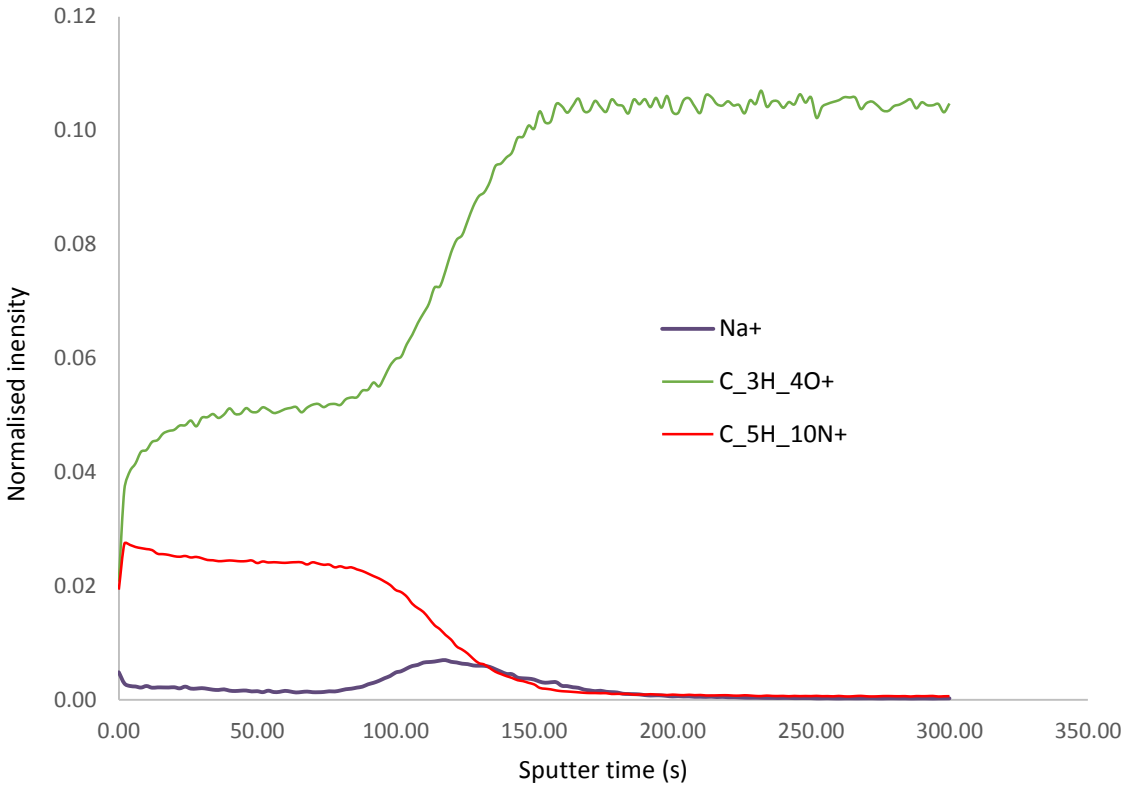


Figure 4.26 ToF-SIMS depth profile showing signal intensity as a function of Ar sputtered depth of drug-coated stent (abluminal surface). Four phases are present in this profile, surface, bulk, interface and substrate (PLLA). The characteristic signals in the positive polarity are sirolimus (red), PDLLA (green) and sodium (purple).

The ToF-SIMS depth profile data Figure 4.26, specifically of drug and of polymer, reveal a surface that is composed mostly of sirolimus followed by a region that is depleted of the drug. Beyond the drug-depleted region, a fairly uniform distribution of drug and PDLLA is observed. Sodium and PDMS were also monitored as part of this investigation, more details are provided with regard to contaminants is explained in Chapter 5 as part of *in vitro* degradation study.

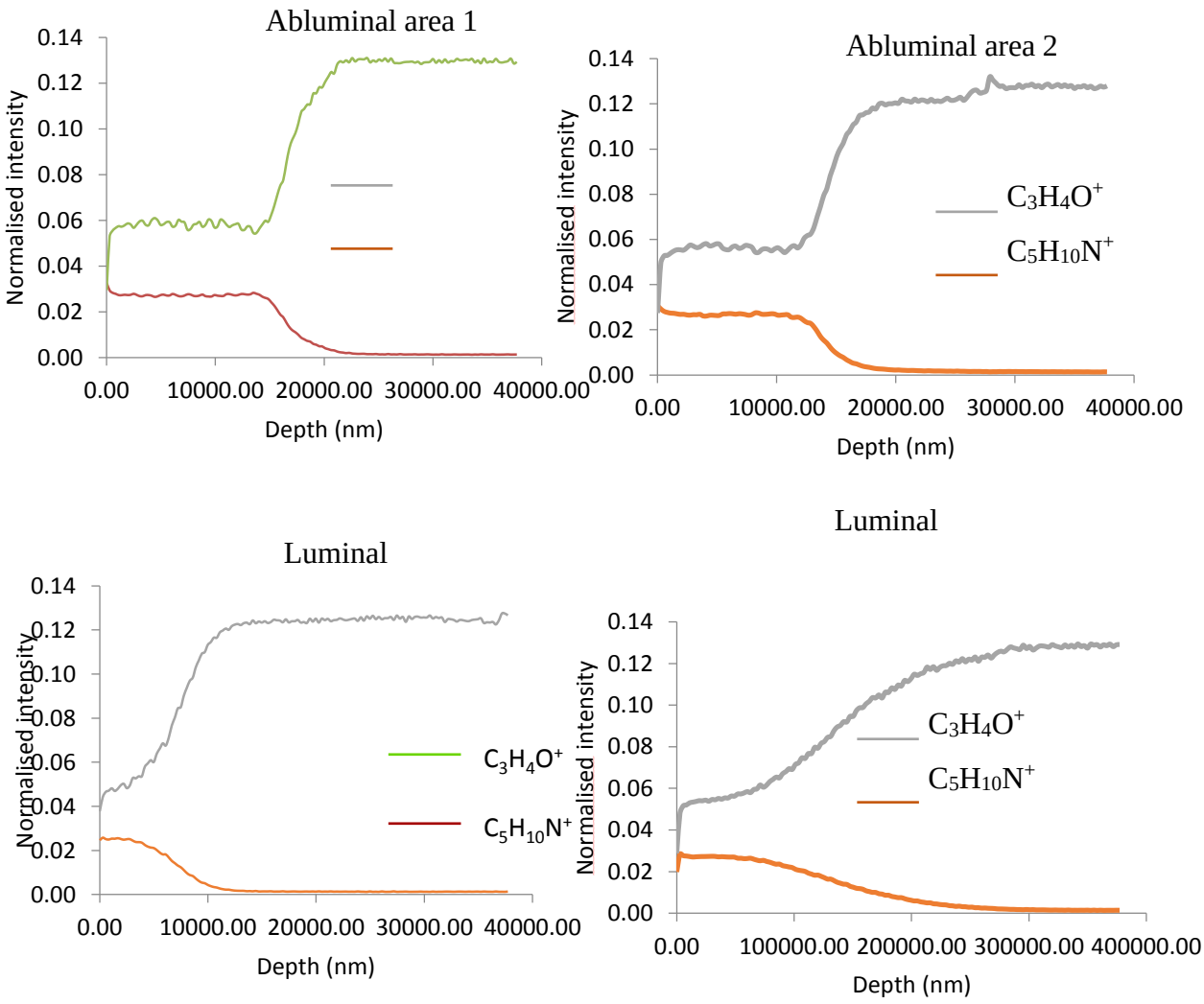


Figure 4.27 ToF-SIMS depth profile of two areas taken from the abluminal and luminal side of the drug-coated stent. Secondary ion intensities for selected fragments plotted as a function of depth. Drug enriched regions are observed in all depth profiles.

It is observed in Figure 4.27, the depth profile of the luminal side appears somehow fairly similar to the abluminal side, with the drug being enriched at the surface, and nonetheless we already know the coating layer on the abluminal side is thicker than the luminal.

The drug seems to be enriched at the surface followed by a concentration gradient as a function of depth. From the depth profile data, the thickness of the drug coating was calculated to be approximately 4 µm for the top surface. It is evident the drug is enriched at the surface and shows a decrease intensity throughout the bulk. The depth profile implies there is drug at the near surface and successive polymer enrichment in the bulk area. In another word, the depth profile for all drug coated scaffolds give a trend of being divided into 4 areas: surface, bulk, interface and substrate (scaffold-PLLA), as shown in Figure 4.27. The drug appears to be enriched at the surface, then the intensity of the drug drops at around 100 nm and the polymer takes an opposing trend; this trend is consistent in all analysed areas.

4.4.3 3D Image Reconstruction

3D reconstruction images were reconstructed from the depth profile data. These images have mapped the variation in drug/polymer distribution. ToF-SIMS imaging with argon cluster sputter depth profiling provided detailed insight into the three-dimensional (3D) chemical composition of a series of polymer coatings. A uniform sputter rate was obtained in these samples.

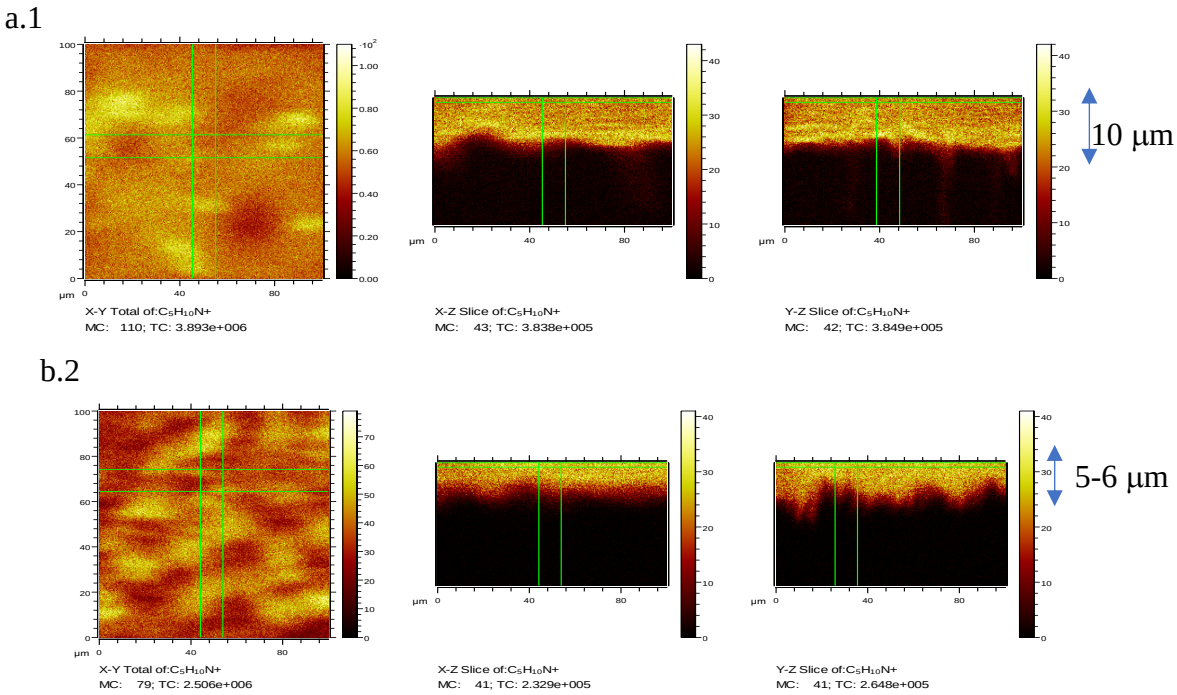
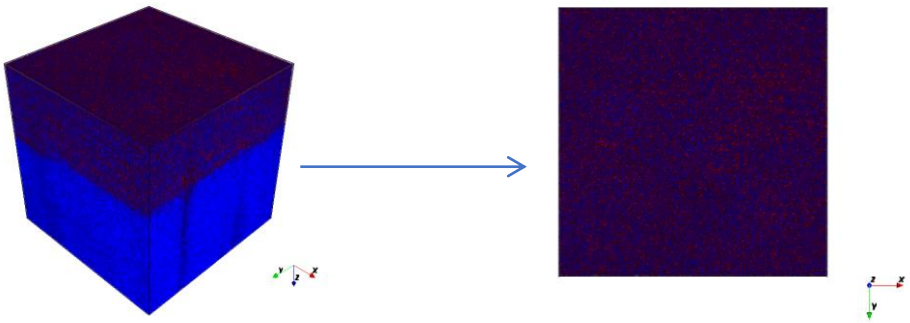


Figure 4.28 Reconstructed 3D cross sectional view of the positive ion data taken from depth profile of sirolimus in the a.1, abluminal and b.2, luminal surface coating of Arteriosorb^{TM} scaffold.

The coating layer on the abluminal side of the scaffold thicker than the luminal area as shown in Figure 4.28 and Figure 4.29. The distribution of the drug in the coating-layer was investigated using 3D chemical imaging. The ToF-SIMS data were constructed as XYZ and XY, examples of which reported in Figure 4.28. A set of 3D images of the control stent, constructed from the 2D images at each cycle of the positive polarity depth profile, are rendered in Figure 4.29 and Figure 4.30. The heterogeneous appearance of the coating layer was observed in 3D image volume as shown in Figure 4.30.



3D Render Overlay of: $C_5H_{10}N+$, C_3H_4O+

Figure 4.29 3D SIMS images at depth extracted from abluminal surface of ArterioSorb™, acquired in the positive polarity using 3D-render in volume view mode. The colour in blue represents the polymer and in red is sirolimus.

The 3D ToF-SIMS images deduced using volume mode are difficult to interpret the interior organisation of the drug and polymer. Therefore iso-surface mode was used as a main tool to explain the distribution of the drug in the coating layer of the stent. The 3D ToF-SIMS images of as-fabricated stents, showing the iso-surface of sirolimus, $C_5H_{10}N^+$ (red), and PDLLA, $C_3H_4O^+$ (green), are rendered in Figure 4.30.

Iso-surface mode is a useful method of 3D chemical imaging as many components may be imaged together, and the opacity of each layer was reduced to view the interior of the image volume. Before generation of each iso-surface, an intensity value (threshold) was selected to allow features of the chemical distributions to be identified and amplify the subsurface domain structure (Figure 4.30). The choice of threshold is critical and needs to be optimised for each sample. Changing the value of threshold can drastically change the visualisation result. In another words, the rendering process makes sense if there is a clear separation between regions with signal that is higher or lower than the selected threshold value [246].

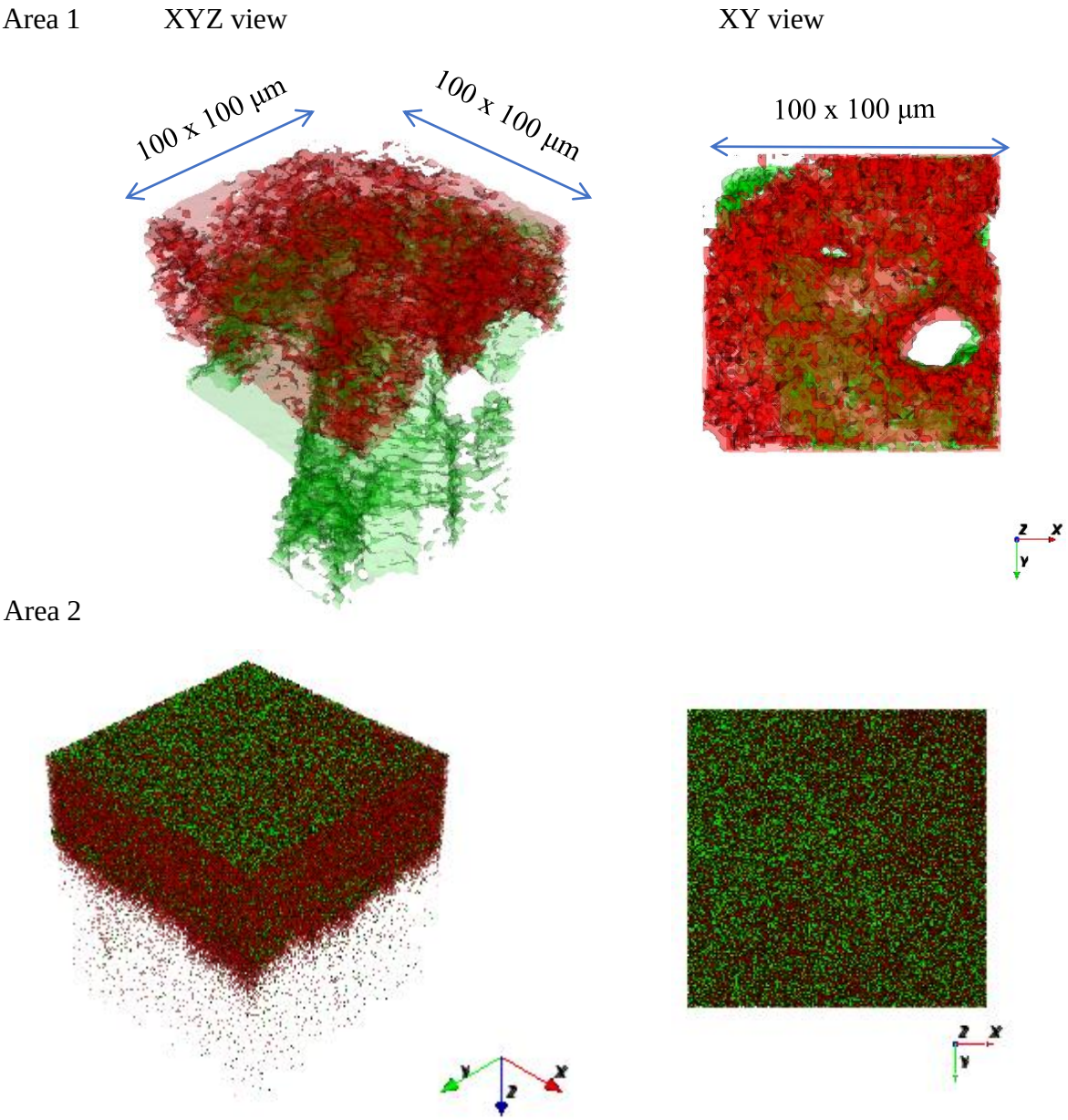


Figure 4.30 3D SIMS overlay visualisation at-depth acquired from the depth profile on abluminal surface of a coronary scaffold coating containing sirolimus/PDLLA. Data acquired in the positive polarity. Sputter erosion was performed using Ar cluster ion beam. The field of view of each image is 100 × 100 µm. Iso-surface overlay of sirolimus at (m/z= 84, red), and PDLLA at (m/z = 56, green), showing the surface view. The opacity of the polymer was reduced so that the interior of the image can be clearly observed.

The iso-surface images in Figure 4.30 reveal the subsurface distribution of both the polymer and drug matrix. The drug is enriched at the surface and also the subsurface

region contains some of the drug component as well.

4.4.4 Surface Composition of Sirolimus/PDLLA Coating in ArterioSorb™ Scaffold by XPS

Since ToF-SIMS is not a quantitative method and the matrix effect has an influence on the intensity of ions and their environment; XPS was used to provide quantitative data[212]. XPS was carried out to permit the determination of the chemical composition of the coating-layer (sirolimus/ PDLLA) in bioresorbable PLLA stent as received. XPS work carried out in this chapter was done on the ThetaProbe at Nexus, Newcastle.

XPS characterisation provided quantitative measurements with a depth of 10 nm. The peak positions of elements in XPS spectra are affected to their chemical status, for instance, carbon peak positions in CO_2 are not the same to those in saturated hydrocarbons. This is known as chemical shift which essentially provide extra information for chemical analysis [244]. First the analysis was conducted on standard reference samples (PDLLA and Sirolimus), structure of both sirolimus and PDLLA shown in Figure 4.31, followed by the characterisation of the actual stent as received. Refer to Chapter 3 for XPS analysis of the starting materials.

XPS has been performed on both the abluminal and luminal side, but only the abluminal side has been presented in this chapter. The theoretical atomic percentage of sirolimus and PDLLA were reported in Chapter 3. Peak identification in spectra was the primary task in quantifying the elements present on the surface of the stent.

a. Sirolimus

b. PDLLA

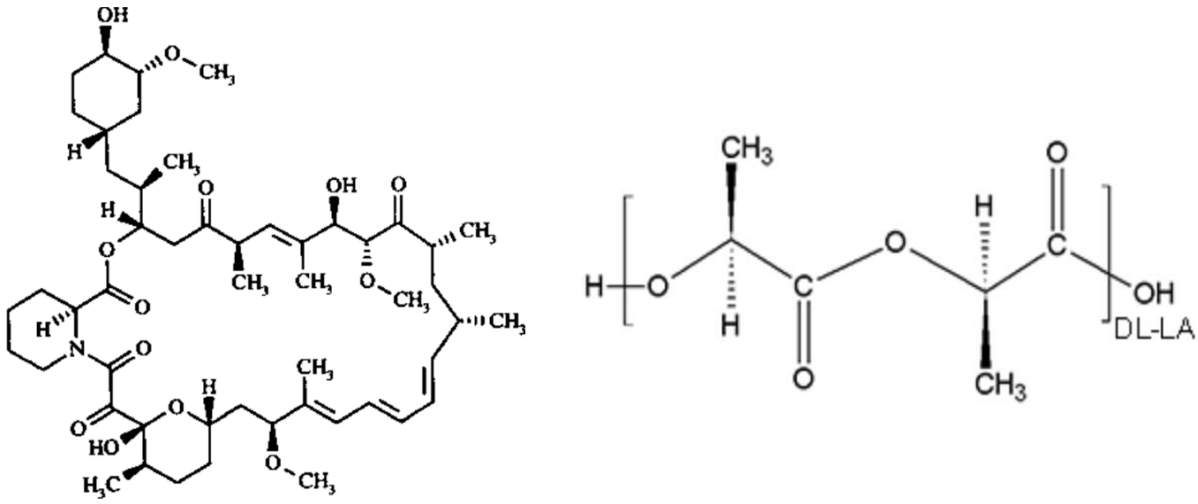


Figure 4.31 Chemical structure of a. Sirolimus and b. PDLLA [247,248].

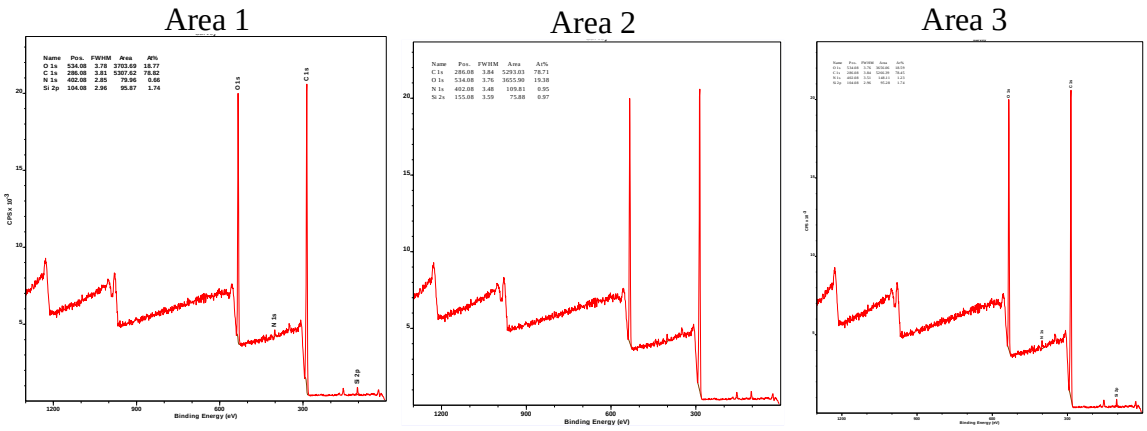


Figure 4.32 Wide-scan XPS spectra of sirolimus/PDLLA coated bioresorbable stent of 3 areas of abluminal coating layer of ArterioSorb™. Spectra were acquired with a monochromated Al Kα (1486.7 eV, Ar_{800+}).

Figure 4.32 shows typical wide scan XPS spectra of a sirolimus/PDLLA spray coated stent with a drug/polymer loading of 50 % / 50% weight ratio. The spectra show peak intensities for C 1s, O 1s and N 1s. A nitrogen peak was observed on the chemical composition spectra of stent as received, which is the diagnostic marker for the drug (sirolimus, $C_{51}H_{79}NO_{13}$) in this case, since it is the only material containing nitrogen in this medical device, because there is no nitrogen in the molecular structure of PDLLA or PLLA. Some other peaks were also observed such as silicon and fluorine (data not shown for the fluorine), this often due to contamination from the stent packaging or sample handling. These materials were previously detected by ToF-SIMS.

The nitrogen level in pure sirolimus is 1.54 %, in contrast the nitrogen level of sirolimus in as-fabricated scaffold % 63 (0.9/ 1.54) x 100. This is undoubtedly more than the designed bulk ratio of the drug of 50 %, indicating a drug-rich surface of the sirolimus/PDLLA bioresorbable scaffold. A similar phenomenon was found on sirolimus/PDLLA coated stent analysed by ToF-SIMS (Figure 4.30). The amount of diagnostic chemical groups detected can be directly correlated to the amount of sirolimus and PDLLA present at the surface. For stents, as received, the relative amount of C, O and N are relatively similar to the expected composition of sirolimus and this suggests the significant presence of sirolimus at the surface compared to the bulk.

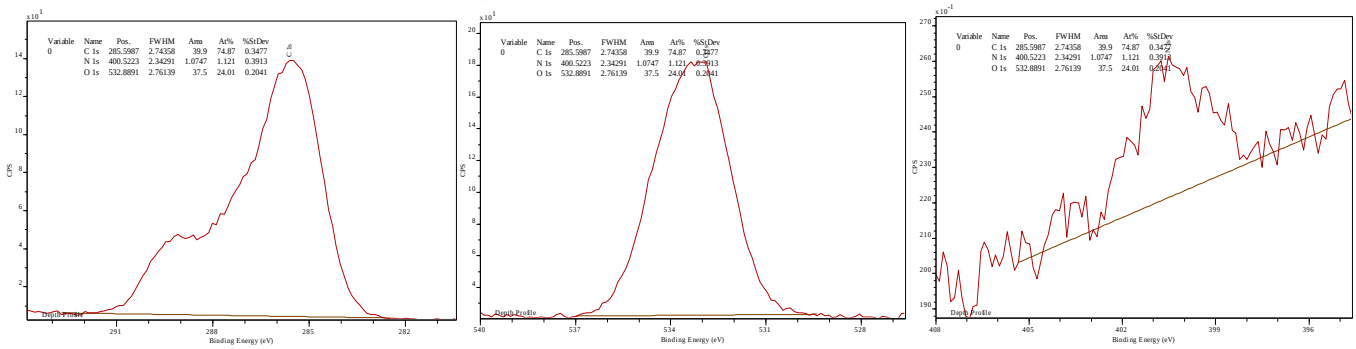
Table 4.4 XPS elemental % of characteristic components present in the abluminal coating in Arteriosorb™ of three different areas.

Sample ID	C1s	N1s	O1s
Abluminal: area 1	78.82	0.66	18.77
Abluminal area 2	78.45	1.23	19
Abluminal area 3	78.71	0.95	19.38

From Table 4.4 there seem to be an increase number of carbon due to adventitious hydrocarbon from the environment or reduction of oxygen.

Abluminal

C 1s O 1s N 1s



Luminal

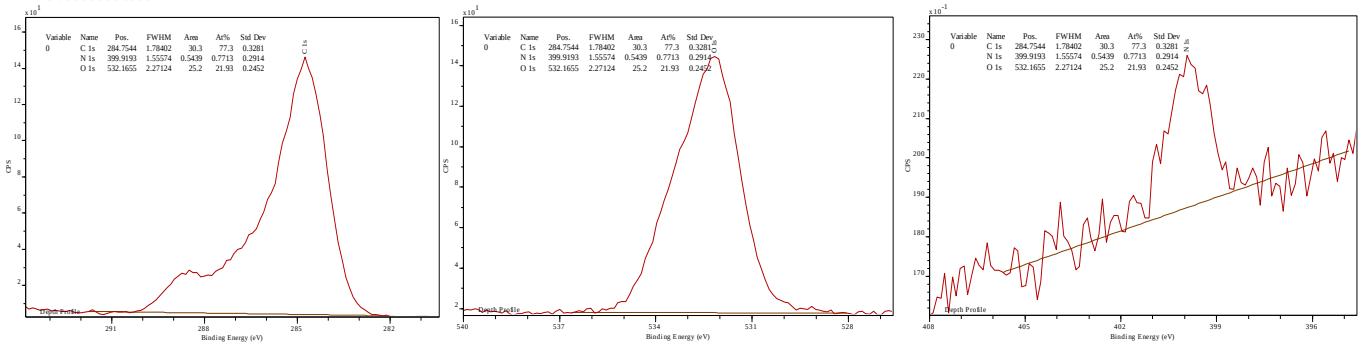


Figure 4.33 XPS high resolution spectra obtained in snapshot mode using ThetaProbe XPS (Nexus, Newcastle University). The spectra show C 1s, O1s and N 1s for the abluminal and luminal surface of ArterioSorb™ scaffold.

Figure 4.33 shows high resolution spectra of C1s, O1s and N 1s. The spectra show that the highest level of N 1s relative to the presence of sirolimus on the abluminal coating of the stent, in contrast less N was observed on the luminal side of the stent.

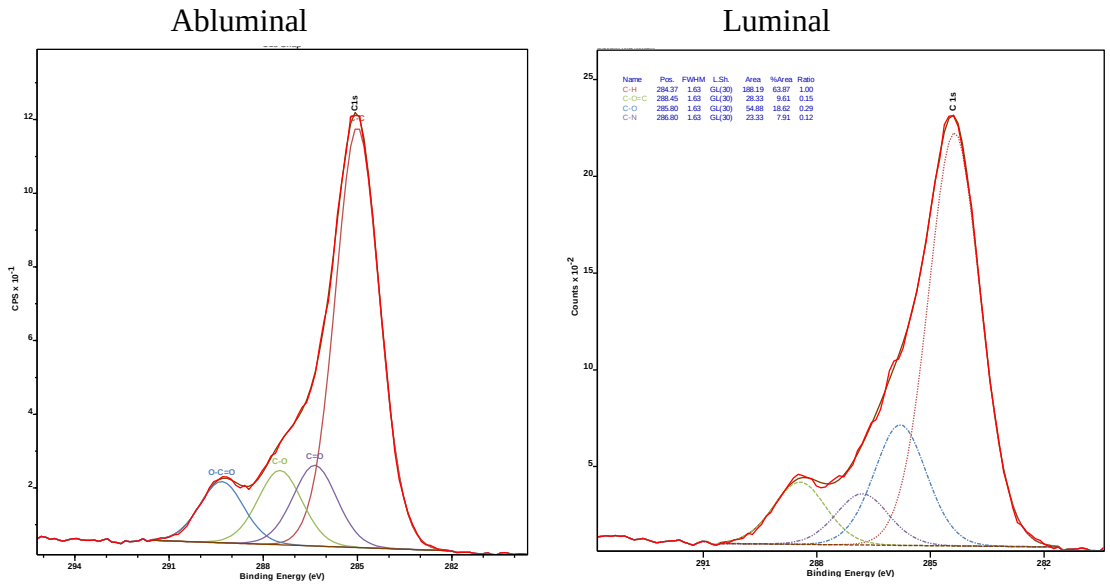


Figure 4.34 C1s XPS spectra of the abluminal and luminal surface of ArterioSorb™ coated stent at depth = 0 nm.

A multi component envelope was applied on the C 1s region. Figure 4.34 highlights the components whitin the C 1s envelope. Three carbon components were previously observed in PDLLA at 285, 287 and 289 eV (Chapter 3), these peaks are C-C, C-O and O-C=O, confirming there is no drug in them. With regard to sirolimus, it has a theoretical atomic percentage of N of 1.5 %, C 1s of 78.5 % and O 1s of 20 %. The XPS experimental data obtained using Thetaprobe XPS suggested a ratio for atomic percentage of abluminal surface of N (0.9 %), C (77%) and O is (21%). Suggesting drug predominantly enriched on the surface of the scaffold.

Figure 4.34 shows carbon atoms in different environment generate three peaks, as described above. The XPS spectra with defined peak positions and relative peak intensities can be used as fingerprint to identify sirolimus and PDLLA. Two components were associated with the N1s region of the XPS spectra, these components related to the nitrogen within the sirolimus molecule. The hydrogen atom from the carboxylic acid in the polymer protonate a portion of the nitrogen in the sirolimus to make the signal in Figure 4.34. A small shift in the binding energy have produced an overlap as shown in Figure 4.34. The overlap was resolved carefully with assistance of CasaXPS software by using fit component and also the FHMW was fixed[153]. Four peaks are representative of

the drug and these peaks are 285,286,287 and 289 eV, however the peak at 287 eV is contributed to from the polymer only, which has also displayed other peaks that have been overlapped with 285 and 289 eV, i.e. are representative of the drug.

Component peaks of the C1s spectra were chosen based upon the shape of the core level envelope. The spectra showed contribution from C-O functional groups at 287 eV and from O-C=O at 289 eV from the polymer. The contribution from nitrogen forming N-C=O and C-N-C expected to appear at 286 and 285 eV, however these peaks overlapped with peaks at 285 and 287, that (C-O) and (C=O), respectively, due to a small chemical shift. Binding energy shifts from the polymer were consistent with literature values [249]. Peaks at 287 and 288 eV are exclusive peaks of sirolimus, which can also display the peaks at 286 and 289 eV that overlap with PDLLA peaks.

XPS presented variability in drug composition. The reason for this difference might be due to solvent evaporation kinetics. This explains the phenomena behind the variability of drug composition on each area of the stent. XPS analysis was conducted on series of stents (additional data described in Appendix D), and it was evident some areas of the stent have presented higher drug concentration than others, showing heterogeneity in drug loading, causing drug concentration gradient. This was observed in ToF-SIMS. Another reason to this finding might be due to drying process of the coating, where de-mixing of the drug and the polymer occurs with preferential surface segregation of the drug.

The XPS data reported in Figure 4.32 shows presence of Si. The presence of such material could come from possible contamination during stent manufacturing or sample handling. The presence of substances such as Si or Na contribute to a matrix effect, that lead to enhance ionisability of sirolimus/PDLLA and ion yields near the surface [150]. The drug percentage on the surface is higher than the bulk, meaning the drug ratio on the surface is close to the bulk design, suggesting the chemistry information at the top surface less than 10 nm in depth can be acquired by XPS, reflecting the bulk information up to microns.

4.4.5 XPS Depth Profiling

XPS depth profiling of the chemistry of the surface layer of bulk materials was generated on spray coated stents an example of which is shown in Figure 4.35 and Figure 4.36.

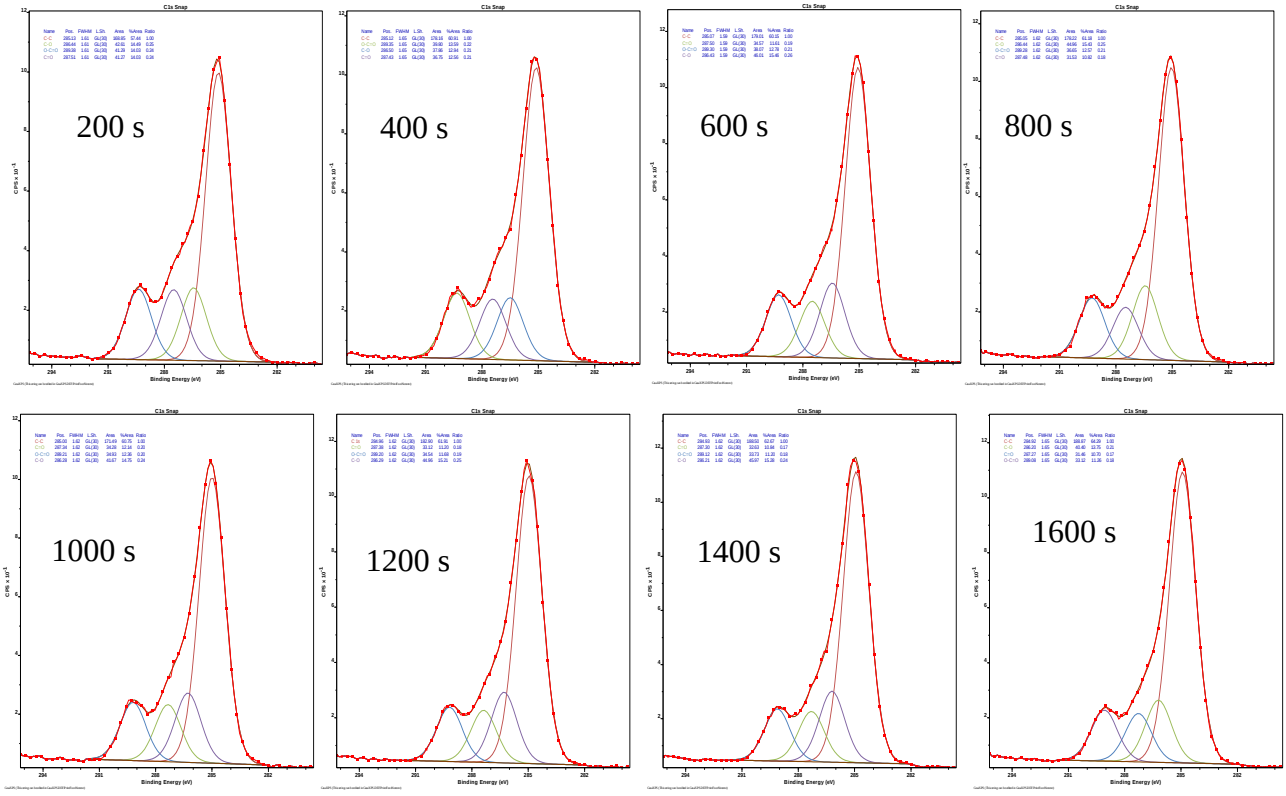


Figure 4.35 High resolution spectra of the C 1s region envelope fitted with components of the abluminal area of ArterioSorb™ as a function of sputter time.

Figure 4.35 shows the C1s spectra of the abluminal surface of spray coated stent as fabricated. The depth distribution of sirolimus is monitored by the profile of nitrogen (green) and of PDLLA is indicated by the profile of oxygen (blue), there is a higher fraction of oxygen in the molecular structure of PDLLA than that of sirolimus. The carbon intensity of the polymer (C-O) of sputtered surface was observed to be less than one of pure polymer, this small decrease in intensity is assigned to chain scission of the polymer at the ester linkage forming a carbonyl group [250].

The C-C (hydrocarbon chains) increases with depth suggesting depletion of the drug and exposing the substrate (PLLA), Table 4.5. However, the shape of the peak in Figure 4.35

has not changed significantly at 1600 sputter time, suggesting longer analysis run is required to get into the substrate.

Table 4.5 Quantification table of C1s envelope components of ArterioSorb™ scaffold displaying percentage atomic concentration as a function of depth.

	% area under C1s envelope			
Sputter time (s)	C-C	C-O	C=O	O-C=O
0	66.05	12.67	11.67	9.61
200	57.44	14.49	14.03	14.03
400	69.91	12.94	12.56	13.59
600	60.15	15.46	11.61	12.78
800	61.18	15.43	10.82	12.57
1000	60.75	14.75	12.14	12.36
1200	61.91	15.21	11.20	11.68
1400	62.67	15.28	10.84	11.20
1600	64.29	13.75	10.70	11.26

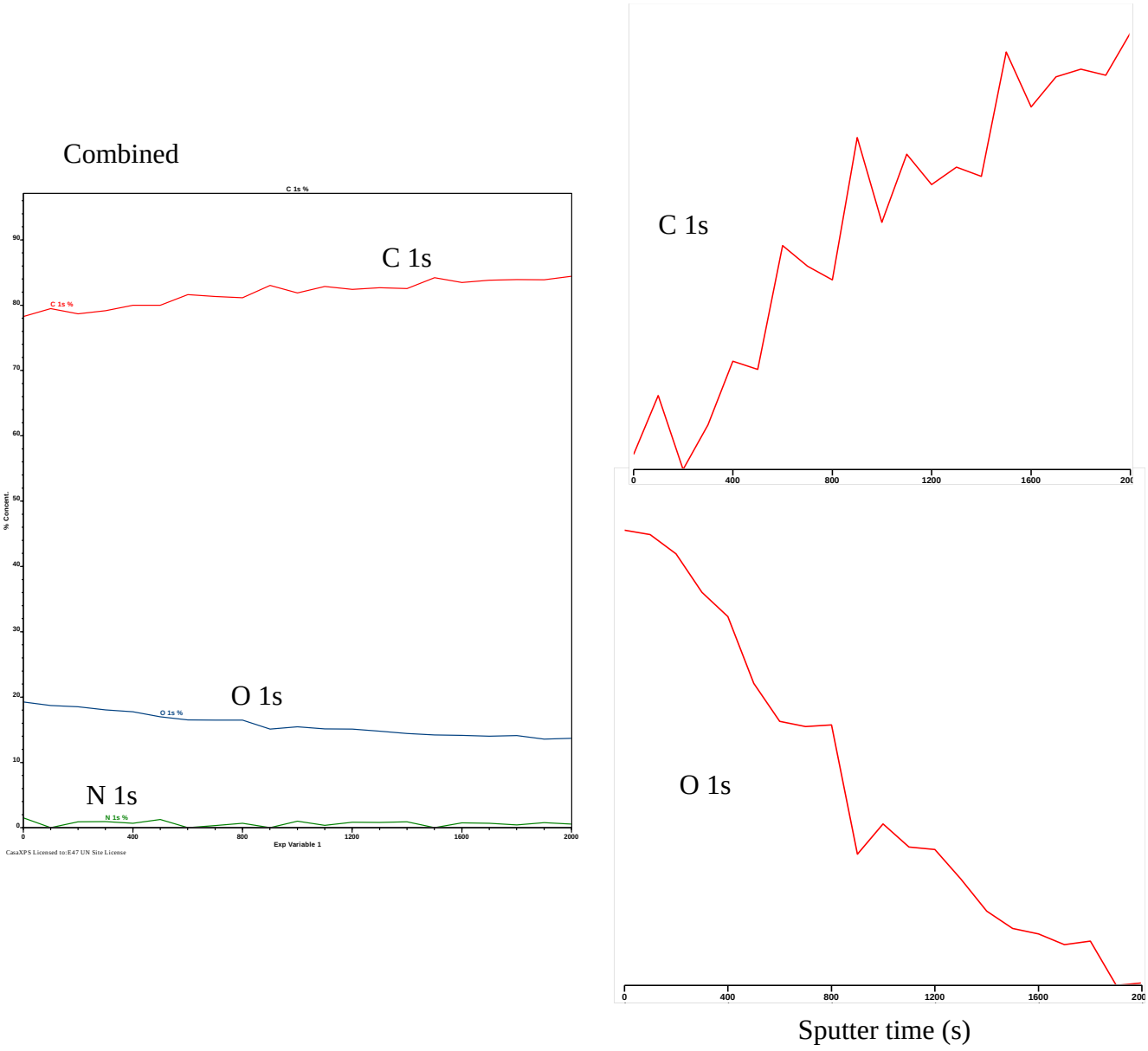


Figure 4.36 XPS depth profile of the stent coating, showing O 1s and C 1s. The atomic composition is shown as a function of sputter time.

The XPS data showed that the presence of sirolimus in ArterioSorb^{TM} scaffold could be quantitatively measured from the surface and within. However, XPS data analysis was not an easy process, for instance, factors such as chemical shift and surface charge can complicate peak identification, also the presence of auger peaks may affect the identification process of peaks. The spatial distribution of N 1s on the surface of bulk sample should be of an interest for future work and a perfect comparison between ToF-

SIMS and XPS. Due to the lack of spatial resolution of the XPS method there is an open question to how the coating layer is distributed over the surface of ToF-SIMS, which was the main focus to answer this question with regard to homogeneity or heterogeneity of the applied coating on the stent. Nitrogen and oxygen analysis, reveal a surface that is composed predominantly of sirolimus followed by a region that is depleted of the drug. The differences between the interface observed in TOF-SIMS and the one in XPS are dissimilar and this difference due to the heterogeneity and morphological variation from one batch to another.

4.5 Compositional with Depth by Raman Spectroscopy

Confocal Raman mapping (CRM) was used as a correlative method for the ToF-SIMS analysis to provide a 3D understanding of the morphology of components (Sirolimus and PDLLA) across the surface and also within the bulk of PLLA stent. Raman spectroscopy was used to differentiate each component found in the ArterioSorb^{TM} sirolimus-eluting coronary stent. Raman microscopy has been used to characterise coating material such as polymer [251] or diamond (carbon) [252], Active pharmaceutical ingredient (API) distribution or polymer thickness in drug-eluting coatings [253,254].

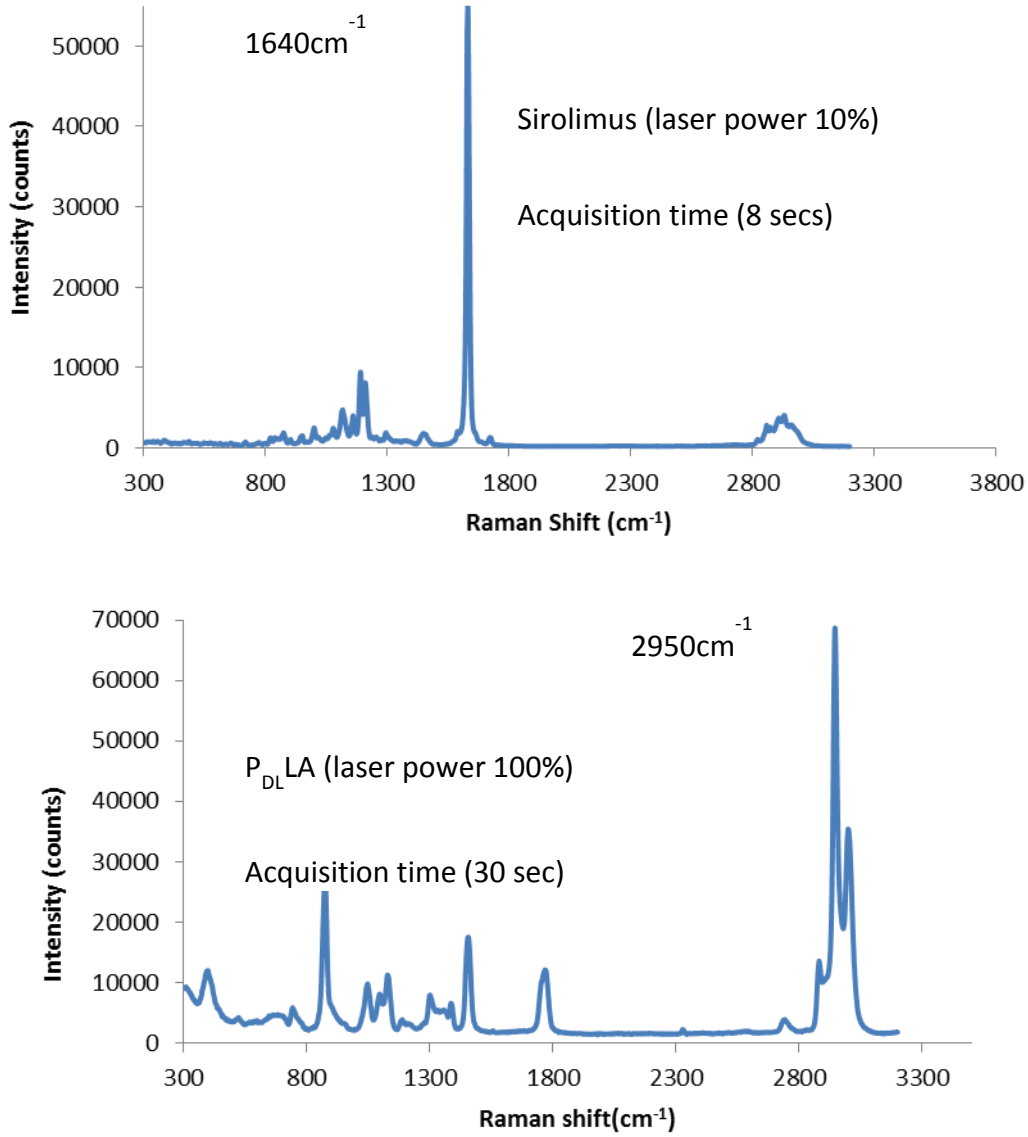


Figure 4.37 Raman spectra of pure sirolimus and PDLLA.

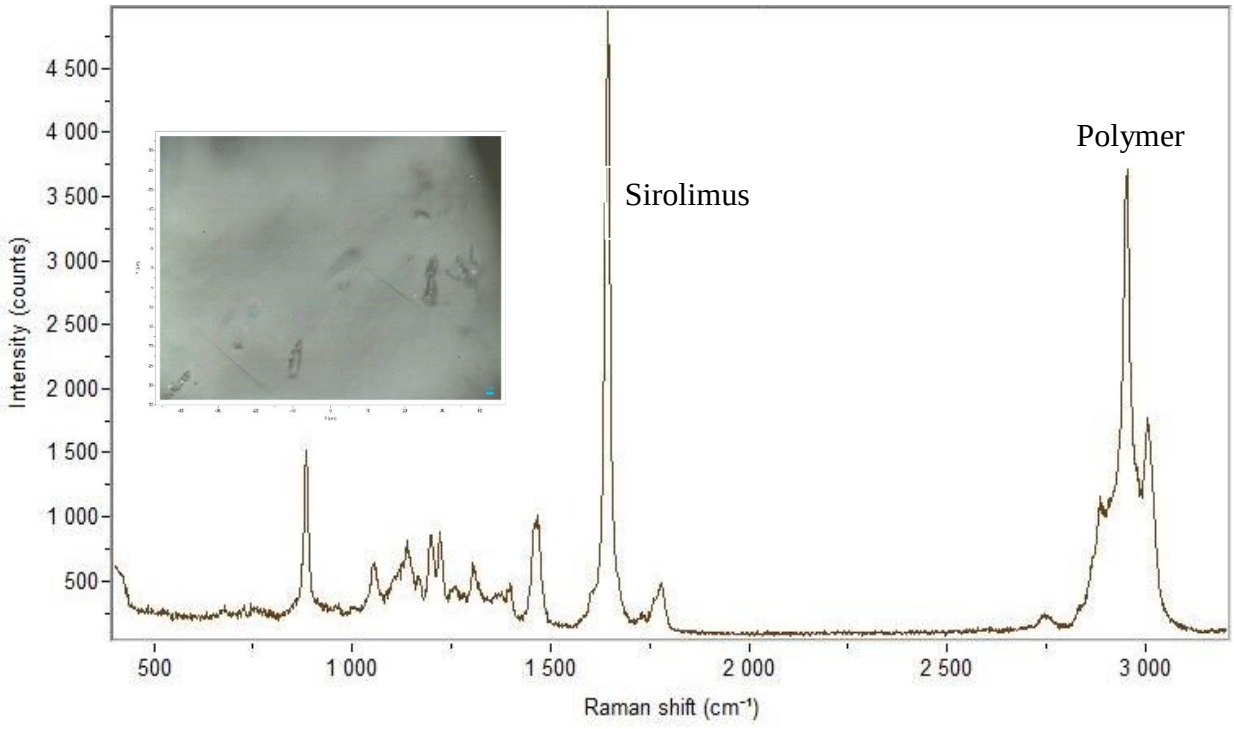


Figure 4.38 Typical Raman spectra of drug coated stent using a green 532 nm laser.

CRM data show drug present all over the surface of the scaffold but with areas of high localisation of drug intensity, again agreeing with ToF-SIMS data showing that the drug distribution is heterogeneous at the micron scale. Intensity of the signals associated with the sirolimus in the region between 1600 and 1700 cm^{-1} and for the polymer 2950 cm^{-1} [255], as shown in Figure 4.37. Spectra of powdered sirolimus and PDLLA were obtained at wavelength of 532 nm, as shown in Figure 4.37. Prior to *in vitro* degradation study, the 50/50 sirolimus/PDLLA coating appeared homogenous and thick, and the spectra of sirolimus and PDLLA show no evidence for chemical changes in the PLLA polymer.

Previous studies have reported two spectral bands that are related to the amorphous and crystalline phase of PLLA. These peaks are found at 755 cm^{-1} and 869 cm^{-1}. The peak of 755 cm^{-1} is assigned to the crystalline phase, while the peak at 869 cm^{-1} relates to the amorphous phases [256,257]. The Raman images of sample as received in Figure 4.39 (z stacks) show a transition from drug-enriched surface of sirolimus to region enriched in the polymer. Below the surface the area is composed of PLLA. A false colour overlay is

given in Figure 4.39, where sirolimus is red and PDLLA is green. The Raman images show the surface to have large areas rich in sirolimus and smaller areas rich in PDLLA showing a similar structure to that observed in the ToF-SIMS images. Also, obvious separation for the sirolimus and PDLLA is evident, where there was a distinct layer of sirolimus in the upper half of the coating.

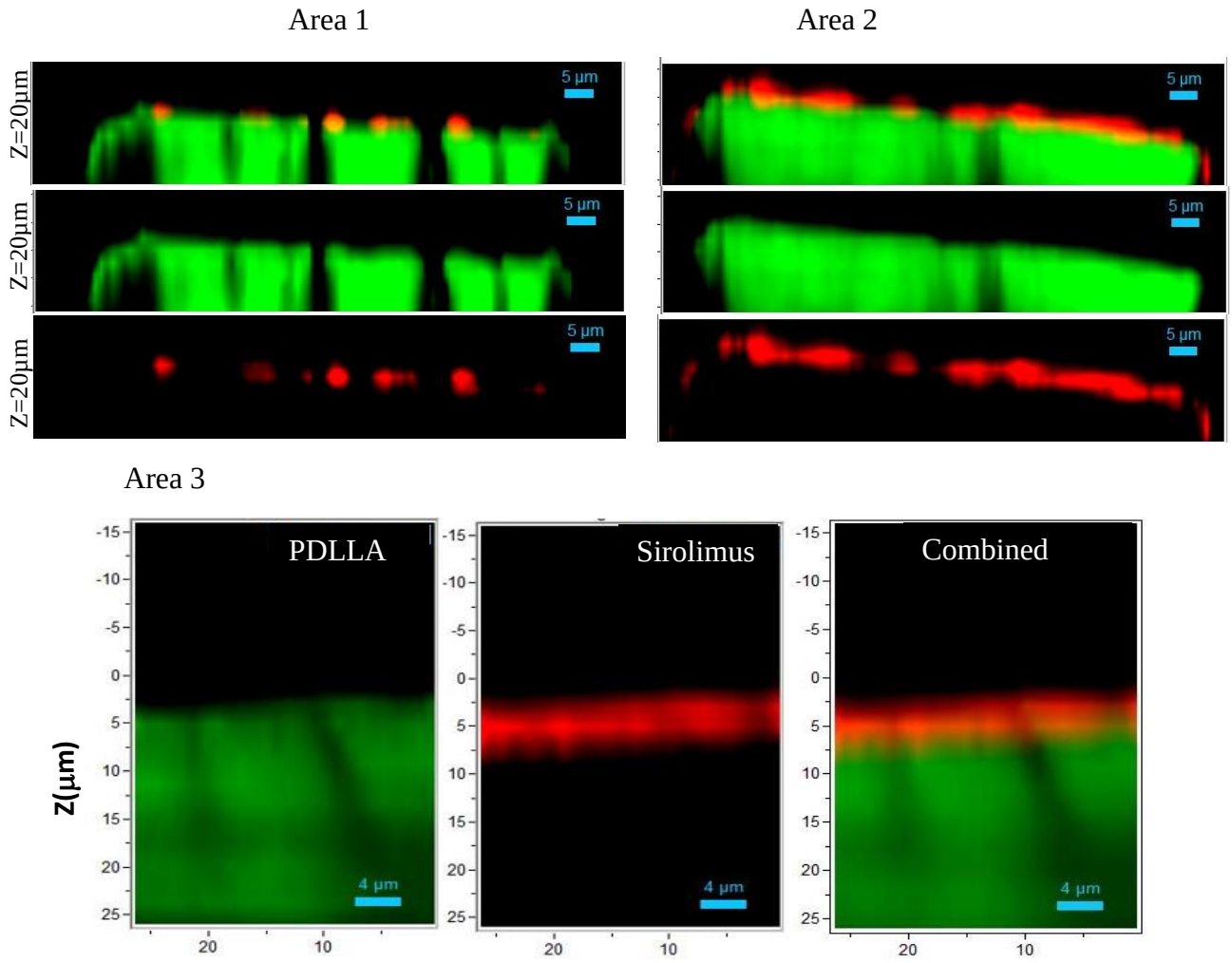


Figure 4.39 Raman microscopic images of the ArterioSorb™ stent, taken from three areas of abluminal surface. The dark region above the coating represents void. The colour of the images relates to relative Raman signal intensity of sirolimus (red) and PDLLA (green). Overlapping regions of sirolimus and PDLLA yields shades of orange and yellow.

The Raman images display a transition from a drug-enriched surface to region enriched in the polymer. Data obtained from analytical techniques describe the distribution of the drug and the polymer within the coating layer, where AFM gave an insight into the organisation and topography of the sample, ToF-SIMS and Raman enabled us in understanding drug distribution in 3D at nano-meter and micro-meter resolution and XPS was useful in quantifying the distribution of drug.

4.6 Conclusions

Surface sensitive techniques demonstrated here is in this thesis, have been successfully used to characterise the surface morphology and drug distribution heterogeneity in series of ArterioSorb^{TM} stents. Using an amorphous polymer such as PDLLA gives good solid dispersion and potentially a homogenous system. Features observed on the coating layer of the scaffold were semi-crystalline by definition, which leads to a phase observed

The use of inert and friendly coatings results in the improvement of drug eluting stents, which are also modified to changeable wall sheer conditions. Bioresorbable polymeric stents are a highly attractive concept with a desirable goal of preventing potential (metal) stent fracture during restenosis. Although magnesium, iron and zinc their alloys can be used as an alternative bioresorbable material and they can disappear. Thinner struts are one of the key areas under intense research because of their prominence in terms of providing a reduced cross-sectional profile within the vessel, improved stent flexibility, and potentially reduced restenosis. The work described in this thesis has been undertaken in order to allow a greater understanding of the use of surface analytical techniques for the characterisation of fast evolving medical devices. It is an established fact that the complementary use of multiple surface analytical techniques is capable of providing a deep understanding of the chemical and molecular structure of the sample. The AFM technique has the advantage of recording the change in the surface morphology from one area to another. This allows the evolution of surface morphology to be followed. This combined approach of using the analytical techniques of ToF-SIMS (imaging and depth profiling), confocal Raman and other complimentary methodologies provides a powerful tool-set for the study of the spatial chemical distribution of biomolecules and excipients such as surfactants within controlled release formulations

such as stents. The high lateral resolution in ToF-SIMS imaging achieved providing valuable characterisation results, fulfilling an aim of this thesis. Chemical heterogeneity was observed in the surface and the bulk of the stent. AFM and SIMS have provided analysis of the outer surfaces of the coating on the stent, where AFM was helpful in obtaining atomic scale imaging as well as provided a direct measurement of the intermolecular forces. Raman helped in the generation of images illustrating the distribution in the interior of the coating-layer. Chemical information was obtained in 3-D at depths. The concentration of sirolimus decreases with depth, although the drug was present throughout the coating layer, which indeed confirmed the potential of this cutting-edge technology to be used as a prolonged drug delivery system. Only limited work was done by XPS, however, was enough to provide an understanding of materials in ArterioSorb^{TM} scaffold. XPS analysis confirmed the existence of sirolimus on the surface of the stent with high percentage compared to the bulk implying a drug rich region, where ATR data maintained relative drug rich region of up to 1 µm. Our analysis has revealed a complex and heterogeneous organisation of sirolimus distribution within the stent that is likely to have considerable influence on the kinetics and mechanism of release of the bioactive molecule (sirolimus) from the polymer network in such a medical device.

5 UNDERSTANDING THE DISTRIBUTION OF SIROLIMUS AND RELEASE FROM THE PDLLA COATING LAYER

The previous chapter showed how the complementary analytical techniques of AFM, ToF-SIMS, XPS and confocal Raman microscopy were used to characterise the novel fully bioresorbable scaffold. The drug release profile of drug eluting stents is important, as the drug release profile may affect the subsequent neointimal formation after stent implantation[258]. In this chapter, the release of sirolimus from the bioresorbable matrix (sirolimus/PDLLA) was studied.

Release data of drug eluting stents such as the CYPHER^{TM} stents are not easy to study, due to the low solubility of drug used in these devices, the long period of release and the small amount of sirolimus used[96]. Drug-eluting coatings[259] are applied to biomedical implants (ArterioSorb^{TM})[51] to achieve sustained release of APIs (sirolimus in this case) to specific regions of the body. Biodegradable polymers maintain their properties for a limited period of time *in vivo* and gradually degrade into materials that can be soluble or are metabolised and are excreted from the body[260]. In order to be used for *in vivo* applications, the polymers used for such systems must have favourable properties for biocompatibility[261], processability, sterilisation[262] and shelf life[263]. *In-vitro* investigation of degradation kinetics of biopolymers is crucial not only for a fundamental understanding

of the nature of the degradation process but also for the design and optimisation of implantable biomedical devices. The release of drug from drug eluting stents can typically arise as a result of the hydrolysis of the polymer at the interface with the biological system. Hydrolysis is the major degradation mechanism of PLLA. Therefore, the release of the drug, and hence its therapeutic activity, is directly connected to the surface erosion of the polymer (Figure 5.1)[264,265]. The degradation behaviour strongly depends on the physical form of the polymer and drug. Drug release behaviour influences drug persistence in the arterial wall, which can impact the healing process of the blood vessel. Visualising the whole dosage forms during dissolution testing may contribute to understanding the performance of dissolution and unravelling the performance mechanism[71,266,267].

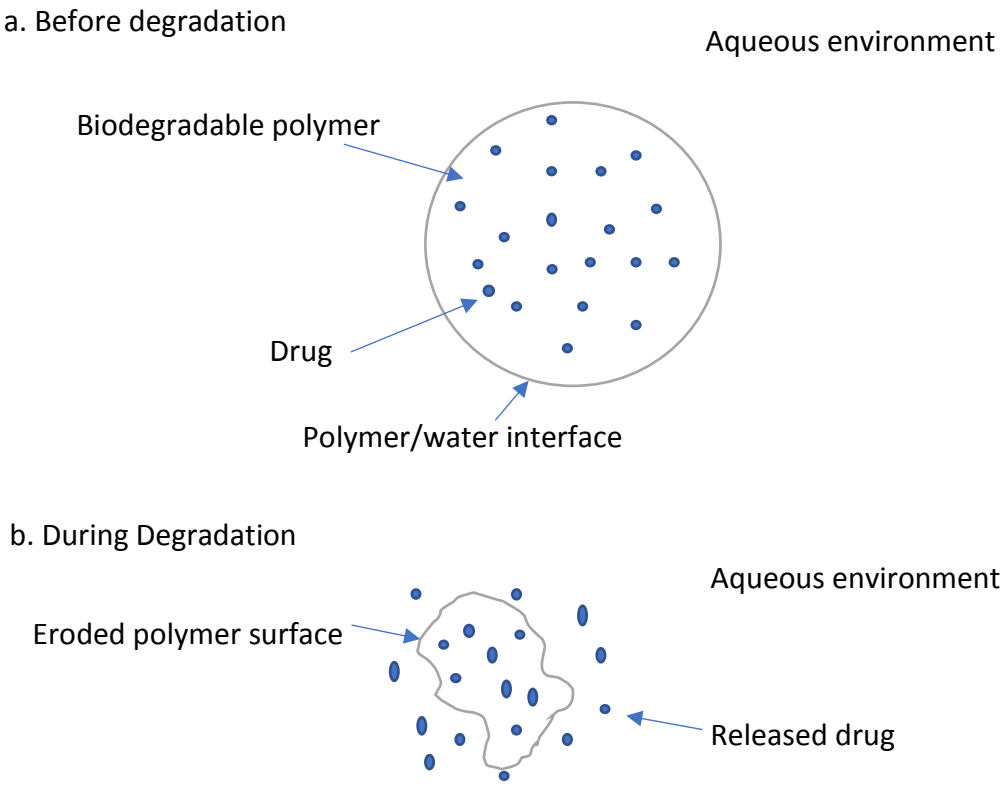
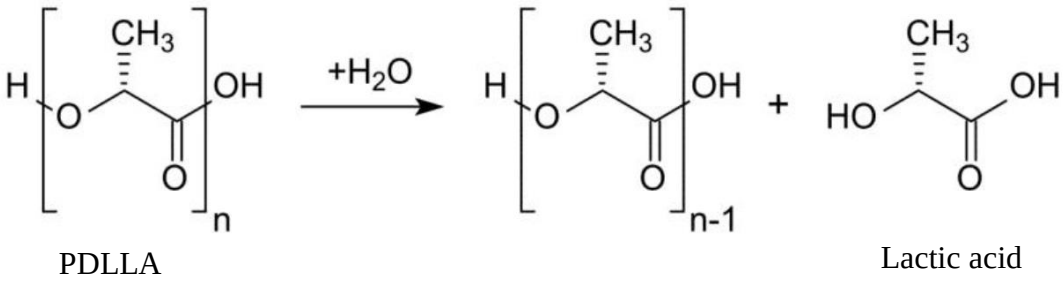


Figure 5.1 Schematic diagram of the mechanism of action of surface eroding biodegradable polymer devices.

There are two commonly observed release profiles for drug eluting stents: linear release profile without burst release and two-phase release profile with burst release[258]. The degradation behaviour of PLLA (Figure 5.2) and factors influencing its degradation

kinetics have been extensively studied. The drug release can be influenced by various factors, such as loading amount of drug, polymer-drug miscibility, and Tg[268]. From literature it can be concluded that the degradation of the polymer in aqueous solution occurs preferentially in the bulk[269].



PDLLA Lactic acid

Figure 5.2 Chemical structure of PDLLA and its degradation process in aqueous environment [270].

Here the micro-structural and morphological changes of the polymer/drug surface induced by the polymer degradation have been systematically studied by analytical techniques mentioned in chapters above. The scope of this chapter is not to assess the biocompatibility of the device or the drug/polymer coating but to visualise the depth and lateral distribution of sirolimus in the PDLLA coating layer during its degradation in simulated physiological conditions. Similar analytical techniques to the ones employed above have been used.

5.1 Experimental Methods and Materials

All the samples and experiments described previously in Chapter 2 and 4. The PLLA biodegradable coronary stents used in this chapter were provided by Arterius Ltd (Leeds), produced by a using ultrafast laser cutting machine to cut PLLA oriented tubing to achieve the scaffold structure. All scaffolds were crimped onto the surface of the balloon.

In terms of the XPS experiments some samples were analysed using a different XPS instrument and this was due to ion gun being out of order on the ThetaProbe (Nexus). The parameters were kept as similar as possible to those described in Chapter 2, 3 and

4. All samples analysed were cut open and flattened out gently and analysis was performed on flat areas of the scaffold as the side edges of samples might be distorted as a result of excessive tensile stress during sample preparation and mounting. For XPS analysis used via ThetaProbe 8KeV Ar_{300}^{+} snap shot mode was used. Later on, measurements were acquired on a Thermo Scientific K-Alpha XPS spectrometer (described in Appendix D) and Kratos Axis ULTRA. Analysis areas of 300 x 500 μm was used in all the measurements for sample analysed at Nexus (Newcastle) and 2x2 mm etch area, 10 kV Ar_{1000+}, analysis area 100 μm spot for sample analysed at Kratos Analytical Ltd (Manchester) on the Kratos Axis ULTRA. In order to check for the centred alignment for the X-ray spot a measurement was done on a phosphorous sample before measurements on stents. Charge compensation was used throughout the measurements.

5.1.1 In Vitro Drug Release Studies

The degradation studies of first and second iteration scaffolds were conducted in PBS at 37°C with a pH of 7.4. A number of scaffolds immersed in falcon tubes containing 3 mL of sterilised PBS pH 7.4. The PBS in each tube was collected and replaced with fresh medium (sampling time described in Chapter 2). Subsequently the samples were analysed by a plate-reader equipped with UV-VIS spectrometers at 278 nm.

5.2 Results and Discussion

5.2.1 Release Profile

Drugs formulated in medical devices are typically released by diffusion through the polymer matrix, by degradation of the polymer materials or a combination of both mechanisms. *In vitro* experiments were performed to study the degradation of sirolimus loaded PDLLA coating deposited on PLLA scaffolds. PLLA tends to undergo bulk erosion however, drug release is not limited to degradation alone. The two main mechanisms involved in drug elution are diffusion-controlled release and degradation/erosion-controlled release. At the start concentration gradients and the shape of the drug delivery

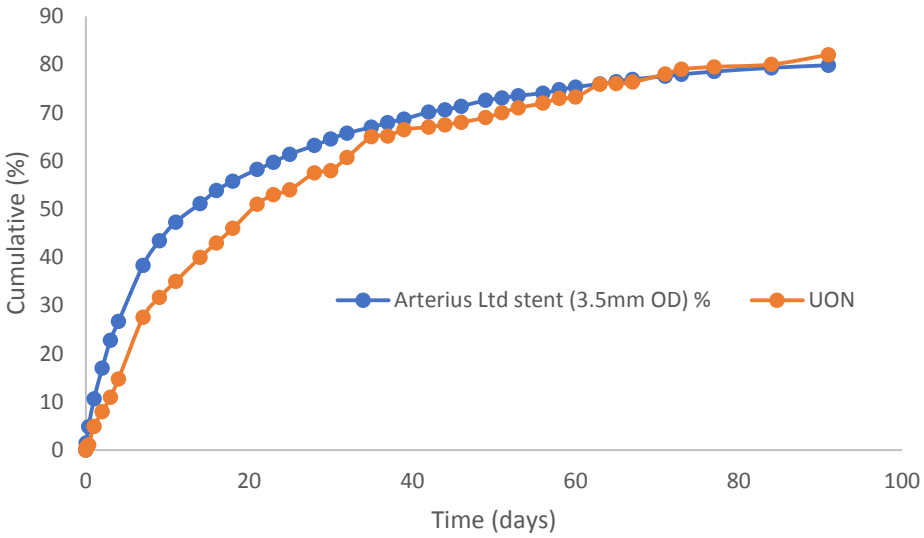
medical device control drug release[271]. In the later stage of the drug release, degradation of the polymer matrix starts to prevail, the release kinetics become controlled by degradation or erosion. The release kinetics from drug eluting stents is generally governed by the coating (material properties, coating thickness and ratio of drug/polymer), drug (drug diffusion coefficient and drug properties) and process parameters[272]. The most important aspect of such factors that may influence the drug release of the drug include the coating thickness, the ratio of drug/polymer and the drug diffusion coefficient[272]. Water diffusion coefficients in polylactide are within a somewhat narrow range, regardless of whether polymer is amorphous or crystalline. It is estimated that in a glassy PLLA, it takes water molecules 1 microsecond to diffuse a distance of 1 nm (about a monomer length), and it takes a few days to diffuse through 1 mm (a typical sample size). The saturated concentration of water in the amorphous PLLA is also the same as that in the crystalline state; both are about 1 wt%[273]. In crystalline polymers, mobility may be lower than that in amorphous polymers. Nevertheless, it has been determined that the diffusion rate of water in crystalline polymers is about identical to that in amorphous polymers of the same chemical compositions[273]. It was reported in the literature[273] that diffusion of polymer and water chains do not control the hydrolysis rates. As a result, the crystalline polymer should degrade at the same rate as an amorphous polymer of a similar chemistry. The same hypothesis goes for oriented polymers[273].

Clinically, an initial rapid release of drug is a desirable effect as it achieves high drug concentration in the targeted tissue followed by the slow release of the drug controlled by the degradation rate of the polymer [274]. The surface area is another factor that can determine the type of the drug release. As the PLLA matrix degrades through the formation of pores, the surface area which the drug can diffuse out into an aqueous environment increases to produce an increased drug release.

This chapter focuses on studying the changes related to the surface and subsurface of the drug/polymer on ArterioSorb™ eluted for 2 days, 16 days, 1 month, 2 months and 3 months. Scaffolds are designed to release sirolimus over a prolonged period of time to overcome restenosis. The distribution of sirolimus in the matrix can influence the release behaviour, where drug enrichment at the surface of the scaffold may promote a burst

release effect whereas a more uniform mixing of the drug and the polymer may provide a more uniform release profile. The release profile of sirolimus was monitored over the course of 3 months. The data in Figure 5.3 shows the drug release from ArterioSorb™ scaffolds with different wall thickness to the scaffold struts, one was done by Arterius Ltd (Leeds) and other was carried out here at the University of Nottingham.

a.



b.

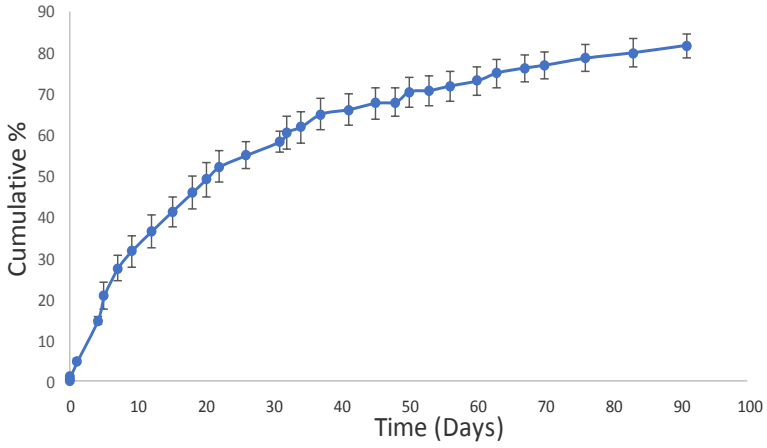


Figure 5.3 *in vitro* release profile of cumulative amount of sirolimus eluted from PDLLA coating as a function of elution time in PBS. A. represents release profile of sirolimus from ArterioSorb™ coating with different strut thickness. B. Release profile of sirolimus from Arteriosorb™ with wall thickness of 95 μm. The error bars represent one standard deviation based on three measurements at each time

interval.

The drug release rate is controlled by diffusion through an arrangement of pores, with developing structure as the polymer matrix degrades. Water is absorbed by polymeric materials, a process that is faster than drug release[275]. This process leads to water filled pores over time. The size of these pores gets larger leading to large enough pores to facilitate drug release[276].

The release of sirolimus is displayed in Figure 5.3 and demonstrates drug release of ArterioSorb™ scaffold in a controlled manner with relatively rapid release of the drug within the first days of elution, about 40 % drug released. After the rapid release, there was a nearly linear sustained and slower release period. The burst release is not preferable in the DESs as it may increase the risk of toxicity associated with a large amount of drug release[277]. The elution behaviour of scaffolds studied in Nottingham and by Arterius Ltd are relatively similar (as shown in Figure 5.3). Difference and similarity factors F1/F2 (FDA equivalent test) was performed to show if both release profiles are statistically the same (data shown in Appendix E, Figure E.2). It is acceptable to say a substantial amount of the drug is released within 3 months of dissolution, however some portion of sirolimus is retained in the polymer even after 3 months, and this could be due to matrix construction.

This elution profile was similar to release profiles that have been reported in a similar study (Figure 5.4)[278,279], although this study was done in a different format but the polymer and the drug is the same. You can see how changing the amount of the drug and polymer plays a role in changing the release profile. Figure 5.4 shows drug release of sirolimus loaded PDLLA nanoparticles with different drug concentration in the polymer. The release profile with 30 % content of sirolimus/PDLLA nanoparticle shows the highest rate of release and highest release efficiency reaching 70 % than others with low drug contents[280]. The difference in the drug release profiles is likely to be caused by the dispersion state of sirolimus in polymer. As higher drug content could lead to the formation of a continued drug release channel and therefore, more drug could be released through these interconnected channels, i.e. a stent with a high drug loading, based on same release rate can release the drug for a longer time.

It has been reported[26] that drug eluting stents that release of sirolimus over a month was more effective in suppressing neointimal hyperplasia and diminishing major adverse cardiovascular events than stents that release drugs over a shorter period of time. Drug elution beyond 30 days, yet, could also be theoretically unfavourable, as this may delay endothelialisation of the stent, with the potential risk of stent thrombosis.

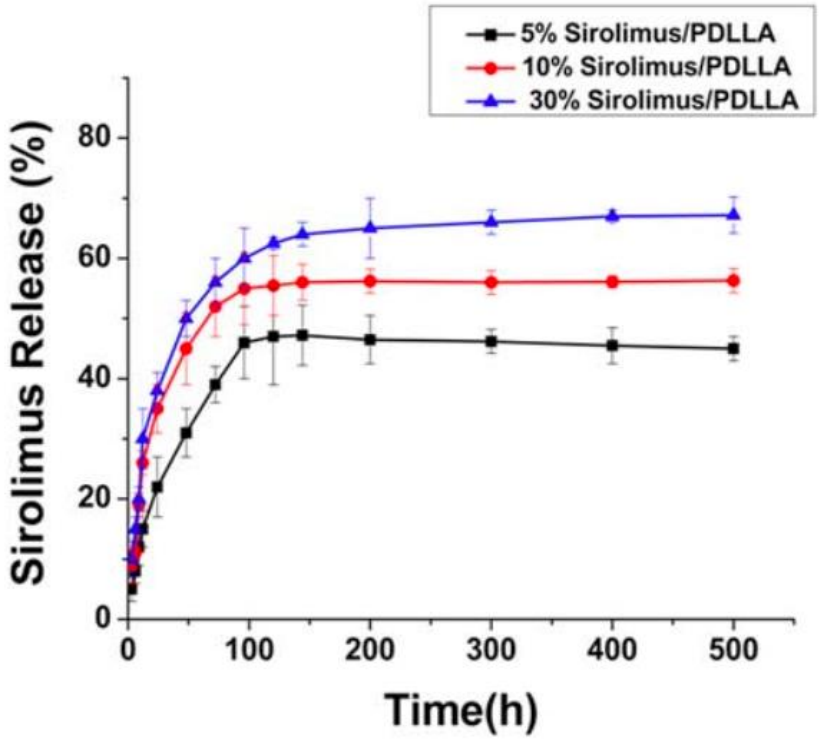


Figure 5.4 Drug release profile of sirolimus in PDLLA nanoparticles. Figure adapted from [280].

The observed drug release from the spray coating layer (Figure 5.3) exhibits a diffusion-controlled release post an initial rapid drug release (day 9-22) and after 22 days a degradation dominated release can be observed. The slow rate of polymer degradation makes diffusion through the ArterioSorb™ scaffold the only possible mechanism for drug release. Drug release in Figure 5.3 accounts for almost 80 % of the drug in the coating over the course of 3 months. The remaining of the drug left on the stent after 3 months of degradation could be due to strong interaction between the drug and polymer and

could only be released by complete degradation of the polymer matrix, i.e. more than 3 months.

5.2.2 Surface Morphology of Dissoluted Stents

The surface morphologies of dissoluted ArterioSorb™ scaffolds as well as drug coated oriented tubing were examined by ESEM and AFM to give a more detailed insight into the polymer degradation on the micro-scale level. It is useful to compare the surface morphology of scaffold as fabricated described in Chapter 4 to those dissoluted for 3 months (data shown in Appendix A, Figure A.6). Controlling surface smoothness and coating thickness are very important in drug coating for drug eluting scaffolds. Rough surface and thick layer of coating may provoke an injury at the lesion site post stent implantation[281]. As seen from SEM images in Figure 5.5 polymer erosion has occurred, along with possible phase separation between the drug and the polymer.

The SEM analysis showed significant changes in the morphology of the coating surface during the degradation period in PBS (tubing Figure 5.5 and ArterioSorb™ in Figures 5.6-5.9). The surface coating started to break, and the consequent cracks become larger (in particular on the surface of first generation of ArterioSorb™ scaffolds). Interconnected and globular porous structures were also formed. Samples exposed to aqueous environment possessed, pitted and roughened areas, with obvious pits (100 – 200 nm in diameter) being quite large and of a depth compared to the untreated surface.

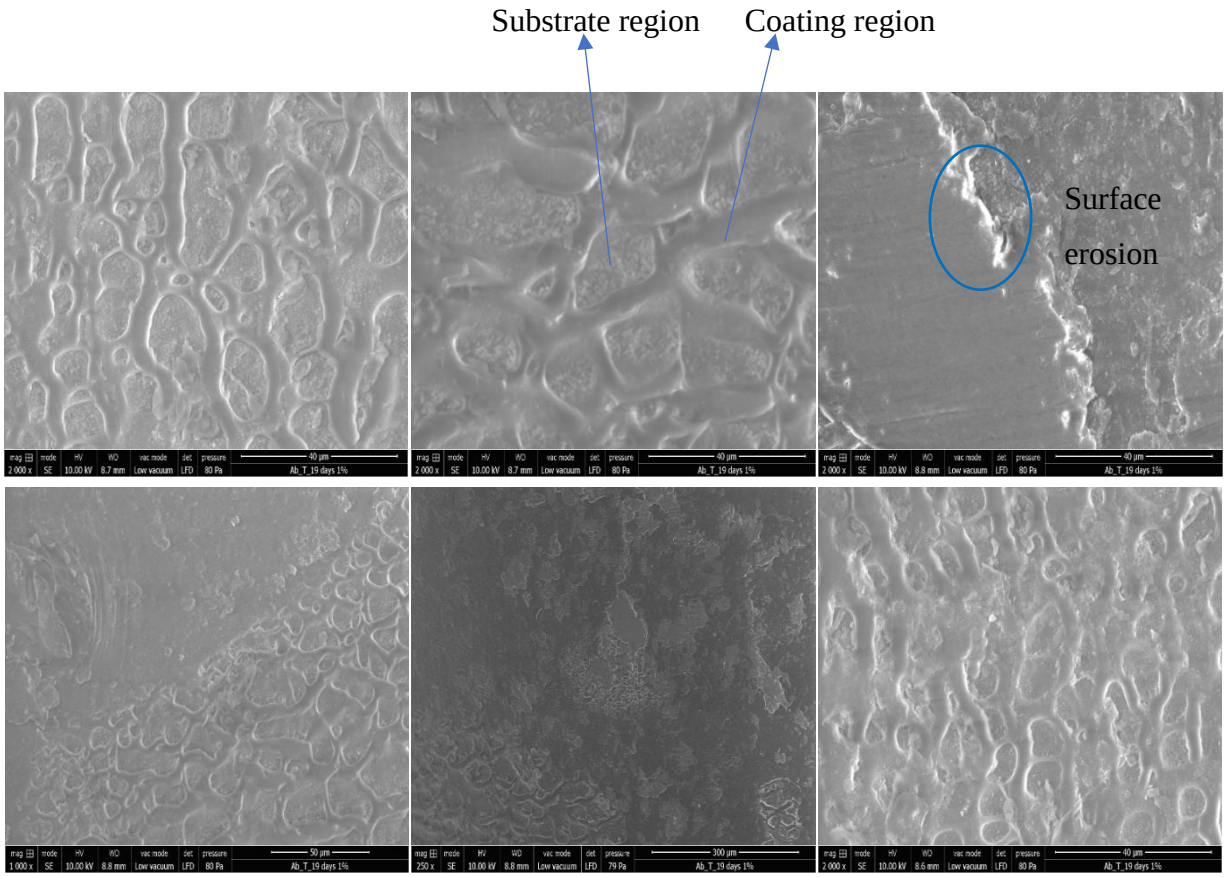


Figure 5.5 SEM images of drug coated die-drawn PLLA tubing in PBS for 2 weeks.

SEM images taken at different degradation times post exposure to PBS, show small wrinkles appeared on the surface and these wrinkles grew in size leading to porous surface. The surface in Figure 5.5 shows evidence of surface erosion highlighted in blue circle. Blue arrows indicate erosion of coating revealing substrate. The formation of these porous features might be due to diffusion of sirolimus from the coating film and penetration of water in the coating layer.

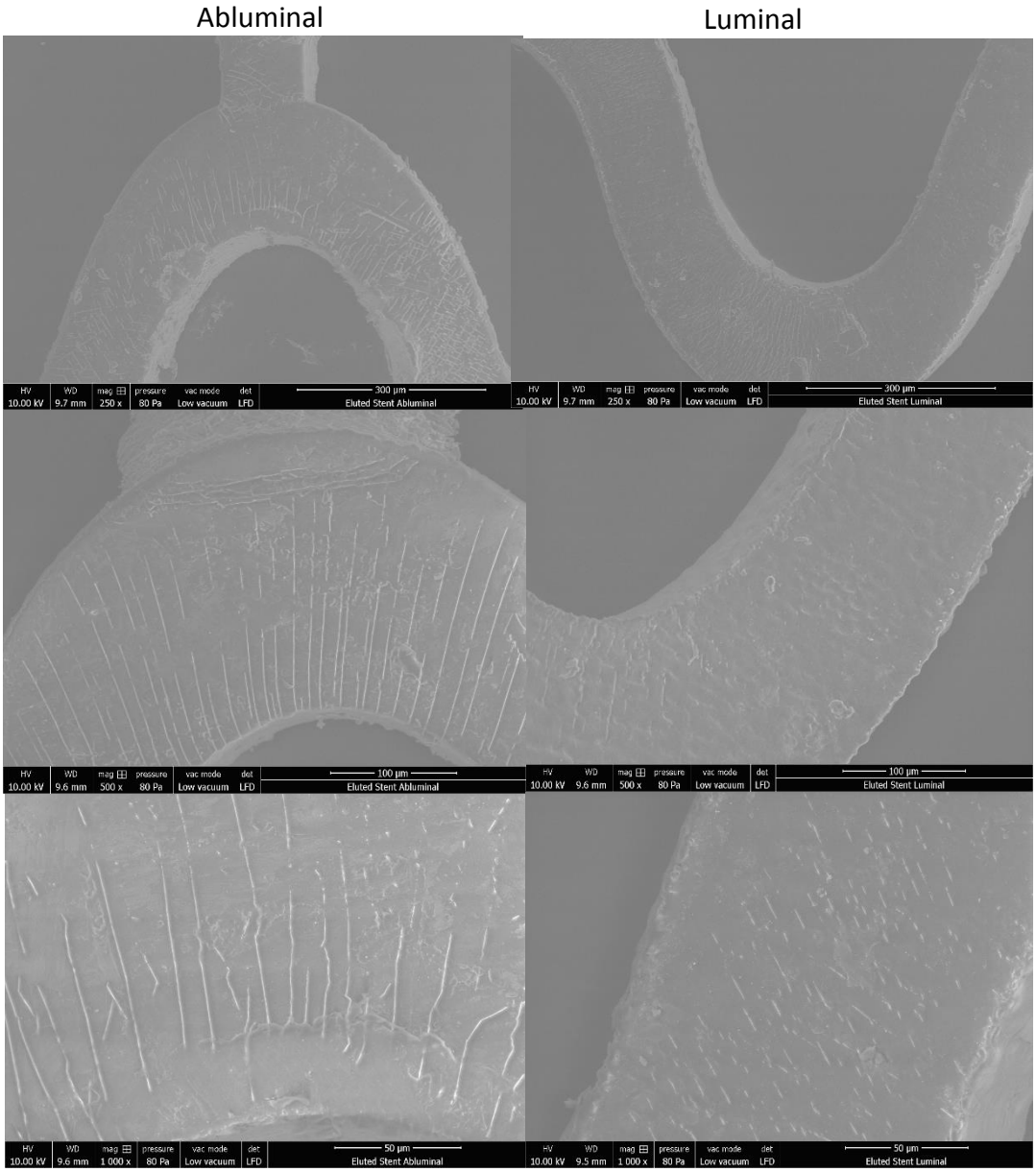


Figure 5.6 SEM images of drug coated ArterioSorb™ scaffold in PBS for 2 days, showing top and bottom surfaces.

The images in Figure 5.6 did not show significant morphological changes, thus more scaffolds were left in dissolution media for a longer time. The SEM images in Figure 5.7 illustrate the changes in morphology of the coating due to the degradation at the end of 2 weeks. The progressive nature of the degradation process is showed in the figure. The

morphology of the drug/polymer coating in Figure 5.7 shows the formation of pores due to the degradation of the polymer, which are the first noticeable sign of degradation.

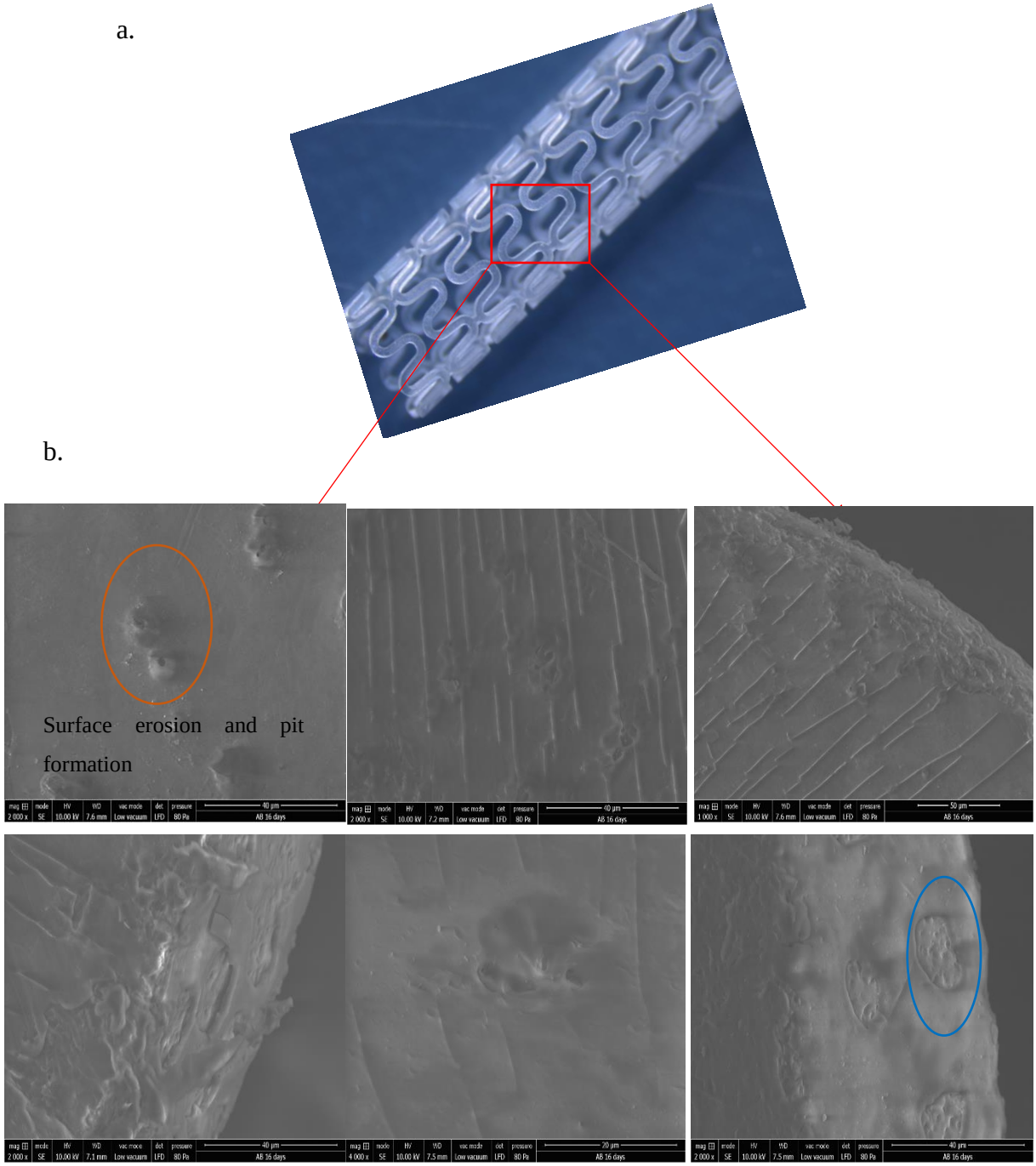


Figure 5.7 a. The fully bioresorbable drug eluting scaffold, b. SEM images of drug coated ArterioSorb™ scaffold in PBS for 2 weeks.

Blue circles in Figure 5.7 indicate areas where the coating has completely disappeared leaving the PLLA substrate below degrades more slowly and has similar pore visible.

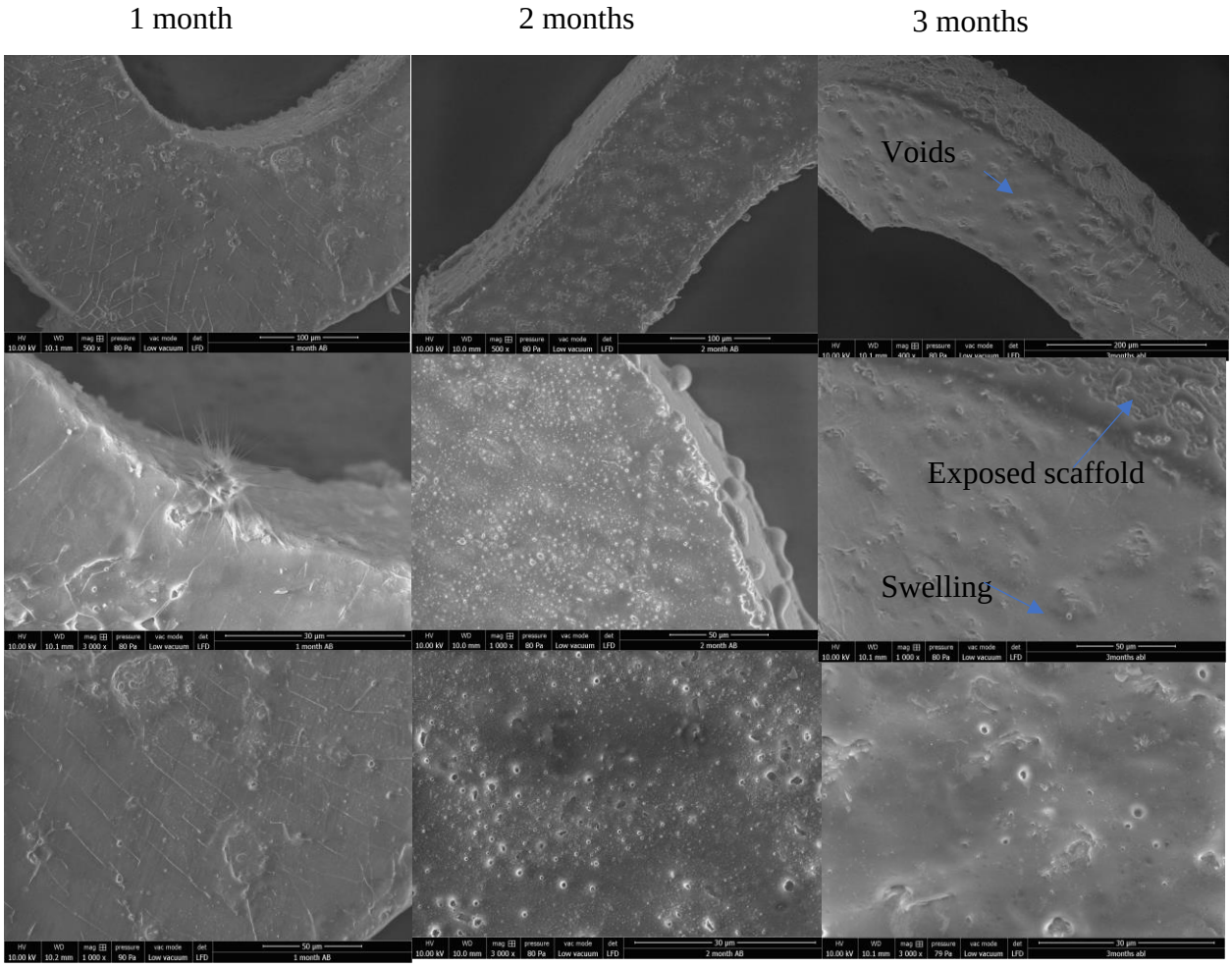


Figure 5.8 SEM images of the spray coated stent (Abluminal side) at the end of 1, 2 and 3 month (s) degradation.

Figure 5.8 and Figure 5.9 show further degraded samples resulting in large number of pores as well as an increase in the surface roughness, presumably related to the beginning of polymer mass loss.

The hydrolysis of ester bonds in the polymer that takes place following water contact leads to lactic acid production, which catalyses the hydrolysis process further leading to heterogeneous degradation within the polymer matrix. The surface of the degraded

scaffold shows evidence of heterogeneity with phase separation. As indicated in the SEM images where the drug coating layer started to flake off, leading to potentially exposing the substrate of the device (PLLA). The degradation process occurred across the entire sample, as can be seen from Figure 5.8, however the degradation rate seems to be relatively non-uniform in different areas along the scaffold structure.

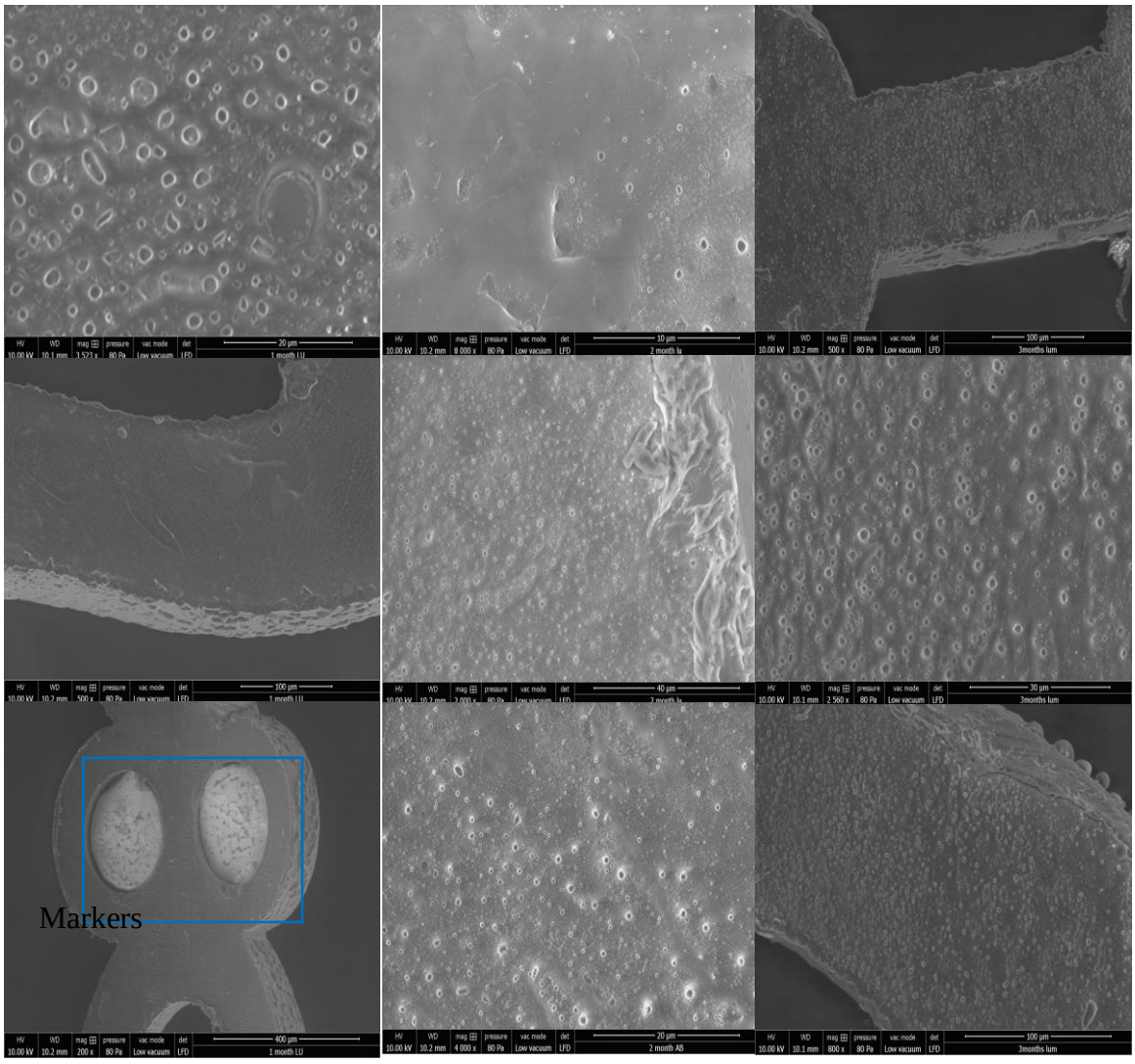


Figure 5.9 SEM images of the spray coating scaffold showing luminal side at the end of 1, 2 and 3-month(s) degradation.

Comparison of the surface coating of first and second generation ArterioSorb^{TM} scaffolds carried out by Arterius Ltd and Nottingham University after several months of dissolution testing, are described in Appendix A. Combination of SEM and AFM have been used to demonstrate the difference if any between the two coating layers.

Pore formation is quite evident in Figure 5.9, these pores occur due to water absorption in the polymer matrix. Over time, absorption causes the polymer to swell as shown in Figure 5.7, creating holes that are drug may elute from. The origin of pore formation could be due to a demixing process that involves phase separation of polymer mixture occurring under specific conditions of spray coating. In addition to pore formation, other factors such as polymer-drug interactions and drug-drug interactors may influence drug release. Similar holes were reported with paclitaxel/PDLLA and simvastatin/PDLLA coatings on coronary metal stents[235]. The reason why PDLLA was used for the top coating, is that it possesses more desirable degradation properties than the PLLA. PDLLA has a Tg of 50-60 °C and a lower mechanical strength of 1.9 GPa compared to PLLA which has a Tg of 60-65 °C and a mechanical strength of 4.8 GPa[157]. After 3 months of the device being in aqueous solution, the enduring hydrolytic degradation leads to a PDLLA/sirolimus coating layer with a high degree of porosity.

The degradation process can be broken down into three phases. The first phase indicates a rapid uptake of water by the polymer, this arises within the first 12 hours of degradation, whilst the second phase relates to the hydrolysis of the polymer and lasts for 7.5 months. In this phase, the production of lactic acid takes place in the polymeric matrix subsequently generating autocatalytic effect. Most of the drug is released in this phase of the degradation process. The last phase is the rapid breakdown of the polymer, in this phase the rate of lactic acid production in the matrix is less than the lactic acid when ousted into the aqueous solution, leading to a reduction of lactic acid concentration[266]. Although this study should have been continued for 12 months but due to the length course of this research and limited number of samples it had to be completed within 3 months.

SEM analysis does not yield chemical or physical property distribution information. Therefore, AFM and 3D chemical analysis can be useful. AFM work was extensively focused on imaging the abluminal areas, since this region comes to contact with the targeted tissue after implantation. The surface coverage of the domains described previously in Chapter 4 was lost after 1 month of degradation, these domains indicated in Figure 5.10 – 5.15 described in the shape of pits.

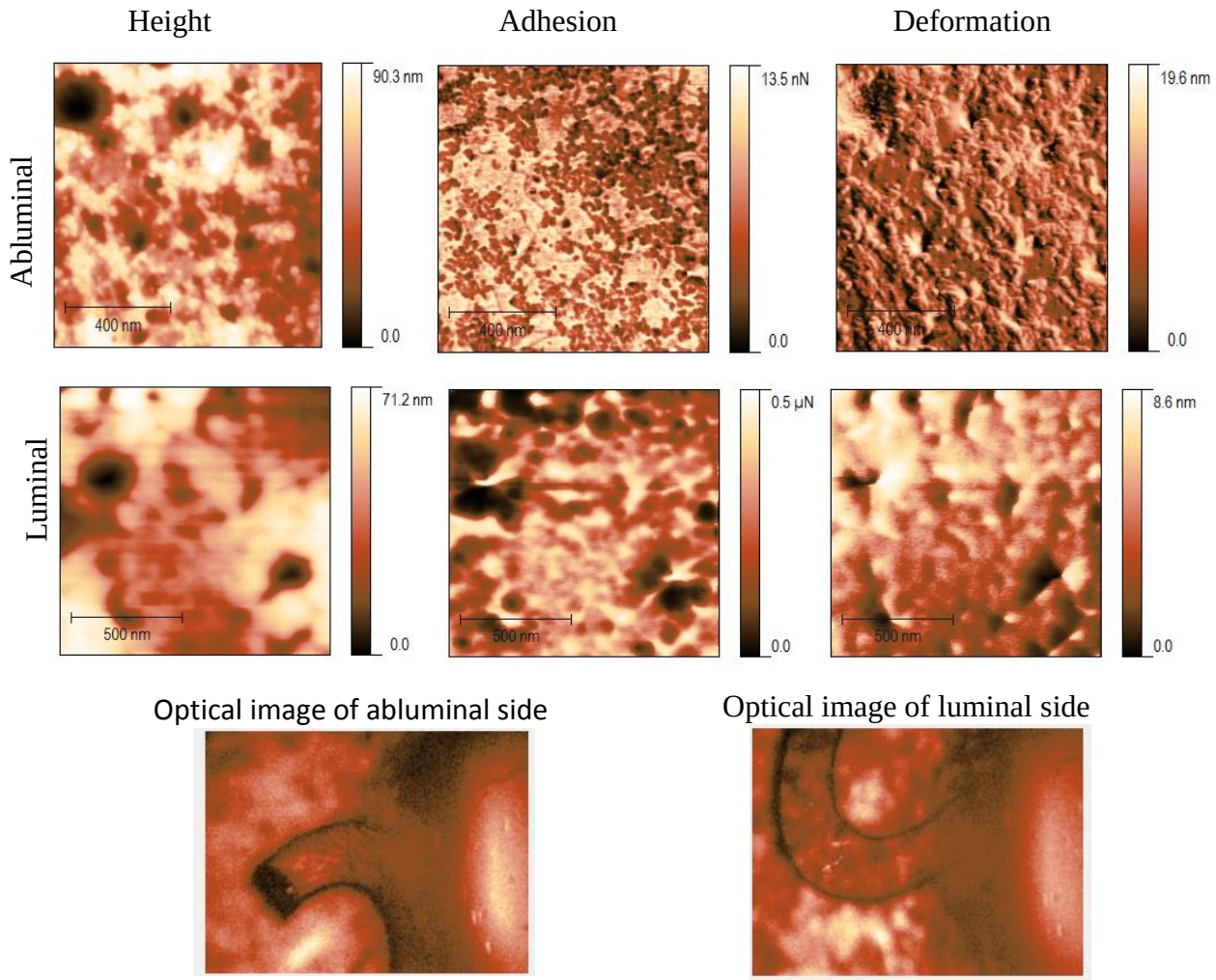


Figure 5.10 AFM surface images from dissolution study of abluminal and luminal surface of ArterioSorb™ scaffold post 2 days in PBS, with scan size of (1 x 1μm) and (1.21 x 1.21 μm), respectively. Roughness measurement 9 nm and 6 nm, respectively.

Formation of pits in Figure 5.10 suggests the loss of the globular features from the top surface within 1 month. Similar features were reported on a comparable investigation[282]. Spray coated stents exposed to an aqueous environment for 2 days showed bright areas, these bright domains existed in previous scaffolds reported in Figure 4.12 and Figure 4.13, suggesting a rapid loss of domains from the surface.

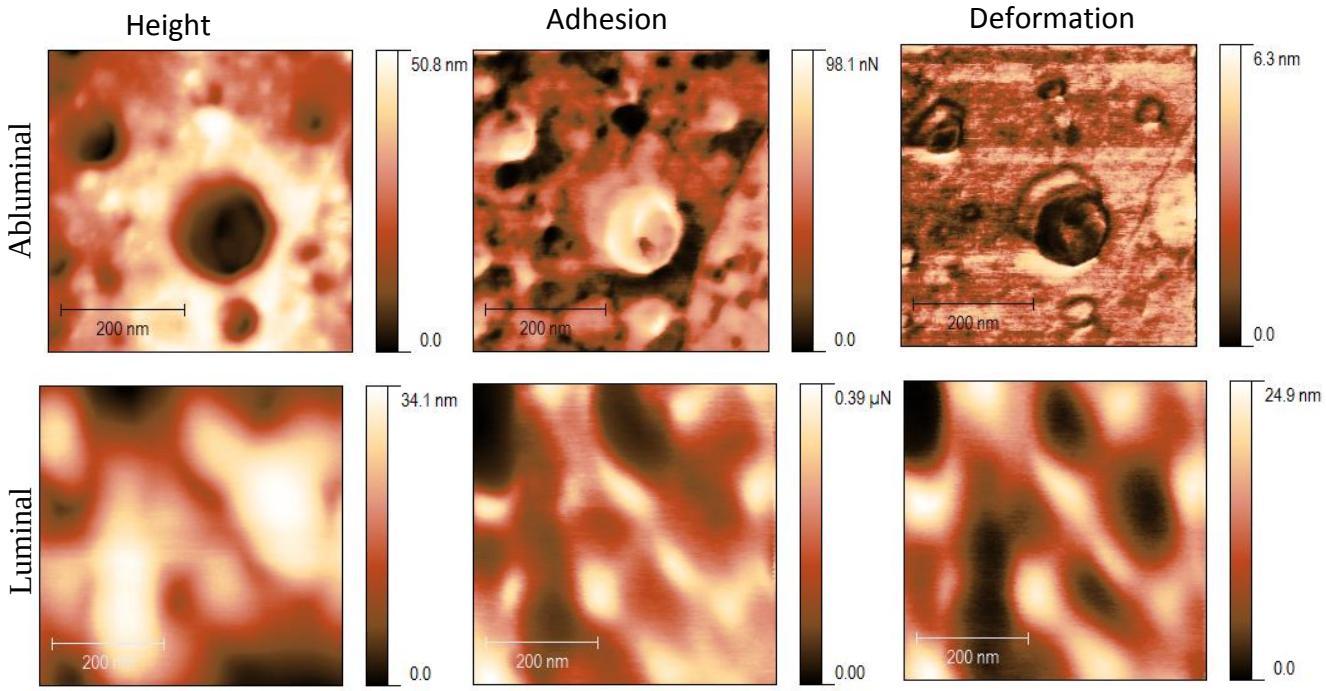


Figure 5.11 Close up AFM surface images taken from abluminal and luminal surface of ArterioSorb™ scaffold after 2 days in aqueous environment. RMS of 8 nm and 6 nm, respectively.

The drug rich pockets appeared previously in the as-fabricated scaffolds described in previous Chapter 4 and appears as voids within the polymer. Due to the topography and geometry of the scaffold.

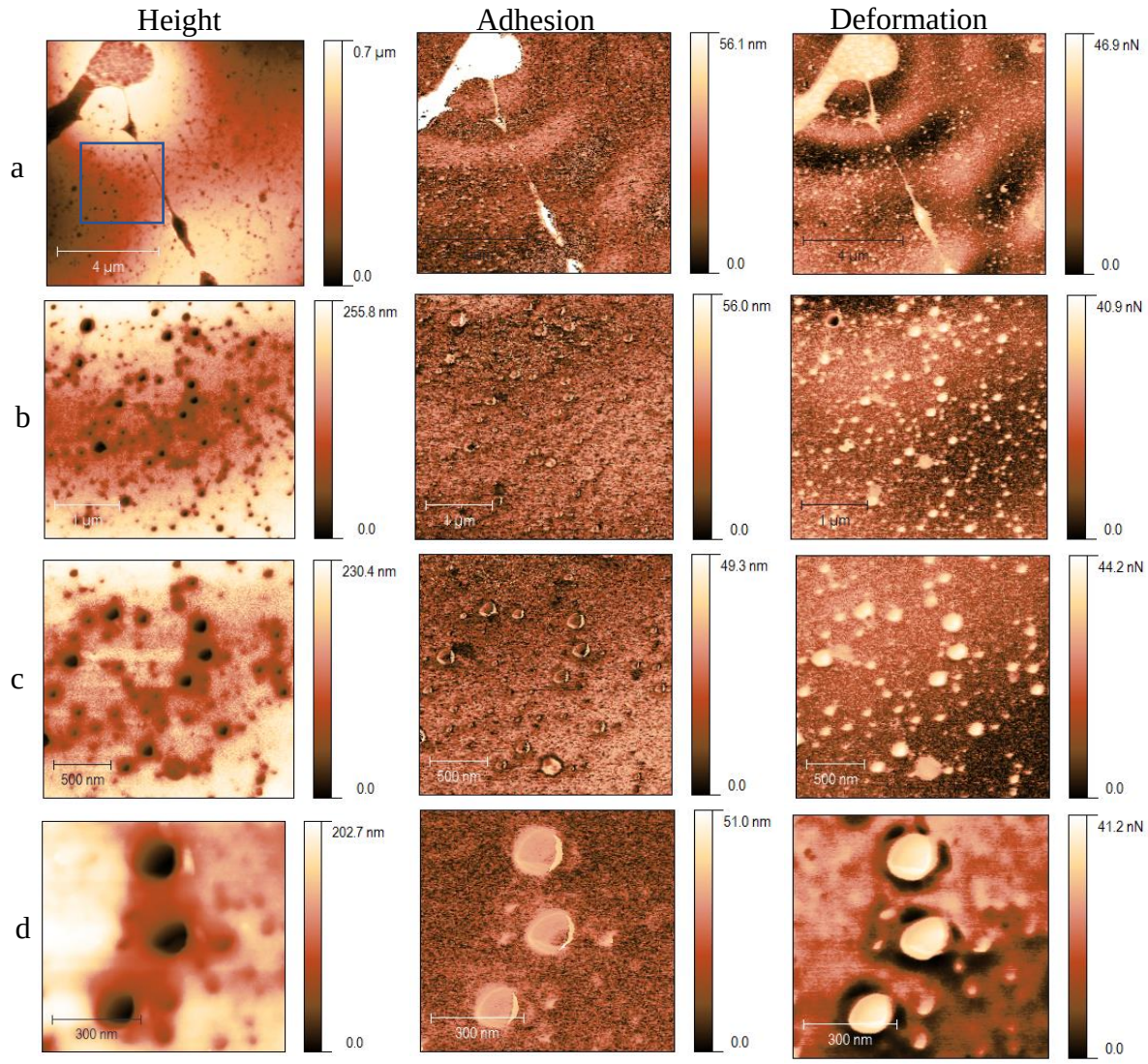


Figure 5.12 AFM surface images in tapping mode of an area of abluminal surface of the sirolimus/PDLLA coating layer (area 1) of ArterioSorb™ scaffold after 1 month in aqueous environment. The AFM images a, b, c and D are taken from same area but different magnification, a. (10 x 10 µm), b (3.8 x 3.8 µm), c (2.1 x 2.1 µm), d (0.81 x 0.81 µm).

The small features (pores) highlighted in blue square in Figure 5.12 have been magnified to show a region with multiple pore throats. These features are remnants of drug rapid release and expose the degree to which drug from deep within coating has direct access to the surface.

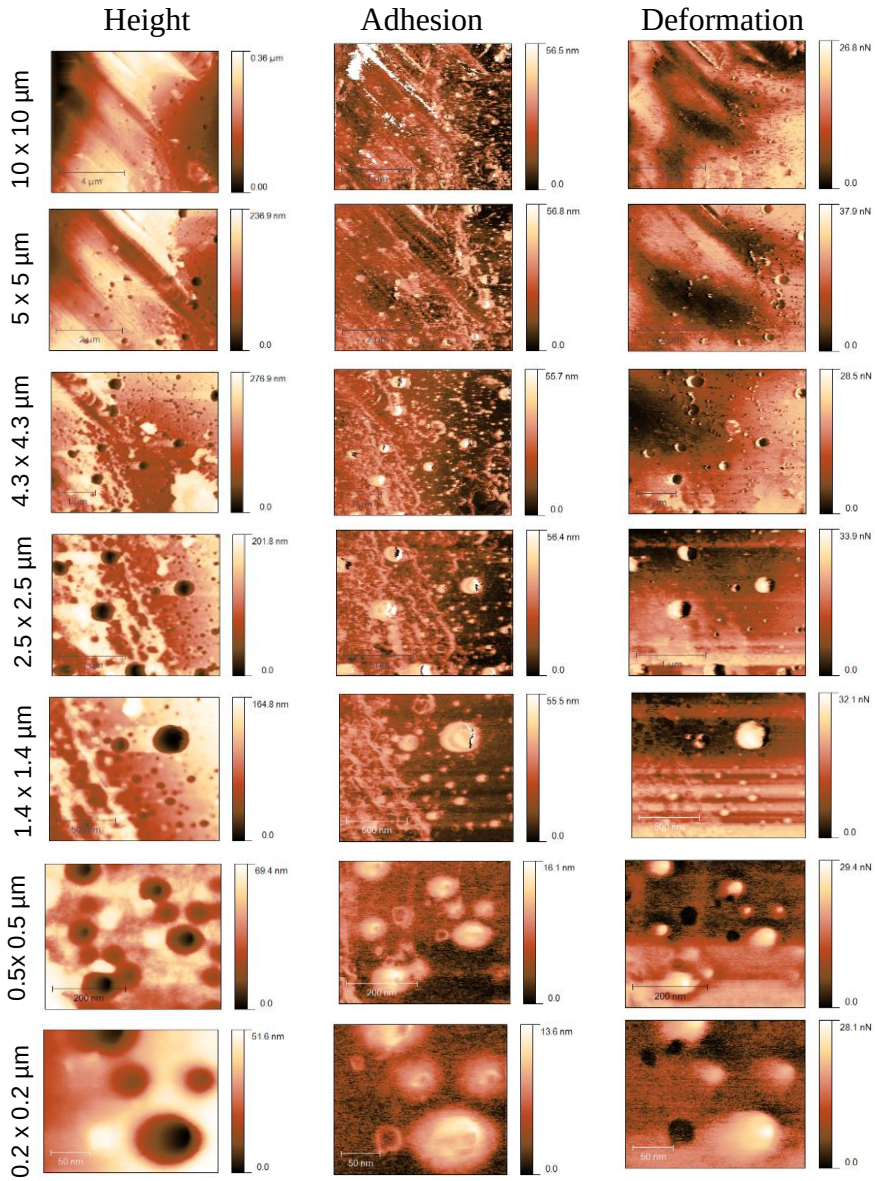


Figure 5.13 AFM surface images in tapping mode at the surface of a sirolimus/PDLLA coating (area 2) of stent eluted in PBS for 1 month. AFM images are magnifications of first set of images (magnification of selected areas of stent struts).

The lactic acid matrix degrades to allow pore formation (as shown in Figure 5.13), increasing the surface area for fabrication, leading to a rapid release of the drug. Since PDLLA and PLLA are both fully biodegradable, once the stent has degraded it leaves only small tantalum markers at the edges of the scaffold. It has been reported a similar

type of scaffold has been implanted in porcine arteries for 1 month and up to 3 years, the evaluation of such preclinical studies demonstrated lower rates of vascular inflammation and neointima formation in contrast with permeant drug eluting stent containing sirolimus[283]. Large and deep pits were formed post dissolution as shown in Figure 5.14. The micro network observed in scaffolds as-fabricated have been evacuated at 3 months, and voids appeared (blue arrows). The pores were deeper and wider in comparison to the 2 days surface.

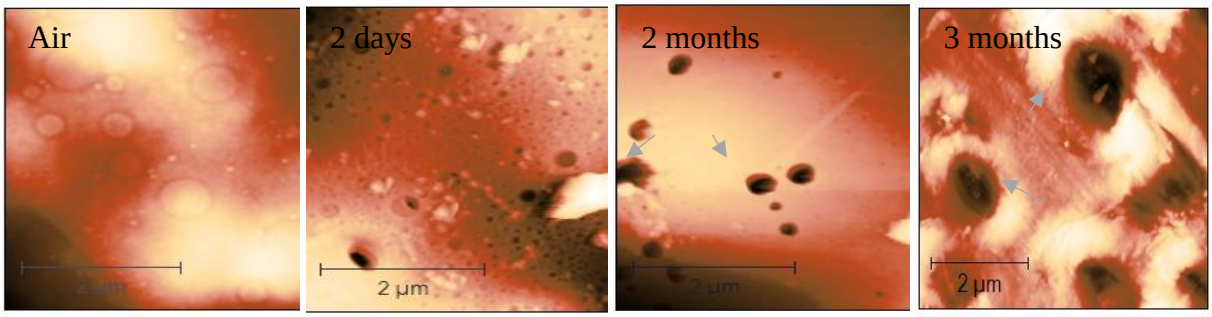


Figure 5.14 Example of topographical surface images acquired in tapping mode in air, taken from abluminal surface ArterioSorb™ scaffolds after degradation in PBS at 37 °C. Scan size of these images 5 x 5 µm.

The AFM images reveal pores and depressed regions that directly replaced the drug enriched region protruding mounds at the surface were observed at the surface of scaffolds as fabricated, this is marking a direct link between the pore formation and drug release in ArterioSorb™ scaffold. The depth of pore formation varies from 10 nm to 200 nm, data collected from more than 3 areas (Figure 5.15). The largest pore extends to a depth (0.5 µm) beneath the surface with some structure at the base, representative of pores. These pores provide a direct route for drug release. These features are likely remnants of drug rapid release and expose the degree to which sirolimus from deep within the coating-layer has direct contact to the surface.

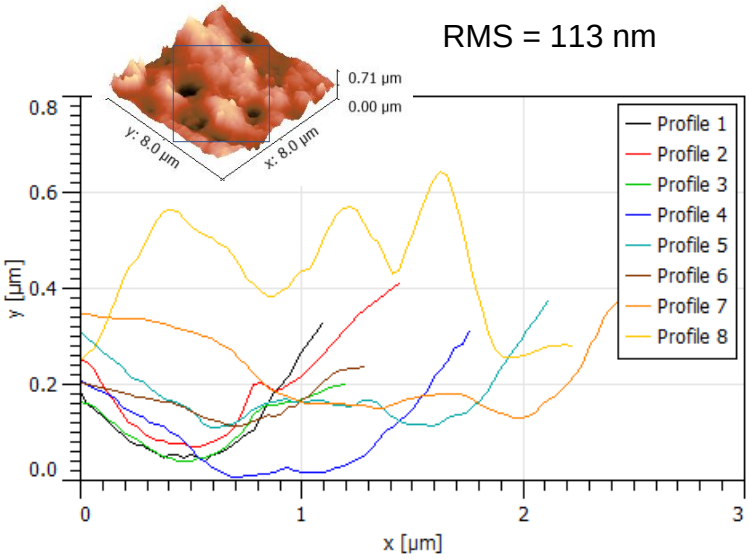


Figure 5.15 AFM line scan profiles taken from a scaffold eluted for 2 months indicating the depth of pores present at the surface of ArterioSorb™ scaffold.

5.2.3 Surface Chemical Chemistry by ToF-SIMS

ToF-SIMS has the potential to facilitate a clear understanding of changes in the surface organisation at the interface of bioresorbable scaffolds, whereas AFM showed how such variations in surface chemistry maybe related to surface morphology. Changes in the surface chemistry of this scaffold have led changes in surface topography on dissolution. Such surface morphology changes are likely to have an effect on release profile of the sirolimus. Build-up of the drug at the surface is consistent with the early rapid release of the drug (Figure 5.3). This effect was known from the dissolution profile. For example, if phase separation is seen potentially a method of control needs to be used to control the drug release. This method of control could include increasing the drying rate as well as solvent used in order to manipulate drug release profile and potentially making more or less drug at the surface of scaffolds. The release rate profile can be manipulated by varying the radial distribution of the drug coating, the mixing method or the amount of drug material, and crosslink density of the polymeric material[284].

The ToF-SIMS spectra of the virgin and dissoluted scaffold as well as tubing are shown for the mass m/z 84 and m/z 56 in Figure 5.16. Using the diagnostic markers identified in previous Chapters, the ToF-SIMS spectra were reconstructed as images to characterise the distribution of sirolimus/PDLLA at the surface of the scaffold and within (Figure 5.16). Positive and negative polarities were collected however, the work here was focused on positive polarity as described in previous chapters. The negative polarity was obtained just in case if we needed to check for other ions such as sulphur or chlorine (data not shown).

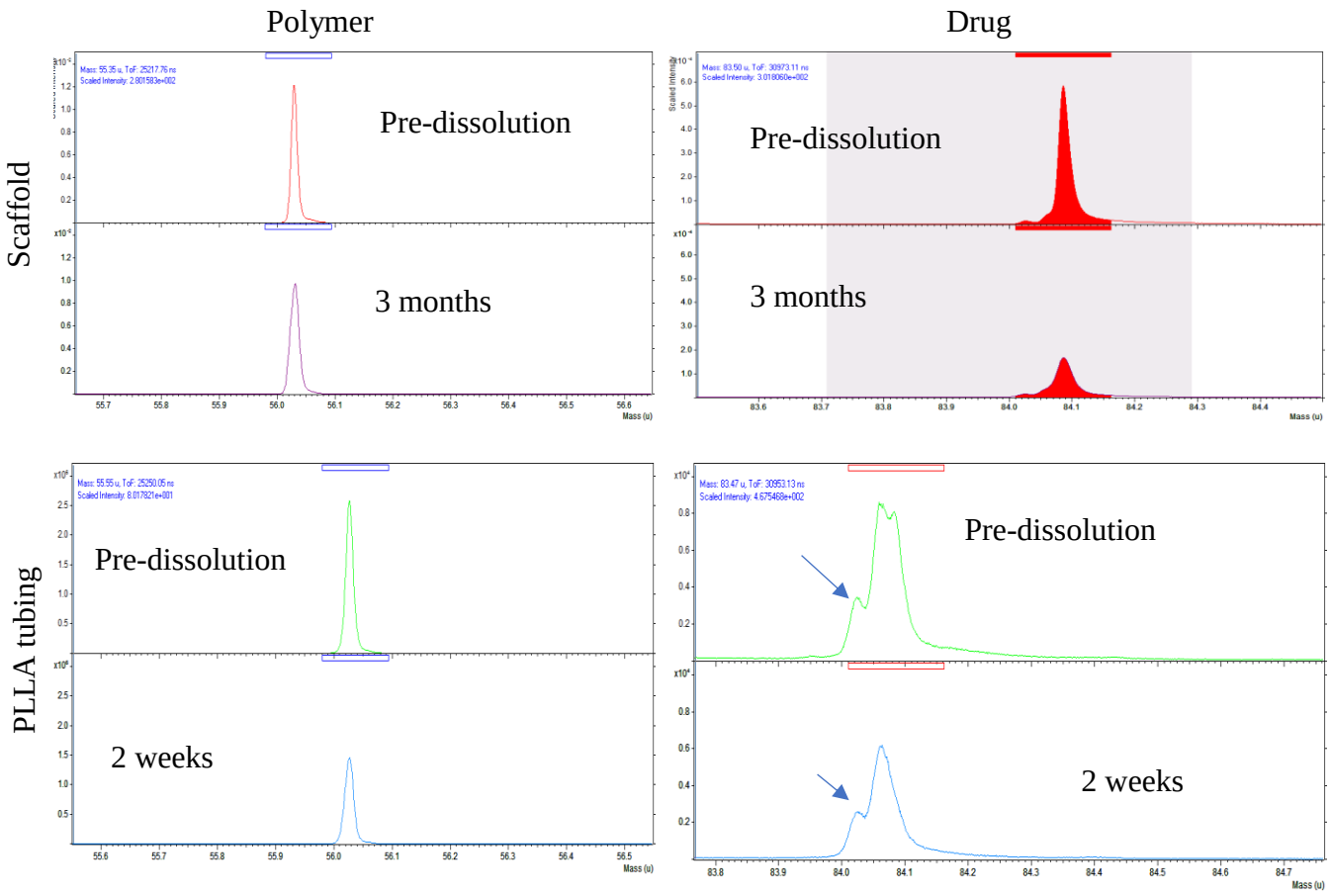


Figure 5.16 ToF-SIMS spectra of characteristic fragments of the drug and polymer in scaffold and polymeric tubing.

The shape of the peak at m/z 84 for eluted tubing is not the same as the peak seen on the scaffold. It is likely the additional peak highlighted in blue arrows in Figure 5.16

suggests presence of hydrocarbon due to the deposition of adventitious hydrocarbon .

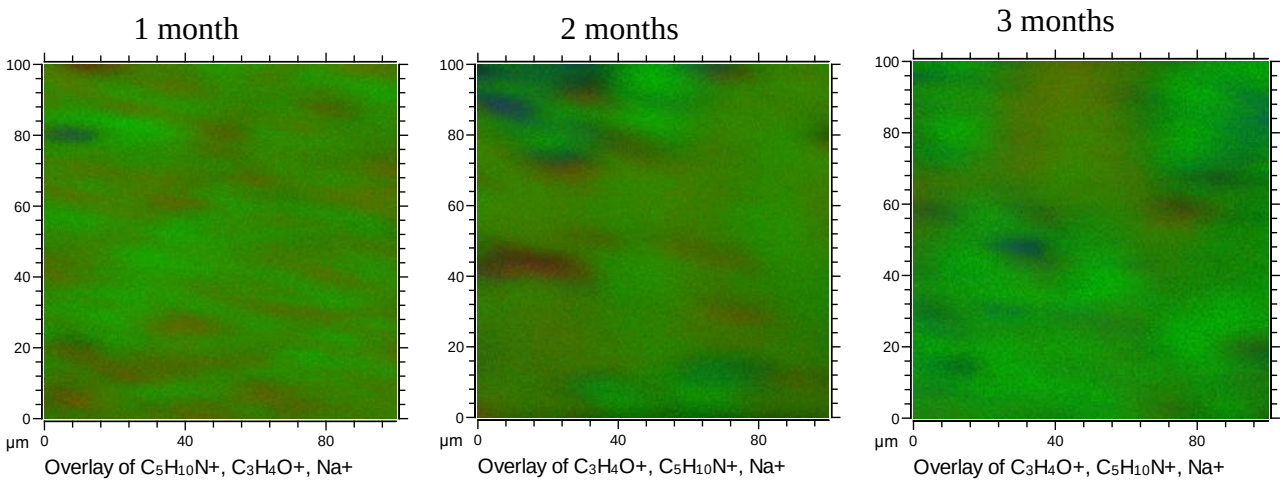


Figure 5.17 2D ToF-SIMS images of scaffold abluminal surface immersed in PBS for 1, 2 and 3 months. Overlay images of sirolimus in (red), polymer in (green) and Na^+ in blue.

2D images in Figure 5.17 are colour overlay of the sirolimus signal in red, the polymer in green and the Na in blue. Morphology within the coating changes as sirolimus elutes and the distribution of sirolimus is heterogeneous on these samples (Figure 5.17).

The set of images in Figure 5.17 highlights variation in the surface morphology of the coating layer, leading to a porous appearance. In comparison to the coating layer of as-fabricated scaffold, sodium (blue) appears more in the surface region, this observation makes sense the fact that elution medium contained sodium.

As described in Chapter 4, as-fabricated scaffolds pose a thick surface layer of sirolimus on the abluminal side. Post elution the thickness of the coating layer was decreased, since it has been in contact with aqueous environment. ToF-SIMS 3D reconstructed images display domain formation at the surface as well as bulk regions with fissures like feature running within (Figure 5.18).

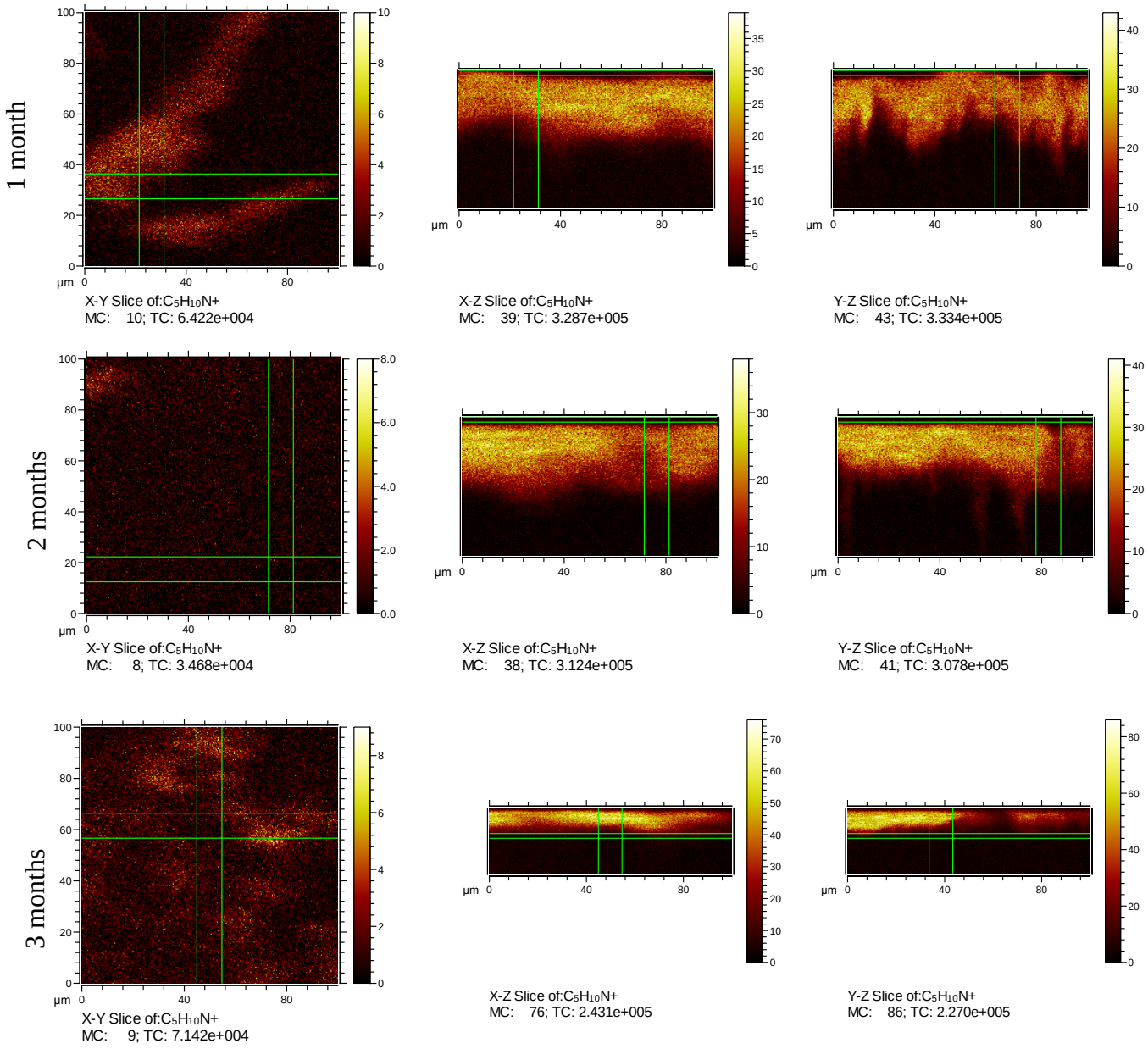


Figure 5.18 3D reconstructed images of Sirolimus as a function of elution time.

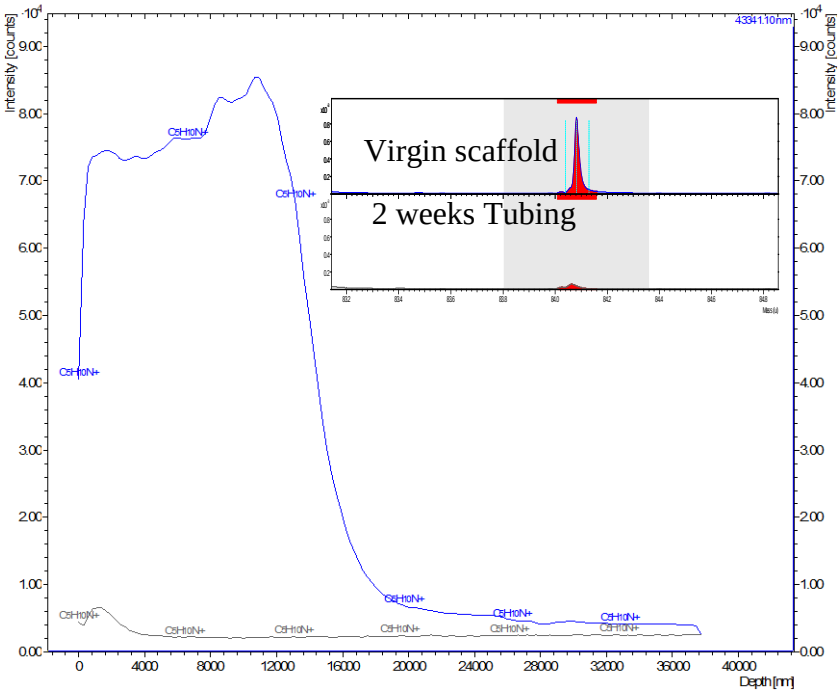


Figure 5.19 ToF-SIMS profile of as-fabricated scaffold and drug coated tubing post exposure to aqueous environment for 2 weeks. The line in the blue represents virgin scaffold and the line in grey is 2 weeks eluted tubing in PBS.

The comparison between the depth profile data of untreated scaffold versus eluted tubing (exposed to PBS at 2 weeks) illustrate loss of the drug from the top surface, hence rapid release. This evaluation was done as a prove of concept. The embedded spectra in Figure 5.19 show the decrease in drug intensity of scaffold eluted for 2 weeks as compared to the drug present on the surface of as-fabricated scaffold. More ToF-SIMS depth profile data of untreated scaffold (as-fabricated) and a scaffold eluted for 2 weeks is shown in Appendix C, Figure C.12.

Sodium, PDMS were also monitored alongside characteristic fragments of the drug and polymer. Figure 5.19 shows high concentration of Na^+ and PDMS on the top surface of the scaffold. Sodium is a common contaminant, but it could be this time coming from the PBS solution and as for PDMS, double side tape was used for the mounting of the sample. These contaminants were observed in previous samples described in chapter 4.

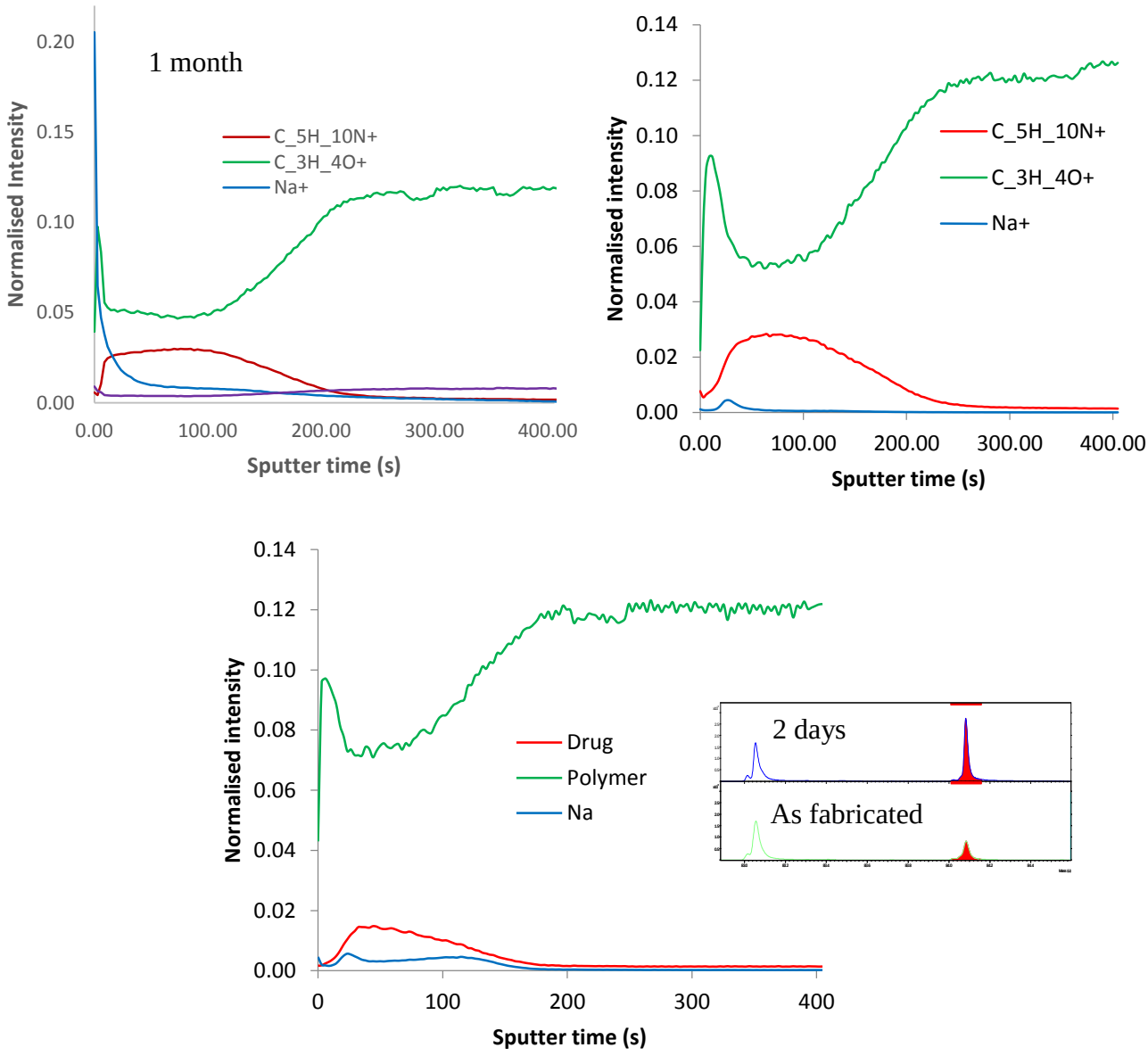


Figure 5.20 ToF-SIMS depth profile of abluminal surface of ArterioSorb™ as a function of elution time.

Phase separation was observed in these samples suggesting, in the context of this work, that the drug is phase separating from the polymer or at least enriching in local areas (therefore minimising its interaction with the polymer in these regions). After 3 month of elution, sirolimus was less concentrated at the surface and depleted with depth exposing PLLA substrate.

For ease of comparison only positive polarity were discussed. ToF-SIMS profiles for abluminal surface of scaffolds eluted for 0, 2 days, 2 weeks, 1, 2 and 3 month(s) are described in Figure 5.21 but then only 2 and 3 months eluted scaffolds were described as a function of depth later on in this thesis. ToF-SIMS depth profile of dissoluted samples indicate that there is less sirolimus at the surface compared to the as-fabricated sample. Also, it was observed that there is more PDMS and other contaminants such as F and K+ and Na. This observation makes sense in the light of the fact that the aqueous solution used for dissolution study contains sodium for instance, as drug eluted from the coating layer, Na becomes a remnant. This observation will be described later in XPS analysis.

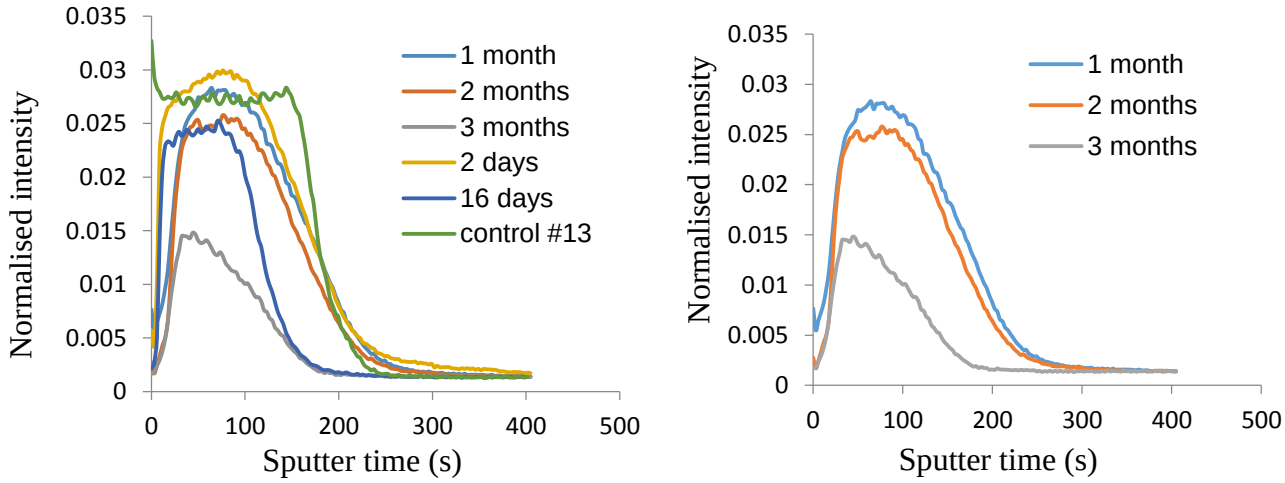


Figure 5.21 ToF-SIMS depth profiles of abluminal surface of ArterioSorb™ scaffolds eluted for over 3 months. A. SIMS profiles of all different scaffold and b. SIMS profiles of abluminal surface of scaffolds eluted for 1, 2 and 3 months showing sirolimus as a function of elution time.

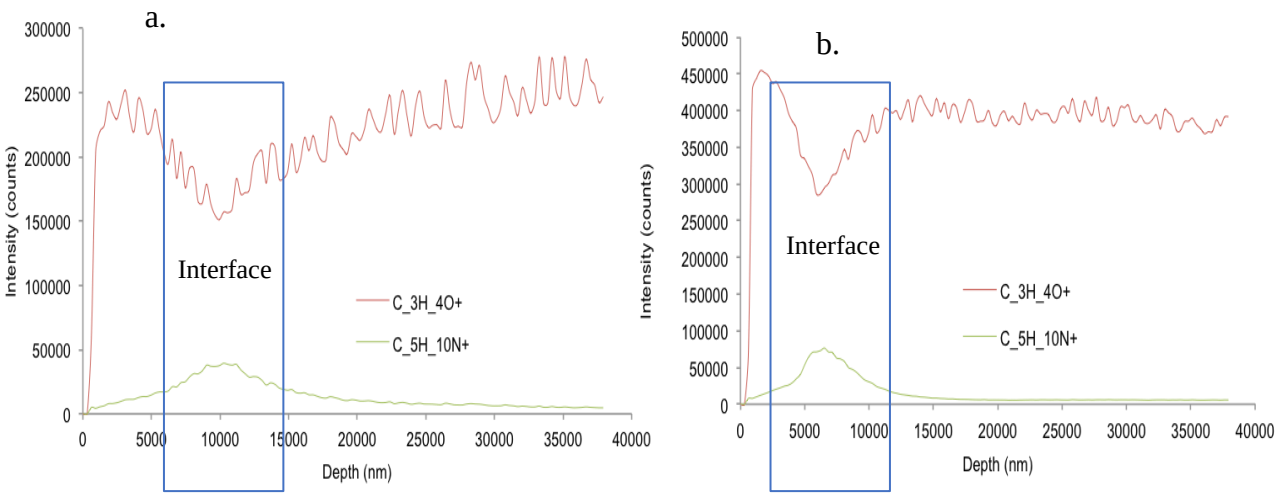


Figure 5.22 ToF-SIMS depth profiles of a bioresorbable scaffold showing signal intensity of the sirolimus and polymer as a function of Ar^+ sputtered depth. The drug sirolimus shows in the (green) and $P_{DL}LA$ in (red). The characteristic signals in the positive polarity are $C_5H_{10}N^+$, and $C_3H_4O^+$. a. represents depth profile of the 2 months scaffold suspended in PBS and b. depth profile of the 3 months scaffold suspended in PBS. Total depth of approximately 4 μm in the positive polarity.

The depth profiles of the 2 and 3 months eluted scaffolds in Figure 5.22, reveal that there is thick layer of polymer coating in 2 months eluted stent as compared to ToF-SIMS profile of 3 months eluted scaffold. The interface of sirolimus shifts from 1 μm to around 0.5 μm after 3 months of dissolution.

We investigated the degree of drug coverage on the scaffold with using 3D ToF-SIMS imaging before (Chapter 4) and after dissolution here in this chapter. Figure 5.23 describes 3D SIMS mapping of drug distribution in the coating using positive polarity. The iso-surface data related to the drug is coloured in red and the polymer is in green.

Note the substrate polymer is not completely showing in 3D SIMS images is because we have chosen an iso-value to make it easier to visualise in this thesis. Clearly there is polymer here as seen in depth profile spectra (Figure 5.22) but actually it is the drug location we are interested in and it had to be done for clarity.

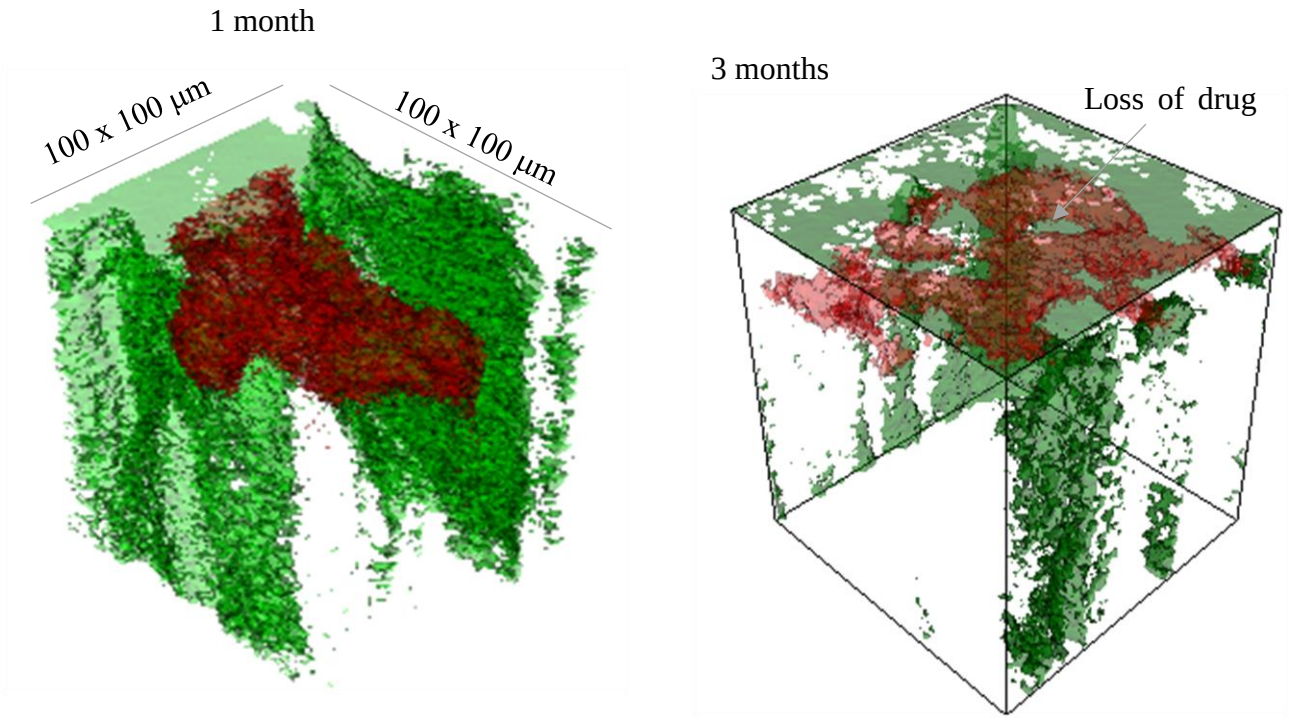


Figure 5.23 A set of 3D images taken from abluminal areas of eluted bioresorbable stent immersed in PBS at different time intervals. 3D images built from the 2D images at each cycle of the positive polarity depth profile, are rendered. The 3D images are iso-surface overlay of the sirolimus ($C_5H_{10}N^+$, red), and $P_{DL}LA$ ($C_3H_4O^+$, green). As elution proceeds, the surface layer becomes thin and porous.

The distribution of the drug was inferred by mapping the intensity of $C_5H_{10}N^+$ in the area of analysis. In this thesis, peaks at m/z 84 and 56 were used to map the drug and polymer, respectively. The data in Figure 5.23 shows loss of drug domains and less sirolimus at the surface as compared to non-eluted scaffolds (Chapter 4, Figure 4.30). From the iso-surface overlay images, it can be seen the remaining sirolimus in the coating surface has become quite thin and porous than that observed in the images of the as-fabricated stent.

5.2.4 Surface Chemical Composition by XPS

5.2.4.1 Surface film

XPS was carried out to investigate the chemical changes in surface chemistry of bioresorbable scaffold as a function of elution time. Samples mounted and pressed down onto a silicon-free carbon tape, as shown in Figure 5.24. Visually, there are issues with the stents not being perfectly flat. This will evidently have an influence on XPS sampling depth and sputter rate for depth profiling, which will be described later in this chapter.

The surface atomic compositions were calculated from core line areas using a straight-line background divided by the appropriate sensitivity factors. The obtained data were used to calculate the concentration of all elements detected in the composition of the coating layer and the distribution profiles were plotted.

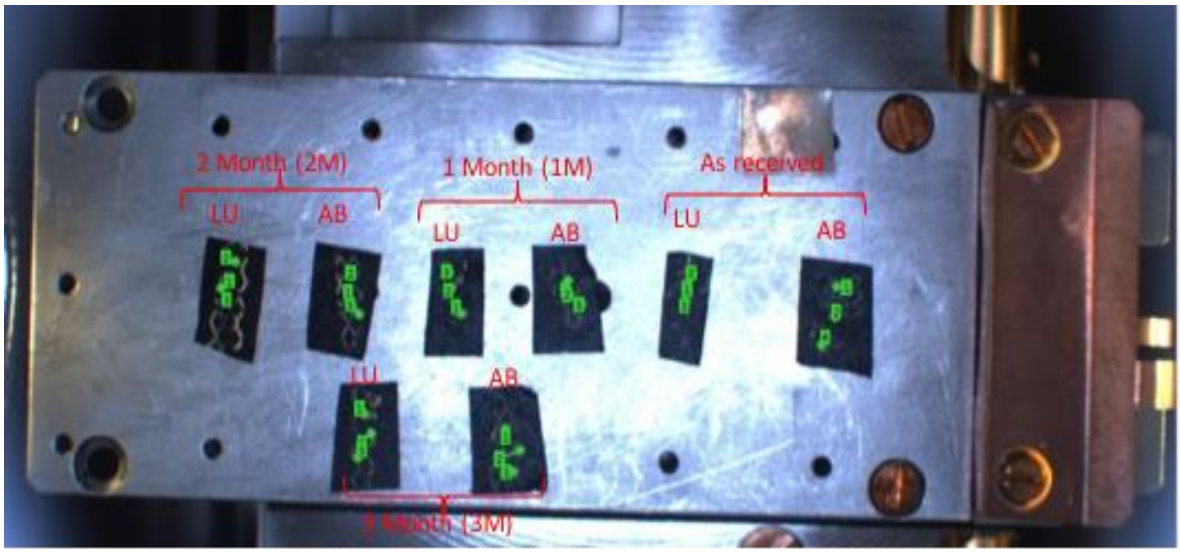


Figure 5.24 A Picture of ArterioSorb™ Scaffold mounted on stage, showing abluminal and luminal surfaces. (Kratos Analytical Ltd, Manchester).

Primarily, the survey spectra for starting materials were established in the previous chapters. The theoretical percentage of PDLLA for the C1s and O1s based upon bulk composition reported in Chapter 3 (60 and 40 %), respectively. The experimental percentage of these elements shows a slight difference with enrichment of C1s at the

surface. Contamination of the materials (sirolimus and PDLLA) is possible from handling or could be due to atmospheric contaminants (adventitious hydrocarbons). Characterising a surface in XPS without carbon contamination is almost impossible. As mentioned in Chapter 3, pure PDLLA/PLLA produces three carbon peaks the same position, which confirms the loss of sirolimus on surface of the scaffold (Figure 5.25).

Quantification of the scaffold as a function of elution time (pre-depth profiling) was carried out by applying a background subtraction to the high-resolution spectra not the survey spectra. A constraint for the FWHM was applied for all high-resolution spectra. The experimental proportions of the elements detected are tabulated in (Table 5.1) for the sirolimus/PDLLA coating layer at different elution time points, pre-depth profiling. The atomic percentages were quantified using empirically derived relative sensitivity factors provided by Kratos Analytical Ltd. Data were recoded using Kratos Vision II software and data were then transferred to VAMAS file and processed using CASAXPS. The possible errors in the atomic percentage were calculated using CasaXPS software. The software calculates the standard deviation of a peak using a Monte Carlo method[285]. During this calculation, fitting trials are conducted in which synthetic noise is added to the measured data, followed by a peak fit.

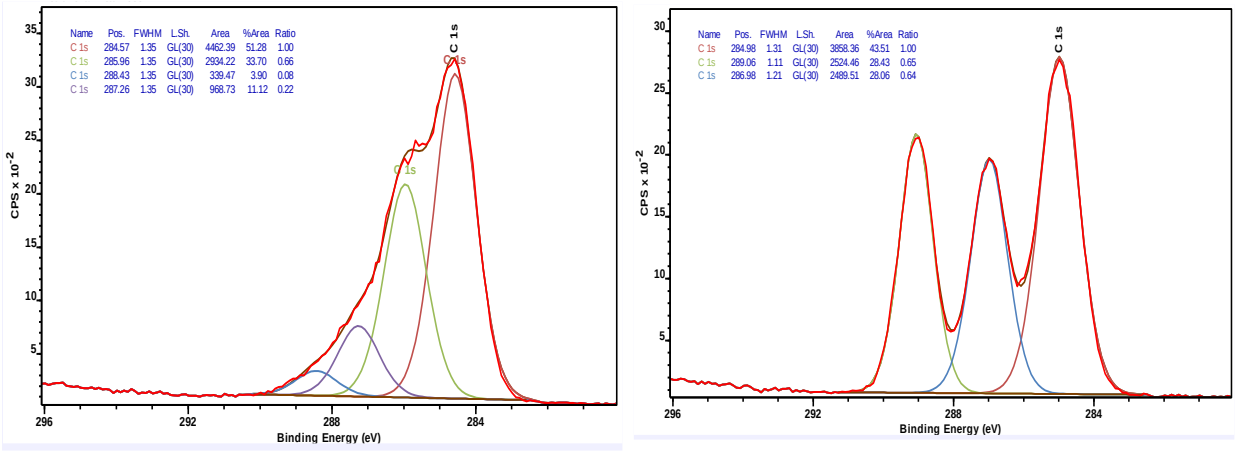


Figure 5.25 XPS data of high resolution scan for pure drug and polymer, using ThetaProbe XPS (Nexus, Newcastle).

Table 5.1 Experimental atomic % for abluminal and luminal surface of coating layer of ArterioSorb™ scaffolds.

Abluminal As fabricated	**Atomic con %**	**Error %**	**Luminal As fabricated**	**Atomic conc %**	**Error %**
C1s	74.60	0.50	C1s	74.40	0.40
O1s	24.40	0.50	O1s	24.30	0.40
N1s	0.82	0.08	N1s	0.60	0.06
Si2p	0.66	0.03	Si2p	0.77	0.07
Abluminal 1 month	Atomic con %	Error %	Luminal 1 month	Atomic conc %	Error %
C1s	68.10	0.50	C1s	59.15	0.62
O1s	22.70	0.41	O1s	23.65	0.48
N1s	0.19	0.06	N1s	0.17	0.07
Si2p	9.11	0.15	Si2p	17.02	0.32
Abluminal 2 months	Atomic con %	Error %	Luminal 2 months	Atomic conc %	Error %
C1s	66.12	0.52	C1s	68.32	0.47
O1s	30.69	0.46	O1s	26.29	0.43
N1s	0.11	0.21	N1s	0.12	0.07
Si2p	3.06	0.26	Si2p	5.25	0.19
Abluminal 3 months	Atomic con %	Error %	Luminal 3 months	Atomic conc %	Error %
C1s	67.82	0.44	C1s	64.78	0.44
O1s	25.60	0.38	O1s	25.70	0.39
N1s	0.2	0.06	N1s	0.32	0.06
Si2p	6.38	0.20	Si2p	9.18	0.21

Figure 5.26 shows the wide scan spectra of as fabricated and dissoluted scaffolds obtained using Kratos Axis ULTRA XPS, on both abluminal and luminal regions of the scaffold.

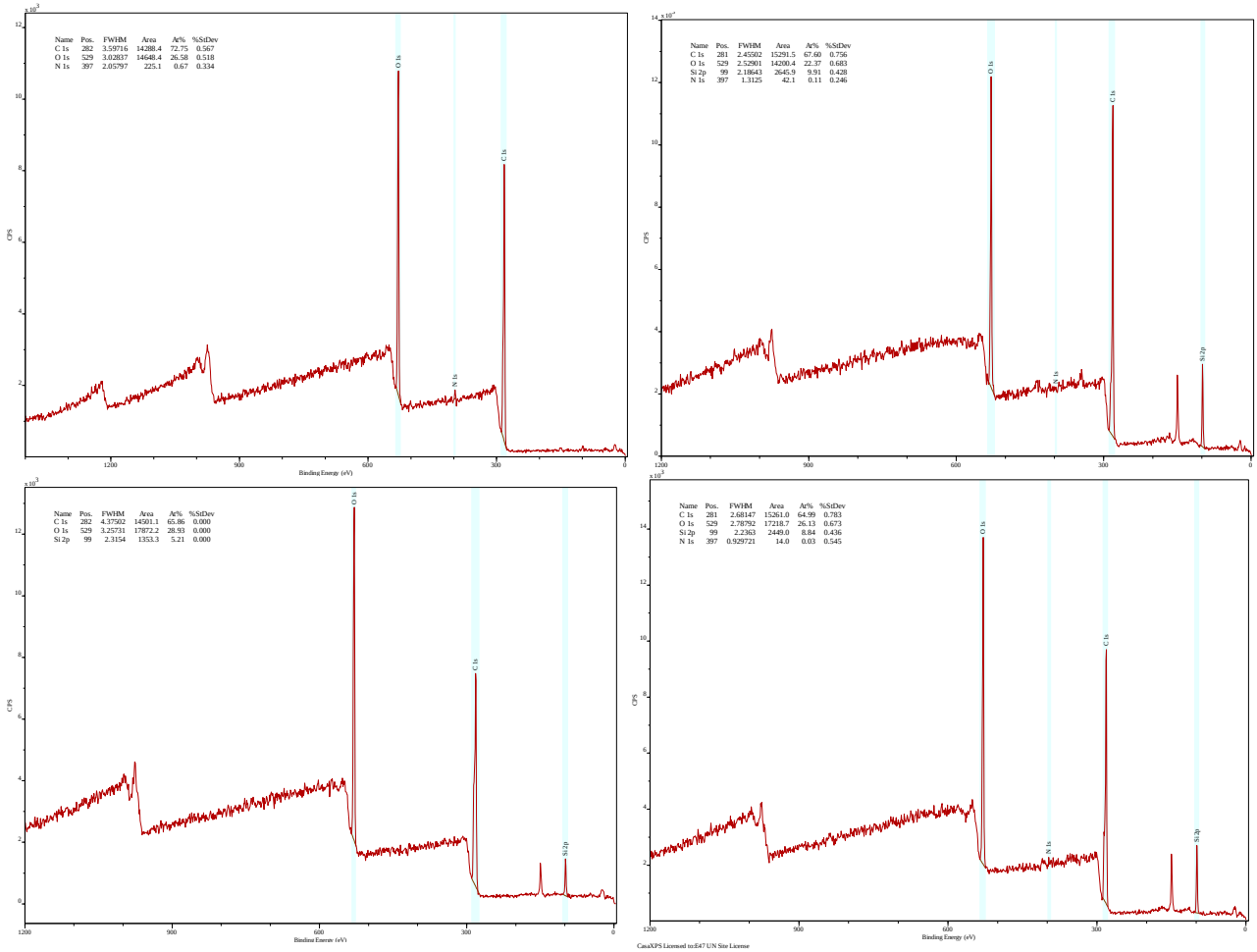


Figure 5.26 XPS spectra of wide scans of luminal coating layer of stents subjected to dissolution media (Nottingham), measurements were acquired on a Kratos Axis ULTRA XPS spectrometer.

5.2.4.2 Peak fitting

High resolution spectra were acquired with higher energy resolution to investigate the chemical state for the elements at the surface and within. Peak model was used to demonstrate points relating to quantification regions. Carbon fitting was performed using the CasaXPS software (version 2.3.18).

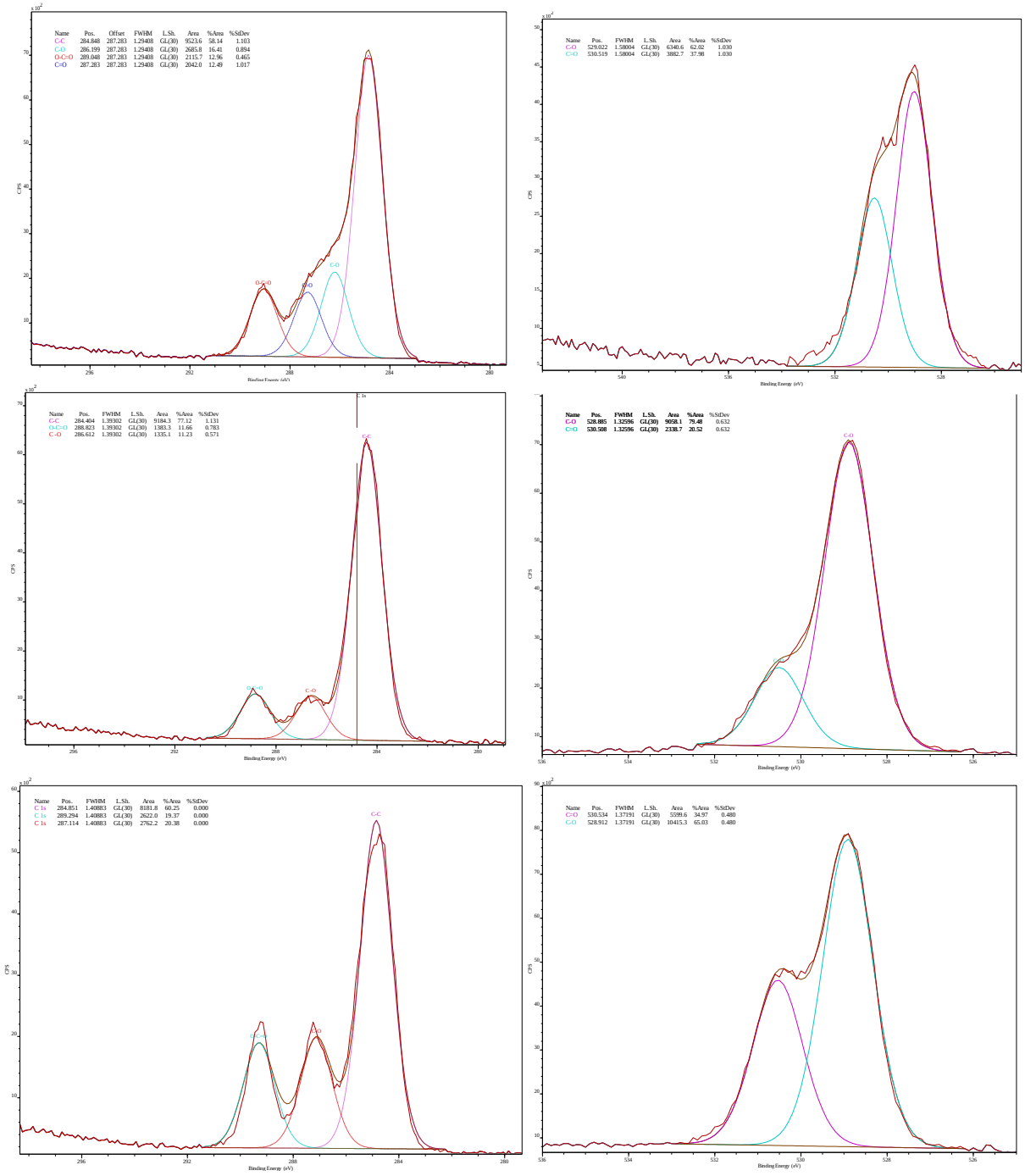


Figure 5.27 High resolution spectrum of the C1s and O1s regions in abluminal ArterioSorb™ as fabricated versus dissoluted scaffold for 3 months.

Four chemical states of carbon are fitted to each C 1s peak envelope for sirolimus. Prior dissolution the coating layer of ArterioSorb™ exhibited a shape similar to the one

described for pure sirolimus (Figure 5.25). After dissolution, the peak shape was changed due to the loss of drug domains. Figure 5.28 shows the high resolution XPS spectra for the C 1s and O1s regions for as-fabricated scaffold. It can be observed from the figure that for as-fabricated and dissoluted, the deconvoluted C 1s spectra showed the possibility for peaks at 284.8 ± 1.1 eV, 286.1 ± 1.1 eV and 287.3 ± 1.0 eV and 289.0 ± 0.5 eV. These peaks correspond to C-C, C-O, C=O and O-C=O which are mainly due to polymer/drug coating. The oxygen region was deconvoluted (Figure 5.28), showing two peaks, and low binding energy component attributes to C=O and high binding energy attributes to C-O group.

5.2.5 XPS Depth Profiling

The distribution within the XPS analysis depth is of great interest in studies involving surface work[153]. Depth profiles of ArterioSorb™ scaffolds at different elution time was obtained in conjunction with Ar ion beam sputtering.

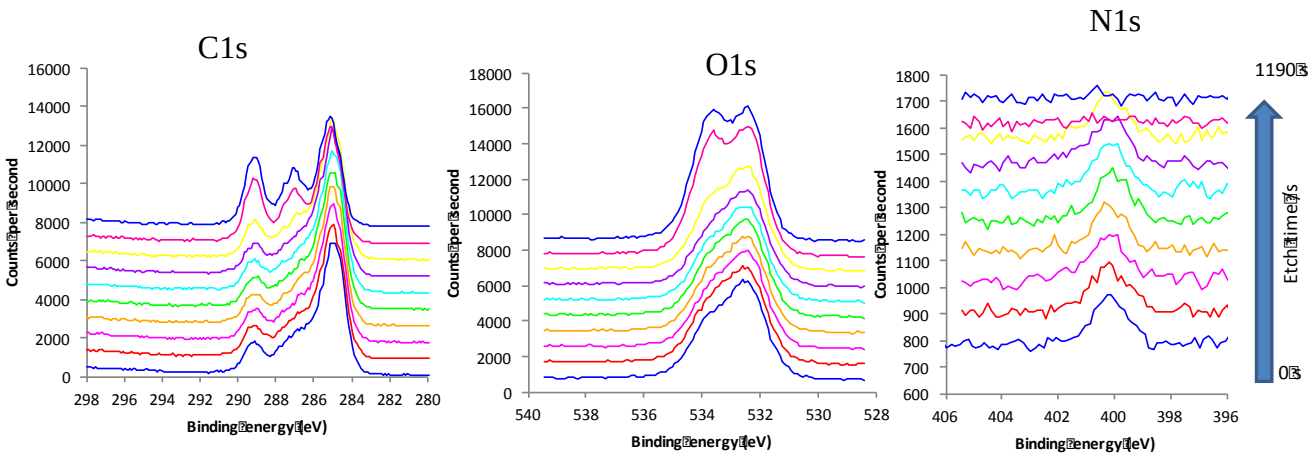


Figure 5.28 Depth profile spectra of C1s, O1s and N1s regions for abluminal ArterioSorb™ scaffold as received as a function of depth.

The XPS profile data in Figure 5.29 show high resolution and depth profiling spectra of C and O and N for as-received scaffold. Before etching the sample, the C 1s peak showed the possibility for the existence of sirolimus and polymer bonds for all first and second generation of ArterioSorb™ scaffolds. (Data of 1st generation dissoluted scaffolds are described in Appendix D). After etching the samples for 30 seconds (~ 4 nm), showed a

reduction of C-C and C-O peaks. The XPS depth profile in Figure 5.29, in particular of oxygen and nitrogen shows the surface is composed of sirolimus followed by depletion of it. This phenomenon was prominent characteristic of the 3D SIMS mapping (described in the previous chapters). There are hence differences between the XPS and SIMS data regarding the depletion region of the drug. This difference might be due to sample variations within each scaffold as well as mechanical heterogeneity. The peak shape in the dissoluted samples (as shown in Figure 5.28) confirm the depletion of the drug in the top 10 nm of the coating. The drug peak disappeared displaying features of similarity to PDLLA/PLLA, confirming what was seen previously by AFM (Chapter 4). Where dark regions are drug rich areas and bright areas where the surface was exposed of polymer dominated system.

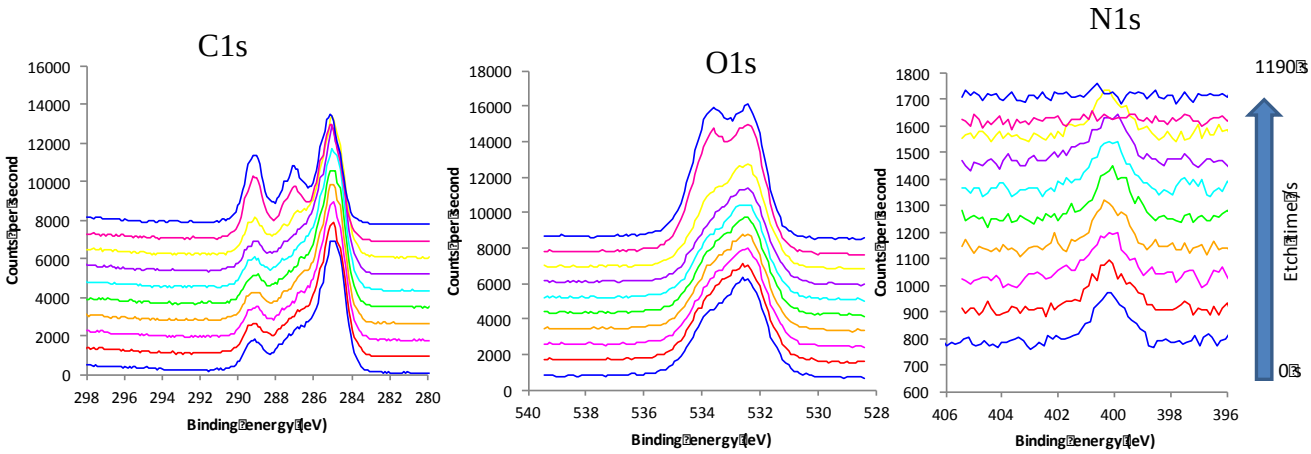


Figure 5.29 XPS depth profile of abluminal ArterioSorb scaffold (as fabricated), of a. C1s, O1s and N1s regions. B. XPS profile of zoomed in N 1s as a function of depth. Analysis area 100 µm spot size. Sputter ion beam was rastered over an area of 2x2 mm etch area, (10 kV Ar_{1000+}).

For the scaffolds which had been in solution, Nitrogen is not seen at the surface at the same level as the as-received sample. As can be seen from Figure 5.30, after 1 etch cycle the concentration decreases to <0.1%. Further etching shows an increase in N followed by a decrease in N concentration. Reduction in the intensity of O 1s peak on increasing depth can correspondingly be witnessed from the Figure 5.29. It's apparent that O 1s peak shape ties in with the N concentration change, as shown in Figure 5.30. The XPS depth profile of nitrogen shows the surface is composed predominately of drug

followed by depletion at around 200 seconds of sputtering, followed by areas enriched of sirolimus then eventually depleted. The zoomed in profile of the N 1s region shows a steep dip after 1000 seconds, showing N 1s no longer observed, as it is below the limit of detection.

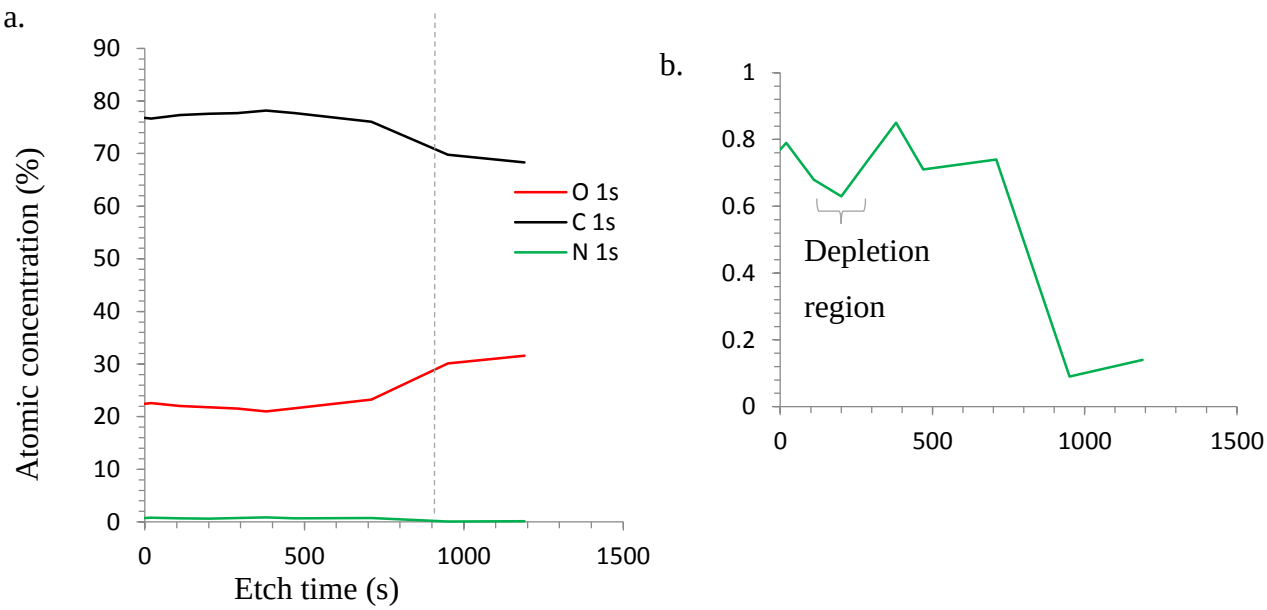


Figure 5.30 a. XPS depth profile of nitrogen region of abluminal surface of ArterioSorb scaffold after 1 month in PBS, b comparison of high resolution spectra of O1s regions obtained for a scaffold been in PBS for 1 month. O1s spectra after 0, 1 and 10 etch cycle, respectively. There is a possible change in the elemental composition due to degradation.

Figure 5.31 (b) shows high resolution spectra of O 1s region of dissoluted scaffold at different sputter cycle. The peaks observed for O 1s at 529.0± 1.0 eV, 530.5 ± 1.0 eV can be attributed to C-O and C=O. Un-etched oxygen is dominated by surface contamination, first etch reveals an O 1s peak similar in shape to the PLLA polymer (O1s peak of the polymer described in Appendix D). Subsequent etching shows the peak shape return to the shape of the drug/polymer seen in the as-received sample (as shown in Figure 5.29).

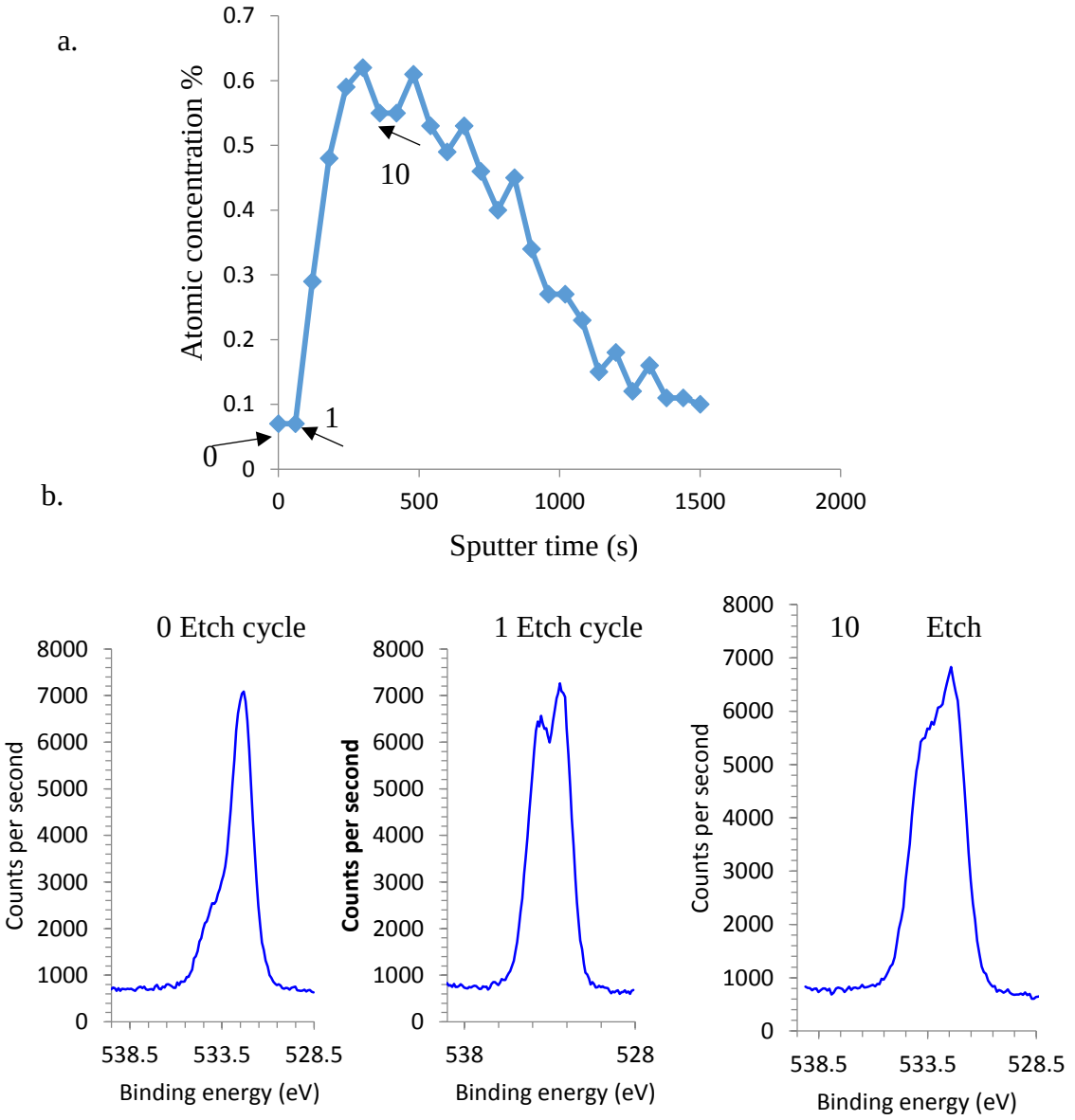


Figure 5.31 Comparison of abluminal surface of ArterioSorb™ depth profiles of N1s region at different elution time.

Figure 5.32 shows the high-resolution spectra of the N 1s region obtained after different dissolution time intervals. From the N1s region, reduction in the intensity of peak (and therefore the amount of drug) with an increase in immersion time was observed.

Heterogeneity is observed in both scaffold generations, as can be seen from ToF SIMS images of samples as-fabricated (Chapter 4, Figure 4.21, Figure 4.22 and Figure 4.30). There are polymer enriched areas surrounded by drug enriched areas. The analysis of the underlying layers of the coating layer shows the polymer enriched domains increase until covering most of the surface at 3000 nm depth. Three measurements were taken on three different areas of the coating layer for both abluminal and luminal side. Some areas seem to have higher drug content than others, showing heterogeneity in drug loadings. The range of values in drug contents is due to heterogeneity of the coating. This is consistent with ToF-SIMS at least qualitatively. The presence of silicon could be from the lubricant used during the product manufacturing or during sample handling.

XPS allowed us to investigate the elemental distribution and to evaluate uniformity of the polymer layers as across the surface of scaffolds as well as composition of polymer drug-containing layer through the depth. Depth profiling using XPS confirms that the drug is enriched at the surface, posing significant implications for drug coated polymer delivery systems. There is very little in the literature about characterisation of stent by XPS depth profiling, as a result this work has provided a valuable insight into the potential of surface characterisation and dynamic of drug release from such complex system.

5.2.6 Raman

The Raman data is complementary to ToF-SIMS and is consistent with added functionality of clearly revealing large holes (phase separation), which is related to the drug release.

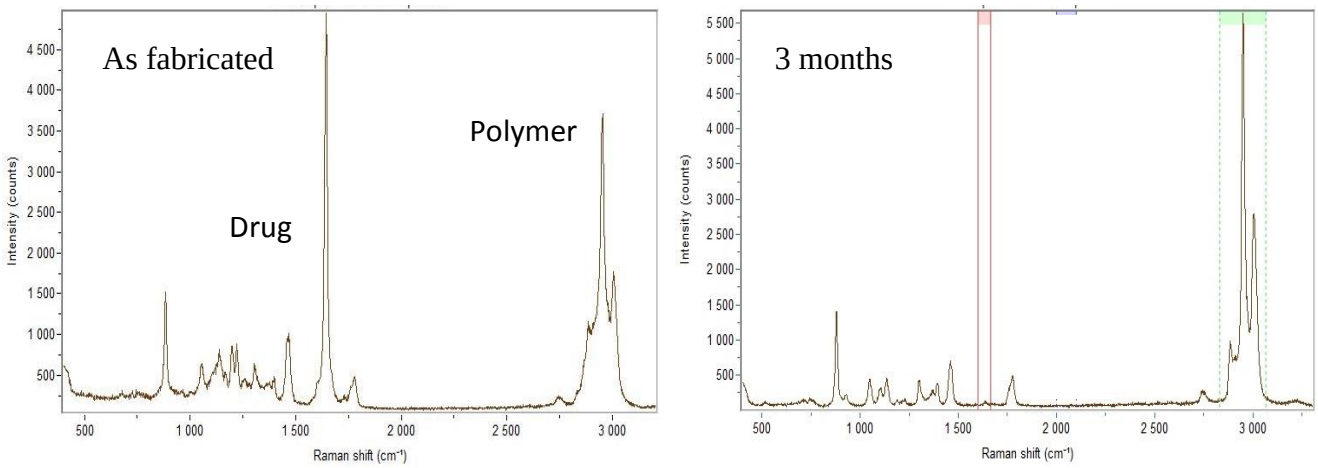


Figure 5.32 Spectra showing intense peak of the polymer at (2900 cm^{-1}) post dissolution, and drug peak (1631 cm^{-1}) seems to be less intense as compared to a spectrum extracted from as fabricated surface of ArterioSorb™.

Figure 5.33 shows the strong peak at 1640 cm^{-1} associated with the drug decreases as elution proceeds, leaving a spectrum similar to PLLA (Chapter 4, Figure 4.37).

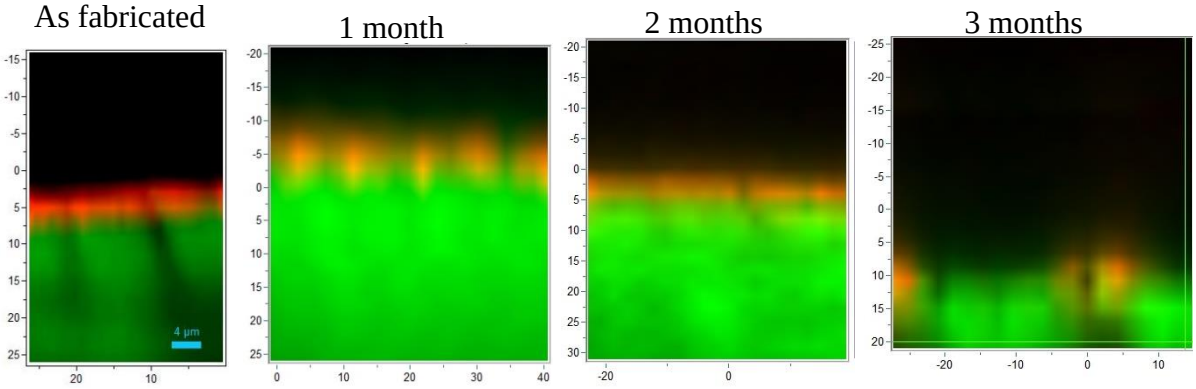


Figure 5.33 Confocal Raman maps of stent coating-layers distribution (Z: 20 µm deep) as a function of elution of sirolimus from 50 % sirolimus 50 % PDLLA coating. Indicating sirolimus as (red), PDLLA as (green) and (black) is air.

Also, there seem to be concentrated areas of the drug, where the drug accumulated at the surface and the polymer less strong at the surface and became heterogeneous (Figure 5.34). As the surface is eroded the distribution of drug becomes more

heterogeneous. As expected, sirolimus decreases in respect to the polymer as sirolimus eluted from the coating. The peak associated with sirolimus at 1640 cm^{-1} essentially disappear as elution proceeds, leaving a spectrum similar to the one described in Chapter 4 (Figure 4.37). Raman data show drug present all over the surface of 0-month scaffold (described in Chapter 4, Figure 4.39) but there are areas of high localisation of drug intensity, again agreeing with ToF-SIMS data showing that the drug distribution is heterogeneous. After elution, the surface exposed to aqueous environment appears to be less thick as compared to surface of control stent (as fabricated).

Several areas were measured by Raman to ensure that the trend is reproducible, however it was very time-consuming experiment as each sample took almost 14 hours to analyse. Raman images are displayed at elution time points of 0, 1, 2 and 3 month(s). To sum up, the Raman images above highlight the inhomogeneous distribution of drug in red and polymer in green. The images at 0-month elution show areas enriched in sirolimus (as shown previously in AFM analysis) corresponding to high topographical regions. The Raman images reveal areas of low and high drug concentration. Over the course of 3 months elution the majority of the drug (80 %) has been released as demonstrated by the surface Raman image. Coating rearrangement is apparent on a large-scale. The coating arrangement is something that may occur post elution, where the polymer fills in porous features and separate pockets that have been observed previously. Some part of the scaffold starts to flatten out over the course of elution, due to loss of drug-rich domain from within the coating.

5.3 Near Surface Chemistry by ATR-IR

ATR was acquired to identify the chemical information, it was discussed in previous chapter the characteristic peak associated with sirolimus is at 1645 cm^{-1} and PDLLA at 1268 cm^{-1}. After dissolution, the spectra show weakening of sirolimus peak.

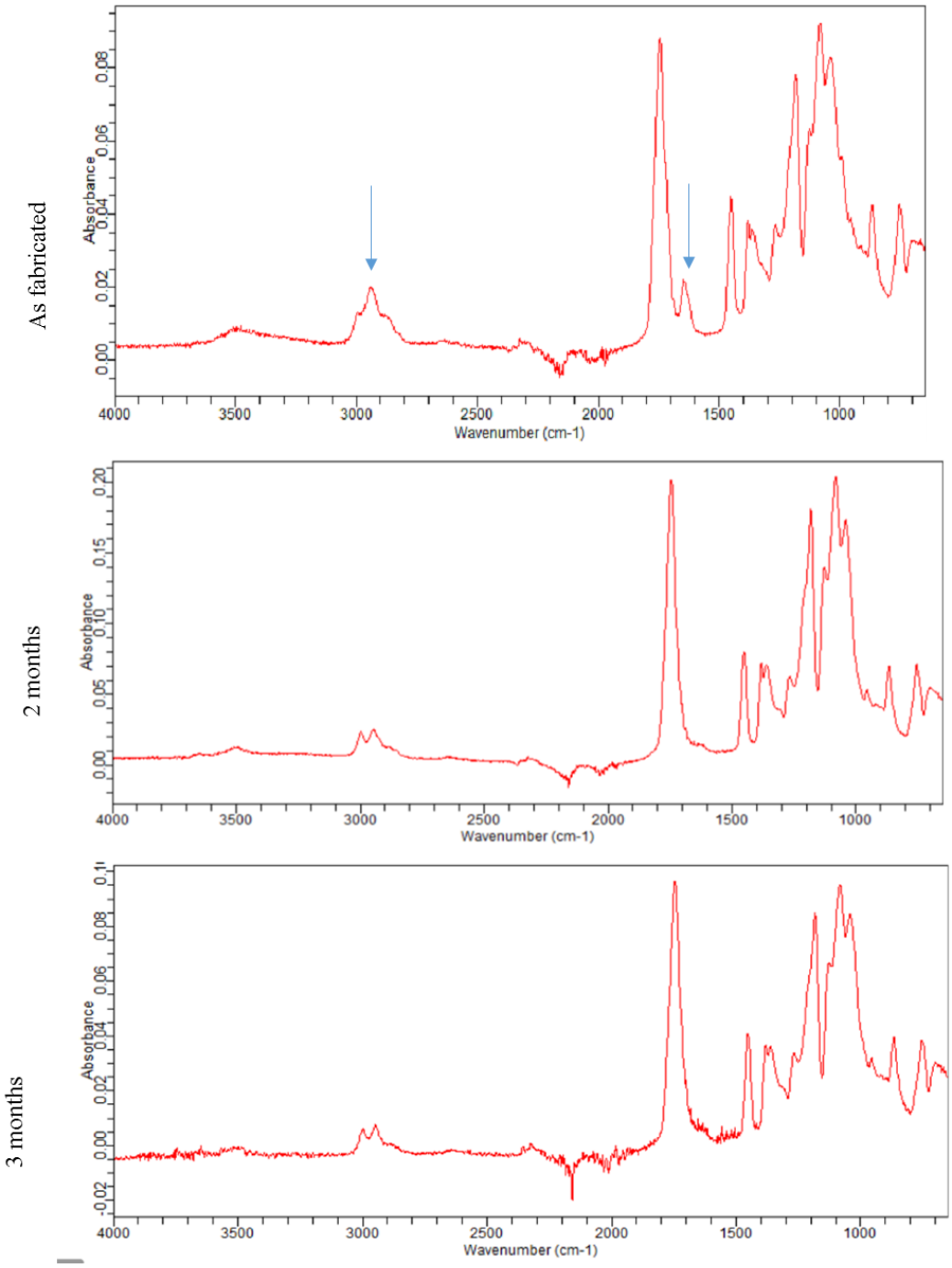


Figure 5.34 ATR spectra of dissoluted sirolimus/PDLLA laser cut scaffold at 0, 2 and 3 months in PBS.

Taken together the experiments undertaken using different complementary analysis techniques a possible drug release mechanism from ArterioSorb^{TM} was revealed. A rapid

release of sirolimus from the top surface occurred due to diffusion of the drug from the near-surface and bulk of the scaffold, this might have occurred via buried drug rich domain, through pits generated after rapid release of the drug, another reason to this release mechanism obtained in this chapter might be due to the loss of drug rich domain followed by slower erosion of the bulk material over months of degradation in PBS under physiological conditions.

5.4 Conclusions

The work presented in this Chapter has exposed important morphological features related to drug release in the ArterioSorb™ scaffold, these features correlated to the chemical identity. Pore formation was evident at the surface on the ArterioSorb™ coating layer post *in vitro* investigation. The correlation between the data using analytical techniques mentioned above is a powerful method that can connect the chemical properties with the physical morphology of fully bioresorbable scaffold coatings during elution procedure. Combinations of techniques was also demonstrated by Belu *et al*. in their analysis of rapamycin loaded in PLGA using XPS and ToF-SIMS coupled with Raman[97].

The release profile done by Arterius Ltd and one carried out in Nottingham display similar characteristic diffusion profiles as was observed in actual scaffolds. *In vitro* studies of the degradation kinetics of polymers are essential for the design and optimisation of implantable biomedical devices. The choice of a suitable release medium is an essential characteristic in the development of *in vitro* drug release testing. The successfully performed experiments and obtained results demonstrate the potential of field-effect devices as a novel and promising tool for the real-time analysis. AFM topographical information has provided a significant understanding into the structural changes that occurs at the surface interface. AFM was quite useful to confirm the mechanical properties of the coating and confirm the coating sustained its adhesion to the scaffold (PLLA), this is useful validation of the preclinical data. AFM suggested that the spray-coated layer (sirolimus in PDLLA) was firmly adhered to the surface of the scaffold before elution and was relatively smooth but became heterogeneous upon dissolution testing and yet maintaining the integrity of the coating. The surface morphologies showed

possible hydrolysis occurred at localised areas on the coating film leading to the formation of pits, which converged to form larger areas of degradation. Phase separation at the drug-polymer coating surface. The phase separation of polymer/sirolimus during spray-coating conditions leads to the formation of nano-pores via the spinodal decomposition mechanism.

The 3D distribution of sirolimus in the PDLLA coating as a function of elution time was assessed by ToF-SIMS imaging and depth analysis with further information gleaned from optical profilemetery. XPS was also used to probe the elemental composition of the coating-layer, confirming the loss of the drug post dissolution. Finally, the chemical morphology of a 50:50 sirolimus/PDLLA coating-layer on scaffolds was examined using CRM, from the surface through the bulk of the coating-layers, where large areas of sirolimus domains were distinct at the surfaces and then were depleted following 3 months of elution.

The overall work successfully described the physical properties and the *in vitro* drug release mechanism of sirolimus/PDLLA coated stents. In our coating system, sirolimus was released in a sustained manner from PDLLA coating layer coated on the stent. However, if the experiment was to be repeated it's recommended to use a surfactant and ethanol to improve solubility (Tween 80 and ethanol), this is what Pharma use. The drug has to be in amorphous phase to dissolve quickly. The morphology of the coating layer was stable without irregularity or roughness under optimal conditions of ultrasonic spray coater. Illustrating how the technique can be used to identify what is left after dissolution to complement the information from the dissolution of what has come off. The morphology and chemical composition of a novel bioresorbable drug eluting scaffold was successfully characterised at the nano and micro-scale. The release mechanism and the location of the drug are both important aspects of the design of a controlled drug release delivery system. Consequently, monitoring the distribution of the drug and the polymer were investigated in order to understand the release kinetics associated with ArterioSorb™ stent. The association between drug-enriched regions and the coating morphologies allowed a correlation between drug release and pore-formation at each stage in the process. The 3D molecular compositional information acquired was useful for

understanding the performance in a drug delivery device such as a stent/scaffold. 3D molecular information displayed an enrichment of the drug at the surface for all analysed scaffolds and decrease in homogeneity as drug elutes out of the stent, leaving areas on the scaffold rich in sirolimus and areas that are mainly PLLA substrate. The data obtained from ToF-SIMS correlate well with Raman images. Although the area of analysis was not the same. Images obtained by both analysis display qualitatively similar features on a comparable size and depth scale. The 3D spatial distribution of the drug obtained by ToF-SIMS and Raman indicated a drug-enriched surface region in the coating on control samples (as-fabricated), where sirolimus regions are large and distinct at the surface of the non-eluted stent (as-fabricated) however, upon elution the drug is also eluted from throughout the coating layer, as shown by Raman imaging. The data indicated a switch in drug composition from rich in sirolimus (prior elution) to rich in polymer post elution. XPS depth profile did prove difficult, however surface analysis was much easier. The depth profile of the drug was identified by the profile of nitrogen.

6 GENERAL CONCLUSIONS AND FUTURE DIRECTIONS

This thesis has shown how surface analytical techniques have been successfully employed to characterise the surface chemical character of a fully bioresorbable scaffold with potential to be used for the treatment of cardiovascular diseases. Due to complications in geometry of the scaffold a series of starting materials including extruded and oriented polymeric tubing with different dimensions, coated and uncoated have used as “model system” before looking into the characterisation of the full product. The information gleaned from the characterisation of these tubes proved to be very useful in evaluating the practicability of the surface analysis techniques presented in this thesis.

Complementary techniques, SEM, AFM, DSC, ATR-IR, ToF-SIMS, XPS and Raman were used to characterise these tubes. In summary, the analysis technique SEM and AFM have shown a homogenous surface for the PLLA tubing. This was in agreement of the ToF-SIMS chemical mapping data. In addition, AFM imaging of PLLA tubing as presented in Chapter 3 revealed that the PLLA presents a homogenous surface prior processing. In the results presented in Chapter 3, attention was paid to height and AFM phase images revealed regions of different tip-sample interactions indicating heterogeneity at the nanoscale. DSC was used to scrutinise the crystallinity of the polymeric tubing prior processing and post laser cutting. This is important as the physical state of the polymeric surface helps in predicting scaffold performance *in vivo*. As the rate of degradation *in vivo* depends on existence of amorphous region. Moreover, the degree of crystallinity has an impact on the polymer solubility[286]. The higher the crystallinity, the more likely the polymer will be brittle under biological conditions. ATR-IR enabled us to

assess the structure of PLLA, confirming the C=O, C-O-C and C-C peaks were visible at 1754, 1175 and 1200 cm^{-1}, respectively.

Stents are characteristically composed of scaffolding that includes a network or pattern of interconnecting structural elements or struts. These patterns were produced by laser machining of oriented PLLA tubing. The effect of laser cutting in polymer materials was investigated in Chapters 3 and 4. The laser cutting procedure was not fully disclosed due to confidentiality. However, ultra-short pulses are used as they have an advantage over longer pulse lasers[224,287]. Series of laser cut scaffolds were supplied by Arterius Ltd, all of which have been cut using different laser parameters. Some of these scaffolds had shown small heat affected zones as compared to other areas. These areas were referred to as HAZ[124]. Melting of the polymer can result in unwanted decrease or increase in crystallinity once the polymer re-solidifies. Moreover, laser cutting could induce the formation of amorphous material. The surface morphology of laser cut scaffold was investigated by SEM and AFM. AFM images of the laser cut samples revealed formation of pits, and spherulite features. Also, areas where polymer melting on the edge of the scaffold were observed, such phenomena might have happened due to temperature used during the cutting of the scaffold. Nano-thermal analysis confirmed the presence of these laser cut features. The analysis of ToF-SIMS was carried out on abluminal surface of the extruded and die-drawn PLLA tubing, however it was quite difficult to get into the inside of the tube due to the curvature, hence bad topography. ToF-SIMS employing $C60^{++}$ was utilised to obtain in depth information from the PLLA tubing where fluorine, chlorine and nitrogen were found to be on the surface in small amounts. The surface composition was determined by XPS. The detected elements that are present in the PLLA tubing by XPS were reported to be carbon and oxygen as expected although other elements have been detected, namely silicon and nitrogen. PLLA samples have three types of carbon bonding environment: C-O, C-C(C-H) and O=C-O that correspond to their theoretical composition. The surface of PLLA tubing showed enrichment of C1s which might be due to adventitious hydrocarbon.

In Chapter 4 the morphology and chemical composition of a novel bioresorbable drug eluting scaffold was successfully characterised at the nano and micro-scale. The surface

and depth characterisation of the coating surface layer provided valuable information with regard to the distribution of the drug. The SEM and AFM images of the drug coating surface layer show a structure of varying topography, with some areas that are relatively homogenous and others that contain features which appear as openings in the surface. The phase separation of polymer/sirolimus during spray-coating conditions led to the formation of nano-pores via a proposed spinodal decomposition mechanism.

Nano and microthermal analysis was successfully described in Chapter 3 and 4. The analysis of the abluminal side of the laser cut scaffolds showed differences in state composition. For as-cut PLLA scaffold (crimped) multiple transitions were observed confirming the amorphous status of the surface. It is very possible that the heating step associated with crimping had introduced some crystalline feature on the surface of the stent. The thermal maps (AFM Nano-IR) helped in identifying the materials based on their thermal properties. The distribution of the drug was investigated using ToF-SIMS using an Ar cluster ion beam for depth profiling and Bi_3 for surface analysis. 3D visualisation of the chemical constituents in drug eluting stent was achieved. Surface morphology changes might have an effect on release profile of the sirolimus. XPS provided a quantitative understanding of the distribution of the drug within the samples. XPS data confirmed surface drug enrichment was observed.

A control study was not performed on different application methods of coating such as spin-cast or dip coating or different thickness, however other studies [87,97] have reported methods of coating are significant factors that may have an impact on early release of sirolimus. The approach presented in this chapter has revealed important morphological features related to drug release in the ArterioSorb™ scaffold first and second generation and has related these features to the chemical identity. The study of *in vitro* degradation proved potential surface disruption of the samples (drug coated tubing) over time. *In-vitro* studies of the degradation kinetics of polymers are essential for the design and optimisation of implantable biomedical devices. The results of the presented *in vitro* study in Chapter 5 showed the outcome of release testing of ArterioSorb™ stent on the specific experimental conditions. Elution was shown to happen from drug enriched areas on a relative short time, followed by gradual elution from subsurface regions. The *in vitro*

degradation study of ArterioSorb^{TM} revealed initial rapid release of the drug from the top surface followed by controlled drug release over time. The drug release rate is controlled by diffusion through an arrangement of pores, with developing structure as the polymer matrix degrades. The SEM analysis revealed that the coating surface maintained its integrity and adhesion to the strut during degradation. AFM studies confirmed circular features on the coating layer for the as-fabricated scaffold. These features are presumably drug related and upon elution loss of these domains were visible by development of pore formation. In general, regions of the polymer look to be saturated with drug, whilst some areas had areas consist of sirolimus and little of PDLLA. The thickness of the drug (in ToF-SIMS, XPS and Raman) appeared to be variable due to elution study. Below certain areas of drug-rich domains, there seemed to be areas depleted of sirolimus, also beneath other areas that are enriched of drug, showing the heterogeneous distribution in 3D. The drug elutes from the surface and from within drug concentrated subsurface. During elution, the coating contracts (as shown in SEM analysis and AFM) causing some sodium or other substances to be present at the surface (as shown in ToF-SIMS and XPS), this is due to sodium (alkali ions) remains in solution when the sample is extracted from aqueous elution medium. Little was mentioned about sodium in this work as this was not part of thesis scope. The established work was visualised by ToF-SIMS and Raman imaging, both of which provided strong evidence of pore network formation post *in vitro* study and polymer reorganisation as a function of time.

A series of arterial stents has been studies using varies cutting edge analytical techniques. Hight resolution level set of data were obtained from a complex system. On the microscale there is some element of heterogeneity. However, taking the device as a whole we can conclude there is an even distribution of drug in the coating. From ToF-SIMS data we can detect the effects of drug coming out of the coating. The drug distribution was measured at the microscale showing an even distribution of sirolimus in the coating and the drug being released evenly. The drug can phase separate from polymer due to relative kinetic energy and results evidence of this understanding as shown in AFM images.

Taken together analysis done throughout this thesis, three different stages of drug release were observed from the ArterioSorb™ scaffold: a rapid release of the drug from the top surface as a result of loss of the drug domains (drug-enriched region), followed by a slow release erosion of the bulk material. Drug release from the bulk of the sample occurs through generation of pits post rapid release followed by diffusion of the polymer matrix. Dissolution data showed an instant loss of sirolimus from the surface even though the surface was intact after 3 months of dissolution. Data obtained from AFM as well as CRM images reveal pore formation and depressed regions that are directly replaced by drug enriched region. These features (pores) provide direct route for drug release mechanism.

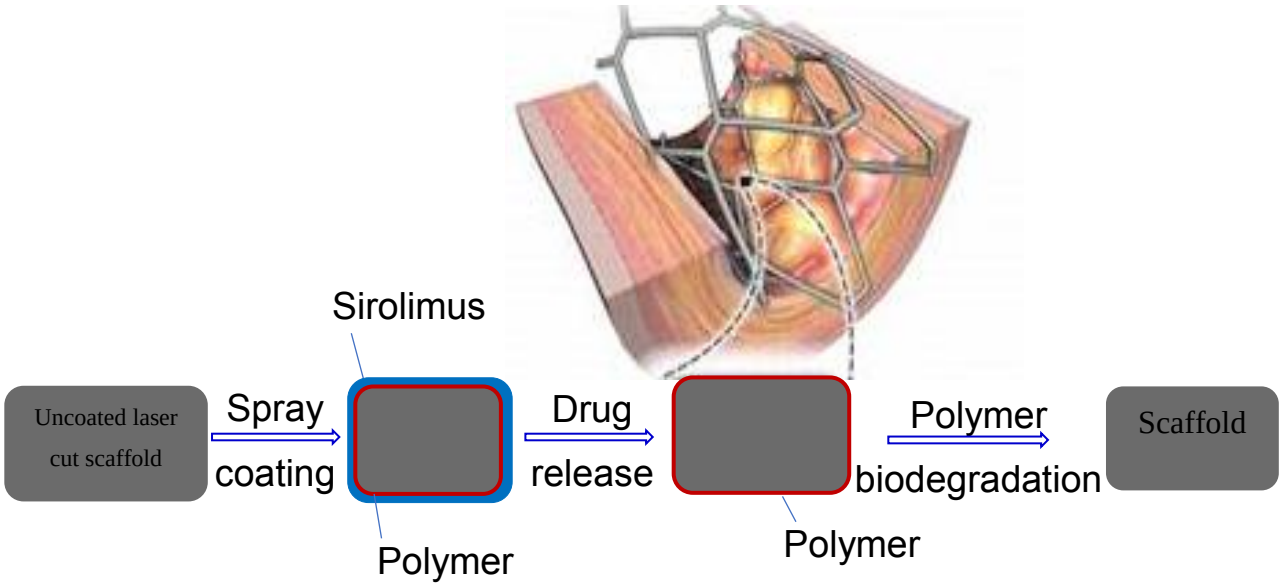


Figure 6.1 Schematic of proposed mechanism for degradation of the polymer and drug release.

Data obtained in thesis helped in developing an understanding of the distribution of the drug as a whole, which helped in justifying the observed drug release profiles. The drug in ArterioSorb™ scaffold is likely to be released from coating by rapid release of drug followed by even release of drug over time and as the coating layer breaks up sirolimus is released in sustained manner.

Rich layer of sirolimus was observed at the surface of Raman as well as ToF-SIMS and a drop of drug concentration after dissolution was reasonably apparent in 3D ToF-SIMS models. Over time pits form and eventually islands where the coating left, and the coating lose its integrity and polymer degrade. It's important to know this as the outer layer goes due to drug release. The initial rapid release of sirolimus could be due to the combined process of faster drug diffusion than polymer degradation of the matrices. This mechanism provides an insight into drug release mechanism from surface eroding versus bulk eroding polymer. A combination of methods helped identify the materials used in this device. The distribution in the coating and drug release was characterised in a 3D model, which helped us in establishing that the drug is released via polymer erosion and pit formation from a microscale phase separated system. Drug concentration profiles in the film suggest diffusion of the drug through the polymer coating. This work connects manufacture parameters to device structure and *in vitro* performance. This information can be used to make better devices.

The research presented in this thesis leaves some questions unanswered. There are several lines of potential research arising from this work which should be pursued. These include:

- As mentioned previously sirolimus has a very low solubility in aqueous solutions, several stabilisation studies of the formulations should be considered. Moreover, using different release media, like cell culture medium to understand its effect on the release profile in contrast to PBS.
- Study the uptake of sirolimus, the effect of pH and temperature on the degradation behaviour of the scaffold. The degradation of the polymer is potentially highly dependent on the temperature especially when the temperature is higher than the Tg of the polymer-drug mixture. In terms of drug release and maintaining the homogeneous local drug concentrations in the tissue, is to release different amounts of a drug. This approach relays on the coating thickness of the struts. In theory, different drug release profiles can be achieved, by using different amount of a drug at different sites on the scaffold.
- The mechanical properties of the device could be investigated in more depth, by using sensitive force-sensing probes. In addition, Nano/micro scratch testing is a

possibility to study the mechanical property of the device[262]. Some of the commercially available testing tools that might be useful to consider in the future include, Electroforce® DES test instrument. 12 samples can be instantaneously analysed using such technology, with pulsatile expansion and particle capture technology to show any flaking and cracking of the coating layer during simulated use over test periods up to ten years simulated life time.

- Sterilisation of the device is a crucial aspect that need to be considered before supplying the device to patients. The work I have carried out during this project did not involve aseptic conditions of the device. Therefore, this is something that should taking into account for future work. Few researchers[262] have addressed the problem with sterilisation, as certain components of the product might be changed with by the sterilisation process. Therefore, it's essential to have a full understanding of the characterisation method to keep the product unchanged during sterilisation testing. Techniques such as nuclear magnetic resonance (NMR) or HPLC can be used to determine if the sterilisation process has altered the property of the drug after extraction.
- Shelf life is an important parameter that should be considered. Shelf life studies test drug and formulation stability. The device should be tested against its release specification to make sure it still continues to do its job as predicted. Extracting the drug from the coating layer of the device could be done by a validated method such as HPLC and to ensure that the drug has not undergone any degradation.
- Shipping studies are also required for the evaluation of the device. Humidity and temperature should be considered during shipping and consideration should be paid to the integrity of the packaging.

APPENDIX A: SEM

PLLA is considered a brittle material but does not fracture during crimping. PLLA scaffolds were made by laser cutting away the wall of PLLA tubing into a mesh scaffold structure. SEM provided an identification of different features such as heat affected zones (HAZs) depending on the selected resolution. Blue arrows in Figure A.1 show molten areas due to laser cutting effect

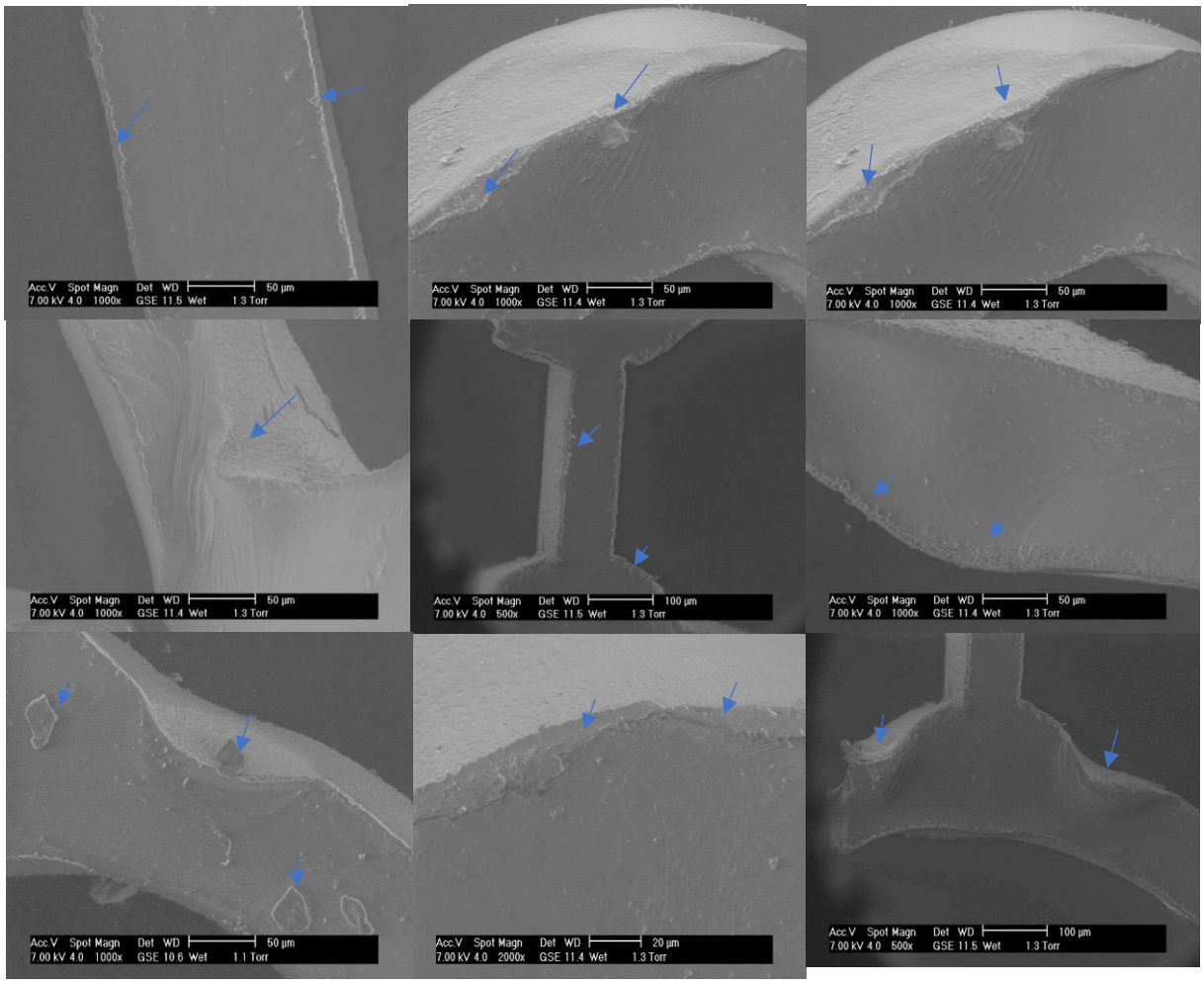


Figure A.1 SEM images of luminal surface of PLLA only scaffold using different laser cut methods. The use of femtosecond laser machining has been shown to reduce the size of HAZs, due to short beam/material interaction time. Blue arrows show heat affected zones.

Laser cut scaffolds were analysed on both sides, luminal and abluminal. SEM of crimped scaffolds in Figure A.1 show that melted zones are localised at the sidewall of the stent and occur at the inner bend causing the material to bulge out.

EDX analysis was occasionally used to provide basic elemental identification and quantitative compositional information of what is on the coating surface. For instance, the spectrum in the Figure A.2 shows elements such as Na and Si present on the surface of laser cut PLLA scaffold, which was in agreement with ToF-SIMS data as well as XPS. Although these elements are not part of the coating layer, but could have deposited on surface as a result of contamination during either sample preparation or due to being in contact with packaging bag that have been used to store samples in. Another assumption might be due to unclean lead end and exist end of the mandrel as well as die used in the die drawing process.

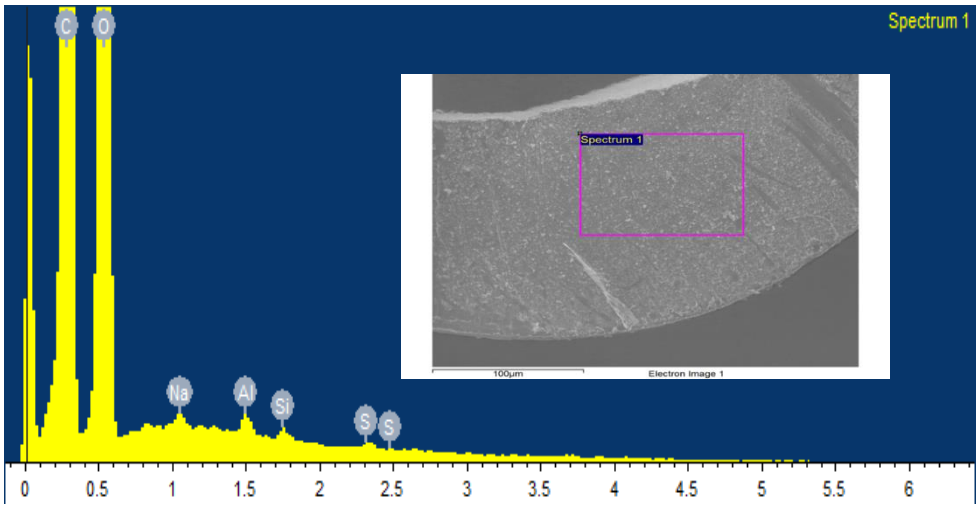


Figure A.2 EDX spectrum of luminal surface of laser cut PLLA scaffold, showing some elements such as Na and Al.

The EDX spectrum shows oxygen, carbon as expected but also Na, Al, Si and S. Presence of these elements could be due to contamination. The presence of PDMS could originate from the lubricant used during the manufacturing process. The coating surface of first generation of ArterioSorb^{TM} scaffold post *in vitro* dissolution testing was investigated by SEM. Initially the surface of these scaffolds was gold coated since PLLA is non-conductive. SEM images in Figure A.3 revealed a change in the surface

morphology as dissolution testing experiment proceeds. Although it is difficult to decide whether the coating that looks like it is flaking off is part of the gold sputtering or actual coating surface that has started to degrade. For this reason, it was decided it was better to image these samples using low vacuum SEM throughout the thesis.

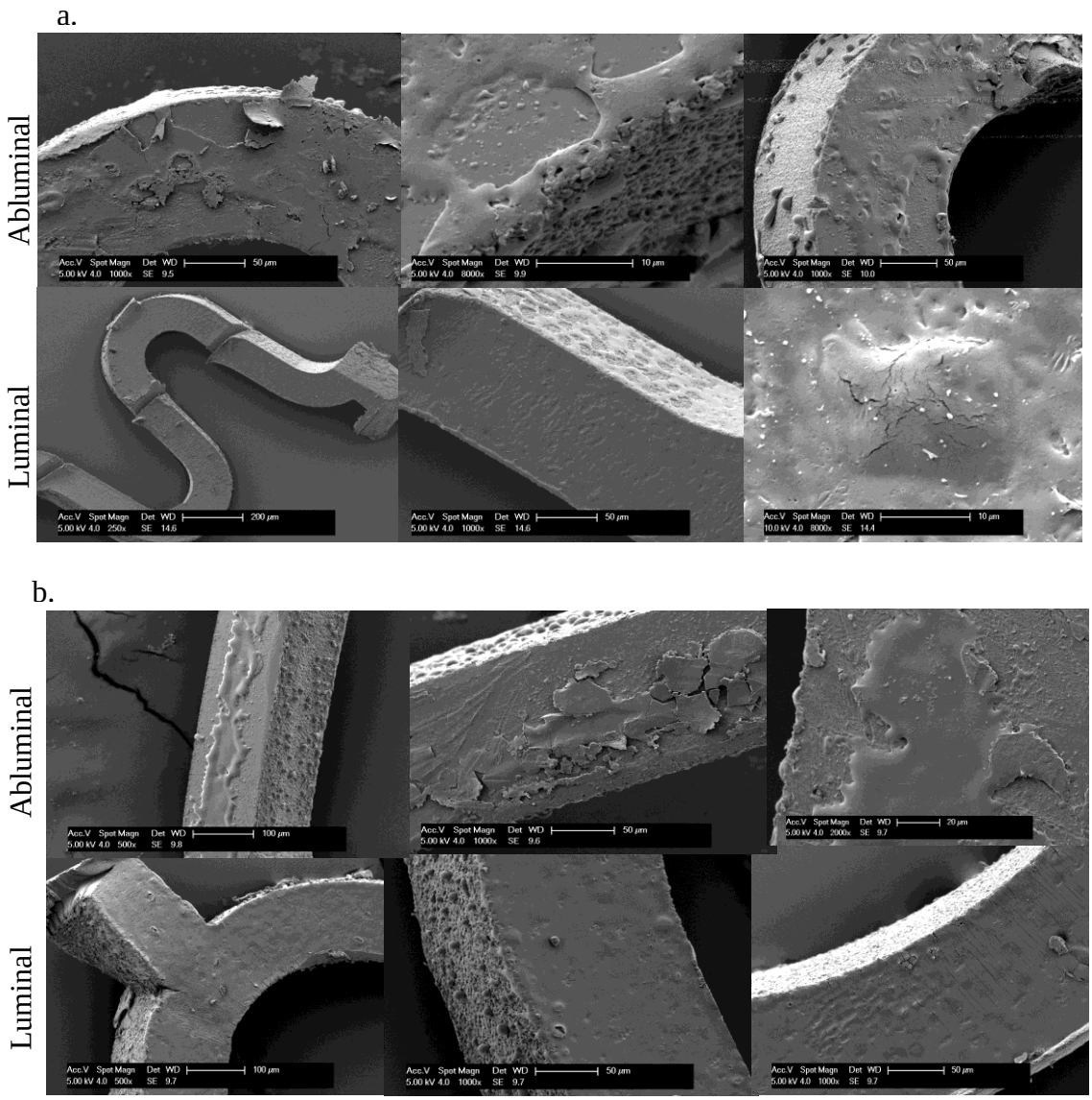


Figure A. 3 SEM images of dissoluted scaffold over 3 months in PBS. a. abluminal and luminal surface of ArterioSorb^{TM} scaffold suspended in PBS for 2 months, and b. abluminal and luminal surface of ArterioSorb^{TM} scaffold suspended in PBS for 3 months.

Scaffolds imaged in Figure A.3 were washed with water after being in PBS and left to dry at ambient condition overnight before analysis. Its hypothesis PBS droplets at the surface can crystallise to form surface features that look like the ones present in Figure A.3. The cracks on the surface of these scaffolds offer a way for diffusion of oligomers from the bulk of the polymer.

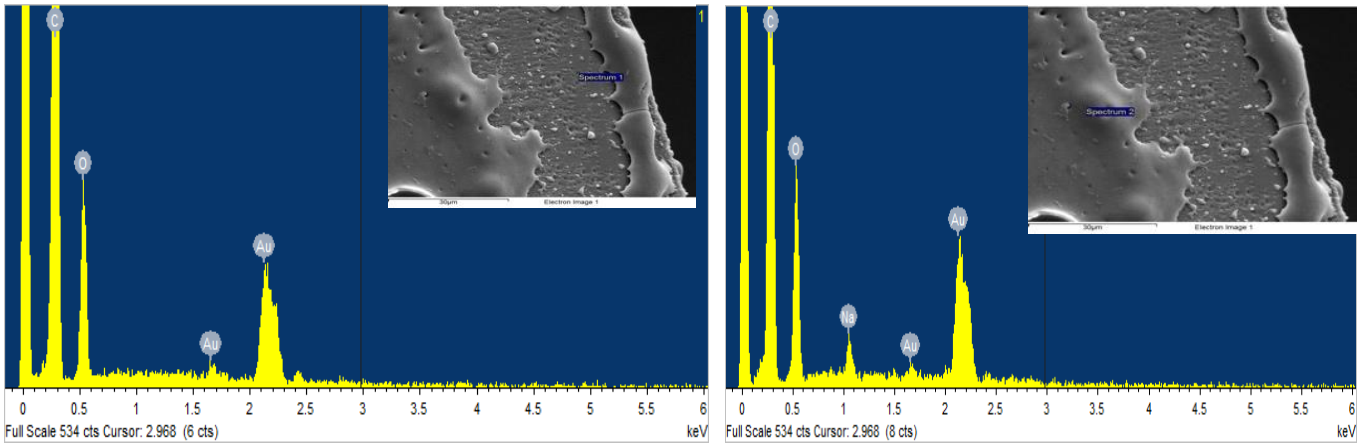


Figure A.4 EDX spectra of two areas on abluminal surface of ArterioSorb™ suspended in PBS for 2 months.

Figure A.4 show spectra of elements that present on the surface of the stent post elution.

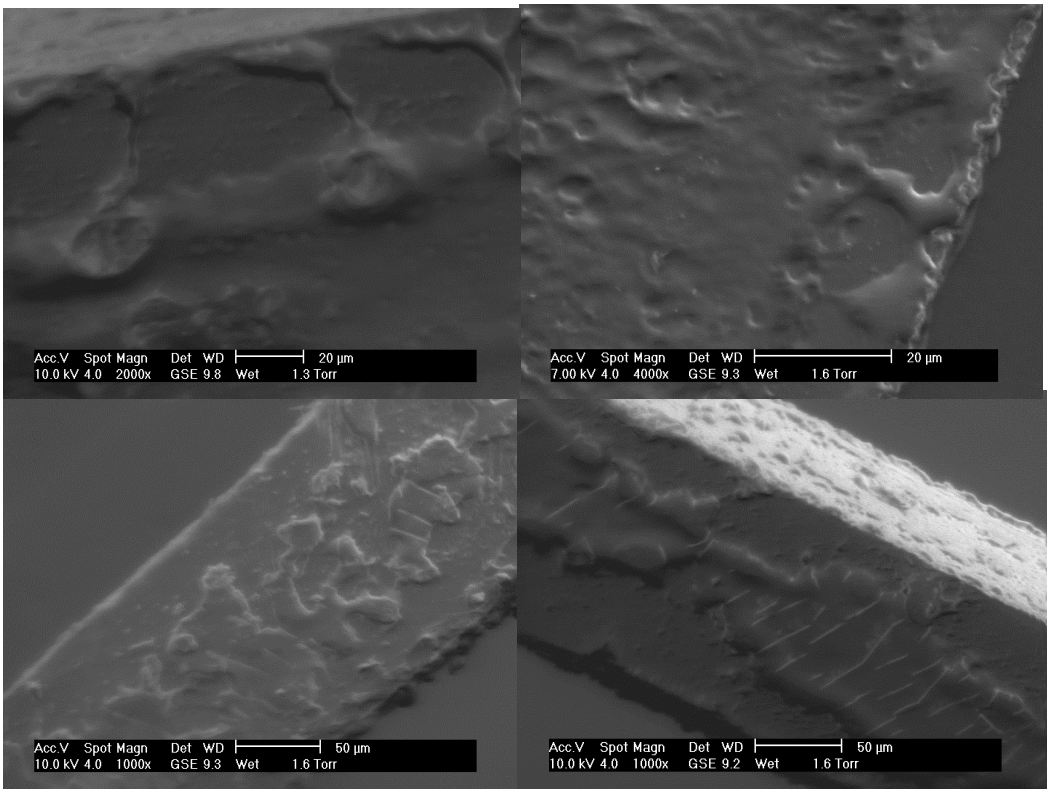


Figure A. 5 SEM images of abluminal surface of first generation ArterioSorb™ scaffold, suspended in PBS for 2 and 3 months, respectively. Analysis was carried out using low vacuum SEM.

SEM images in Figure A.5 of the abluminal side of the polymer coating following 2 and 3 months dissolution in PBS media (carried out by Arterius) revealed irregularities of the polymer in all scaffolds. The polymer coating displayed regions of uneven coating and polymer flaking, also coating cracking within the inner curvature and linker bards. These features were observed throughout the length of the scaffold.

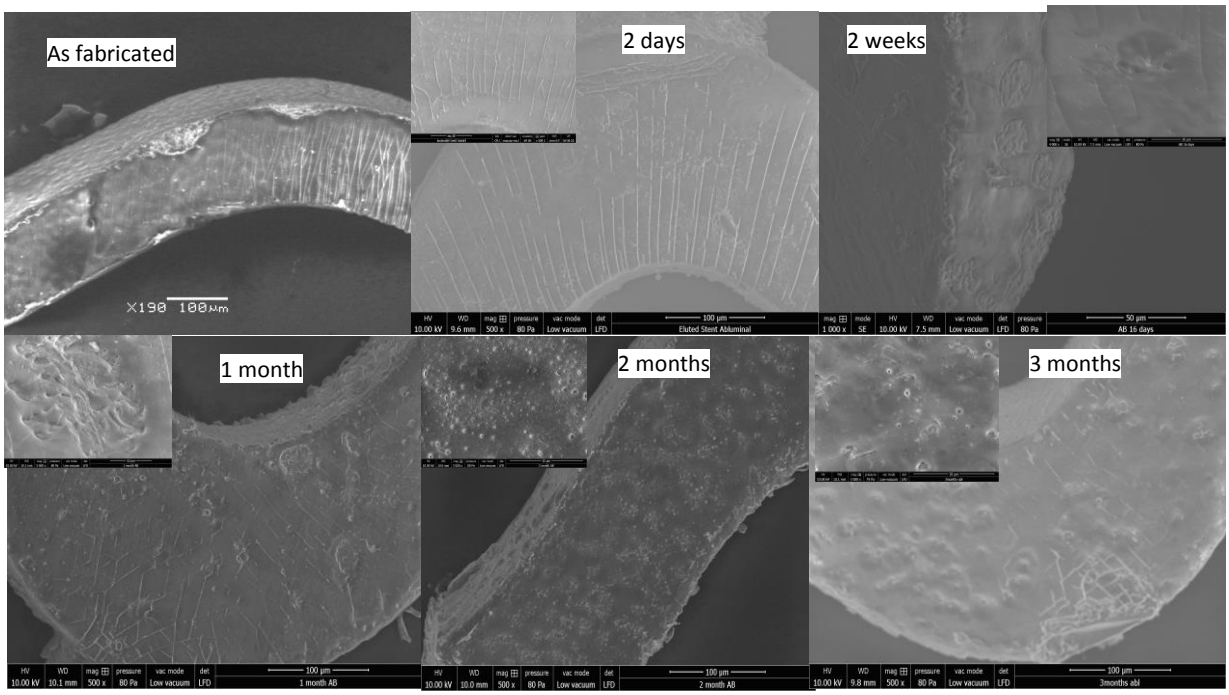


Figure A. 6 SEM images of abluminal surface of ArterioSorb™ scaffolds, suspended in PBS for 0, 2 days, 2 weeks, 1, 2 and 3 month(s), respectively. Analysis was carried out using low vacuum SEM.

APPENDIX B: AFM

Table B.1 The root mean square (RMS) roughness of the surface measured using AFM, data obtained from 5 measurements taken from abluminal surface of ArterioSorb scaffold.

Sample ID	Scan size	RMS
As fabricated stent	5 μm	120 nm
3 months in PBS	3 μm	60 nm

The roughness of the stent changes from one area to another due to loss of the drug domains, leading to the exposure of PLLA scaffold only.

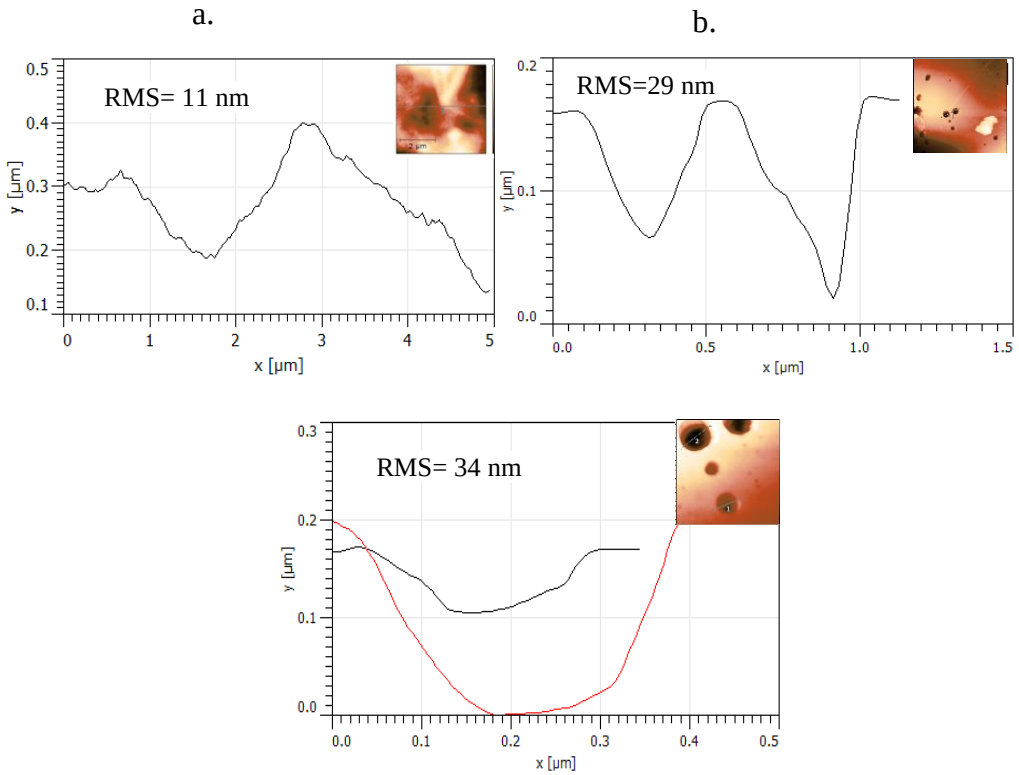


Figure B.1 AFM depth profiles of abluminal area of ArterioSorb a. as-fabricated, b.2 months and c zoomed in area into 2 months scaffold. Scan size for a and b of 5 x

5 μm and c. 3 x 3 μm.

Samples in PBS for 2 and 3 months were measured using the nanoIR2 system. The mechanical heterogeneity of the coating layer might be due to not enough drying of the coating or due to drying conditions that do not provide uniform and complete removal of the solvent. The drug peak in Figure B.2 is no longer present post elution.

Material	Structure	IR-Absorption CM^{-1}
$P_{DL}LA$	OH hydroxyl	3500
	CH_3	2945
	C=O	1756
	C-O	1300-1050
Sirolimus	C-H	2950
	C=N	1645-1717
	C-N	1636

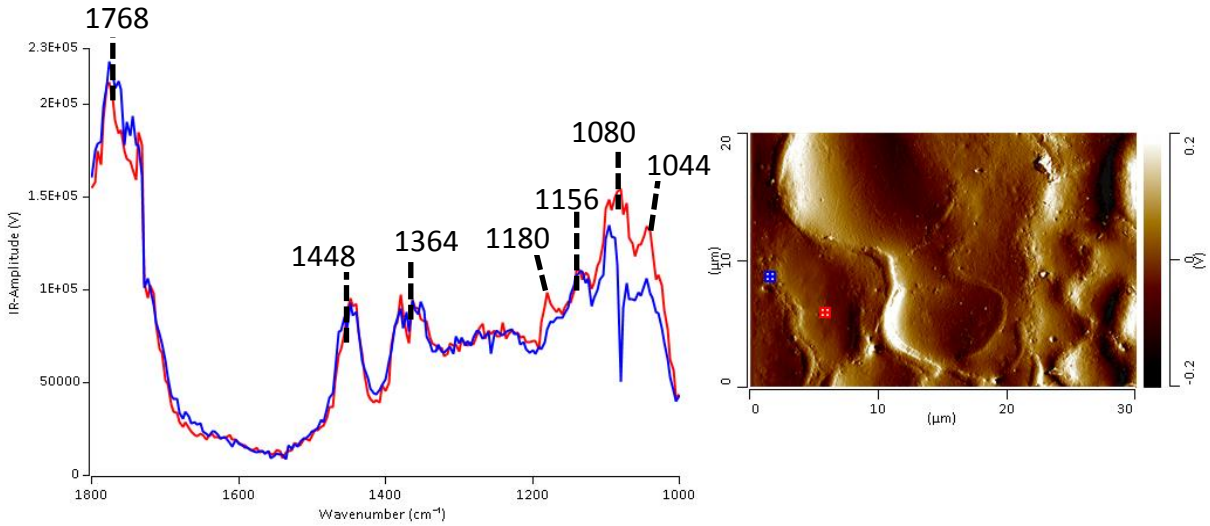


Figure B.2 AFM thermal analysis of abluminal surface of ArterioSorb™ post 2 months in PBS. AFM scan size 20 x 30 μm.

APPENDIX C: TOF-SIMS

ToF-SIMS provides molecular information from the outermost atomic layer of material providing an understanding of changes in the surface chemistry of the interfaces.

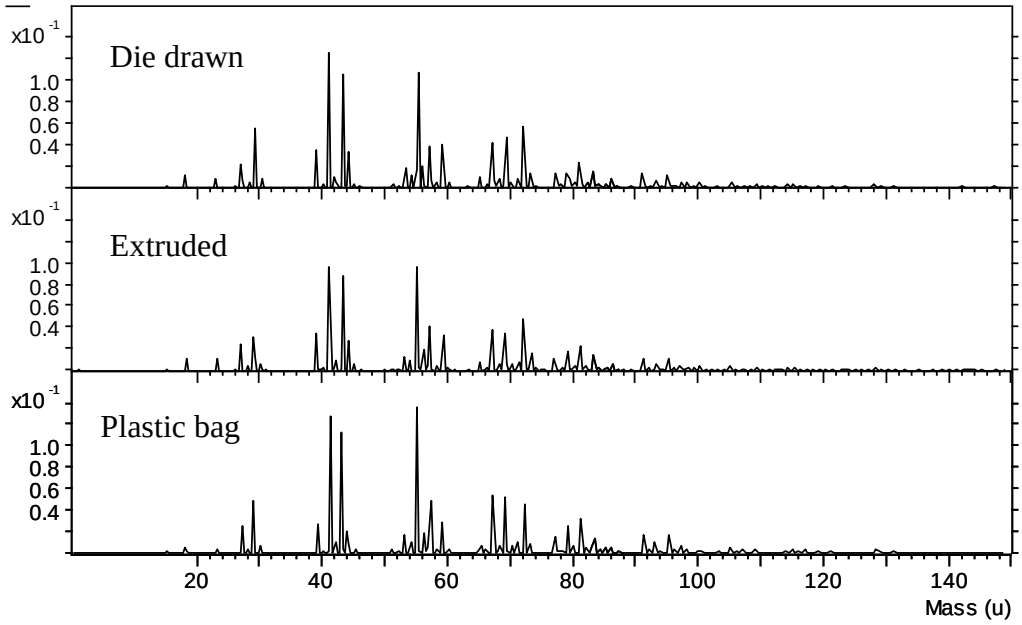


Figure C.1 ToF-SIMS spectra in positive polarity of die-drawn, extruded tubings and plastic bag, respectively.

In Figure C.1 the spectra of the abluminal areas show main characteristic ion markers of the polymer and plastic bag used to store samples in. There is not much of a difference between die-drawn PLLA tubing and extruded sample. It is clearly evident from Figure C.1 that the spectra reveal very similar chemical compositions in the extruded and die drawn tubing. In contrast, the spectrum of the plastic bag shows contribution of of sodium at m/z 24. This peak suggests the presence of sodium on the surface of the scaffold.

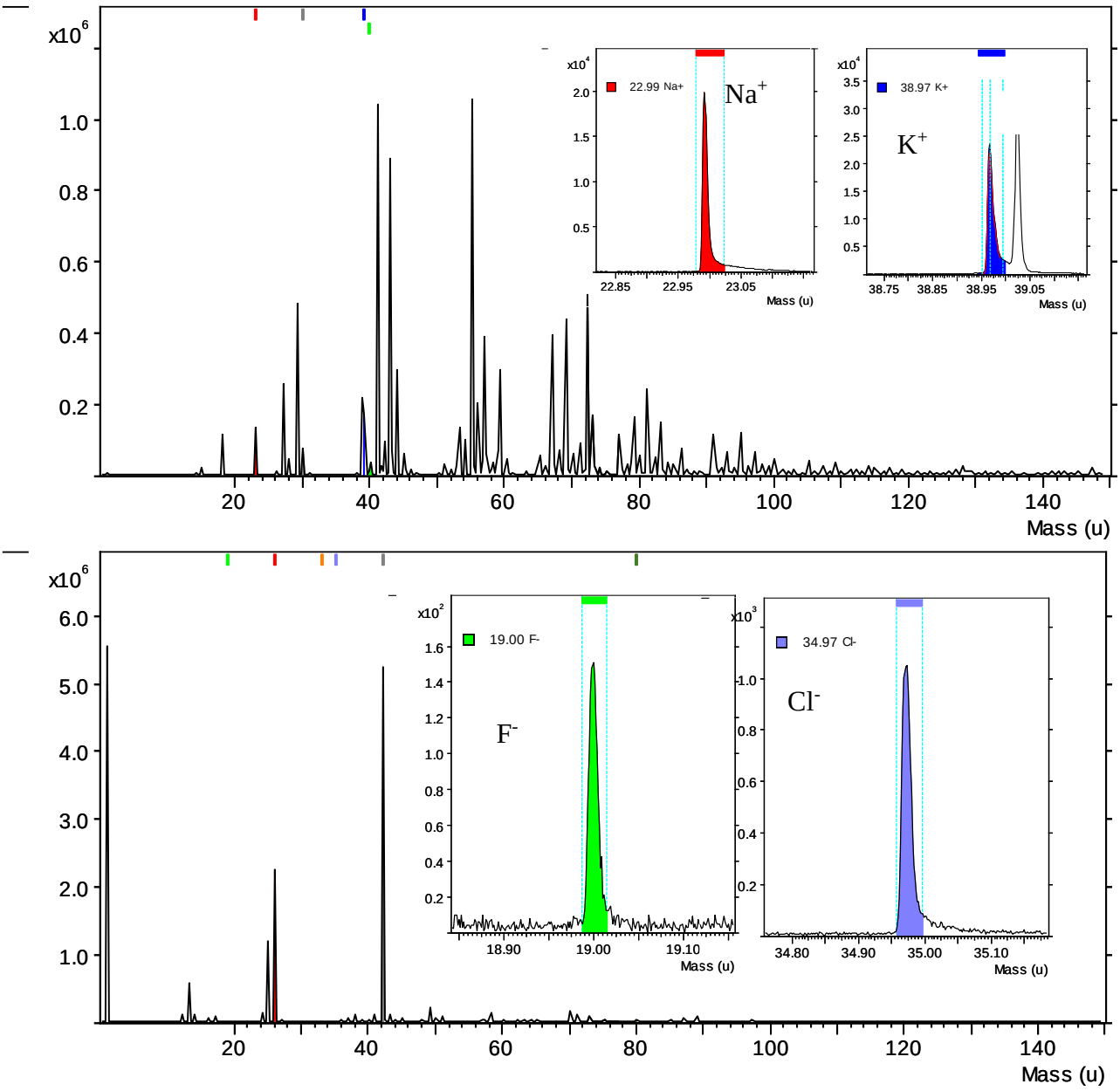


Figure C.2 ToF-SIMS spectra of abluminal surface of extruded PLLA tubing in the positive and negative polarity, prior depth profiling.

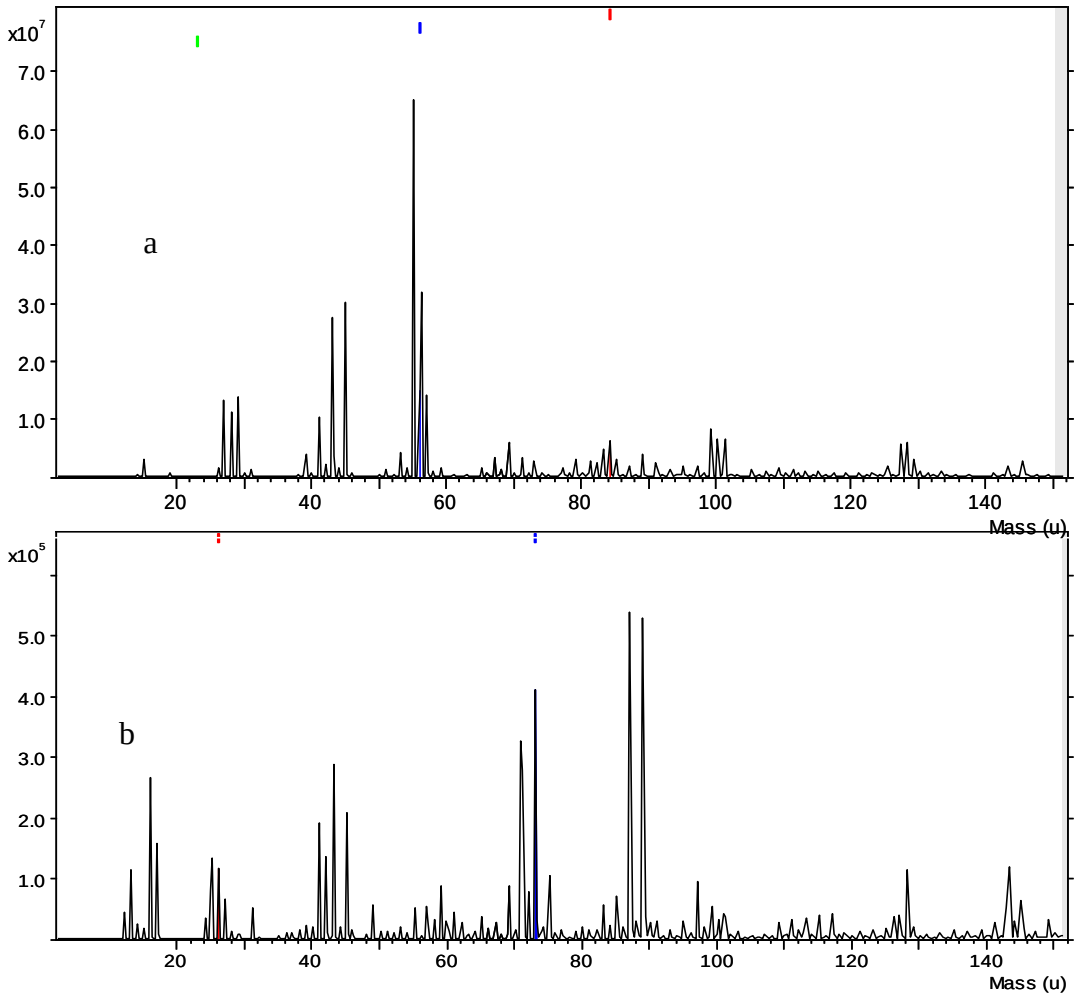
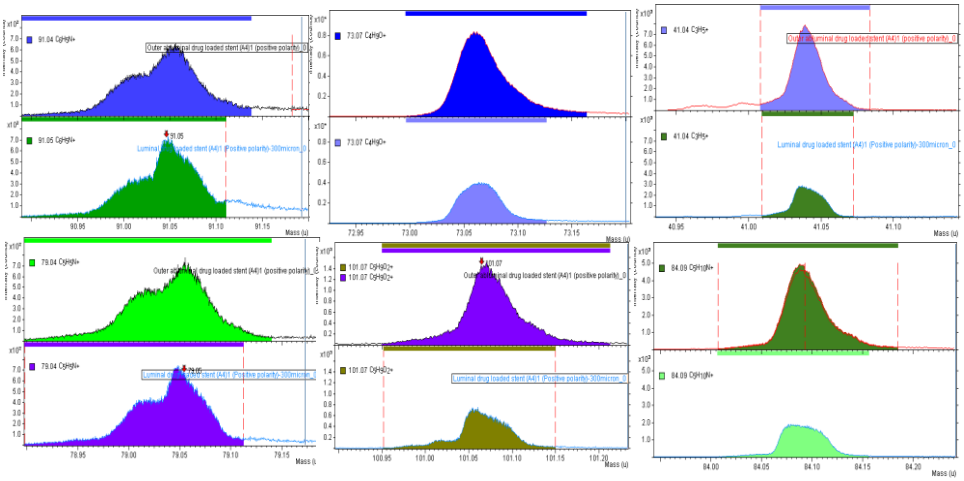


Figure C.3 ToF-SIMS spectra in a. positive and b. negative polarity of abluminal surface of coating layer in scaffold as received.

Positive and negative polarities were collected on ArterioSorb™ scaffolds. However, the work was mainly focused on positive polarity. Negative polarity was recorded to check for other ions such as sulphur or chlorine.

Drug



Polymer

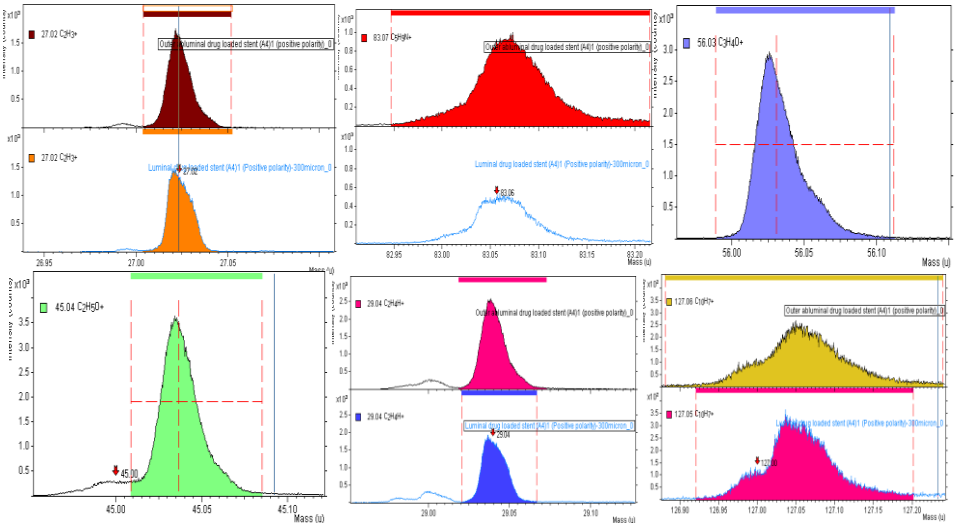


Figure C.4 Identified Characteristic peaks of the drug and the polymer on the abluminal and luminal surface of ArterioSorb™ scaffolds using ToF-SIM. Selected secondary ion intensities were acquired in the positive polarity. Peaks of the drug are 91, 79, 101, 73, 41 and 84 m/z and of polymer are 27, 29, 45, 56, 127 m/z).

Figure C.4 shows some mass ions that are characteristics of polymer and drug. However, in this thesis, we used the peak at 84 m/z ($C_5H_{10}N^+$) for sirolimus and the peak at 56 m/z ($C_3H_4O_2^+$) for the polymer to investigate the distribution of the drug in the coating layer of the ArterioSorb™ scaffold. These peaks have the best signal-to-background with which to achieve high contrast imaging.

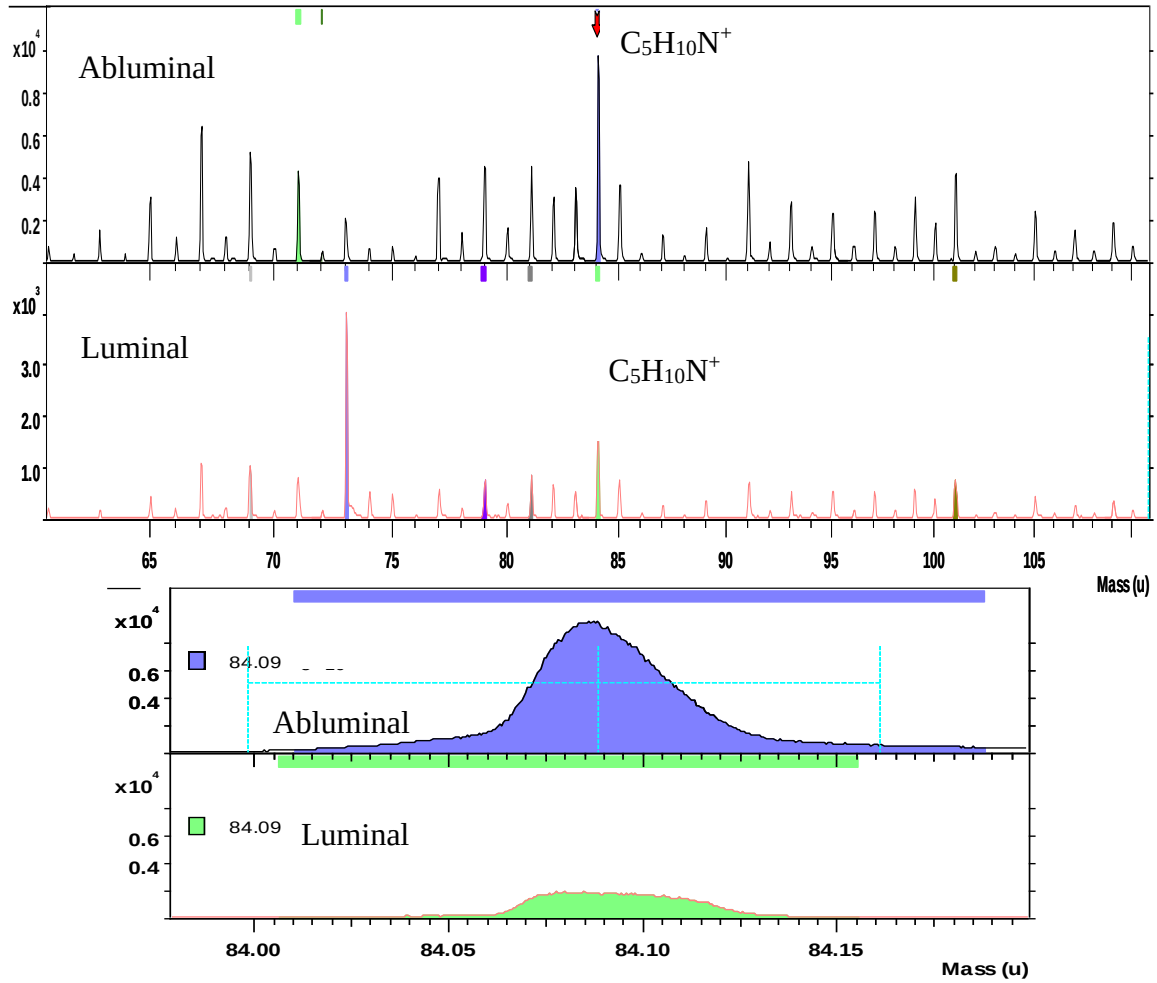


Figure C.5 High mass resolution positive ion spectra from selected region of the abluminal/luminal surface of sirolimus in PDLLA polymeric scaffold. Showing abluminal and luminal presence of sirolimus at 84 m/z.

The intensity of the drug in Figure C.5 appears high on the abluminal side of the scaffold as compared to the luminal. This finding bears a close resemblance to what has been reported by Arterius Ltd, in that the coating layer on the abluminal surface was approximately 15 μm compared to the luminal side of the stent.

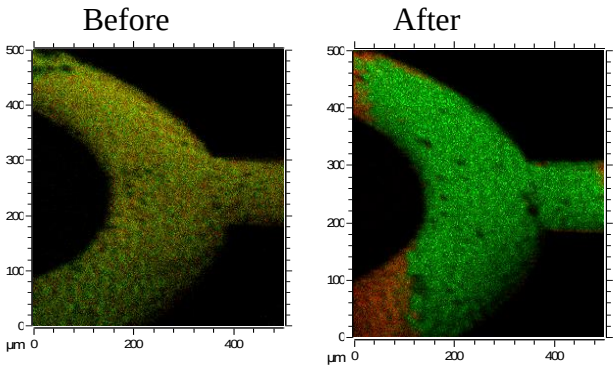


Figure C.6 ToF-SIMS 2D images in positive polarity of abluminal surface of as received scaffold pre-depth profiling versus post depth profiling. The overlay colour represents the polymer in green, and the drug in red.

Images in Figure C.6 demonstrated that ion beam alignment was maintained post depth profiling.

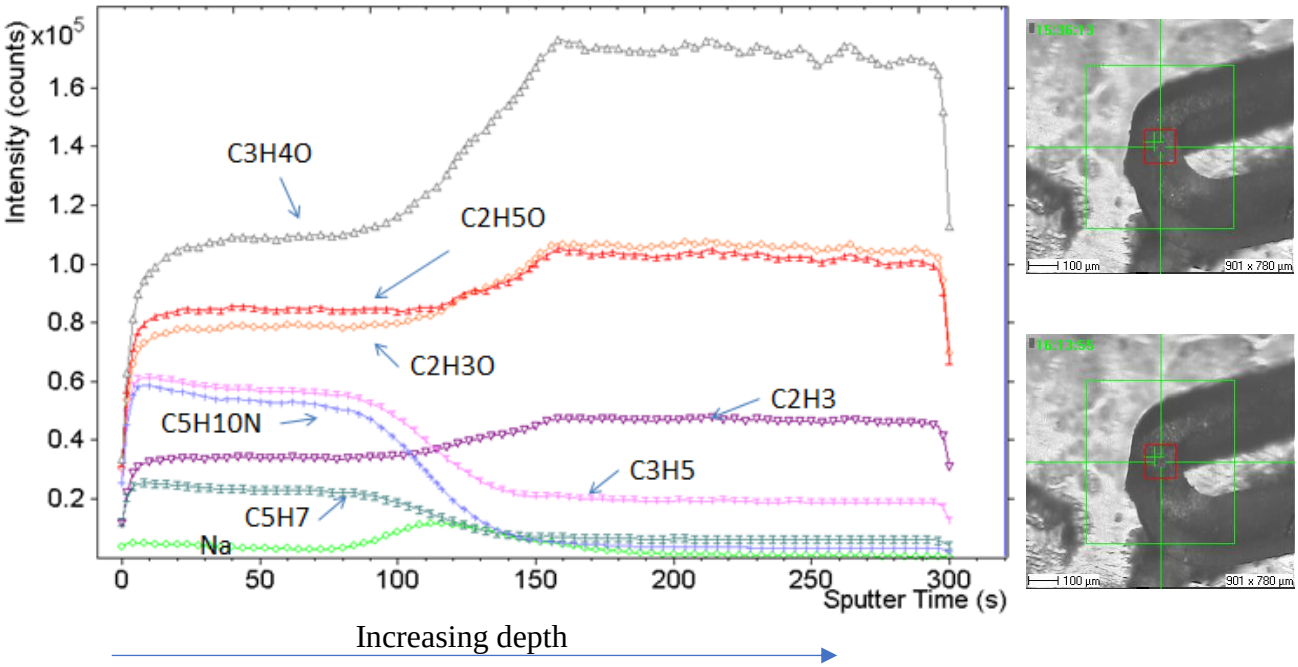


Figure C.7 ToF-SIMS depth profile of abluminal surface of ArterioSorb™ pre-dissolution showing some of the potential secondary ion intensities plotted as a

function of depth.

From the plot in Figure C.7 we can conclude that, the ion markers for the polymer and drug behave similarly, although seem to have a higher sensitivity. Also, one can establish the thickness of the drug overlayer and relate it to the performance characteristic of the device. Drug ions appear to be enriched at the surface then start to deplete gradually as a function of time, whereas the polymer ions follow the same opposing trend. Sodium appears to be at the interface. In summary, distinctive characteristic peaks such as Na^+, $C_5H_{10}N^+$ and $C_3H_4O^+$ were used throughout this thesis. The depth profiles were divided into 4 areas: surface, bulk, interface and substrate (the scaffold-PLLA).

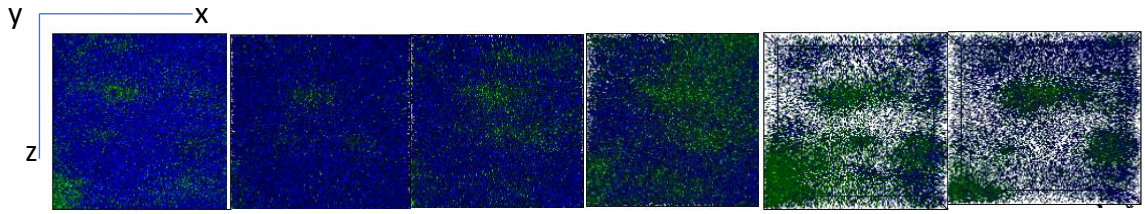


Figure C.8 ToF-SIMS 2D images of abluminal surface of ArterioSorb™ as function of depth of selected markers of the drug and sodium. Positive secondary ion polarity distribution of sirolimus (blue) and sodium (green) at depth intervals 400 nm.

Lateral distribution of sirolimus is visualised in Figure C.8 via 2D images at depth. To understand the spatial distribution of the ions in 3D, ToF-SIMS data was reconstructed as XY image taken at different depth intervals. Selected secondary ions in the X Y plane taken at regular data point intervals for the abluminal side of the stent. The surface appears to be composed mostly of the drug (blue), whilst the underlying layer at the interface is composed of sodium (green) as shown in Figure C.8. The drug is observed to be relatively enriched at the surface of the coating layer then decreases gradually as a function of depth, whereas the intensity of Na decreases gradually as a function of depth

The depth profile was carried out on different portions of the sample.

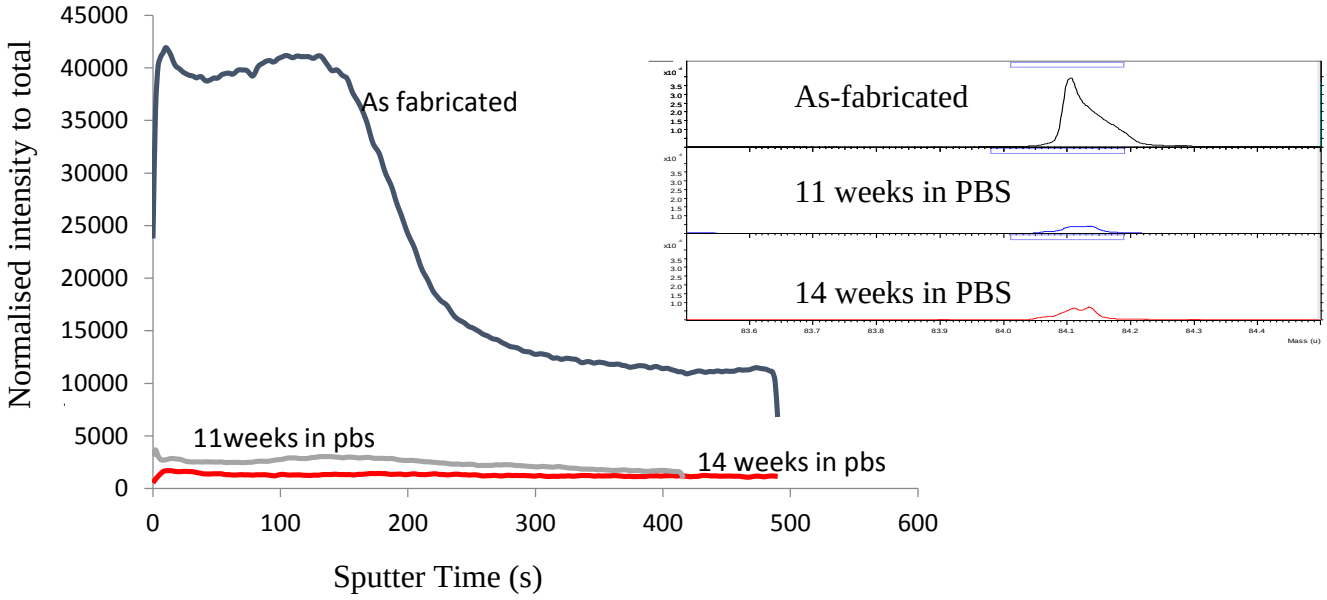


Figure C.9 ToF-SIMS depth profile of ArterioSorb scaffolds (first generation) as a function of elution time, using $C60^{++}$. Dissolution testing was carried out by Arterius Ltd.

The embedded spectra show characteristic fragment of the drug at 84 m/z as a function of elution time. Increased secondary ion intensity yield was much more noticeable in the data obtained by Ar cluster ion beam as compared to the depth profile obtained by the use of $C60^{++}$.

3D images were constructed from the raw data files in order to understand the spatial distribution of the ions and relate the structure to the release characteristics. It is observed that the surface is mainly composed of the drug and the underlying layers show increasingly polymer rich regions until they cover the whole area which is supposed to be the scaffold (PLLA).

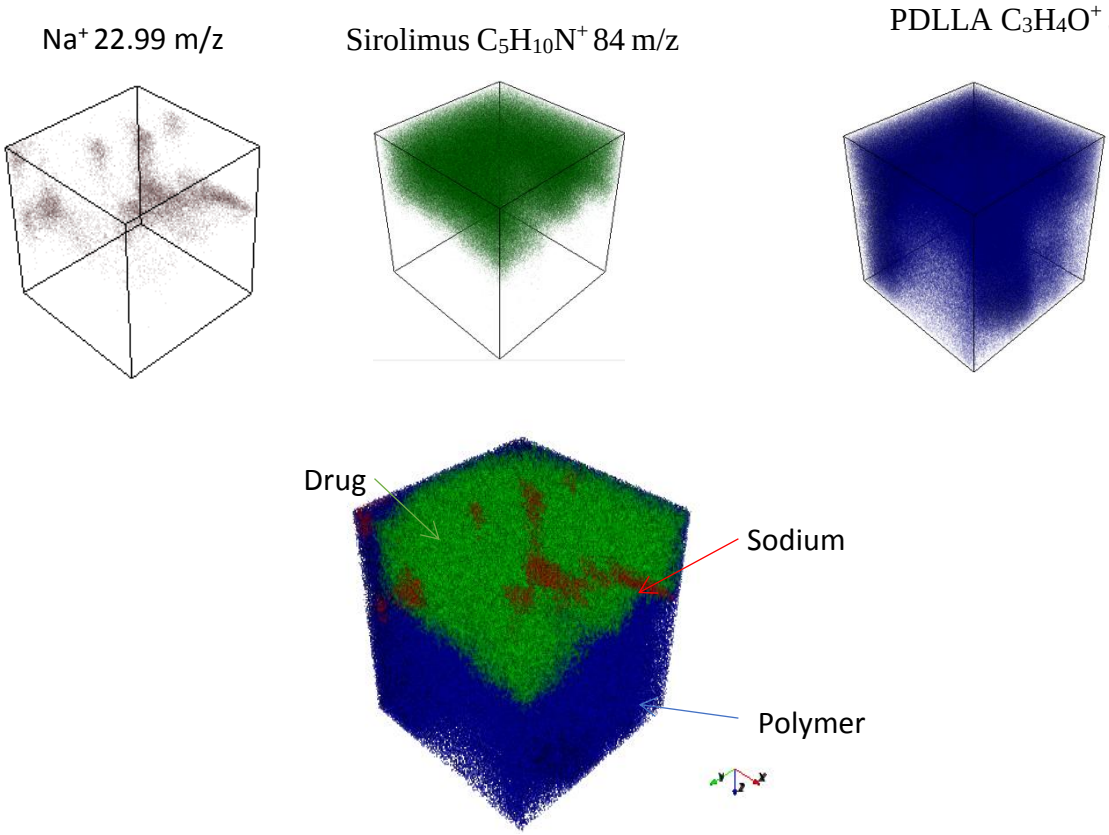


Figure C.10 ToF-SIMS 3D image of abluminal surface of as-fabricated scaffold using $C60^{++}$.

ToF-SIMS images of abluminal region of drug coated scaffold in Figure C.10 show the drug homogenously distributed and polymer distributed throughout the drug as expected.

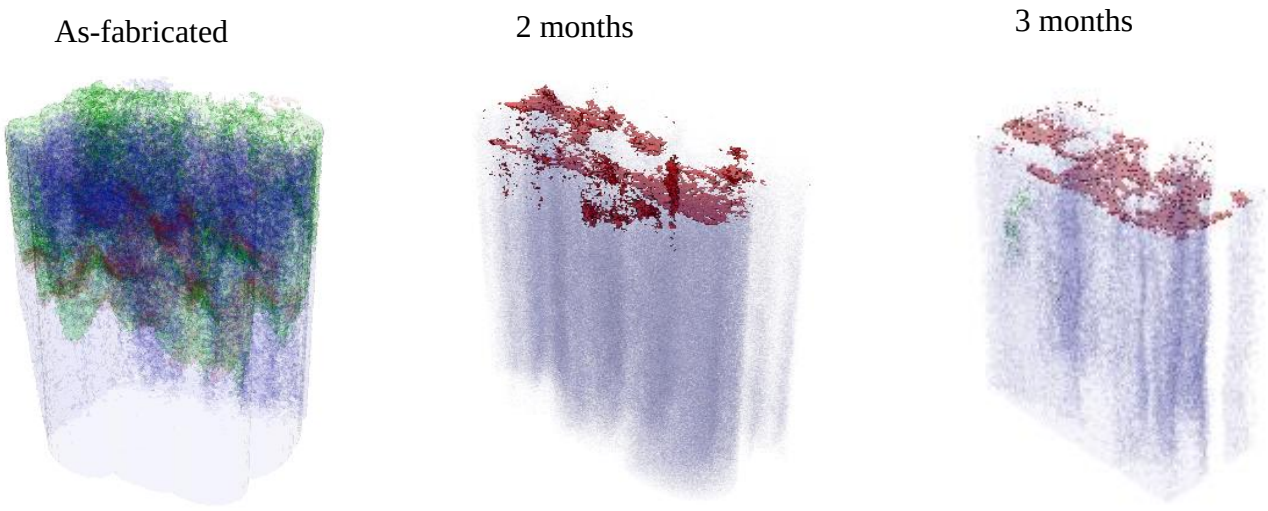


Figure C.11 A set of 3D images taken from an abluminal area of control and dissoluted samples at different time intervals, constructed from the 2D images at each cycle of the positive polarity depth profile, are rendered. The 3D images are iso-surface overlay of the sirolimus (red), and $C_3H_4O^+$ (dark blue) and Na^+ (green). These samples were eluted by Arterius Ltd.

The 3D spatial distribution of the drug obtained by ToF-SIMS quantitatively indicated a drug-enriched surface region followed by a drug-depletion region and finally a constant-composition region of PLLA substrate. Molecular depth-profiling using ToF-SIMS of coatings on scaffold was feasible and resulted in a 3D molecular compositional distribution of the drug within the coating polymeric film, as described above.

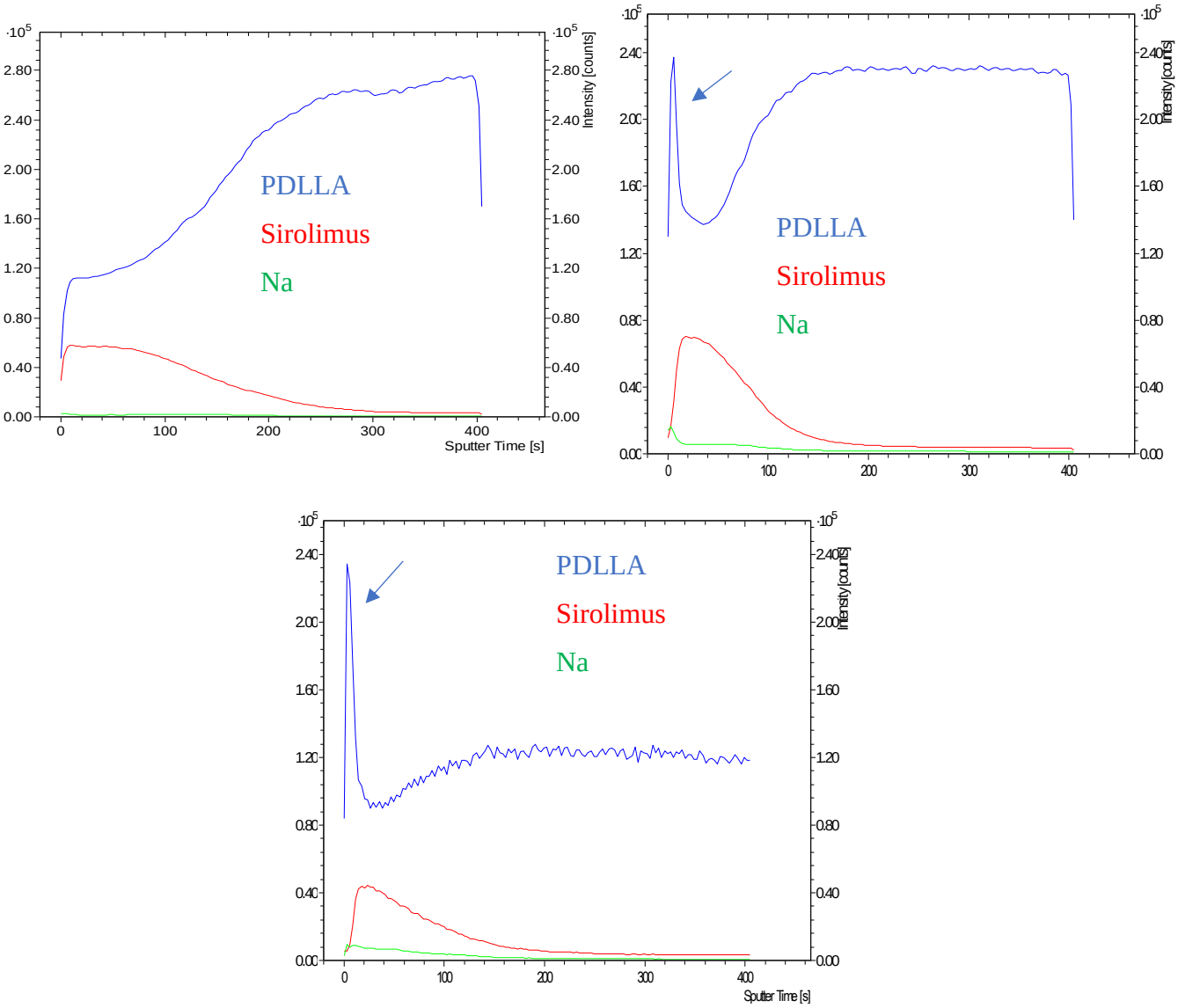


Figure C.12 Depth profile of luminal surface of as fabricated, 2 days and 16 days scaffolds suspended in PBS. Distribution of sirolimus (red) is heterogeneous on these samples.

The SIMS profiles for scaffolds exposed to PBS for 2 and 16 days suggest thin polymer coating at the surface, as indicated by blue arrows in Figure C.12

The coating layer on the sample is rather heterogeneous, therefore profile of sirolimus in PDLLA have different concentration gradients. Secondary ion intensities for 2 and 16 days suggestive of thin polymer coating at the surface.

Heat affected zones were also investigated by ToF-SIMS on laser cut bioresorbable scaffolds (uncoated).

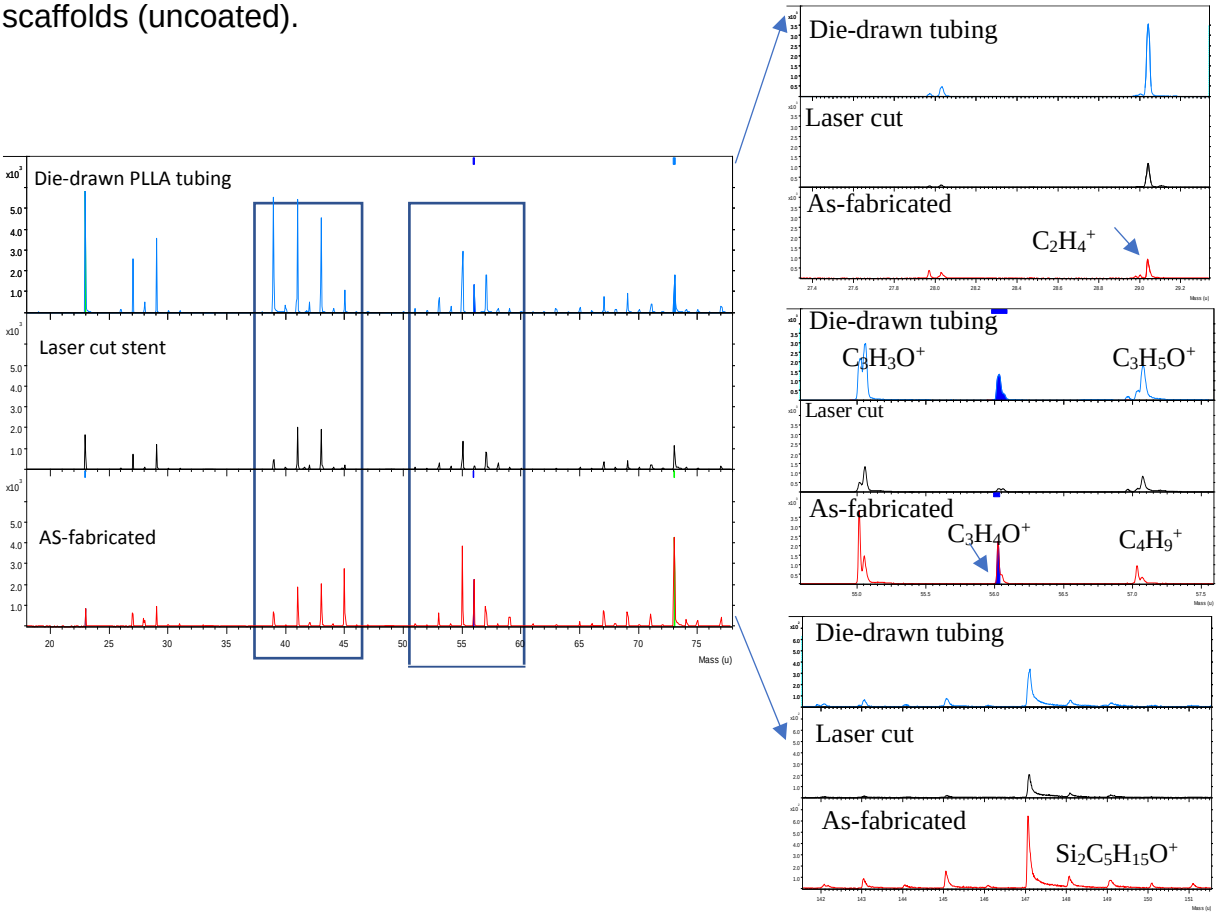


Figure C.13 ToF-SIMS spectra of heat affected zones versus non-laser cut PLLA tubing.

The differences between the abluminal areas of die-drawn tubing, laser-cut, and as-fabricated samples are highlighted in Figure C.13. increased magnification figure shows the presence of Si on the die-drawn PLLA tubing and as-fabricated stent and hydrocarbon peaks are much intense on the tubing which is characteristic of PLLA. The peak at 147 m/z suggests presence of PDMS on all analysed areas. PLLA related ions ($C_xH_yO_z^+$) are observed in all analysed areas in particular die-drawn PLLA tubing.

APPENDIX D: XPS

XPS was used to establish the elemental composition of the coating surface. It allowed us to investigate the elemental distribution as well as composition of polymer drug-containing layer through the depth. Different types of XPS instruments were used in this thesis, in the main body of my thesis we exploited Thetaprobe XPS in Chapter 4 and Kratos Axis ULTRA XPS in Chapter 5. Slight change in measurements were observed.

Heat affected zones were studied using Thetaprobe XPS (Nexus) on laser cut scaffolds (uncoated) of both abluminal and luminal sides.

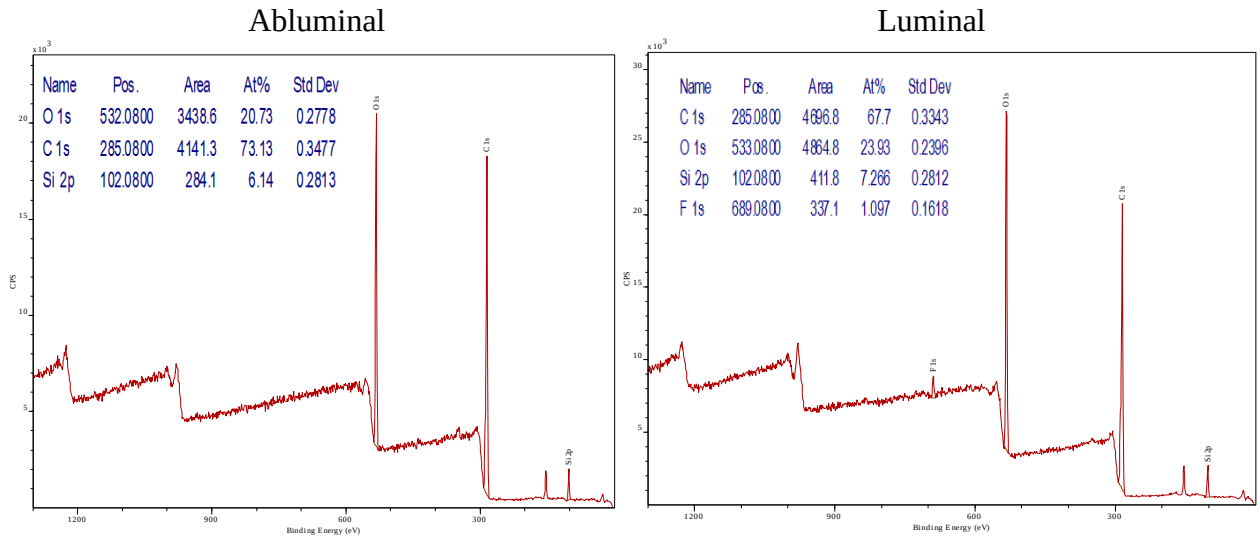


Figure D.1 Wide scan XPS spectra of abluminal and luminal surface of laser cut uncoated ArterioSorb.

XPS wide scan analysis of uncoated scaffold interestingly appears to be contaminated with silicon on both sides, although more pronounced on the luminal surface. Also, fluorine is on luminal surface of the scaffold. This might be due to contamination during sample mounting on double sided tape. Cross contamination from the residual of a previous extrusion and orientation run or even there might have been different processes being undertaken at the same time of extrusion/laser cutting process.

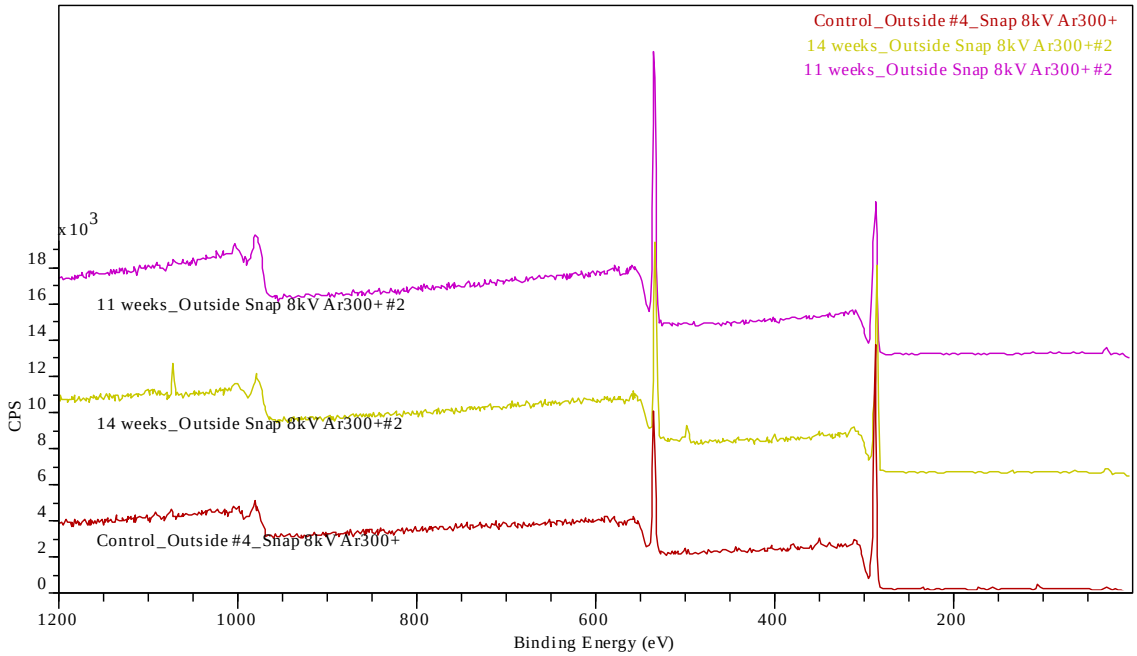


Figure D.2 Wide scan XPS spectra of abluminal surface of ArterioSorb as a function of elution time. Analysis was done on the ThetaProbe XPS (Nexus, University of Newcastle).

a. b.

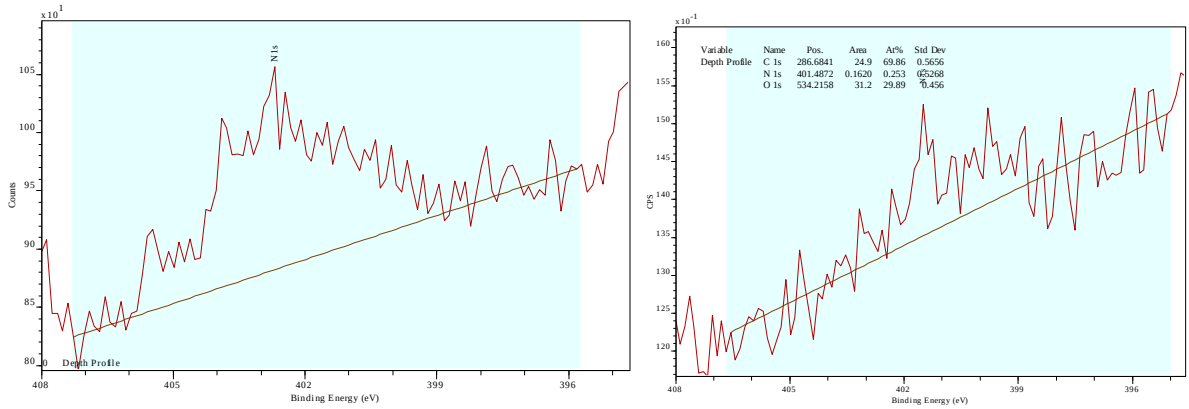


Figure D.3 High resolution spectra of characteristic element (N1s) present on the abluminal surface of ArterioSorb a.as fabricated, and b. 2 months in PBS.

XPS high resolution spectra in Figure D.3 show the elemental composition of the surface was C, N and O as expected for sirolimus and PDLLA and allowed a determination of their relative composition against design expectation.

Further analysis was carried out using XPS depth profile. The most striking observation in depth profile is variability of drug distribution. Bear in mind, integration of N1s peak is very difficult during this analysis. Data processing may vary from one user to another. Apart from this issue, the result in Figure D.4 has strengthened our findings that the distribution of the drug on coating surface is heterogeneous.

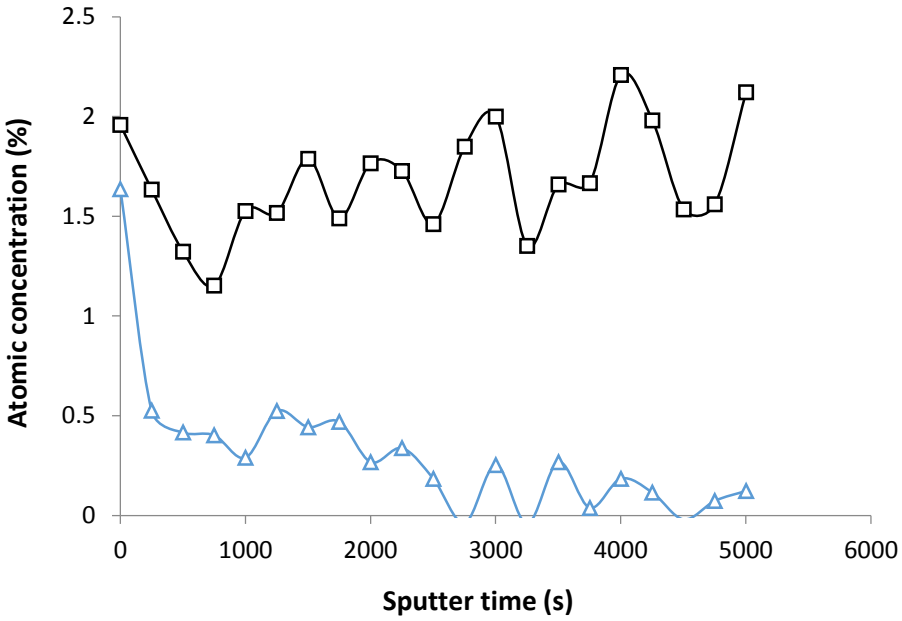


Figure D.4 XPS depth profile of abluminal surface of ArterioSorb™ as fabricated (black) versus 2 months in PBS (blue). The nitrogen observed to be reaching the detection of limit (0.14 %).

Depth profiles in Figure D.4 show obvious chemical heterogeneity of the polymer coating of ArterioSorb™. The spectra confirm the loss of drug concentration as function of elution time. The presence of carbon (C1s) and oxygen (O1s) was determined by the content of organic components - polymer coating and drug, the presence of nitrogen (N1s) was determined by the content of the drug substance (sirolimus), the presence of other elements as observed in Figure D.1 was determined by the composition of the substrate used for mounting sample on.

The depth profile of sodium was not monitored, as it was below the detection limit of XPS. The obtained data in Figure D.4 confirm the results of the SEM analysis of the non-

uniformity of the polymer coating. Another XPS experiment was carried on a Thermo Scientific K-Alpha XPS spectrometer. This work was done to evaluate if there is a difference in measurements between XPS instruments that have been used in the previous chapters. X-ray spot (analysis area) of nominally 300 x 150 micron was used in all the measurements. In order to check for the centred alignment for the X-ray spot a measurement was done on a phosphorous sample before the actual measurements on stents.

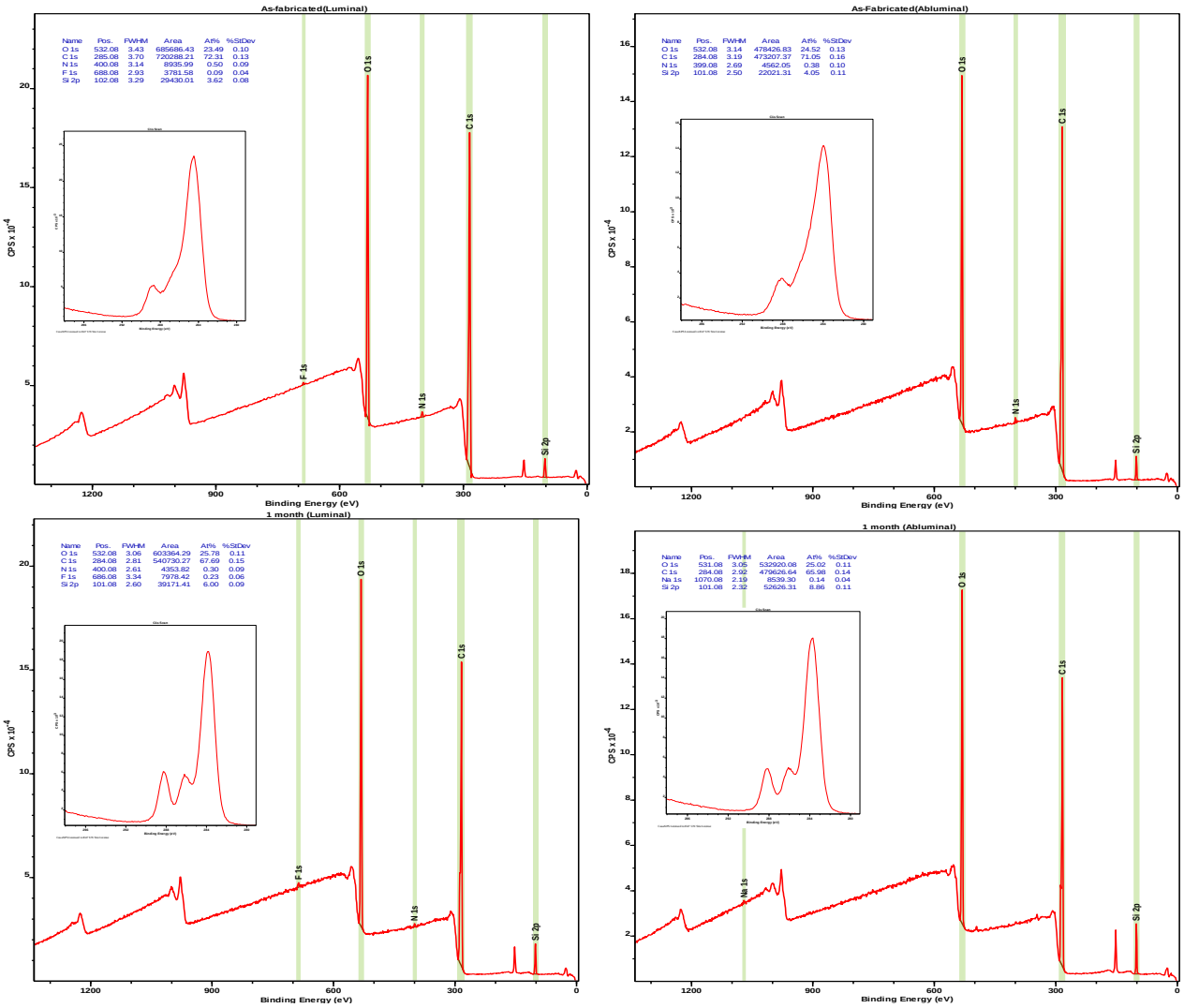


Figure D.6 Wide scan spectra of luminal and abluminal ArterioSorb™ scaffolds as a function of elution time. High-resolution spectra of C 1s region are embedded within each wide scan spectrum.

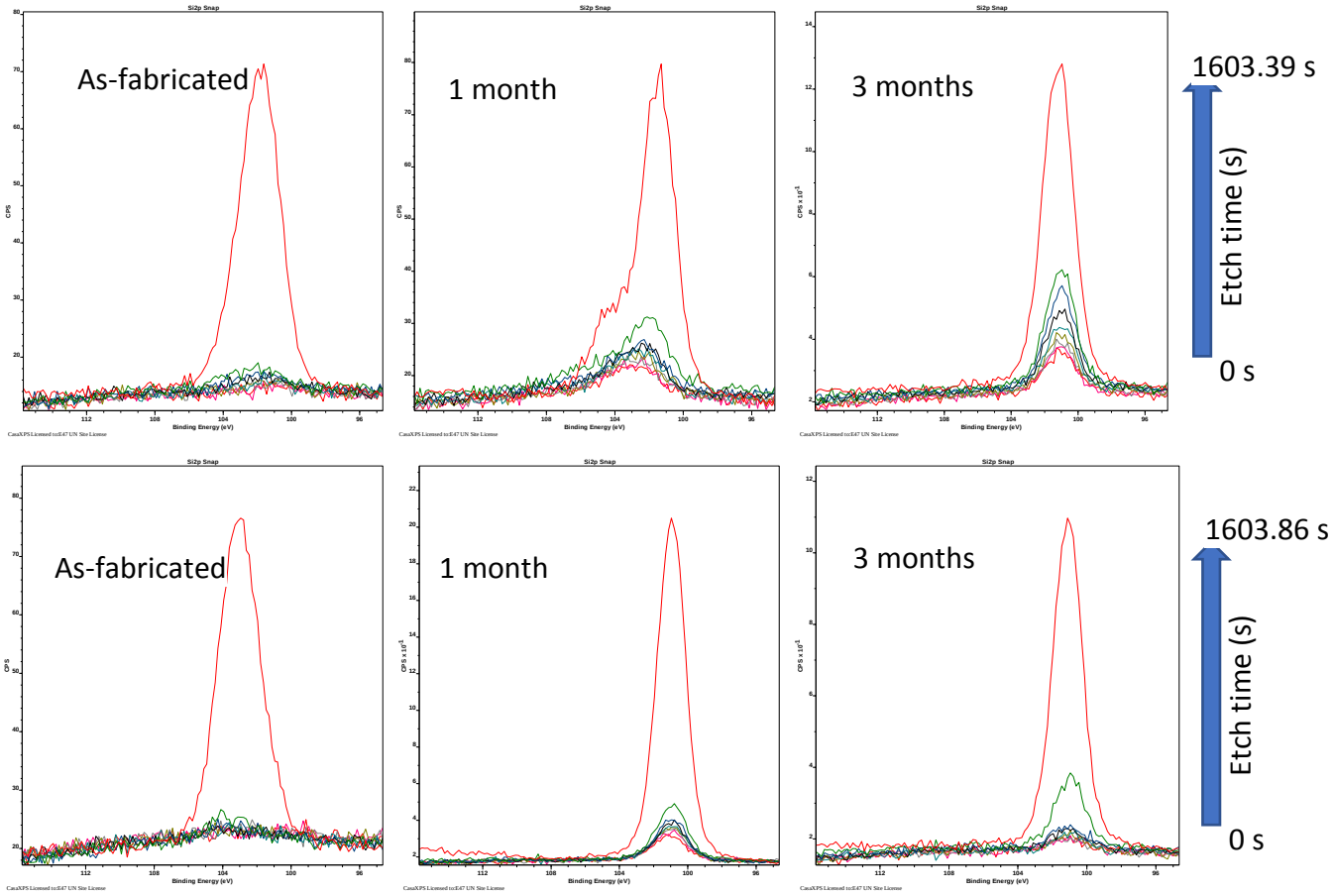
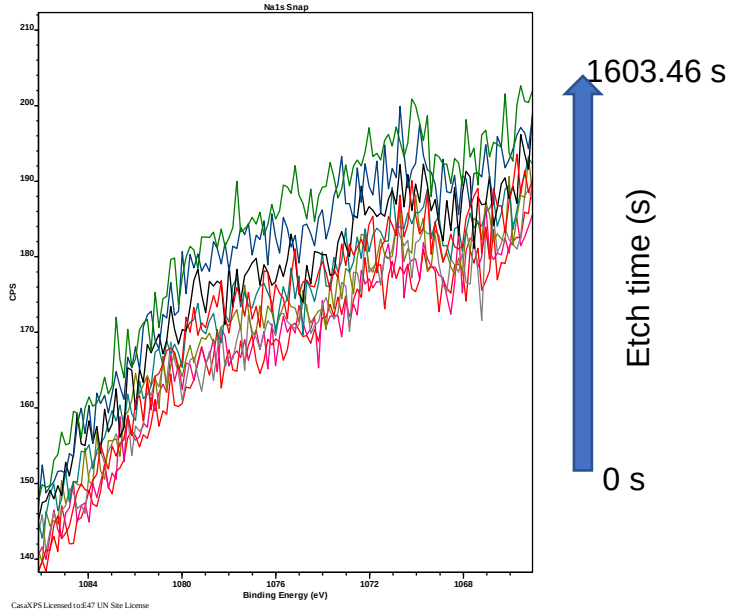


Figure D.7 High-resolution depth profile spectra of Si2p region for abluminal and luminal surface of Arteriosorb^{TM} scaffolds, as a function of elution time.

The findings in Figure D.7 indicate high level of Si 2p present on the surface and within the scaffold. The reason to this event is might be due to samples being left on carbon tape for over week or so before being analysed by Thermo Scientific K-Alpha XPS spectrometer (Nexus, Newcastle University).

a.



b.

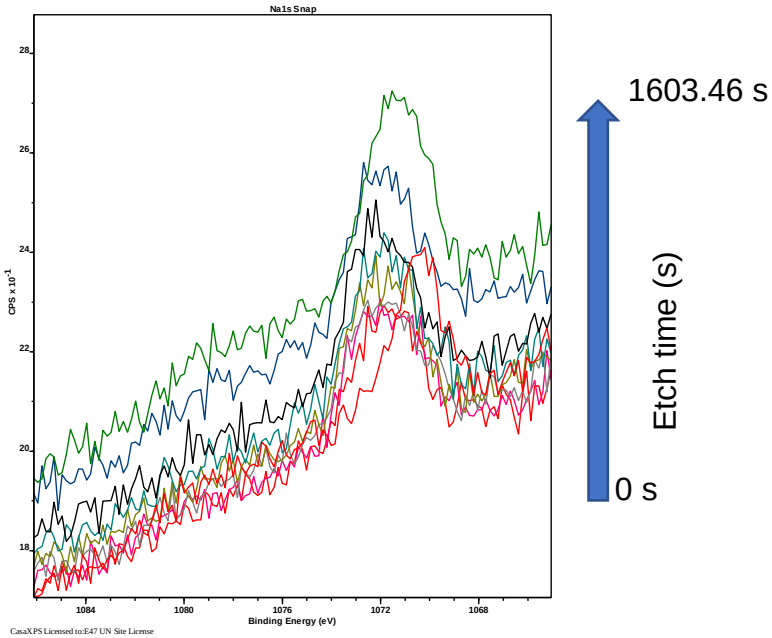


Figure D.8 High resolution depth profile spectra of Na 1s region for abluminal ArterioSorb™, a. as-fabricated and b. 1 month dissoluted.

APPENDIX E: DISSOLUTION TESTING

For drug-release testing, it is ideal that the medium mimics the in-use conditions as close as possible. Elution into water is of limited value and as a minimum, PBS was recommended by Arterius Ltd as it possesses a physiologically relevant concentration of ions. The drug release mechanism might be dependent upon ion-exchange processes. Ions and salts typically have low solubility in polymers. Consequently, ions such as H^+ and OH^- from elution testing solutions do not have major effects on the degradation of polymers as they do not migrate into the samples. However, if there are organic acids in the test media that can diffuse into the polymers, the degradation may be enhanced.

Different approaches were undertaken such as the use of the SOTAX USP4 flow-through cell to mimic the artery wall condition. This approach was particularly challenging as we were required to match dissolution condition Arterius had used for their dissolution testing on first generation scaffold. Small volume of PBS was not sufficient enough to carry out the experiment for a period of 3 months. Additives were needed to accelerate the release of the drug. In the literature, most researches had used a solvent (Dichloromethane) to enhance the release of the drug and large volume of media but that would defeat the objective of working under physiological condition. Some issues were associated with the use of the SOTAX USP4 flow-through cell, it is recommended to use a large volume of elution medium but even though the amount of the drug on the device is still considerably low, which had led to a difficulty detecting the amount of the drug release by HPLC. Drug eluting scaffolds are relatively expensive and due to the limited availability, it was difficult to use several of the scaffolds in order to find out which approach is most suitable for drug release. Hence the standard method developed in Arterius Ltd was employed. Therefore, a couple of scaffolds were suspended in small volume of elution medium (typically 3 mL) and the drug release in the medium was taken over time and analysed using UV-VIS.

The objective of different dissolution approaches is the use of a reproducible, robust and validated method. Thus, to compare dissolution profiles from different runs, mathematical treatment of the elution data should be considered. Figure E.1 illustrates the calibration curve was used to construct the release profile described in Chapter 5.

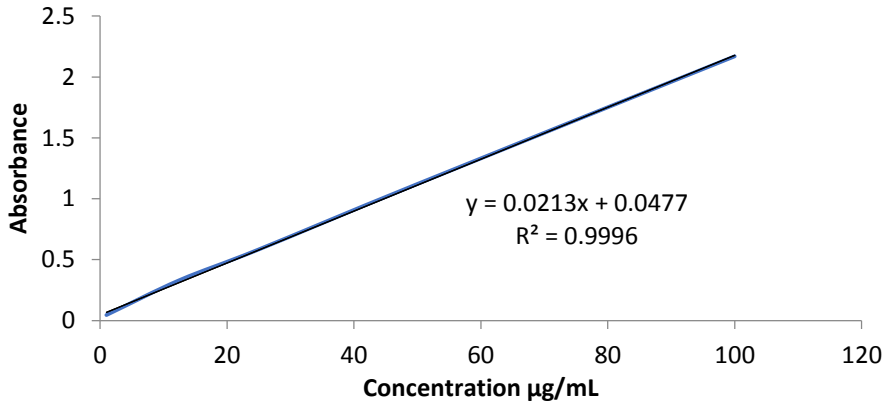


Figure E.1 Standard calibration curve

Using regression analysis, the following equation was obtained for sirolimus in methanol. Some preliminary work was carried out to look at the degradation of PLLA tubing only. The preliminary work was focused primarily on the mass loss of PLLA over time.

The difference factor (f1) determines the % difference between the two dissolution curves at each time point and is a measurement of the relative error between the two curves. Whereas, the similarity factor (f2) is a measurement of the similarity % in the two dissolution curves.

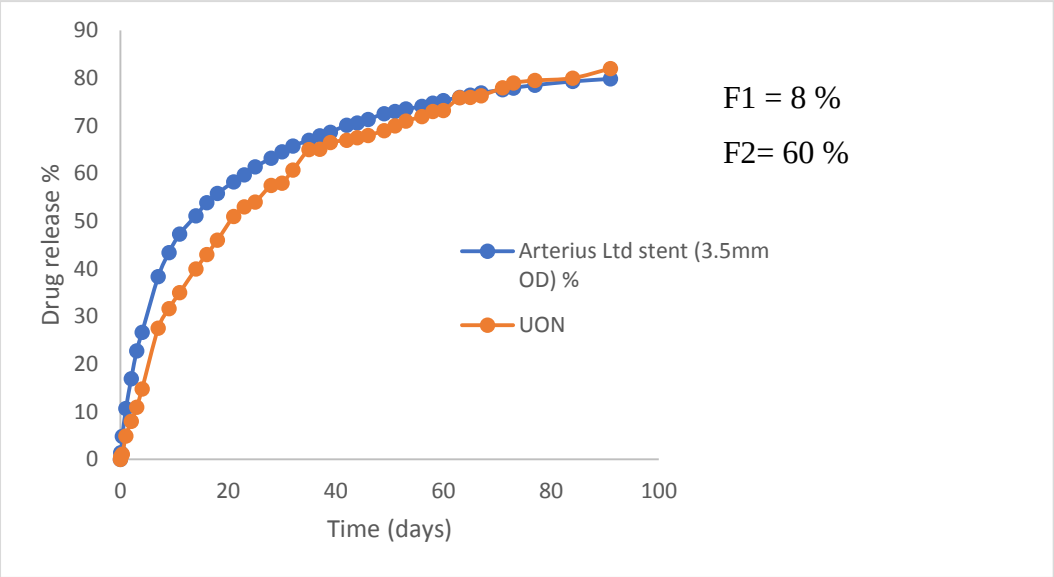


Figure E.2 Statistical Comparison of dissolution profiles of ArterioSorb™ stent exposed to PBS for over 3 months using similarity (F2) and difference factors (F1). Similarity factor = 60 % and difference factor = 8 %.

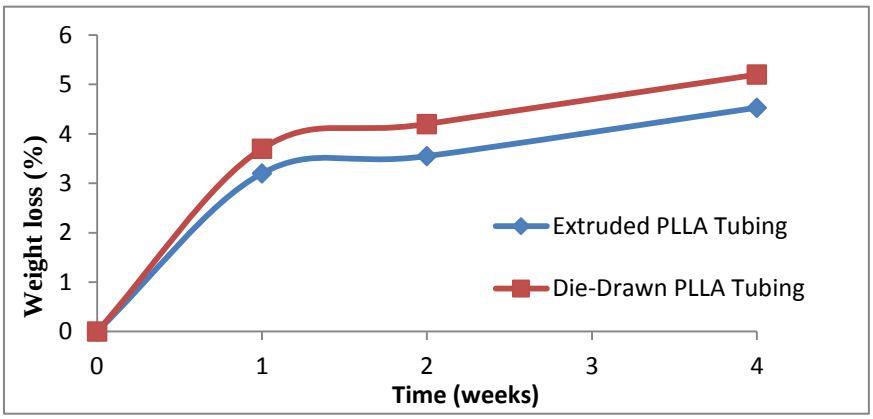


Figure E.3 Weight loss fraction of extruded and die-Drawn PLLA tubing during in vitro degradation for 4 weeks.

Our *in vitro* study of mass loss for PLLA tubing (extruded versus die-Drawn PLLA) showed some mass loss but not significant as it was only carried out for a short period of time. The results from the weight loss show that extruded PLLA tubing degrade more slowly than the die-Drawn PLLA tubing.

In conclusion, the morphology of the bioresorbable eluting scaffold (ArterioSorb) varies from one position to the next. Upon drying of the coating layer, sirolimus/PDLLA de-mixing occurs with preferential surface separation of the drug. The 3D spatial distribution of the drug in as-fabricated scaffolds obtained by ToF-SIMS indicates a drug-enriched surface region followed by a drug-depleted region and finally a constant-composition region of PLLA substrate.

APPENDIX F: CRIMPING AND EXPANSION BENCH TESTING

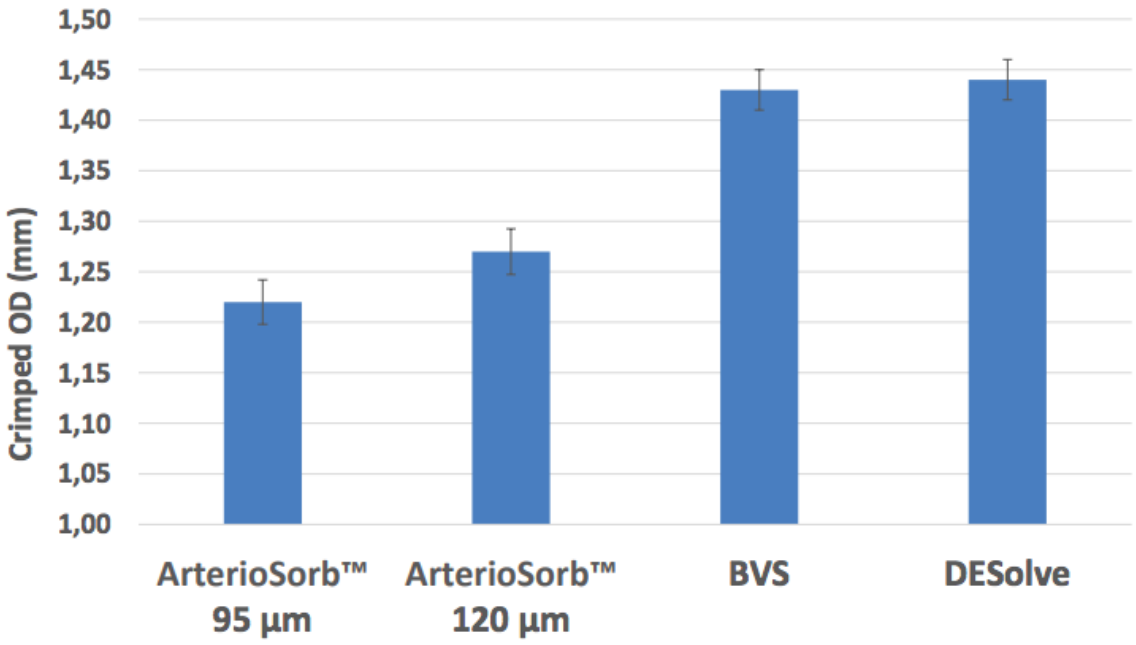


Figure F.1 Comparison of crimping and expansion testing of different bioresorbable scaffolds. Figure provided by Arterius Ltd.

The mechanical property of ArterioSorb™ and other bioresorbable scaffold was compared. Low crimp profiles for ArterioSorb™ scaffold was achieved compared to other bioresorbable scaffolds in the market

CONFERENCES AND AWARDS

- UK Surface Analysis Forum (UKSAF) 2017, Pavilions Teignmouth: Won the Seah Award £250 for Best Overall (Oral + Poster) Presentation.
- Presented at the Controlled release society (CRS), Seattle (2016) and Boston (2017).
- UK Society for Biomaterials (UKSB) 2016, University of Westminster, London: Won first prize for best oral poster presentation.
- Poster presentation at the European Society for Biomaterials (ESB), Krakow (2015).
- Poster titled “Investigation of a Novel Bioresorbable Polymer-Coated Drug-Eluting Scaffold” published on Arterius Ltd web page.

References

1 Geetha, M., Singh, A., Asokamani, R. & Gogia, A. Ti based biomaterials, the ultimate choice for orthopaedic implants–a review. *Progress in materials science* **54**, 397-425 (2009).

2 Helmus, M. N. Overview of biomedical materials. *MRS Bulletin* **16**, 33-38 (1991).

3 Bonfield, W. Materials characteristics versus in vivo behavior. *New York: New York Academy of Science* **173** (1988).

4 Ducheyne, P. Bioceramics: material characteristics versus in vivo behavior. *Journal of biomedical materials research* **21**, 219 (1987).

5 Anderson, J. M. & Zhao, Q. Biostability of biomedical polymers. *MRS Bulletin* **16**, 75-77 (1991).

6 Anderson, J. M., Rodriguez, A. & Chang, D. T. in *Seminars in immunology.* 86-100 (Elsevier).

7 Ferraro, A. in *IOP Conference Series: Materials Science and Engineering.* 012021 (IOP Publishing).

8 Milinkovi, I. *et al.* Aspects of titanium-implant surface modification at the micro and nano levels. *Materials and technology* **46**, 251-256 (2012).

9 Wen, C. *Surface coating and modification of metallic biomaterials*. (Woodhead Publishing, 2015).

10 Lewis, A. *Drug-device combination products: delivery technologies and applications*. (Elsevier, 2009).

11 Waller, D. G. *Cardiovascular E-Book: Key Articles from the Medicine journal*. (Elsevier Health Sciences, 2016).

12 Sidney, S., Rosamond, W. D., Howard, V. J. & Luepker, R. V. (Am Heart Assoc, 2013).

13 Nazneen, F. *et al.* Surface chemical and physical modification in stent technology for the treatment of coronary artery disease. *Journal of Biomedical Materials Research Part B: Applied Biomaterials* **100**, 1989-2014 (2012).

14 Libby, P., Ridker, P. M. & Maseri, A. Inflammation and atherosclerosis. *Circulation* **105**, 1135-1143 (2002).

15 Kolansky, D. M. Acute coronary syndromes: morbidity, mortality, and pharmacoeconomic burden. *The American journal of managed care* **15**, S36-41 (2009).

16 Schiff, A. F. The development of coronary artery bypass surgery. *Coronary Artery Disease* **1**, 121-132 (1990).

17 Yu, Y. Enhancing the biocompatibility of coronary artery stents. (2015).

18 Hinohara, T. Percutaneous coronary intervention: current perspective. *The Keio journal of medicine* **50**, 152-160 (2001).

19 Galvin, E. *Characterisation of the performance of an absorbable magnesium stent by experimental and numerical analysis*, Dublin City University, (2014).

20 Keren, G. in *Analytical and Quantitative Cardiology* 187-196 (Springer, 1997).

21 Anderson, H. V. Restenosis after coronary angioplasty. *Disease-a-Month* **39**, 617-670 (1993).
22 Agema, W. R. *et al.* Current PTCA practice and clinical outcomes in The Netherlands: the real world in the pre-drug-eluting stent era. *European Heart Journal* **25**, 1163-1170 (2004).
23 Topol, E. J. *et al.* A comparison of directional atherectomy with coronary angioplasty in patients with coronary artery disease. *New England Journal of Medicine* **329**, 221-227 (1993).
24 Serruys, P. W. *et al.* A comparison of balloon-expandable-stent implantation with balloon angioplasty in patients with coronary artery disease. *New England Journal of Medicine* **331**, 489-495 (1994).
25 Subbotin, V. M. Excessive intimal hyperplasia in human coronary arteries before intimal lipid depositions is the initiation of coronary atherosclerosis and constitutes a therapeutic target. *Drug discovery today* **21**, 1578-1595 (2016).
26 Yin, R.-X., Yang, D.-Z. & Wu, J.-Z. Nanoparticle drug-and gene-eluting stents for the prevention and treatment of coronary restenosis. *Theranostics* **4**, 175 (2014).
27 Topol, E. J. & Califf, R. M. *Textbook of cardiovascular medicine*. (Lippincott Williams & Wilkins, 2007).
28 Butany, J. & Collins, M. Analysis of prosthetic cardiac devices: a guide for the practising pathologist. *Journal of clinical pathology* **58**, 113-124 (2005).
29 Bandar, A.-M., Mongrain, R. & Yue, S. Coronary stents fracture: an engineering approach. *Materials Sciences and Applications* **4**, 606 (2013).
30 Schmid, E., Morris, A. & Nguyen, J. D. (Google Patents, 2012).
31 Farrar, D. F., Al-Lamee, K. G. & Motley, J. N. (Google Patents, 2008).
32 Paryab, N. *et al.* Uniform expansion of a polymeric helical stent. *Journal of Medical Devices* **6**, 021012 (2012).
33 Al-Lamee, K. G. (Google Patents, 2010).
34 Wang, L. *et al.* Long-term Outcomes of Drug-eluting versus Bare-metal stent for ST-elevation Myocardial Infarction. *Arquivos brasileiros de cardiologia* **102**, 529-538 (2014).
35 Ribeiro, P. A. *et al.* A new expandable intracoronary tantalum (Strecker) stent: early experimental results and follow-up to twelve months. *American heart journal* **125**, 501-510 (1993).
36 DePalma, V., Baier, R., Ford, J., Gott, V. & Furuse, A. Investigation of three-surface properties of several metals and their relation to blood compatibility. *Journal of Biomedical Materials Research Part A* **6**, 37-75 (1972).
37 Palmaz, J. C. Intravascular stents: tissue-stent interactions and design considerations. *AJR. American journal of roentgenology* **160**, 613-618 (1993).
38 Fattori, R. & Piva, T. Drug-eluting stents in vascular intervention. *The Lancet* **361**, 247-249 (2003).
39 Erne, P., Schier, M. & Resink, T. J. The road to bioabsorbable stents: reaching clinical reality? *Cardiovascular and interventional radiology* **29**, 11-16 (2006).
40 Neamtu, I. *et al.* Current concepts on cardiovascular stent devices. *Mini reviews in medicinal chemistry* **14**, 505-536 (2014).
41 Kereiakes, D. J. *et al.* Usefulness of a cobalt chromium coronary stent alloy. *The American journal of cardiology* **92**, 463-466 (2003).
42 Sketch, M. H. *et al.* Evaluation of the Medtronic (Driver) cobalt-chromium alloy coronary stent system. *The American journal of cardiology* **95**, 8-12 (2005).

43 Chen, M. S. *et al.* Bare metal stent restenosis is not a benign clinical entity. *American heart journal* **151**, 1260-1264 (2006).
44 Puranik, A. S., Dawson, E. R. & Peppas, N. A. Recent advances in drug eluting stents. *International journal of pharmaceutics* **441**, 665-679 (2013).
45 Gogas, B. D., McDaniel, M., Samady, H. & King, S. B. Novel drug-eluting stents for coronary revascularization. *Trends in cardiovascular medicine* **24**, 305-313 (2014).
46 Giacoppo, D. *et al.* Treatment strategies for coronary in-stent restenosis: systematic review and hierarchical Bayesian network meta-analysis of 24 randomised trials and 4880 patients. *BMJ* **351**, h5392 (2015).
47 Leon, M., Abizaid, A. & Moses, J. The CYPHER™ stent: a new gold standard in the treatment of coronary artery disease. *The Cardiovascular Research Foundation, New York, NY* (2003).
48 Lockwood, N. A. *et al.* In vitro and in vivo characterization of novel biodegradable polymers for application as drug-eluting stent coatings. *Journal of Biomaterials Science, Polymer Edition* **21**, 529-552 (2010).
49 Yazdani, S. K. *et al.* In vitro and in vivo characterisation of biodegradable polymer-based drug-eluting stent. *EuroIntervention* **7**, 835-843 (2011).
50 Ge, J. Limus-eluting stents with Poly-L-lactic acid coating. *Asia-Pacific Cardiol* **1** (2007).
51 Al-Lamee, K., Kelly, A., Coates, P. D., Thompson, G. P. & Caton-Rose, P. (Google Patents, 2013).
52 Mani, G., Feldman, M. D., Patel, D. & Agrawal, C. M. Coronary stents: a materials perspective. *Biomaterials* **28**, 1689-1710 (2007).
53 Di Mario, C. *et al.* Drug-eluting bioabsorbable magnesium stent. *Journal of interventional cardiology* **17**, 391-395 (2004).
54 Wu, M. *et al.* Surface characterization of poly (lactic acid)/everolimus and poly (ethylene vinyl alcohol)/everolimus stents. *Drug delivery* **17**, 376-384 (2010).
55 Yokoyama, M. Block copolymers as drug carriers. *Critical reviews in therapeutic drug carrier systems* **9**, 213-248 (1991).
56 Kumar, N., Ravikumar, M. N. & Domb, A. Biodegradable block copolymers. *Advanced drug delivery reviews* **53**, 23-44 (2001).
57 Kavanagh, C. A., Rochev, Y. A., Gallagher, W. M., Dawson, K. A. & Keenan, A. K. Local drug delivery in restenosis injury: thermoresponsive co-polymers as potential drug delivery systems. *Pharmacology & therapeutics* **102**, 1-15 (2004).
58 Chen, M.-C. *et al.* A novel drug-eluting stent spray-coated with multi-layers of collagen and sirolimus. *Journal of controlled release* **108**, 178-189 (2005).
59 Tenekecioglu, E. *et al.* Bioresorbable scaffolds: a new paradigm in percutaneous coronary intervention. *BMC cardiovascular disorders* **16**, 38 (2016).
60 Garg, S. & Serruys, P. W. Coronary stents: looking forward. *Journal of the American College of Cardiology* **56**, S43-S78 (2010).
61 Tenekecioglu, E., Torii, R., Bourantas, C. V., Al-Lamee, R. & Serruys, P. W. Non-Newtonian pulsatile shear stress assessment: a method to differentiate bioresorbable scaffold platforms. *European Heart Journal* **38**, 2570-2570 (2017).
62 Islambulchilar, Z., Ghanbarzadeh, S., Emami, S., Valizadeh, H. & Zakeri-Milani, P. Development and validation of an HPLC method for the analysis of sirolimus in drug products. *Adv Pharm Bull* **2**, 135-139 (2012).
63 Wang, C. P., Chan, K. W., Schiksnis, R. A., Scatina, J. & Sisenwine, S. F. High

performance liquid chromatographic isolation, spectroscopic characterization, and immunosuppressive activities of two rapamycin degradation products. *Journal of Liquid Chromatography & Related Technologies* **17**, 3383-3392 (1994).
64 Paine, M. F. *et al.* Identification of a novel route of extraction of sirolimus in human small intestine: roles of metabolism and secretion. *Journal of Pharmacology and Experimental Therapeutics* **301**, 174-186 (2002).
65 Paine, M. F., Leung, L. Y. & Watkins, P. B. New insights into drug absorption: studies with sirolimus. *Therapeutic drug monitoring* **26**, 463-467 (2004).
66 Osmulski, P. A. & Gaczynska, M. Rapamycin allosterically inhibits the proteasome. *Molecular pharmacology* **84**, 104-113 (2013).
67 Il'ichev, Y. V., Alquier, L. & Maryanoff, C. A. Degradation of rapamycin and its ring-opened isomer: role of base catalysis. *Arkivoc* **12**, 110-131 (2007).
68 Hallensleben, K., Raida, M. & Habermehl, G. Identification of a new metabolite of macrolide immunosuppressant, like rapamycin and SDZ RAD, using high performance liquid chromatography and electrospray tandem mass spectrometry. *Journal of the American Society for Mass Spectrometry* **11**, 516-525 (2000).
69 Strohbach, A. & Busch, R. Polymers for cardiovascular stent coatings. *International Journal of Polymer Science* **2015** (2015).
70 Wessely, R. New drug-eluting stent concepts. *Nature Reviews Cardiology* **7**, 194-203 (2010).
71 Auras, R., Harte, B. & Selke, S. An overview of polylactides as packaging materials. *Macromolecular bioscience* **4**, 835-864 (2004).
72 Bergström, J. S. & Hayman, D. An overview of mechanical properties and material modeling of polylactide (PLA) for medical applications. *Annals of biomedical engineering* **44**, 330-340 (2016).
73 van Alst, M., Eenink, M., Kruft, M. & van Tuil, R. ABC's of bioabsorption: application of lactide based polymers in fully resorbable cardiovascular stents. *EuroIntervention: journal of EuroPCR in collaboration with the Working Group on Interventional Cardiology of the European Society of Cardiology* **5**, F23-27 (2009).
74 Onuma, Y. *et al.* Five-year clinical and functional multislice computed tomography angiographic results after coronary implantation of the fully resorbable polymeric everolimus-eluting scaffold in patients with de novo coronary artery disease: the ABSORB cohort A trial. *JACC: Cardiovascular Interventions* **6**, 999-1009 (2013).
75 Domb, A. J. & Kumar, N. *Biodegradable polymers in clinical use and clinical development*. (John Wiley & Sons, 2011).
76 Li, S., Garreau, H. & Vert, M. Structure-property relationships in the case of the degradation of massive poly (α-hydroxy acids) in aqueous media. *Journal of Materials Science: Materials in Medicine* **1**, 198-206 (1990).
77 Jamshidian, M., Tehrany, E. A., Imran, M., Jacquot, M. & Desobry, S. Poly-Lactic Acid: production, applications, nanocomposites, and release studies. *Comprehensive Reviews in Food Science and Food Safety* **9**, 552-571 (2010).
78 Rattier, B. D., Hoffman, A. S., Schoen, F. J. & Lemons, J. E. Biomaterials Science: An Introduction to Materials in Medicine. *Journal of Clinical Engineering* **22**, 26 (1997).
79 Cheng, Y., Deng, S., Chen, P. & Ruan, R. Polylactic acid (PLA) synthesis and modifications: a review. *Frontiers of chemistry in China* **4**, 259-264 (2009).
80 Ikada, Y. & Tsuji, H. Biodegradable polyesters for medical and ecological applications. *Macromolecular rapid communications* **21**, 117-132 (2000).

81 Kricheldorf, H. R., Kreiser-Saunders, I., Jürgens, C. & Wolter, D. in *Macromolecular Symposia.* 85-102 (Wiley Online Library).
82 Baratian, S., Hall, E., Lin, J., Xu, R. & Runt, J. Crystallization and solid-state structure of random polylactide copolymers: poly (l-lactide-co-d-lactide) s. *Macromolecules* **34**, 4857-4864 (2001).
83 Tsuji, H. & Ikada, Y. Blends of isotactic and atactic poly (lactide) s: 2. Molecular-weight effects of atactic component on crystallization and morphology of equimolar blends from the melt. *Polymer* **37**, 595-602 (1996).
84 Shimamoto, T., Adachi, M., Oka, T. & Takasawa, H. The Second Far-Eastern Symposium on Biomedical Materials. *Kyoto, Japan* **171** (1995).
85 Kasemo, B. & Lausmaa, J. Biomaterial and implant surfaces: a surface science approach. *International Journal of Oral & Maxillofacial Implants* **3** (1988).
86 Mahoney, C. M. Cluster secondary ion mass spectrometry of polymers and related materials. *Mass spectrometry reviews* **29**, 247-293 (2010).
87 Belu, A. M., Graham, D. J. & Castner, D. G. Time-of-flight secondary ion mass spectrometry: techniques and applications for the characterization of biomaterial surfaces. *Biomaterials* **24**, 3635-3653 (2003).
88 Walls, J. *Methods of surface analysis: techniques and applications*. (CUP Archive, 1990).
89 Ratner, B. D. Surface modification of polymers: chemical, biological and surface analytical challenges. *Biosensors and bioelectronics* **10**, 797-804 (1995).
90 Briguori, C. *et al.* In-stent restenosis in small coronary arteries: impact of strut thickness. *Journal of the American College of Cardiology* **40**, 403-409 (2002).
91 Hercules, D. M. & Hercules, S. H. Analytical chemistry of surfaces. Part I. General aspects. *J. Chem. Educ* **61**, 402 (1984).
92 Kannan, R. Y., Salacinski, H. J., Vara, D. S., Odlyha, M. & Seifalian, A. M. Principles and applications of surface analytical techniques at the vascular interface. *Journal of biomaterials applications* **21**, 5-32 (2006).
93 Kamath, K. R., Barry, J. J. & Miller, K. M. The Taxus™ drug-eluting stent: A new paradigm in controlled drug delivery. *Advanced drug delivery reviews* **58**, 412-436 (2006).
94 Regar, E., Sianos, G. & Serruys, P. Stent development and local drug delivery. *British medical bulletin* **59**, 227-248 (2001).
95 Wormuth, K. in *Confocal Raman Microscopy* 203-223 (Springer, 2010).
96 Abizaid, A. & Costa, J. R. New drug-eluting stents. *Circulation: Cardiovascular Interventions* **3**, 384-393 (2010).
97 Belu, A., Mahoney, C. & Wormuth, K. Chemical imaging of drug eluting coatings: combining surface analysis and confocal Raman microscopy. *Journal of Controlled Release* **126**, 111-121 (2008).
98 Grabow, N. *et al.* A biodegradable slotted tube stent based on poly (L-lactide) and poly (4-hydroxybutyrate) for rapid balloon-expansion. *Annals of biomedical engineering* **35**, 2031-2038 (2007).
99 Pan, C. J., Tang, J., Weng, Y., Wang, J. & Huang, N. Preparation, characterization and anticoagulation of curcumin-eluting controlled biodegradable coating stents. *Journal of Controlled Release* **116**, 42-49 (2006).
100 Nguyen, K. T. *et al.* Molecular responses of vascular smooth muscle cells and phagocytes to curcumin-eluting bioresorbable stent materials. *Biomaterials* **25**, 5333-5346 (2004).

101 Yamawaki, T. *et al.* Intramural delivery of a specific tyrosine kinase inhibitor with biodegradable stent suppresses the restenotic changes of the coronary artery in pigs in vivo. *Journal of the American College of Cardiology* **32**, 780-786 (1998).
102 Lewis, A. *et al.* Phosphorylcholine-based polymer coatings for stent drug delivery. *Journal of Materials Science: Materials in Medicine* **12**, 865-870 (2001).
103 Lewis, A. L. *et al.* Crosslinkable coatings from phosphorylcholine-based polymers. *Biomaterials* **22**, 99-111 (2001).
104 Palmer, R. R. *et al.* Biological evaluation and drug delivery application of cationically modified phospholipid polymers. *Biomaterials* **25**, 4785-4796 (2004).
105 Vogt, F. *et al.* Long-term assessment of a novel biodegradable paclitaxel-eluting coronary polylactide stent. *European Heart Journal* **25**, 1330-1340 (2004).
106 Vedantham, K., Chaterji, S., Kitsongsermthon, J., Garner, J. & Park, K. *Future outlook for drug eluting stents*. (Woodhead Publishing, 2009).
107 Wang, Y., Burgress, D. & Aagaard, J. *Drug Device Combination Products*. (Woodhead Publishing Ltd.: Cambridge, UK, 2010).
108 Langer, R. New methods of drug delivery. *Science* **249**, 1527-1533 (1990).
109 Yang, C. & Burt, H. M. Drug-eluting stents: factors governing local pharmacokinetics. *Advanced drug delivery reviews* **58**, 402-411 (2006).
110 Schwartz, R. S. *et al.* Drug-eluting stents in preclinical studies: updated consensus recommendations for preclinical evaluation. *Circulation: Cardiovascular Interventions* **1**, 143-153 (2008).
111 McKittrick, C., Kennedy, S., Oldroyd, K., McGinty, S. & McCormick, C. Modelling the impact of atherosclerosis on drug release and distribution from coronary stents. *Annals of biomedical engineering* **44**, 477-487 (2016).
112 Varma, M. V., Kaushal, A. M., Garg, A. & Garg, S. Factors affecting mechanism and kinetics of drug release from matrix-based oral controlled drug delivery systems. *American Journal of drug delivery* **2**, 43-57 (2004).
113 StÖrger, H., Grube, E., Hofmann, M., Schwarz, F. & Haase, J. Clinical Experiences Using Everolimus-Eluting Stents in Patients with Coronary Artery Disease. *Journal of interventional cardiology* **17**, 387-390 (2004).
114 Naseerali, C., Hari, P. & Sreenivasan, K. The release kinetics of drug eluting stents containing sirolimus as coated drug: role of release media. *Journal of Chromatography B* **878**, 709-712 (2010).
115 Mikkonen, J. *et al.* Drug-eluting bioabsorbable stents–An in vitro study. *Acta biomaterialia* **5**, 2894-2900 (2009).
116 Waksman, R. Drug-eluting stents: From bench to bed. *Cardiovascular radiation medicine* **3**, 226-241 (2002).
117 Pan, C., Tang, J., Weng, Y., Wang, J. & Huang, N. Preparation and characterization of rapamycin-loaded PLGA coating stent. *Journal of Materials Science: Materials in Medicine* **18**, 2193-2198 (2007).
118 Vert, M., Li, S. & Garreau, H. More about the degradation of LA/GA-derived matrices in aqueous media. *Journal of Controlled Release* **16**, 15-26 (1991).
119 Manjanna, K., Shivakumar, B. & Kumar, T. P. Microencapsulation: an acclaimed novel drug-delivery system for NSAIDs in arthritis. *Critical Reviews™ in Therapeutic Drug Carrier Systems* **27** (2010).
120 Healy, K. E. & Dorfman, G. S. (Google Patents, 1997).
121 Litvack, F., Shanley, J., Parker, T. & Diaz, S. (Google Patents, 2005).
122 Li, J. *et al.* Structure evolution and orientation mechanism of long-chain-branched

poly (lactic acid) in the process of solid die drawing. *European Polymer Journal* **90**, 54-65 (2017).
123 Muhammad, N. B. Laser micromachining of coronary stents for medical applications. (2012).
124 Bäuerle, D. W. *Laser processing and chemistry*. (Springer Science & Business Media, 2013).
125 Steen, W. Laser material processing, 1991. *LIA, Orlando, Fla*.
126 McDermott, M. *et al.* Application of Quality by Design (QbD) Approach to Ultrasonic Atomization Spray Coating of Drug-Eluting Stents. *AAPS PharmSciTech* **16**, 811-823 (2015).
127 Berger, H. L. in *ILASS, 19th Annual Conference on Liquid Atomization and Spray Systems, Toronto, Canada.*
128 Girotto, C., Rand, B. P., Genoe, J. & Heremans, P. Exploring spray coating as a deposition technique for the fabrication of solution-processed solar cells. *Solar energy materials and solar cells* **93**, 454-458 (2009).
129 Selwood, A., Ward, I. & Parsons, B. The production of oriented polymer tube by the die-drawing process. *Plastics and rubber processing and applications* **8**, 49-58 (1987).
130 Smith, I., Ren, F., Baumann, M. & Case, E. Confocal laser scanning microscopy as a tool for imaging cancellous bone. *Journal of Biomedical Materials Research Part B: Applied Biomaterials* **79**, 185-192 (2006).
131 Binnig, G., Quate, C. F. & Gerber, C. Atomic force microscope. *Physical review letters* **56**, 930 (1986).
132 Liu, Y. *Atomic Force Microscopy for Better Probing Surface Properties at Nanoscale: Calibration, Design and Application*, The University of Western Ontario, (2010).
133 Bandyopadhyay, A. & Bose, S. *Characterization of biomaterials*. (Newnes, 2013).
134 Morton, K. C. & Baker, L. A. Atomic force microscopy-based bioanalysis for the study of disease. *Analytical Methods* **6**, 4932-4955 (2014).
135 Höper, R., Gesang, T., Possart, W., Hennemann, O.-D. & Boseck, S. Imaging elastic sample properties with an atomic force microscope operating in the tapping mode. *Ultramicroscopy* **60**, 17-24 (1995).
136 Tomczak, N. & Goh, K. E. J. *Scanning Probe Microscopy*. (World Scientific, 2011).
137 Pittenger, B., Erina, N. & Su, C. Quantitative mechanical property mapping at the nanoscale with PeakForce QNM. *Application Note Veeco Instruments Inc* (2010).
138 Foster, B. New Atomic Force Microscopy(AFM) Approaches Life Sciences Gently, Quantitatively, and Correctively. *American laboratory* **44**, 24-28 (2012).
139 Lee, J., Gilmore, I., Vickerman, J. & Gilmore, I. (Chichester, Wiley, 2009) p, 2009).
140 Graham, D. J. & Ratner, B. D. Multivariate analysis of TOF-SIMS spectra from dodecanethiol SAM assembly on gold: Spectral interpretation and TOF-SIMS fragmentation processes. *Langmuir* **18**, 5861-5868 (2002).
141 Chan, C. M. & Weng, L.-T. Surface Characterization of Polymer Blends by XPS and ToF-SIMS. *Materials* **9**, 655 (2016).
142 Steffens, P., Niehuis, E., Friese, T., Greifendorf, D. & Benninghoven, A. A time-of-flight mass spectrometer for static SIMS applications. *Journal of Vacuum Science & Technology A: Vacuum, Surfaces, and Films* **3**, 1322-1325 (1985).
143 Van Tendeloo, G., Bals, S., Van Aert, S., Verbeeck, J. & Van Dyck, D. Advanced

electron microscopy for advanced materials. *Advanced materials* **24**, 5655-5675 (2012).
144 Taylor, M. *Surface analysis of polymer microarrays*, University of Nottingham, (2009).
145 Spectrometry, S. I. M. Principles and Applications. *Oxford University Press, Oxford* (1989).
146 Ormsby, T. J. *Accurate ultra-low energy SIMS depth profiling of silicon semiconductors*, University of Warwick, (2000).
147 Verlinden, G., Gijbels, R. & Geuens, I. Quantitative secondary ion mass spectrometry depth profiling of surface layers of cubic silver halide microcrystals. *Journal of the American Society for Mass Spectrometry* **10**, 1016-1027 (1999).
148 Mahoney, C. M., Yu, J., Fahey, A. & Gardella, J. A. SIMS depth profiling of polymer blends with protein based drugs. *Applied surface science* **252**, 6609-6614 (2006).
149 Mahoney, C. M., Fahey, A. J. & Gillen, G. Temperature-controlled depth profiling of poly (methyl methacrylate) using cluster secondary ion mass spectrometry. 1. Investigation of depth profile characteristics. *Analytical Chemistry* **79**, 828-836 (2007).
150 Vickerman, J. C. & Gilmore, I. *Surface analysis: the principal techniques*. (John Wiley & Sons, 2011).
151 Kovac, J. Surface characterization of polymers by XPS and SIMS techniques. *Materiali in tehnologije* **45**, 191-197 (2011).
152 Munro, H. & Singh, S. in *Polymer Characterisation* 333-356 (Springer, 1993).
153 Yang, J. & Alexander, M. Techniques for analysing biomaterial surface chemistry. *Surface Modification of Biomaterials. Methods, analysis and applications*, 211 (2010).
154 Rafati, A. *The analysis of polymers for biomedical applications*, University of Nottingham, (2011).
155 Moulder, J., Stickle, W., Sobol, P. & Bomben, K. Handbook of X-ray Photoelectron Spectroscopy (1995) Physical Electronics. *Inc. MN, USA*, 80-81.
156 Mohai, M. XPS MultiQuant: multimodel XPS quantification software. *Surface and interface analysis* **36**, 828-832 (2004).
157 Ulery, B. D., Nair, L. S. & Laurencin, C. T. Biomedical applications of biodegradable polymers. *Journal of polymer science Part B: polymer physics* **49**, 832-864 (2011).
158 Merrett, K., Cornelius, R., McClung, W., Unsworth, L. & Sheardown, H. Surface analysis methods for characterizing polymeric biomaterials. *Journal of Biomaterials Science, Polymer Edition* **13**, 593-621 (2002).
159 Butler, H. J. *et al.* Using Raman spectroscopy to characterize biological materials. *Nature protocols* **11**, 664-687 (2016).
160 Price, D. M., Reading, M., Hammiche, A. & Pollock, H. M. Micro-thermal analysis: scanning thermal microscopy and localised thermal analysis. *International Journal of Pharmaceutics* **192**, 85-96 (1999).
161 Sanders, G. *et al.* Discrimination of polymorphic forms of a drug product by localized thermal analysis. *Journal of microscopy* **198**, 77-81 (2000).
162 Alhijjaj, M. *et al.* Characterization of heterogeneity and spatial distribution of phases in complex solid dispersions by thermal analysis by structural characterization and X-ray micro computed tomography. *Pharmaceutical research*, 1-19 (2016).

163 Zhang, J. *et al.* Nanoscale thermal analysis of pharmaceutical solid dispersions. *Int. J. Pharm.* **380**, 170-173 (2009).
164 Guo, F., Zhu, K., Trannoy, N. & Lu, J. Examination of thermal properties by scanning thermal microscopy in ultrafine-grained pure titanium surface layer produced by surface mechanical attrition treatment. *Thermochimica acta* **419**, 239-246 (2004).
165 Jin, Z. *The micro and nano scale characterization and identification of tablet formulations*, University of Nottingham, (2010).
166 Meyers, G. & Pastzor, A. nano-TA TM: Nano Thermal Analysis.
167 Jeong, W., Hur, S., Meyhofer, E. & Reddy, P. Scanning Probe Microscopy for Thermal Transport Measurements. *Nanoscale and Microscale Thermophysical Engineering* **19**, 279-302 (2015).
168 Weir, N., Buchanan, F., Orr, J. & Dickson, G. Degradation of poly-L-lactide. Part 1: in vitro and in vivo physiological temperature degradation. *Proceedings of the Institution of Mechanical Engineers, Part H: Journal of Engineering in Medicine* **218**, 307-319 (2004).
169 Leica, D. New ZMorf Surface Imaging and Metrology Software for Zeta Instruments Optical Profilers Zeta Instruments and Digital Surf announced that Zeta Instruments is offering ZMorf Surface Imaging and Metrology software with its Zeta.
170 Dazzi, A., Saunier, J., Kjoller, K. & Yagoubi, N. Resonance enhanced AFM-IR: A new powerful way to characterize blooming on polymers used in medical devices. *International journal of pharmaceutics* **484**, 109-114 (2015).
171 Lausmaa, J. *et al.* Surface characterization of biomaterials. *Amsterdam: Elsevier* (1988).
172 Caracciolo, P. C. *et al.* Surface-modified bioresorbable electrospun scaffolds for improving hemocompatibility of vascular grafts. *Materials Science and Engineering: C* **75**, 1115-1127 (2017).
173 Hou, L.-D. *et al.* A review on biodegradable materials for cardiovascular stent application. *Frontiers of Materials Science* **10**, 238-259 (2016).
174 Widmer, M. S. & Mikos, A. Fabrication of biodegradable polymer scaffolds for tissue engineering. *Frontiers in tissue engineering*, 107-120 (1998).
175 Mahoney, C. M., Fahey, A. J. & Belu, A. M. Three-dimensional compositional analysis of drug eluting stent coatings using cluster secondary ion mass spectrometry. *Analytical chemistry* **80**, 624-632 (2008).
176 Serruys, P. W., Kutryk, M. J. & Ong, A. T. Coronary-artery stents. *New England Journal of Medicine* **354**, 483-495 (2006).
177 Shulze, J. E., Betts, R. E. & Savage, D. R. (Google Patents, 2005).
178 Francis, L., McCormick, A., Vaessen, D. & Payne, J. Development and measurement of stress in polymer coatings. *Journal of Materials Science* **37**, 4717-4731 (2002).
179 Gale, D. C., Huang, B., Abbate, A. J., Limon, T. A. & Kleine, K. (Google Patents, 2011).
180 Kleine, K., Gale, D. C., Huang, B., Abbate, A. J. & Limon, T. A. (Google Patents, 2015).
181 Ailianou, A., Ramachandran, K., Kossuth, M. B., Oberhauser, J. P. & Kornfield, J. A. Multiplicity of morphologies in poly (L-lactide) bioresorbable vascular scaffolds. *Proceedings of the National Academy of Sciences* **113**, 11670-11675 (2016).

182 Ramachandran, K., Ailianou, A., Kossuth, M. B., Oberhauser, J. P. & Kornfield, J. Multiplicity of Morphologies in Poly (L-lactide) Bioresorbable Vascular Scaffolds. *Bulletin of the American Physical Society* (2018).
183 Raval, A., Parikh, J. & Engineer, C. Mechanism of controlled release kinetics from medical devices. *Brazilian Journal of Chemical Engineering* **27**, 211-225 (2010).
184 Bhatla, A. & Yao, Y. L. Effect of laser surface modification on the crystallinity of poly (L-lactic acid). *Journal of Manufacturing Science and Engineering* **131**, 051004 (2009).
185 Vasanthakumari, R. & Pennings, A. Crystallization kinetics of poly (L-lactic acid). *Polymer* **24**, 175-178 (1983).
186 Jagtap, R. & Ambre, A. Overview literature on atomic force microscopy (AFM): Basics and its important applications for polymer characterization. *Indian Journal of Engineering and Materials Sciences* **13**, 368 (2006).
187 Areias, A. *et al.* Influence of crystallinity and fiber orientation on hydrophobicity and biological response of poly (L-lactide) electrospun mats. *Soft Matter* **8**, 5818-5825 (2012).
188 Aguilar, C. A., Lu, Y., Mao, S. & Chen, S. Direct micro-patterning of biodegradable polymers using ultraviolet and femtosecond lasers. *Biomaterials* **26**, 7642-7649 (2005).
189 Lasprilla, A. J. R., Martinez, G. A. R. & Hoss, B. Synthesis and Characterization of Poly (lactic acid) for Use in Biomedical Field. *Chem. Eng* **24**, 985-990 (2011).
190 Zhang, J., Duan, Y., Domb, A. J. & Ozaki, Y. PLLA Mesophase and Its Phase Transition Behavior in the PLLA− PEG− PLLA Copolymer As Revealed by Infrared Spectroscopy. *Macromolecules* **43**, 4240-4246 (2010).
191 Martins, K. F., Messias, A. D., Leite, F. L. & Duek, E. A. Preparation and characterization of paclitaxel-loaded PLDLA microspheres. *Materials Research* **17**, 650-656 (2014).
192 Auras, R. Poly (lactic acid). *Encyclopedia Of Polymer Science and Technology* (2010).
193 Yuan, X., Mak, A. F., Kwok, K., Yung, B. K. & Yao, K. Characterization of poly (L-lactic acid) fibers produced by melt spinning. *Journal of Applied Polymer Science* **81**, 251-260 (2001).
194 Carletti, E. *3D scaffolds for tissue engineering produced by microfabrication technology*, University of Trento, (2009).
195 Callister, W. D. & Rethwisch, D. G. *Fundamentals of materials science and engineering: an integrated approach*. (John Wiley & Sons, 2012).
196 Pan, P., Zhu, B., Kai, W., Dong, T. & Inoue, Y. Effect of crystallization temperature on crystal modifications and crystallization kinetics of poly (L-lactide). *Journal of Applied Polymer Science* **107**, 54-62 (2008).
197 Weir, N., Buchanan, F., Orr, J., Farrar, D. & Boyd, A. Processing, annealing and sterilisation of poly-L-lactide. *Biomaterials* **25**, 3939-3949 (2004).
198 Hyon, S.-H., Jamshidi, K. & Ikada, Y. in *Polymers as biomaterials* 51-65 (Springer, 1984).
199 Ahmed, J., Zhang, J.-X., Song, Z. & Varshney, S. Thermal properties of polylactides. *Journal of Thermal Analysis and Calorimetry* **95**, 957-964 (2009).
200 Hsu, S.-T., Tan, H. & Yao, Y. L. Effect of excimer laser irradiation on crystallinity and chemical bonding of biodegradable polymer. *Polymer degradation and stability* **97**, 88-97 (2012).

201 Kaule, T. *et al.* Thermal properties of nanocapsules measured by scanning force microscopy methods. *Microelectronic Engineering* **97**, 223-226 (2012).
202 Royall, P. G., Craig, D. Q. & Grandy, D. B. The use of micro-thermal analysis as a means of in situ characterisation of a pharmaceutical tablet coat. *Thermochimica acta* **380**, 165-173 (2001).
203 Okubo, S. *et al.* Micro-/nanofabrication of cross-linked poly (L-lactic acid) using electron beam nanoimprint lithography. *Applied Physics Express* **5**, 027303 (2012).
204 Calafel, M. I., Remiro, P. M., Cortázar, M. M. & Calahorra, M. E. Cold crystallization and multiple melting behavior of poly (l-lactide) in homogeneous and in multiphasic epoxy blends. *Colloid & polymer science* **288**, 283-296 (2010).
205 Saeidlou, S., Huneault, M. A., Li, H. & Park, C. B. Poly (lactic acid) crystallization. *Progress in Polymer Science* **37**, 1657-1677 (2012).
206 Witzke, D. R., Narayan, R. & Kolstad, J. J. Reversible kinetics and thermodynamics of the homopolymerization of L-lactide with 2-ethylhexanoic acid tin (II) salt. *Macromolecules* **30**, 7075-7085 (1997).
207 Bond, L. *et al.* Differential scanning calorimetry and scanning thermal microscopy analysis of pharmaceutical materials. *International journal of pharmaceutics* **243**, 71-82 (2002).
208 Xing, Q., Zhang, X., Dong, X., Liu, G. & Wang, D. Low-molecular weight aliphatic amides as nucleating agents for poly (l-lactic acid): conformation variation induced crystallization enhancement. *Polymer* **53**, 2306-2314 (2012).
209 Garea, S. A. & Ghebaur, A. FT-IR spectroscopy and Thermogravimetrical Characterization of Prodrugs based on different dendritic polymers and antitumoral drug. *Materiale Plastice* **49**, 1-4 (2012).
210 Garrison, B., Vickerman, J. & Briggs, D. TOF-SIMS: surface analysis by mass spectrometry. *Molecular Dynamics Simulations: The Theoretical Partner to Static SIMS Experiments*, 223-257 (2001).
211 Fisher, G. L., Belu, A. M., Mahoney, C. M., Wormuth, K. & Sanada, N. Three-dimensional time-of-flight secondary ion mass spectrometry imaging of a pharmaceutical in a coronary stent coating as a function of elution time. *Analytical chemistry* **81**, 9930-9940 (2009).
212 Davies, M., Brown, A., Newton, J. & Chapman, S. SSIMS and SIMS imaging analysis of a drug delivery system. *Surface and interface analysis* **11**, 591-595 (1988).
213 Green, F., Shard, A., Gilmore, I. & Seah, M. Analysis of the interface and its position in C60 n+ secondary ion mass spectrometry depth profiling. *Analytical chemistry* **81**, 75-79 (2008).
214 Ma, Z. *et al.* Surface modification of poly-L-lactide by photografting of hydrophilic polymers towards improving its hydrophilicity. *Journal of applied polymer science* **85**, 2163-2171 (2002).
215 Crist, B. V. A review of XPS data-banks. *XPS Reports* **1** (2007).
216 Durand, S. T. D. Handbook of Biopolymer-Based Materials. *Networks* **801**, 849 (2013).
217 Shakesheff, K. *The application of atomic force microscopy in the surface analysis of polymeric biomaterials*, University of Nottingham, (1995).
218 Maitz, M. Applications of synthetic polymers in clinical medicine. *Biosurface and Biotribology* **1**, 161-176 (2015).

219 Hanker, J. S. & Giammara, B. L. Biomaterials and biomedical devices. *Science* **242**, 885-893 (1988).
220 Bhat, S. & Kumar, A. Biomaterials and bioengineering tomorrow's healthcare. *Biomatter* **3**, e24717 (2013).
221 Guerra, A. J. & Ciurana, J. Effect of fibre laser process on in-vitro degradation rate of a polycaprolactone stent a novel degradation study method. *Polymer Degradation and Stability* (2017).
222 Muhammad, N. *et al.* Picosecond laser micromachining of nitinol and platinum–iridium alloy for coronary stent applications. *Applied Physics A: Materials Science & Processing* **106**, 607-617 (2012).
223 Dausinger, F., Hügel, H. & Konov, V. in *Proc. of SPIE Vol.* 107.
224 Momma, C., Knop, U. & Nolte, S. Laser cutting of slotted tube coronary stents—state-of-the-art and future developments. *Progress in Biomedical Research* **4**, 39-44 (1999).
225 Garbassi, F., Morra, M., Occhiello, E. & Garbassi, F. *Polymer surfaces: from physics to technology*. (Wiley Chichester, 1998).
226 Ratner, B. D. *et al.* Biomolecules and surfaces. *Journal of Vacuum Science & Technology A: Vacuum, Surfaces, and Films* **8**, 2306-2317 (1990).
227 Puskas, J. E. *et al.* Drug-eluting stent coatings. *Wiley Interdisciplinary Reviews: Nanomedicine and Nanobiotechnology* **1**, 451-462 (2009).
228 Ma, X., Wu, T. & Robich, M. P. Drug-eluting stent coatings. *Interv Cardiol* **4**, 73-83 (2012).
229 Ruane, P., Perez-Segarra, W. & Reyes, P. (Google Patents, 2006).
230 Bedair, T. M., Cho, Y., Joung, Y. K. & Han, D. K. Biodegradable polymer brush as nanocoupled interface for improving the durability of polymer coating on metal surface. *Colloids and Surfaces B: Biointerfaces* **122**, 808-817 (2014).
231 MOTALEBI, A., NASR-ESFAHANI, M., ALI, R. & POURRIAHI, M. Progress in Natural Science: Materials International. *Volume* **22**, 392-400.
232 Kollum, M. *et al.* Particle debris from a nanoporous stent coating obscures potential antiproliferative effects of tacrolimus-eluting stents in a porcine model of restenosis. *Catheterization and cardiovascular interventions* **64**, 85-90 (2005).
233 Bian, H., Zhou, S., Liang, X., Li, Q. & Han, W. In vitro study of poly (ethylene carbonate) as a drug-eluting stent coating. *Progress in Natural Science: Materials International* **22**, 295-302 (2012).
234 Iannace, S. & Nicolais, L. Isothermal crystallization and chain mobility of poly (L-lactide). *Journal of applied polymer science* **64**, 911-919 (1997).
235 Scoutaris, N. *et al.* Development and biological evaluation of inkjet printed drug coatings on intravascular stent. *Molecular pharmaceutics* **13**, 125-133 (2015).
236 Karagkiozaki, V. *et al.* Development of a nanoporous and multilayer drug-delivery platform for medical implants. *International journal of nanomedicine* **7**, 5327 (2012).
237 Ding, N. (Google Patents, 1999).
238 Li, H., Nie, W., Deng, C., Chen, X. & Ji, X. Crystalline morphology of poly (L-lactic acid) thin films. *European Polymer Journal* **45**, 123-130 (2009).
239 Ratner, B. D. Characterization of biomaterial surfaces. *Cardiovascular Pathology* **2**, 87-100 (1993).
240 Wucher, A. & Winograd, N. Molecular sputter depth profiling using carbon cluster beams. *Analytical and bioanalytical chemistry* **396**, 105-114 (2010).

241 Havelund, R. *et al.* Improving secondary ion mass spectrometry C60 n+ sputter depth profiling of challenging polymers with nitric oxide gas dosing. *Analytical chemistry* **85**, 5064-5070 (2013).
242 Mahoney, C. M., Fahey, A. J., Gillen, G., Xu, C. & Batteas, J. D. Temperature-controlled depth profiling in polymeric materials using cluster secondary ion mass spectrometry (SIMS). *Applied surface science* **252**, 6502-6505 (2006).
243 Nieuwjaer, N., Poleunis, C., Delcorte, A. & Bertrand, P. Depth profiling of polymer samples using Ga+ and C60+ ion beams. *Surface and Interface Analysis* **41**, 6-10 (2009).
244 Leng, Y. *Materials characterization: introduction to microscopic and spectroscopic methods*. (John Wiley & Sons, 2009).
245 Seah, M., Havelund, R., Shard, A. & Gilmore, I. Sputtering yields for mixtures of organic materials using argon gas cluster ions. *The Journal of Physical Chemistry B* **119**, 13433-13439 (2015).
246 Wucher, A., Fisher, G. L. & Mahoney, C. M. Three-Dimensional Imaging with Cluster Ion Beams. *Cluster Secondary Ion Mass Spectrometry: Principles and Applications*, 207-246 (2013).
247 Food & Administration, D. CYPHER™ sirolimus-eluting coronary stent on RAPTOR® over-the-wire delivery system or RAPTORRAIL® rapid exchange delivery system—P020026. *P020026, Part* **3** (2004).
248 Ahmed, J. & Varshney, S. K. Polylactides—chemistry, properties and green packaging technology: a review. *International journal of food properties* **14**, 37-58 (2011).
249 Briggs, D. & Beamson, G. XPS studies of the oxygen 1s and 2s levels in a wide range of functional polymers. *Analytical Chemistry* **65**, 1517-1523 (1993).
250 Rafati, A. *et al.* Quantitative XPS depth profiling of codeine loaded poly (l-lactic acid) films using a coronene ion sputter source. *Journal of Controlled Release* **138**, 40-44 (2009).
251 Udipi, K. *et al.* Development of a novel biocompatible polymer system for extended drug release in a next-generation drug-eluting stent. *Journal of biomedical materials research Part A* **85**, 1064-1071 (2008).
252 Castellino, M. *et al.* Chemico-physical characterisation and in vivo biocompatibility assessment of DLC-coated coronary stents. *Analytical and bioanalytical chemistry* **405**, 321-329 (2013).
253 Balss, K. M. *et al.* Multivariate analysis applied to the study of spatial distributions found in drug-eluting stent coatings by confocal Raman microscopy. *Analytical chemistry* **80**, 4853-4859 (2008).
254 Smith, G. P., McGoverin, C. M., Fraser, S. J. & Gordon, K. C. Raman imaging of drug delivery systems. *Advanced drug delivery reviews* **89**, 21-41 (2015).
255 Balss, K., Llanos, G., Papandreou, G. & Maryanoff, C. Quantitative spatial distribution of sirolimus and polymers in drug-eluting stents using confocal Raman microscopy. *Journal of Biomedical Materials Research Part A* **85**, 258-270 (2008).
256 Younes, H. & Cohn, D. Phase separation in poly (ethylene glycol)/poly (lactic acid) blends. *European polymer journal* **24**, 765-773 (1988).
257 Garlotta, D. A literature review of poly (lactic acid). *Journal of Polymers and the Environment* **9**, 63-84 (2001).
258 Pan, C.-J., Tang, J.-J., Weng, Y.-J., Wang, J. & Huang, N. Preparation and in vitro release profiles of drug-eluting controlled biodegradable polymer coating stents.

Colloids and Surfaces B: Biointerfaces **73**, 199-206 (2009).
259 Glocker, D. & Ranade, S. *Medical Coatings and Deposition Technologies*. (John Wiley & Sons, 2016).
260 Göpferich, A. Mechanisms of polymer degradation and erosion. *Biomaterials* **17**, 103-114 (1996).
261 Boutrand, J.-P. *Biocompatibility and performance of medical devices*. (Elsevier, 2012).
262 A.L, A. in *Biocompatibility and Performance of Medical Devices* (ed J-P. Boutrand) Ch. Methods for the characterisation and evaluation of drug-device combination products, 233–268 (
, 2012).
263 Marin, E., Briceño, M. I. & Caballero-George, C. Critical evaluation of biodegradable polymers used in nanodrugs. *International journal of nanomedicine* **8**, 3071 (2013).
264 Park, T. G. Degradation of poly (D, L-lactic acid) microspheres: effect of molecular weight. *Journal of Controlled Release* **30**, 161-173 (1994).
265 Soares, J. S. & Zunino, P. A mixture model for water uptake, degradation, erosion and drug release from polydisperse polymeric networks. *Biomaterials* **31**, 3032-3042 (2010).
266 Prabhu, S. & Hossainy, S. Modeling of degradation and drug release from a biodegradable stent coating. *Journal of Biomedical Materials Research Part A* **80**, 732-741 (2007).
267 Brannon-Peppas, L.
268 Dave, V. B. (Google Patents, 2006).
269 Schindler, A. & Harper, D. Polylactide. II. Viscosity–molecular weight relationships and unperturbed chain dimensions. *Journal of Polymer Science Part A: Polymer Chemistry* **17**, 2593-2599 (1979).
270 Baura, G. *Medical Device Technologies: A Systems Based Overview Using Engineering Standards*. (Academic Press, 2011).
271 Kamaly, N., Yameen, B., Wu, J. & Farokhzad, O. C. Degradable controlled-release polymers and polymeric nanoparticles: mechanisms of controlling drug release. *Chem. Rev* **116**, 2602-2663 (2016).
272 King, D. & McGinty, S. Assessing the potential of mathematical modelling in designing drug-releasing orthopaedic implants. *Journal of Controlled Release* **239**, 49-61 (2016).
273 Lyu, S. & Untereker, D. Degradability of polymers for implantable biomedical devices. *International journal of molecular sciences* **10**, 4033-4065 (2009).
274 Luderer, F. *et al.* Biodegradable sirolimus-loaded poly (lactide) nanoparticles as drug delivery system for the prevention of in-stent restenosis in coronary stent application. *Journal of biomaterials applications* **25**, 851-875 (2011).
275 Siegel, R. A. & Rathbone, M. J. in *Fundamentals and Applications of Controlled Release Drug Delivery* 19-43 (Springer, 2012).
276 Webber, W. L., Lago, F., Thanos, C. & Mathiowitz, E. Characterization of soluble, salt-loaded, degradable PLGA films and their release of tetracycline. *Journal of Biomedical Materials Research Part A* **41**, 18-29 (1998).
277 Serruys, P. W. *et al.* The effect of variable dose and release kinetics on neointimal hyperplasia using a novel paclitaxel-eluting stent platform: the Paclitaxel In-Stent Controlled Elution Study (PISCES). *Journal of the American College of Cardiology*

46, 253-260 (2005).
278 Sirianni, R. W., Jang, E.-H., Miller, K. M. & Saltzman, W. M. Parameter estimation methodology in a model of hydrophobic drug release from a polymer coating. *Journal of Controlled Release* **142**, 474-482 (2010).
279 Kim, S.-J. *et al.* Development of a biodegradable sirolimus-eluting stent coated by ultrasonic atomizing spray. *Journal of nanoscience and nanotechnology* **11**, 5689-5697 (2011).
280 Zhao, J. *et al.* Drug loaded nanoparticle coating on totally bioresorbable PLLA stents to prevent in-stent restenosis. *Journal of Biomedical Materials Research Part B: Applied Biomaterials* (2016).
281 Joung, Y. K., Jang, B. N., Kang, J. H. & Han, D. K. Precise ultrasonic coating and controlled release of sirolimus with biodegradable polymers for drug-eluting stent. *Biomater. Biomed. Eng* **1**, 13-25 (2014).
282 Ranade, S. V. *et al.* Physical characterization of controlled release of paclitaxel from the TAXUS™ Express2™ drug-eluting stent. *Journal of Biomedical Materials Research Part A* **71**, 625-634 (2004).
283 Wada, R., Hyon, S.-H. & Ikada, Y. Kinetics of diffusion-mediated drug release enhanced by matrix degradation. *Journal of controlled release* **37**, 151-160 (1995).
284 Ding, N. & Helmus, M. N. (Google Patents, 1998).
285 Mc Evoy, K. M., Genet, M. J. & Dupont-Gillain, C. C. Principal component analysis: a versatile method for processing and investigation of XPS spectra. *Analytical chemistry* **80**, 7226-7238 (2008).
286 Fischlschweiger, M. & Enders, S. A Theory for Solubility of Semicrystalline and Branched Polymers in One Solvent. *Macromolecules* **47**, 7625-7636 (2014).
287 Balani, K., Verma, V., Agarwal, A. & Narayan, R. *Biosurfaces: A Materials Science and Engineering Perspective*. (John Wiley & Sons, 2015).